DESIGN AND EVALUATION OF HEAT TRANSFER FLUIDS FOR DIRECT IMMERSION COOLING OF ELECTRONIC SYSTEMS

A Thesis
Presented to
The Academic Faculty

by

Pramod Kumar Warrier Harikumar Warrier

In Partial Fulfillment
of the Requirements for the Degree
Doctor of Philosophy in the
School of Chemical and Biomolecular Engineering

Georgia Institute of Technology
August, 2012

DESIGN AND EVALUATION OF HEAT TRANSFER FLUIDS FOR DIRECT IMMERSION COOLING OF ELECTRONIC SYSTEMS

Approved by:

Dr. Amyn S. Teja, Advisor
School of Chemical and Biomolecular Engineering
Georgia Institute of Technology

Dr. Yogendra Joshi
School of Mechanical Engineering
Georgia Institute of Technology

Dr. Dennis W. Hess
School of Chemical and Biomolecular Engineering
Georgia Institute of Technology

Dr. Charles L. Liotta
School of Chemistry and Biochemistry
Georgia Institute of Technology

Dr. Matthew J. Realff
School of School of Chemical and Biomolecular Engineering
Georgia Institute of Technology

Date Approved: June 18, 2012

To my family.

ACKNOWLEDGEMENTS

I wish to express my sincere gratitude to people who have helped me during the course of my doctoral studies at Georgia Tech. First and foremost, I would like to thank my PhD advisor Prof. Amyn Teja for his support, guidance, numerous helpful discussions, as well as for his comments and critiques. He has taught me not only how to do research but also how to conduct oneself professionally. I will always be indebted to him for that. As this work was in collaboration with Prof. Yogendra Joshi, I would like to thank him for his guidance regarding the heat transfer aspects of this project. I would also like to thank Prof. Joshi for teaching the course on thermal packaging of micro/nano systems that helped me understand the thermal management issues in electronic systems. This work was funded by the Office of Naval Research and I am grateful to them for their support. Synthesis was a big challenge in this project and I am truly thankful to Prof. Stefan France for his help and advice on organic synthesis as well as for allowing me to use his lab. I am also grateful to my thesis reading committee members Professors Charles Liotta, Dennis Hess, and Matthew Realff for their help and advice over the years.

I am thankful to all the faculty members who taught me during the PhD program. Courses taught by Professors Charles Eckert, William Koros, Pradeep Agrawal, Sankar Nair, Christopher Jones, Uzi Landman, Rao Tummala, Zhong Wang, Vladimir Tsukruk, Zhoumin Zhang, Angelo Bongiorno, Andrew Zangwill, David Sherrill, and Sven Behrens have directly or indirectly helped in the successful completion of this thesis. I am also

thankful to Professors Athanasios Nenes, Kobi Abayomi, and Yoshiaki Kawajiri for allowing me to sit in some of their lectures.

I would like to acknowledge Aravind Satyanarayana for the heat transfer experiments, Dr. Ugur Guner for helping with the CAMD code, and Dadasaheb Patil for helping with the synthesis. I would also like to thank Teja group members Dr. Anupama Kasturirangan, Dr. Michael Beck, Angel Olivera, Dr. Pei Yoong Koh, Dr. Yanhui Yuan, Nelson Green, Firman Kurniawansyah, Dr. Feridoun Esmaeilzadeh, Mohamad Zahid Hossain, Jing Yan, Sara Bazdar, and Majid Addous for their support, advice, and friendship. It has been a pleasure to work with all of you.

I have been very fortunate to make lot of good friends in Atlanta and would like to thank Siddharth, Akshay, Prashant, Prabuddha, Ugur, Anil, Ambarish, Aritra, Rohan, Nitesh, Gautam, Surendar, Manoj, Bhandari, Ashish, Divya, Akshi, Swati, Sudipta, Dhruv, Praveen, Meha, Gaurav, Sricharan, Himanshu, Tanu, Shweta, Carlos as well as my batch mates Dhaval, Mike, Hunter, Nathan, and Mohamad for their friendship and support over the years. I would also like to thank members of the Georgia Tech Cricket, Badminton, and Squash clubs for helping me stay active in sports. It was indeed a pleasure and honor to play these sports with you and represent Tech in competitive events.

Most importantly, I would like to thank my family for their unconditional love and support throughout my life. Leaving job to pursue PhD was a difficult decision made easier by your understanding and support.

TABLE OF CONTENTS

LIST OF TABLES

LIST OF FIGURES

SUMMARY

The development of products that have desirable properties is an important goal of chemical product design. In general, new chemical products are identified empirically, based on the potential market for that product and the experience and insight of the designer. This approach is therefore limited by the designer's experience. By contrast, computer-aided molecular design (CAMD) is used in this work to conduct a systematic and exhaustive search of molecular structures and to generate a large number of feasible candidates for a specific application.

The application of interest in the present work is direct immersion phase change cooling of electronic systems. This interest stems from the need to find coolants that can meet the increasing thermal management demands that arise from miniaturization of electronics. Novel heat transfer fluids for direct immersion cooling of electronics were therefore identified using CAMD. In addition, the feasibility of improving existing heat transfer fluids by dispersing small amounts of high thermal conductivity solid nanoparticles in them was also investigated.

Since the CAMD approach requires reliable property estimation methods to screen candidates, group contribution (GC) methods for thermophysical properties relevant to heat transfer were critically evaluated using thermophysical property data for over 150 organic compounds. It was found that the predictive capabilities of the GC

methods were inadequate for organosilicon compounds. Therefore, new GC values were developed for organosilicon compounds and are presented in this work.

The molecules generated by the CAMD algorithm were constrained by limiting their boiling points, enthalpy of vaporization, and thermal conductivity values. The candidates were screened further using a figure of merit (FOM) analysis for pool and flow boiling. A total of 52 compounds were identified after this analysis. From these 52 fluids, 9 fluids were selected for experimental evaluation based on commercial availability and the potential of their synthesis. Two of these fluids (1,1,1-trifluoro-3-methylpentane and 1,1,1-trifluoro-3-(2,2,2-trifluoroethoxy)propane) were synthesized in this work and the remaining 7 were purchased from commercial vendors.

The density, viscosity, and thermal conductivity of the 9 fluids were measured and these values were employed in the validation of the GC methods used in the CAMD approach. Pool boiling heat transfer studies demonstrated that the new fluids possess heat transfer properties that are superior to those of HFE 7200. As most of the new fluids contained fluorine, their environmental properties were also evaluated. A new GC method was developed for radiative forcing (RF) and validated with FT-IR based calculations. RF predictions were then used to calculate the global warming potentials (GWP) of the new fluids. The GWP of new fluids were found to be significantly lower than those of currently used coolants.

The second approach examined for the development of new coolants was the addition of dispersed nanoparticles to existing coolants to enhance thermal conductivity. Since there is considerable disagreement in the literature with respect to the mechanism

of heat transfer in nanoparticle dispersions (or nanofluids), a critical review of experimental data and models for the thermal conductivity of nanofluids was conducted with particular emphasis on the effects of particle size. A modified geometric mean model was developed that takes into account the temperature dependence of the thermal conductivities of the individual phases, as well as the size dependence of the thermal conductivity of the dispersed phase. The rheological properties of nanofluids were also experimentally measured, and the effects of particle concentration, temperature, and shear rate on nanofluid viscosity were evaluated. The viscosity of nanofluids was found to increase by 2 orders of magnitude, while the thermal conductivity increase was found to be only 25 - 30 %. This increase in viscosity when particles are added to liquids suggests that this is not a feasible approach to undertake in order to improve existing coolants for electronics.

CHAPTER 1

INTRODUCTION

Performance enhancement while reducing system size is a universal characteristic of technological development. In the chemical industry, this is known as process intensification. In the microelectronics industry, it is exemplified by Moore's law which states that the number of transistors in an integrated chip doubles every 18-24 months [1]. Similar advancements are also observed in nuclear, automobile, and aircraft systems. With increasing intensification of processes that generate heat, thermal management becomes critical as there is more heat to be dissipated from a smaller area. Hence, thermal management technologies must advance to match the rate at which heat removal demands are increasing. This work therefore deals with identifying and evaluating heat transfer fluids for thermal management of microelectronic systems.

1.1 Microelectronic Systems

Continuous miniaturization of microelectronic systems to improve performance, cost, and reliability has resulted in a significant increase in volumetric heat flux generated in such systems. Indeed, present day microelectronic systems generate heat fluxes in excess of 100 W cm^{-2} for a single chip, and 25 W cm^{-2} for a multichip module [2]. Furthermore, electronic devices of the future are likely to generate heat fluxes of over 1 kW cm^{-2}, and of the same order as the heat flux on the surface of the sun, albeit over a much smaller area. Such large fluxes are available at much lower temperatures in

microelectronic systems, making heat dissipation even more challenging. [3] Thermal management is thus widely regarded as a key bottleneck in further development of electronic systems. [2, 3]

Air has been the preferred fluid for cooling electronic systems for a long time due to low cost, ease of maintenance, and high reliability. [2] However, heat fluxes of over 1 kW cm^{-2} are likely to require forced convection of liquids and/or phase change heat transfer for cooling electronic devices of the future. Liquid cooling methods can be classified into indirect and direct (immersion) cooling. In indirect liquid cooling, electronic components are physically separated from the liquid, whereas they are in contact with the liquid in direct immersion cooling. Direct immersion cooling offers the opportunity to remove heat directly from chips with no intervening thermal conduction resistance and provides greater uniformity of chip temperatures. [4] Direct immersion cooling is also one of the most reliable thermal management techniques with all components residing in a completely sealed liquid environment. [5] Also, physical separation allows the use of water as the liquid coolant. However, electrical and chemical compatibility of the liquid and electronic components pose significant constraints on liquid coolants. This has led to the use of fluoroinerts such as FC-72, FC-86, FC-77, and Novec fluids such as HFE-7100 and HFE-7200 for direct immersion cooling applications. These liquids possess chemical stability, low dielectric constants, and boiling temperatures that lie in the range 50 - 100 °C. [6] However, fluoroinerts and Novec fluids are plagued by low thermal conductivity (about twice that of air) and specific heat (about the same as that of air). Also, they suffer from temperature overshoot in pool boiling applications due to low surface tensions [7], which delays the inception of nucleate

boiling and causes wall temperature to increase significantly above the saturation temperature of the fluid. Moreover, a number of these chemicals have very high global warming potentials. [7] These factors necessitate the development of new heat transfer fluids with improved heat transfer properties for thermal management of future high performance microelectronic systems.

1.2 Approach

New heat transfer fluids for thermal management of electronic systems should possess the following properties in order to be considered superior over current coolants (HFE 7200, FC 72, etc.):

- High thermal conductivity (> 0.07 W m^{-1} K^{-1})
- High enthalpy of vaporization (> 31 kJ mol^{-1})
- High specific heat (> 322 J mol^{-1} K^{-1})
- Low viscosity (< 0.6 cP)
- Low global warming potential (< 59 W year m^{-2} $ppbv^{-1}$)
- Zero ozone depletion potential

In addition, they must be chemically inert, dielectric, compatible with system components, inexpensive, and possess liquid range within the operating heat transfer regime.

The search for heat transfer fluids with these properties can be pursued using any one or a combination of the approaches outlined in the following section [8]:

1.2.1 Ad Hoc Experiments

Ad hoc experiments have been traditionally used to design a large number of consumer products. In such cases, the desired properties must be available or be measured. As experiments are expensive and time consuming, it is not always possible to evaluate all possible candidates. The list of candidates is therefore usually generated by the practitioner's insight or by scanning through chemical property database such as those developed by the National Institute of Standards and Technology (NIST) [9], Dortmund Data Bank [10], or Design Institute for Physical Properties (DIPPR) [11]. However, of the 56 million compounds listed in the Chemical Abstracts Service registry [12], property data are available for a few thousand compounds. Therefore, the search space in this approach is very limited and potential candidates are often not considered.

1.2.2 Computer-Aided Molecular Design

Computer-aided molecular design (CAMD) can be used when validated mathematical models for the estimation of all desired properties are available. In this case, a list of candidate molecules can be quickly generated and tested against property constraints. CAMD, in essence, is the reverse of property prediction, where the objective is to find molecules that possess desired properties. The CAMD approach depends on the accuracy of the property estimation methods used in generating candidates with desired properties. If the estimation methods are not accurate, then there is a possibility that some molecules will not be selected.

Molecules can be generated in the CAMD method by combining atoms (C, H, O, etc.) or functional groups (CH_3, CH_2, OH, COOH, etc.). Combining atoms to generate molecules requires atomic level description of properties, for which time consuming quantum mechanical calculations must be employed. On the other hand, combining functional groups can take advantage of group contribution (GC) methods for estimating properties which can be done very rapidly. GC methods are available for many thermodynamic, physical, and chemical properties. [13]

The CAMD approach using group contribution was employed in this work to identify new heat transfer fluids and mixture formulations for direct immersion cooling of electronics. Depending on the problem description, the CAMD method can yield millions of candidates as it generates all possible combinations of specified groups. These candidates were screened by applying property constraints that narrow the choice from millions to few thousands ($O(10^3)$). As the number of candidates was still very large, an additional screen using figure of merit (FOM) analysis was implemented. The FOM screen brings down the number of potential candidates to an order of 10^1. FOMs are often used to represent heat transfer coefficients and are expressed as a function of the thermophysical properties of the fluid. FOMs of candidates generated by CAMD were compared with those of currently used coolants and candidates with higher FOMs were selected for experimental evaluation. The CAMD-FOM approach used in this work is illustrated in Figure 1.1. [14]

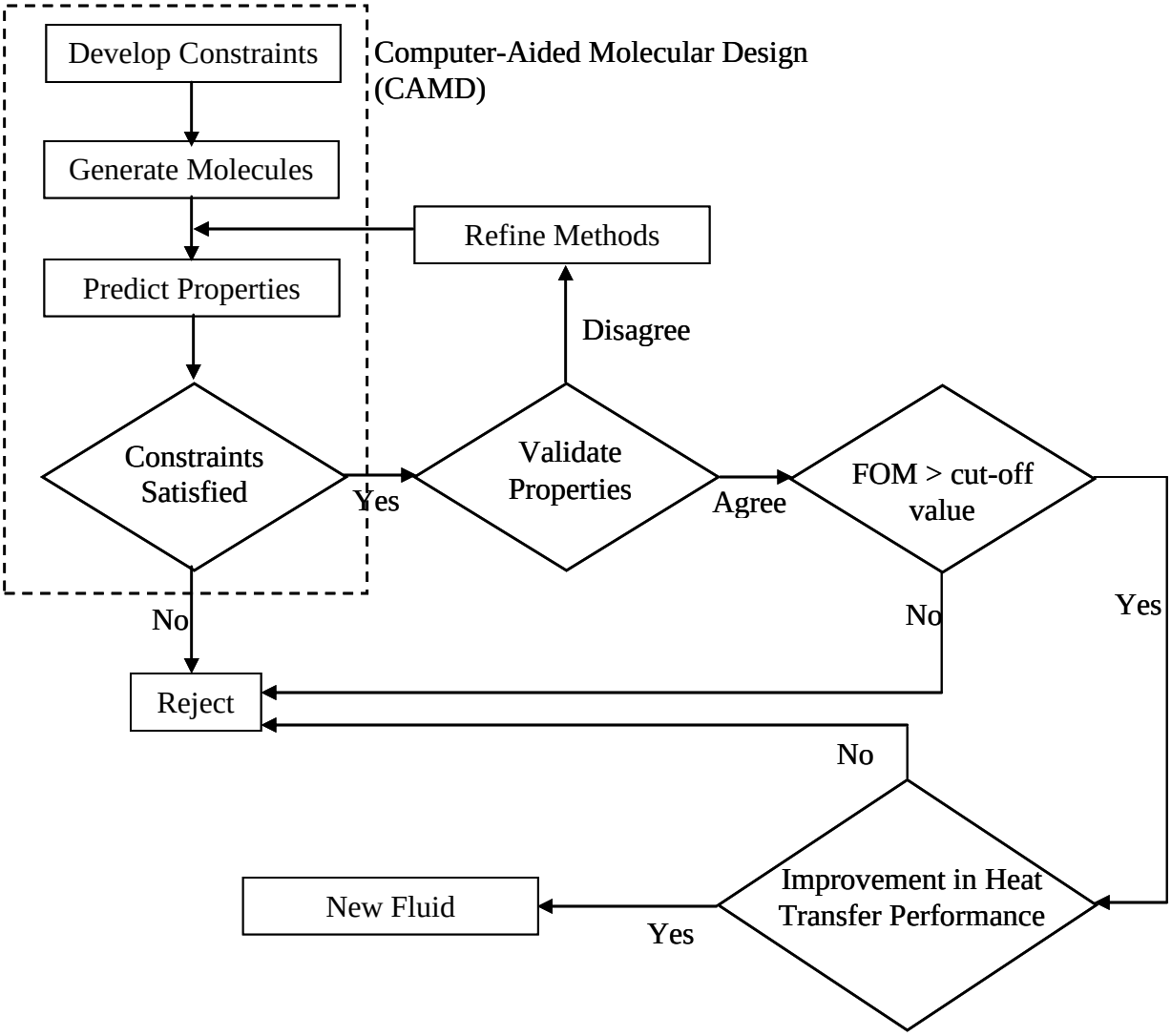

Figure 1.1. CAMD-FOM approach. First 4 steps constitute CAMD.

1.2.3 Enhancing the Properties of Existing Fluids

The properties of known heat transfer fluids can be enhanced for specific applications by adding liquids or solids. Nonlinear dependence on composition for properties of such mixtures offers the potential of yielding formulations with enhanced properties. Customized formulations (i.e. multicomponent mixtures or blends) of

chemicals are routinely used in industry to obtain products with desired properties. For example, lubricants have been formulated that have high chemical stability and specified temperature behavior of the viscosity for automotive applications [15]. CAMD, as described above, was employed in this work to systematically identify liquid additives that improve heat transfer properties of a currently used coolant HFE 7200. HFE 7200 has a boiling point of 76 °C and is, therefore, commonly used in electronics cooling applications where chip temperatures have to be maintained below 80 °C. The same approach can also be used to design additives for other coolants.

Liquids are generally poor conductors of heat (the thermal conductivity of the most common heat transfer fluid, water, is about 0.6 W m^{-1} K^{-1}). As thermal conductivity of solids can be as much as three orders of magnitude greater than that of liquids, addition of more conductive solids to liquids provides an opportunity to increase the thermal conductivity of heat transfer fluids. In this work, dispersions of solid nanoparticles in liquids (nanofluids) were investigated. Since investigations of nanofluids are relatively recent, the underlying physics and effects of various parameters (such as particle size, temperature) on their thermal conductivity are not well understood. This work, therefore, focuses on understanding the fundamental physics of nanofluids. Studies on nanofluids were conducted with water and ethylene glycol based dispersions to compare with the existing literature.

The goal of this work was to design and evaluate new heat transfer fluids for direct immersion phase change cooling of electronic systems. This was achieved using the CAMD-FOM approach illustrated in Figure 1.1. The first task in this work was to

evaluate published property estimation methods used in CAMD. This is discussed in Chapter 2. Chapter 2 also describes the evaluation of new group contributions for organosilicon compounds. The application of the CAMD-FOM approach for the design of heat transfer fluids is presented in Chapter 3. A total of 55 fluids were identified after FOM analysis and 9 were selected for further evaluation. Chapter 4 describes the organic synthesis of 2 of these 9 candidates. The experimental evaluation of 9 fluids including thermophysical property measurements and pool boiling heat transfer studies is presented in Chapter 5. As most of the newly identified fluids were fluorinated compounds and fluorocarbons are known to have significant impact on global warming [16], it is important to assess their impact on the climate. This is discussed in Chapter 6 which describes the development of a new estimation method for radiative forcing as well as experimental evaluation to calculate global warming potential. Finally, Chapter 7 provides a critical review and investigation of the transport properties of nanofluids.

1.3 References

1. Moore, G. E., Cramming more components onto integrated circuits, Electronics, 1965. **38**(8): p.

2. Incropera, F. P., *Liquid cooling of electronic devices by single-phase convection*, 1999. New York: John Wiley & Sons.

3. Tummala, R. R., and Swaminathan, M., *Introduction to System-On-Package (SOP)*: m*iniaturization of the entire system*, 2008. New York: McGraw-Hill.

4. Simons, R. E., *Direct liquid immersion cooling for high power density microelectronics*, Electronics Cooling, 1996. **2**(2): p. 1-6.

5. Tummala, R. R., *Fundamentals of microsystems packaging*, 2001. New York: McGraw-Hill.

6. Mohapatra S. C., *An overview of liquid coolants for electronics cooling*, Electronics Cooling, 2006. **12**(5): p. 1-6.

7. Arik M., and Bar-Cohen A., *Ebullient cooling of integrated circuits by Novec fluids*, Technical Report GRC027, 2002, GE Global Research.

8. Ng, K. M., Gani, R., and Dam-Johansen, K. (eds). *Chemical product design: toward a perspective through case studies*, Computer-Aided Chemical Engineering Volume 23, 2007. Amsterdam, The Netherlands: Elsevier.

9. NIST Chemistry webbook, http://webbook.nist.gov/chemistry/

10. Dortmund Data Bank, http://www.ddbst.com/en/products/DDB-00-Basic-Data.php

11. Rowley, R. L., Wilding, W. V., Oscarson, J. L., Yang, Y., and Giles, N. F., DIPPR® Data Compilation of Pure Chemical Properties, 2010. Design Institute for Physical Properties, http://dippr.byu.edu, Brigham Young University, Provo, Utah.

12. Chemical Abstracts Service, http://www.cas.org/newsevents/releases/research120810.html

13. Poling B. E., Prausnitz J. M., and O'Conell J. P., *The Properties of gases and liquids*, 5th Edition, 2000. New York: McGraw-Hill.

14. Warrier, P., Sathyanarayana, A., Patil, D. V., France, S., Joshi, Y., and Teja, A. S., *Novel heat transfer fluids for direct immersion phase change cooling of electronic systems*, International Journal of Heat and Mass Transfer, 2012. **55**: p. 3379-3385.

15. Rudnick L. R., and Shubkin R. L. (eds.), *Synthetic lubricants and high performance functional fluids*, 1999. New York: Marcel Dekker.

16. Velders, G. J. M., Fahey, D. W., Daniel, J. S., McFarland, M., and Anderson, S. O., *The large contribution of projected HFC emissions of future climate forcing*, Proceedings of the National Academy of Sciences U.S.A., 2009. **106**: p. 10949-10954.

CHAPTER 2

PROPERTY ESTIMATION METHODS

The success of any CAMD approach depends on the availability and accuracy of property estimation methods used to predict the properties of the newly generated molecules. If uncertainties associated with the property predictions are high, then it is possible that potential candidates might be screened out. The performance of four group contribution methods is therefore critically evaluated in this chapter, especially with respect to properties needed in heat transfer calculations. In addition, new group contributions are optimized for thermophysical properties of silicon containing groups.

2.1 Background

Thermophysical properties of substances and their mixtures are important because they have a significant impact on process economics. [1, 2] The role of property estimation methods in process and product design was recently emphasized by Gani and O'Connell [3] who noted that this role consists of:

- *Service* - to provide values of required properties.
- *Service plus advice* - to provide property values as well as advice on feasibility of the design.
- *Integration* - to contribute directly towards the design of the integrated product-process.

Unfortunately, property data are not always available because experimental measurements are expensive and time consuming. Of the 56 million substances listed in the Chemical Abstracts Service registry [4], thermophysical property data are available for only about 20,000 substances [5], and not for all thermophysical properties for these 20,000 substances. For example, the Dortmund Data Bank [5] contains data for the vapor pressure, viscosity, and thermal conductivity for about 9,900, 3,300, and 960 substances, respectively. Consequently, property estimation methods are required to bridge the gap between experimentally measured data and properties needed in calculations.

A property estimation method provides values for the properties of a substance from its molecular structure or from correlations with available data on another property. There are three levels of such methods [1]: empirical, semi-empirical, and first principle methods. Empirical models are usually developed by fitting a mathematical function to literature data. Examples include quantitative structure-property relationships (QSPR) and group contribution (GC) methods. Even though QSPR and GC methods are predictive, they cannot be applied to classes of compounds that were not used in the development of these methods. It is, therefore, useful to correlate properties that are difficult to measure with those that can be accurately measured or predicted. Semi-empirical models represent correlations that are based on a sound physical theory, such as corresponding states theory. First principle methods include detailed calculations based on quantum or molecular mechanics. However, these calculations are often performed for isolated molecules and therefore cannot predict properties in solution. A quantum chemical method, COSMO-RS, is discussed in Appendix G and combines quantum

mechanical calculations with statistical thermodynamics. COSMO-RS can be used to calculate thermodynamic properties in solution.

There are many GC methods available for different properties and it is not possible to discuss and evaluate each one of them. Therefore, only methods that are applicable to a wide variety of compounds and which can predict properties relevant to heat transfer are presented here. QSPR methods were not evaluated in this work as they employ molecular descriptors such as amounts of negatively and positively charged molecular surface area, dipole moment, bond length, and bond angle. Such descriptors require molecular 3D geometry to be optimized using molecular or quantum mechanics. These calculations are time consuming and do not offer much advantage over GC methods in terms of predictive capabilities. GC methods and corresponding states correlations used in this work are described in following sections.

2.1.1 Group Contribution Methods

The development of estimation methods for the thermophysical properties of compounds from their molecular structure has received considerable attention over many years. Group contribution (GC) methods express properties of the molecule as a function of contributions from functional groups that constitute the molecule. For example, the normal boiling point of methanol (CH_3OH) can be calculated from the sum of contributions from CH_3 and OH groups. The basis of GC methods is the presence of certain groupings of atoms (called functional groups) that determine most of the chemical and physical properties of organic compounds. Organic compounds can be systematically organized into classes (alcohols, ethers, esters, carboxylic acids, etc.) with each class

characterized by a particular functional group (OH, O, COO, COOH). A functional group can be defined as a unique collection of chemically bonded atoms that displays distinct set of properties [6]. All alcohols, for example, contain the OH functional group that exhibits similar properties whether it is linked to CH_3, CH_2, or C_6H_5 groups. Therefore, the properties of the OH group are transferable across different organic compounds. GC methods utilize this property of functional groups and further assume that properties are additive. Thus, the contribution of a group towards any property is assumed to be constant and independent of the group to which it is attached. This assumption, while not always valid, provides an opportunity for estimating the properties of a large number of compounds from a much smaller number of parameters that characterize the contributions of individual groups. [7]

GC methods are only approximate methods as the group contributions are not always additive and transferable between different compounds, or even between isomeric forms of the same compound. This is evident from differences in properties of isomeric compounds. For example, the normal boiling points of n-pentane, iso-pentane and neo-pentane are 36, 27.7 and 9.5 °C respectively [8]. Similarly, properties of the COO group are significantly different when it is attached to a hydrogen atom or when it is connected to an alkyl group. Therefore, the definition of a group also play a significant role in GC methods. As a first approximation, groups can be defined as per functional groups of organic chemistry, i.e., CH_3, CH_2, CH, C=C, C≡C, OH, Cl, F, O, CO, COO, CHO, COOH, etc. These groups cannot differentiate between isomers. Accuracy of correlation can be improved by defining groups that can differentiate between isomers such as $CH_2(CH_3)$, $CH(CH_3)_2$. However, as more and more distinctions are made, group tends to

approach the whole molecule and the advantage of GC methods that of representing thousands of compounds by a few groups, is lost. [7, 9] GC methods, therefore, need to compromise between using groups that capture the significant effects of molecular structure while maintaining relatively small number of distinct groups.

The assumption that group properties are transferable was noted by Wu and Sandler [10, 11] who calculated approximate charges on atoms and groups of atoms using *ab initio* quantum mechanical calculations. As properties of atoms or groups are determined by their charge distribution, their calculations provide a theoretical basis for defining groups in GC methods. A rigorous and fundamental explanation for the success of group additivity was also provided by Bader using quantum theory of atoms in molecules (QTAIM) [12-16]. For example, Bader and Bayles [13] studied additivity and transferability of energy and electron delocalization exhibited by the linear hydrocarbons with that obtained for the linear silanes and verified the group additivity relationship for the enthalpy of formation. However, it should be noted that these quantum calculations were performed for isolated molecules and, therefore, their results cannot be extrapolated for solutions or for bulk properties. As GC methods do not consider interactions between molecules, in principle they should only be applicable to properties that can be defined for individual molecules such as heat of formation, dipole moment, acentric factor, polarizability, etc., and not for properties of the bulk medium such as density, thermal conductivity, melting and boiling point, viscosity, etc. Irrespective of these considerations, GC methods are very popular and have proven to be immensely beneficial in chemical process and product design calculations. The following paragraphs

provide an overview of some GC methods, especially those suitable for properties relevant to heat transfer.

It was Kopp [17] in 1855 who first showed that the molar volume of a substance at its boiling point is approximately given by the sum of the atomic volumes of its constituent atoms. Later, during the 1880s, it was observed that molar polarization [18] can be calculated using a group additivity scheme based on constant values assigned to groups comprising each molecule. Similarly, a group additivity scheme was developed by Pascal [19, 20] for magnetic susceptibility. Additivity patterns were observed for many other properties including the parachor [21], specific heat [22], and enthalpy of formation [23]. Benson and Buss [24] were the first to develop a rigorous group additivity scheme for thermodynamic properties. They proposed four levels of additivity rules that accounted for atomic, bond, and group properties. Following the work of Benson and Buss, group additivity schemes have been proposed for many properties with varying degrees of complexity and accuracy. GC methods have even been extended to estimate properties of mixtures. For example, Analytical Solution of Groups (ASOG) [25] and UNIQUAC Functional-group Activity Coefficients (UNIFAC) [7] employ GC method for estimating activity coefficients in mixtures. A detailed and critical review of GC methods and their applications can be obtained from Poling *et al.* [26]. As the focus of this work is on heat transfer and many properties relevant to heat transfer (such as thermal conductivity and heat of vaporization) are estimated using correlations based on corresponding states, GC methods for the estimation of critical properties are discussed first.

Riedel [27] and Lydersen [28] were among the first to develop GC methods for critical properties. They proposed modifications to the Guldberg rule [29], T_c = 1.5 T_b where T_c and T_b are critical temperature and normal boiling point respectively. Writing T_c = T_b/θ, θ can be expressed in Riedel's method as:

$$\theta = 0.574 + \left(\sum n_i C_i\right) \tag{2.1}$$

where n_i is the number of times group i appears in the molecule, and C_i is the contribution of group i. Critical pressure (P_c) was calculated in Riedel's method by:

$$P_c / bar = \frac{M}{\left(0.33 - \sum n_i C_i\right)^2} \tag{2.2}$$

where M is a constant determined by regression. Lydersen [28] extended Riedel's method by evaluating a larger dataset and expressed T_c and critical volume (V_c) as:

$$\theta = 0.567 + \left(\sum n_i C_i\right) - \left(\sum n_i C_i\right)^2 \tag{2.3}$$

$$V_c / cc.mol^{-1} = 40 + \left(\sum n_i C_i\right) \tag{2.4}$$

Lydersen also employed equation 2.2 for P_c but used 0.34 instead of 0.33 in the denominator. With the availability of more experimental data and efficient statistical techniques, many modifications have been proposed for equations 2.1 - 2.4, most notably by Ambrose [30, 31], Daubert [32], Fedors [33], Joback and Reid [34], Constantinou and Gani [35], and Wilson and Jasperson [36]. These methods have been critically evaluated by Poling *et al.* [26] and they recommend methods by Joback and Reid (JR) and

Constantinou and Gani (CG) as these methods can be applied to a wide variety of compounds and provide most of the pure component properties with a single group formulation. Therefore, JR and CG methods were selected for further evaluation in the present work. Marrero and Gani [37] have recently proposed a new modification which was not evaluated by Poling *et al*. Therefore, the Marrero and Gani (MG) method was also selected for evaluation in the present work. None of these methods are applicable to organosilicon fluids, which are an important class of heat transfer fluids that exhibit low viscosity and wide liquid ranges (-100 to 250 °C) [38]. The Wilson and Jasperson (WJ) method does include contributions from silanes and siloxanes, and was therefore considered in this work. These four GC methods (JR, CG, WJ, and MG) have been incorporated into software developed by the Computer Aided Process-Product Engineering Center (CAPEC) of Technical University of Denmark (DTU) and Molecular Knowledge Systems Inc., NH, USA under the names of ICAS [39] and CRANIUM [40] respectively. The JR, CG, WJ, and MG methods are therefore discussed in detail below and a critical evaluation of these methods is presented in the following section.

2.1.1.1 Joback - Reid (JR) Method (1987)

Joback and Reid [34] reevaluated Lydersen's method for critical properties using an expanded dataset and added new functional groups. They also developed new GC methods for other pure component properties that are listed below:

Melting Point (T_m)

$$T_m / K = 122 + \left(\sum n_i C_i\right) \tag{2.5}$$

Normal Boiling Point (T_b)

$$T_b / K = 198 + \left(\sum n_i C_i\right) \tag{2.6}$$

Critical Temperature (T_c)

$$T_c / K = \frac{T_b}{0.584 + 0.965 \times \sum n_i C_i - \left(\sum n_i C_i\right)^2} \tag{2.7}$$

Liquid Viscosity (η) at 298 K

$$\eta / cP = 1000.MW.\exp\left(\sum n_i \, C_{iA} / T + n_i C_{iB}\right) \tag{2.8}$$

Ideal Gas Heat Capacity (C_{pg})

$$C_{pg} / J.mol^{-1}.K^{-1} = \sum n_i C_{iA} + T\sum n_i C_{iB} + T^2 \sum n_i C_{iC} + T^3 \sum n_i C_{iD} \tag{2.9}$$

In equations 2.5 - 2.9, n_i is the number of times group *i* appears in the molecule, C_i is the contribution of group *i*, *MW* is the molecular weight, and *T* is the temperature in Kelvin. For liquid viscosity (equation 2.8), two contribution values were assigned to each group (C_{iA} and C_{iB}). Similarly, four contributions were assigned for each group in the case of ideal gas heat capacity. Joback and Reid employed only 49 groups in the development of their method. Moreover, the groups defined were relatively simple e.g. CH_3, CH_2, C, Cl, F, OH, etc. Their method, therefore, cannot differentiate between isomers.

2.1.1.2 Constantinou - Gani (CG) Method (1994)

Constantinou and Gani [35] considered second order groups (*j*), constructed by combining first order groups (*i*), in order to capture differences in properties of isomers. The CG method employs 78 first order groups that are similar to those used in UNIFAC [7]. In addition, 43 second order groups (*j*) were identified using the conjugation approach described by Mavrovouniotis [41] which include combinations such as $(CH_3)_2CH$, $CH(CH_3)CH(CH_3)$. Interestingly, many second order groups are identical to those found by Wu and Sandler [10] using *ab initio* calculations. The expressions for T_m, T_b, T_c, and enthalpy of vaporization (H_{vap}) in CG method are given by:

Melting Point (T_m)

$$T_m / K = 102.452 \ln\left(\sum_i n_i C_i + \sum_j n_j C_j \right) \tag{2.10}$$

Normal Boiling Point (T_b)

$$T_b / K = 204.359 \ln\left(\sum_i n_i C_i + \sum_j n_j C_j \right) \tag{2.11}$$

Critical Temperature (T_c)

$$T_c / K = 181.128 \ln\left(\sum_i n_i C_i + \sum_j n_j C_j \right) \tag{2.12}$$

Enthalpy of Vaporization (H_{vap}) at 298 K

$$H_{vap} / kJ.mol^{-1} = 6.829 + \left(\sum_i n_i C_i + \sum_j n_j C_j \right) \tag{2.13}$$

2.1.1.3 Wilson - Jasperson (WJ) Method (1996)

The Wilson and Jasperson [36] method was developed only for critical temperatures and pressures of organic and inorganic compounds and employs contributions from both atoms and groups. The critical temperature in this method is given by:

Critical Temperature (T_c)

$$T_c / K = \frac{T_b}{\left[0.048271 - 0.019846 \times n_r + \sum n_i C_i + \sum n_j C_j\right]^{0.2}} \tag{2.14}$$

where n_r, n_i, and n_j are number of rings, atoms of type *i* with contribution C_i, and number of groups of type *j* with contribution C_j, respectively. The WJ method was developed using a dataset of approximately 700 compounds including organics, inorganics, solids, liquids and gases, and employs only 43 atomic and 14 group contributions. The method is, therefore, remarkable in its simplicity as it can be applied to all classes of compounds using only 57 atomic and group contributions. [26]

2.1.1.4 Marrero - Gani (MG) Method

Marrero and Gani [37] extended the work of Constantinou and Gani [35] and included third order groups (*k*), in addition to the first and second order groups defined by Constantinou and Gani. Third order groups are required to model systems of fused aromatic rings, fused aromatic and nonaromatic rings, and systems of nonfused rings joined by chains which include different functional groups. The first order groups describe a wide variety of organic compounds, while the second and third order groups

provide more molecular structural information. In the MG method, therefore, the estimation is performed at three levels, where the first level provides an initial approximation that is improved at the second level and further refined at the third level. For example, estimation of normal boiling point of N-phenyl-1,4-benzenediamine (experimental T_b = 627.15 K) using first, second, and third order groups gives 614.62 K, 616.03 K, and 623.94 K respectively. Similarly, inclusion of third order groups improves melting point estimation of Flutemazepan by approximately 7.5 %. The MG method for various properties of interest is given below:

Melting Point (T_m)

$$T_m / K = 147.45 \ln\left(\sum_i n_i C_i + \sum_j n_j C_j + \sum_k n_k C_k \right) \tag{2.15}$$

Normal Boiling Point (T_b)

$$T_b / K = 222.543 \ln\left(\sum_i n_i C_i + \sum_j n_j C_j + \sum_k n_k C_k \right) \tag{2.16}$$

Critical Temperature (T_c)

$$T_c / K = 231.239 \ln\left(\sum_i n_i C_i + \sum_j n_j C_j + \sum_k n_k C_k \right) \tag{2.17}$$

Enthalpy of Vaporization (H_{vap}) *at 298 K*

$$H_{vap} / kJ.mol^{-1} = 11.733 + \left(\sum_i n_i C_i + \sum_j n_j C_j + \sum_k n_k C_k \right) \tag{2.18}$$

The MG method is complex as it employs 182 first order, 122 second order, and 66 third order groups.

2.1.2 Correlations Based on Corresponding States

The principle of corresponding states derives from the work of van der Waals and relates the configurational thermodynamic properties of conformal substances (i.e. substances that conform to the same intermolecular potential) in a universal way. [26] The principle has been an important tool in the development of correlations for thermophysical properties. Corresponding states correlations that were used in this work are presented below. [39]

2.1.2.1 Enthalpy of Vaporization (H_{vap}) at 298 K

$$H_{vap} / kJ.mol^{-1} = 0.008314.T_c \times \left(R1 + W.R2\right) \tag{2.19}$$

where, R1 = 6.537 $T_r^{0.333}$ - 2.467 $T_r^{0.833}$ - 77.521 $T_r^{1.208}$ + 59.634 T_r + 36.009 T_r^2 - 14.606 T_r^3, R2 = -0.133 $T_r^{0.333}$ - 28.215 $T_r^{0.833}$ - 82.958 $T_r^{1.208}$ + 99 T_r + 19.105 T_r^2 - 2.796 T_r^3, T_r = 1 - 298.15/T_c, and W = (ω - 0.21)/0.25. ω is the acentric factor.

2.1.2.2 Liquid Density (ρ) at 298 K

$$\rho / g.cc^{-1} = 83.14 \times T_c Z_c^A / P_c \tag{2.20}$$

where, Z_c = 0.29056 - 0.08775ω, A = 1 + (1 - T/T_c)$^{0.285714}$, and P_c is the critical pressure.

2.1.2.3 Thermal Conductivity (k) at 298 K

$$k/W.m^{-1}.K^{-1} = \frac{1.11\times\left(3+20\times\left(1-T_r\right)^{0.6666}\right)}{MW^{0.5}\left(3+20\times\left(1-T_{br}\right)^{0.6666}\right)} \quad (2.21)$$

where, $T_r = T/T_c$ and $T_{br} = T_b/T_c$.

2.2 Evaluation of Property Estimation Methods

A wide variety of organic compounds including, alkanes, alkenes, alkynes, carboxylic acids, alcohols, ketones, aldehydes, ethers, esters, amides, fluorinated (F), organosilicon (Si) as well as aromatic and alicyclic compounds were selected for the evaluation of the four GC methods. These families of compounds were selected on the basis of availability of group contributions and their potential in heat transfer applications. Data for approximately ten compounds from each family was compiled from the DIPPR database [42] and used to evaluate the JR, CG, WJ, and MG methods for 8 properties: melting point, normal boiling point, enthalpy of vaporization, surface tension, density, thermal conductivity, viscosity, and specific heat. Enthalpy of vaporization, density, and thermal conductivity were computed using the corresponding states correlations described in equations 2.19 - 2.21 with the values of critical properties computed using the respective GC method. Temperature dependent properties (H_{vap}, σ, ρ, k, η, C_p) were evaluated at 298 K. The evaluation for each property is listed in the following sections. This evaluation was used not only in selecting the best method for each property but also in identifying properties that can be predicted with a reasonable degree of accuracy.

2.2.1 Melting Point

The melting point (T_m) is an important property as it determines the lowest temperature at which a heat transfer fluid can be employed in practical applications. Table 2.1 lists the number of compounds for different functional groups that were used for evaluation of each GC method. Figure 2.1 shows average absolute deviations (AAD)s from DIPPR data for each method. The WJ method does not predict melting points and hence is not shown in Table 2.1 and Figure 2.1.

The overall AADs from DIPPR data for the MG, CG, and JR methods are 12.55, 9.36, and 13.37 % respectively. Relatively large AADs, however, were observed for alkynes, carboxylic acids, and organosilicon compounds. It was also observed that all 3 methods frequently (> 80 % of the time) under-predict T_m for alkanes and over-predict it for alkynes. In addition, the JR method was found to frequently under-predict T_m for aldehydes and ketones while the MG method over-predicted T_m for carboxylic acids.

Table 2.1. Number of compounds used in the evaluation of T_m.

	MG	CG	JR
Alkane	10	9	10
Alkene	8	8	10
Alkyne	10	10	10
Alcohol	10	9	10
Ether	10	8	10
Aromatic	10	10	10
Alicyclic	10	10	10
Aldehyde	9	8	10
Ketone	10	9	10
Ester	10	10	10
Amine	10	9	10
Amide	5	2	5
Carboxylic acid	10	9	10
F	8	3	9
Si	9	N/A	N/A
Total	139	114	134

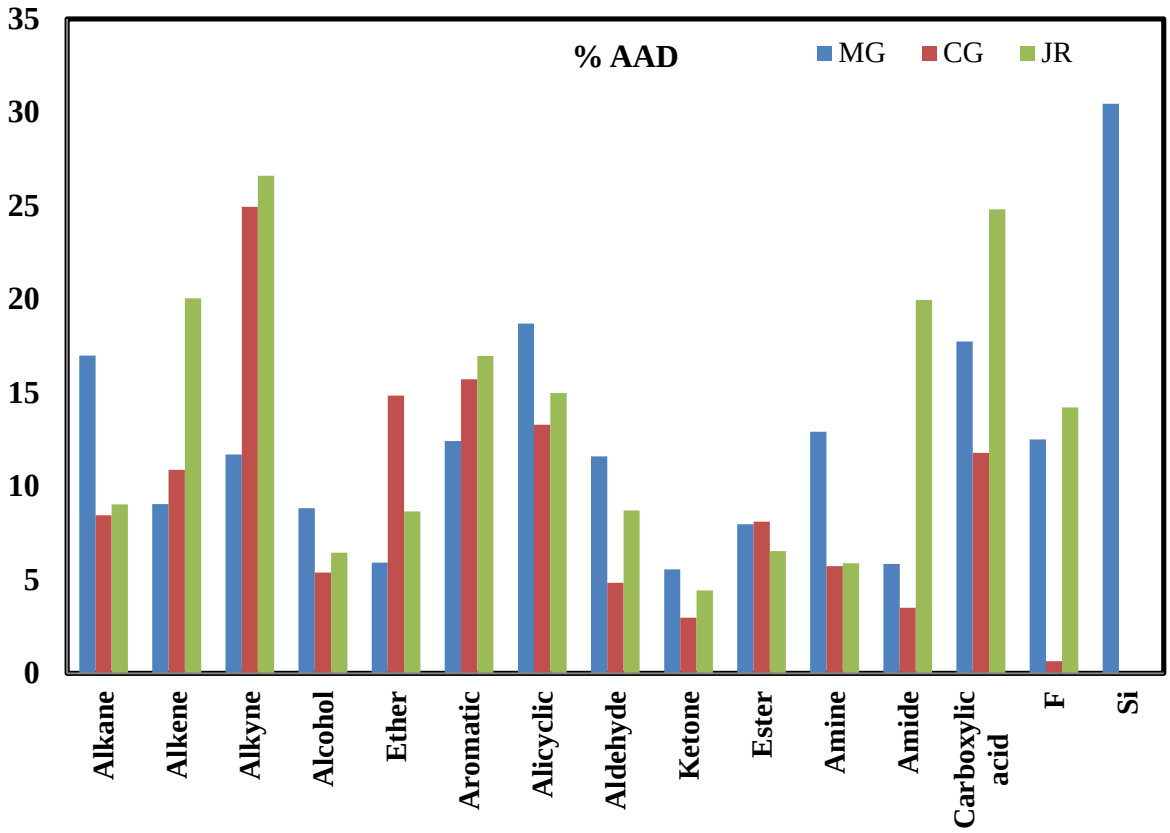

Figure 2.2. AADs for the MG, CG, and JR methods in the prediction of T_m.

2.2.2 Normal Boiling Point

The normal boiling point (T_b) is an important property in pool boiling heat transfer calculations. The performance of the four methods in predicting this property for the 150 compounds from the DIPPR database is shown in Figure 2.2. Table 2.2 lists the number of compounds and the different functional groups used in the evaluation of T_b.

Table 2.2. Number of compounds used in the evaluation of T_b.

	MG	CG	JR	WJ
Alkane	10	9	10	10
Alkene	8	8	9	9
Alkyne	10	10	10	10
Alcohol	10	9	10	10
Ether	10	9	10	10
Aromatic	10	10	10	10
Alicyclic	10	10	10	10
Aldehyde	9	9	10	10
Ketone	10	9	10	10
Ester	10	10	10	10
Amine	10	9	10	10
Amide	5	2	5	5
Carboxylic acid	10	9	10	10
F	9	9	9	9
Si	10	N/A	N/A	10
Total	141	122	133	143

Overall AAD (%) for the MG, CG, JR, and W methods were 3.91, 2.23, 5.18, and 4.27, respectively. The four GC methods, therefore, are able to predict T_b reasonably well. However, deviations were high for amides and therefore these methods should be used with caution for compounds containing the amide functional group. In addition, the MG and WJ methods frequently over-predicted T_b for organosilicon compounds. Given the importance of T_b in boiling heat transfer and the availability of good GC estimation methods for T_b, this property was selected as one of the properties where limits (constraints) could be applied with confidence in CAMD.

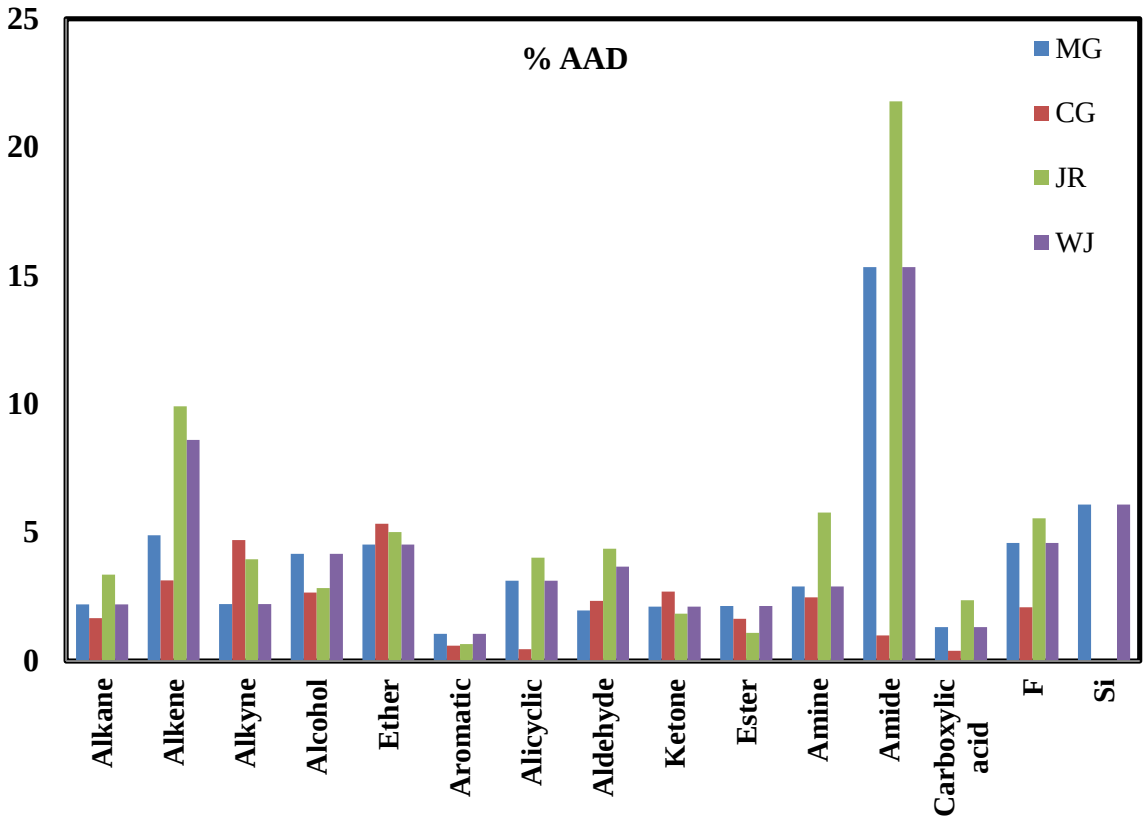

Figure 2.3. AADs for the MG, CG, JR, and WJ methods in the prediction of T_b.

2.2.3 Enthalpy of Vaporization

The enthalpy of vaporization (H_{vap}) significantly influences heat transfer performance in the pool boiling regime. The AADs of the four GC methods in predicting H_{vap} are shown in Figure 2.3. The number of compounds and different functional groups used in the evaluation of H_{vap} are listed in Table 2.3. Overall AAD (%) for MG, CG, JR, and WJ methods were 14.56, 7.67, 15.46, and 9.96 respectively. The MG method was found to frequently (> 80 % of the time) over-predict H_{vap} for all classes of compounds considered in this study except for carboxylic acids and fluorinated compounds. Also, the JR method frequently over-predicted H_{vap} for alkanes, alkenes, alkynes, alcohols,

aldehydes, fluorinated, and aromatic compounds. Overall AAD indicates that H_{vap} can be predicted reasonably well by the CG method. Noting its importance in phase change heat transfer and the availability of good GC estimation methods, H_{vap} was also selected as one of the properties where limits (constraints) could be applied with confidence in CAMD.

Table 2.3. Number of compounds used in the evaluation of H_{vap}.

	MG	CG	JR	WJ
Alkane	7	6	7	7
Alkene	3	3	3	3
Alkyne	9	9	9	9
Alcohol	10	9	10	10
Ether	9	9	9	9
Aromatic	8	8	8	8
Alicyclic	8	8	8	8
Aldehyde	8	8	8	8
Ketone	9	9	9	9
Ester	10	9	10	10
Amine	7	6	7	7
Amide	2	N/A	2	2
Carboxylic acid	4	7	5	4
F	9	9	9	9
Si	N/A	N/A	N/A	10
Total	103	100	104	113

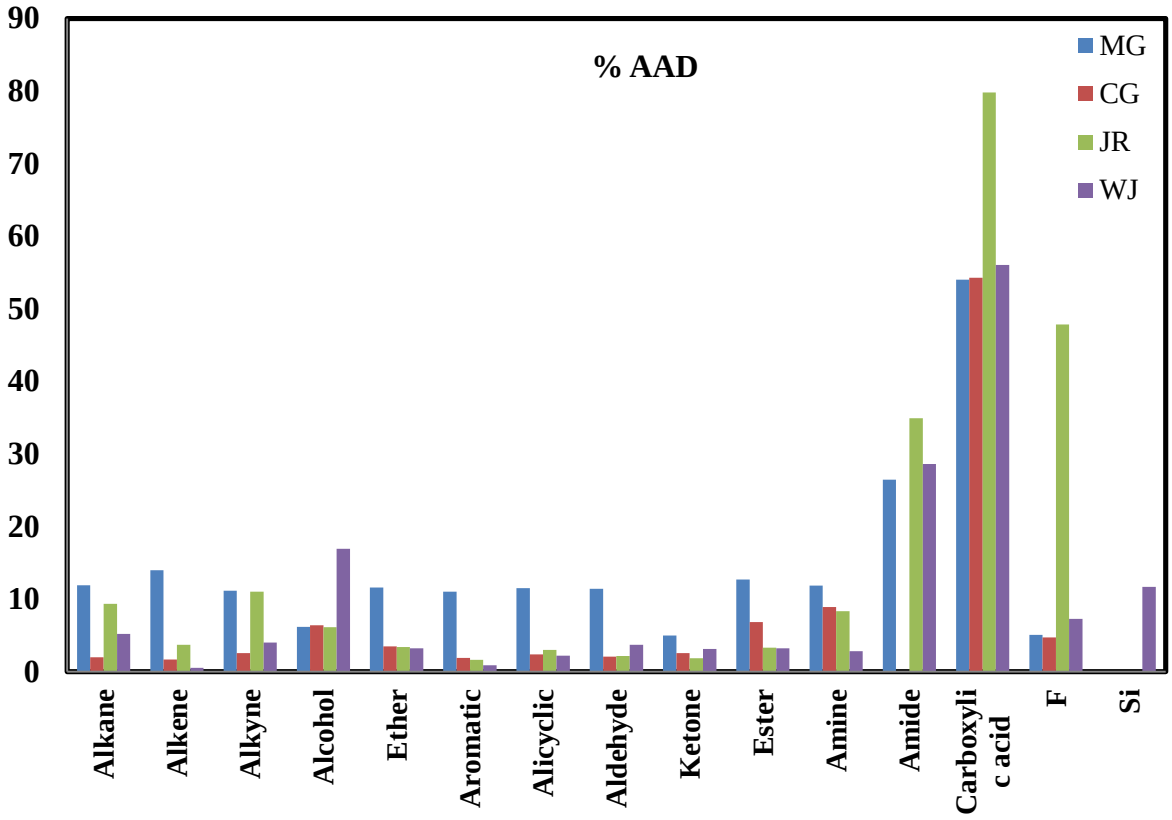

Figure 2.4. AADs for the MG, CG, JR, and WJ methods in the prediction of H_{vap}.

2.2.4 Surface Tension

Surface tension (σ) plays an important role in heat transfer as it determines the ability of the liquid to wet heated surfaces. The number of compounds and AADs are shown in Table 2.4 and Figure 2.4 respectively. Overall AAD (%) for MG, CG, JR, and WJ methods are 11.76, 11.69, 16.17, and 13.60 respectively. Very high AADs of over 50 % were observed for alcohols when σ was predicted using the CG, JR, and WJ methods. It was observed that with the exception of the MG method, all methods frequently over-predicted σ for alkanes, aldehydes, ketones, esters and amines, and under-predicted it for aromatic compounds. In addition, the MG, JR, and WJ methods were found to frequently under-predict σ for fluorinated compounds.

Table 2.4. Number of compounds used in the evaluation of σ.

	MG	CG	JR	WJ
Alkane	7	6	7	7
Alkene	3	3	3	3
Alkyne	9	3	9	9
Alcohol	10	9	10	10
Ether	9	9	9	9
Aromatic	8	8	8	8
Alicyclic	8	8	8	8
Aldehyde	8	8	8	8
Ketone	9	9	9	9
Ester	10	9	10	10
Amine	7	6	7	7
Amide	2	N/A	2	2
Carboxylic acid	10	9	10	10
F	8	2	9	8
Si	6	N/A	N/A	10
Total	114	89	109	118

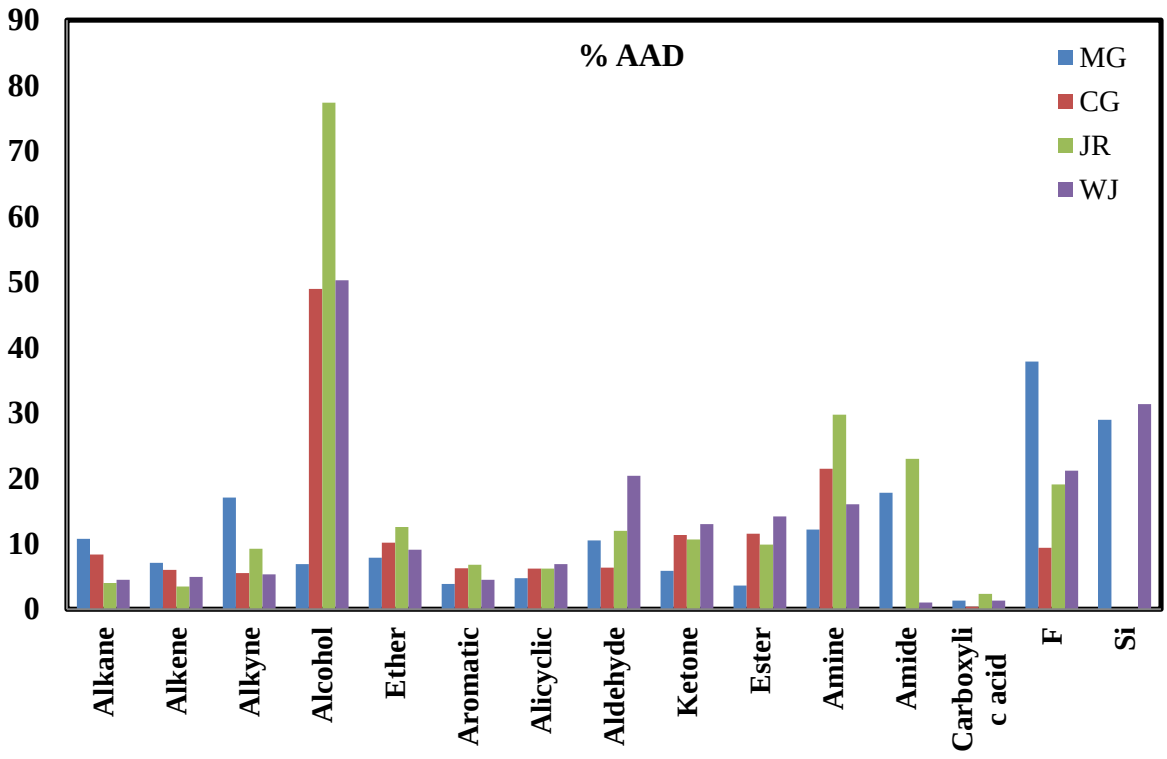

Figure 2.5. AADs for the MG, CG, JR, and W methods in the prediction of σ.

2.2.5 Liquid Density

The liquid density (ρ) does not influence heat transfer as significantly as the enthalpy of vaporization or thermal conductivity, but it is an important property in the determination of requirements and transportation of fluids. The liquid density also appears in heat transfer correlations. The number of compounds used in the evaluation of ρ and the AADs are shown in Table 2.5 and Figure 2.5 respectively. Overall AAD (%) for MG, CG, JR, and WJ methods are 9.53, 7.37, 8.20, and 8.34 respectively. All four methods frequently over-predicted ρ for ethers. In addition, CG, JR, and WJ methods were also observed to frequently over-predict ρ for alcohols, aldehydes, and amines.

Table 2.5. Number of compounds used in the evaluation of ρ.

	MG	CG	JR	WJ
Alkane	7	6	7	7
Alkene	3	3	3	3
Alkyne	9	6	9	9
Alcohol	10	9	10	10
Ether	9	9	9	9
Aromatic	8	6	8	8
Alicyclic	8	8	8	8
Aldehyde	8	8	8	8
Ketone	9	9	9	9
Ester	10	7	10	10
Amine	7	6	7	7
Amide	2	N/A	3	3
Carboxylic acid	4	7	6	4
F	8	3	9	8
Si	N/A	N/A	N/A	10
Total	102	87	106	113

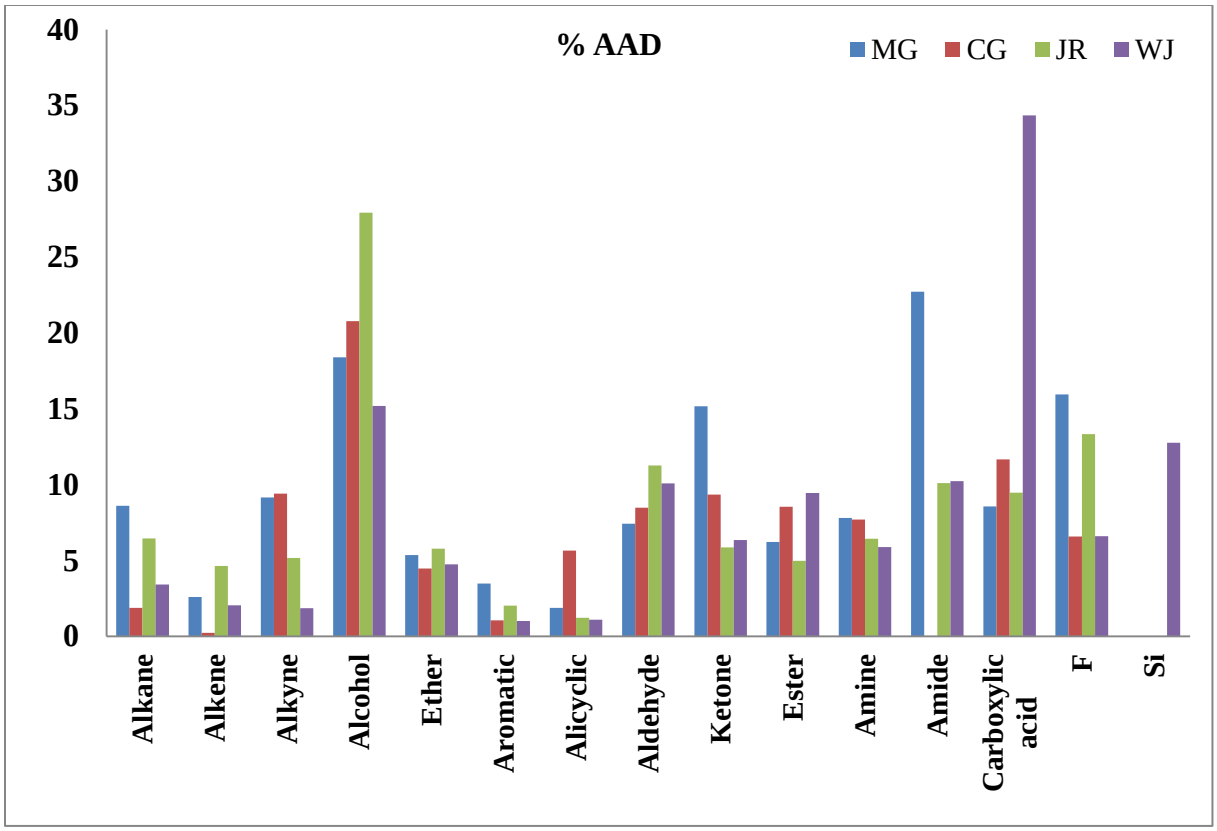

Figure 2.6. AADs for the MG, CG, JR, and W methods in the prediction of ρ.

2.2.6 Liquid Viscosity

The liquid viscosity (η) significantly affects heat transfer as well as liquid pumping and transportation. The number of compounds and AADs are shown in Table 2.6 and Figure 2.6 respectively. The WJ method is not available for viscosity and is therefore not shown in Table 2.6 and Figure 2.6. Overall AAD (%) for MG, CG, and JR methods are 23.38, 16.45, and 24.79 respectively. The MG method was observed to frequently under-predict η for alkynes, alcohols, ketones, esters, and fluorinated compounds. Among fluorinated compounds, very high deviations (~ 80 %) were observed for perflourinated molecules. It should also be noted here that there are no

methods available for estimating liquid viscosity for organosilicon compounds. Due to lack of reliable methods, it was decided not to use viscosity as a constraint in CAMD calculations.

Table 2.6. Number of compounds used in the evaluation of η.

	MG	CG	JR
Alkane	7	7	7
Alkene	3	3	3
Alkyne	6	N/A	N/A
Alcohol	10	10	10
Ether	9	9	9
Aromatic	8	8	8
Alicyclic	8	7	7
Aldehyde	8	8	8
Ketone	9	9	8
Ester	9	9	10
Amine	7	N/A	N/A
Amide	2	N/A	N/A
Carboxylic acid	7	7	6
F	8	N/A	N/A
Si	N/A	N/A	N/A
Total	101	77	76

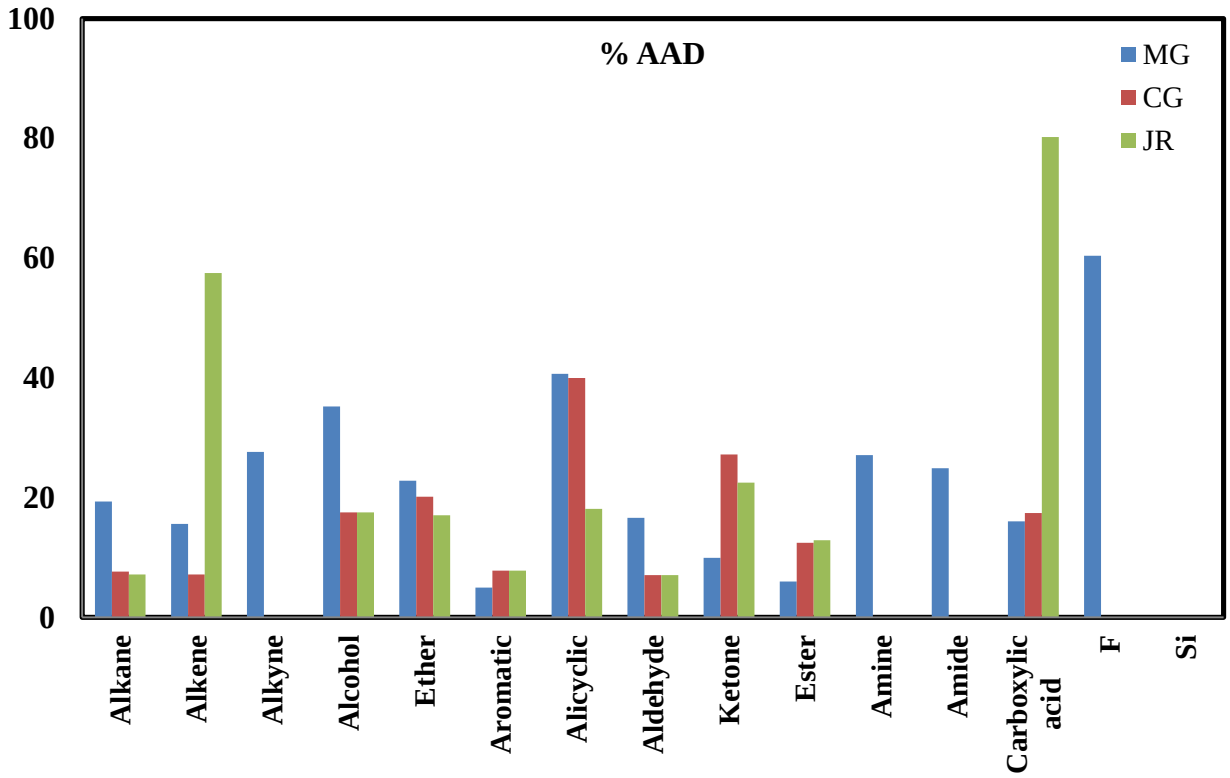

Figure 2.7. AADs for the MG, CG, and JR methods in the prediction of η.

2.2.7 Liquid Thermal Conductivity

The liquid thermal conductivity (k) plays an important role in heat transfer and hence is of significant importance in this work. The performance of the four GC methods in predicting thermal conductivity is shown in Figure 2.7. Table 2.7 lists the number of compounds and the functional group used in the evaluation of k. Overall AAD (%) of 9.14, 7.65, 9.45, and 9.73 for the MG, CG, JR, and WJ methods respectively indicate that k can be estimated reasonably well using these methods. Frequent over-prediction, however, was observed for all four methods for aromatic, alicyclic, amines, and fluorinated compounds. Given its importance in heat transfer and the availability of reliable estimation methods, k was selected as one of the properties where constraints could be applied in CAMD.

Table 2.7. Number of compounds used for the evaluation of *k*.

	MG	CG	JR	WJ
Alkane	7	6	7	7
Alkene	3	3	3	3
Alkyne	9	9	9	9
Alcohol	10	9	10	10
Ether	10	9	10	10
Aromatic	8	8	8	8
Alicyclic	8	8	8	8
Aldehyde	8	8	8	8
Ketone	9	9	9	9
Ester	10	10	10	10
Amine	7	7	7	7
Amide	2	N/A	2	2
Carboxylic acid	4	7	6	4
F	8	9	9	8
Si	N/A	N/A	N/A	10
Total	103	102	106	113

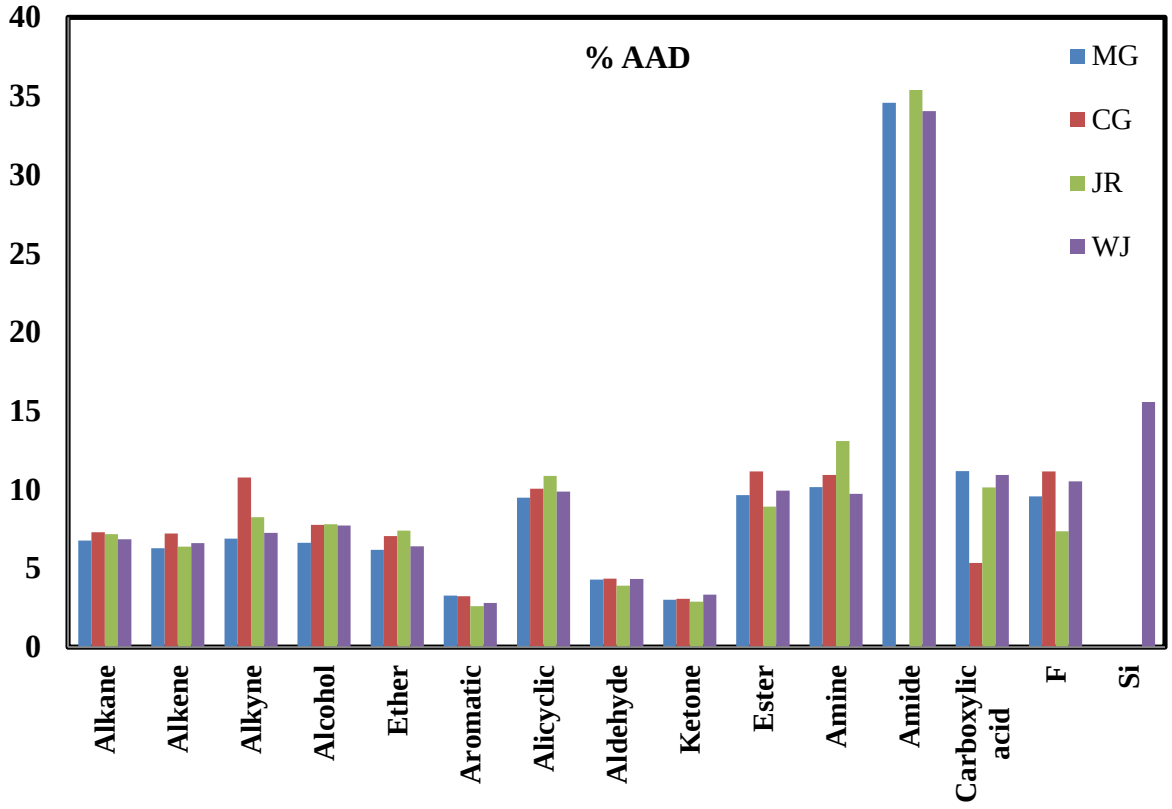

Figure 2.8. AADs for the MG, CG, JR, and W methods in the prediction of *k*.

2.2.8 Liquid Specific Heat

Liquid specific heat (C_p) is also an important heat transfer property as it determines the thermal mass of the fluid. The number of compounds and AADs are shown in Table 2.8 and Figure 2.8 respectively. Group contributions for C_p were not available in the MG, CG, and WJ methods and hence only the JR method was evaluated in this work. Overall AAD for the JR method was 6.19 %. The JR method was, however, found to frequently over-predict C_p for alkanes, alcohols, aldehydes, and carboxylic acids.

Table 2.8. Number of compounds used for the evaluation of C_p.

	JR
Alkane	7
Alkene	3
Alkyne	9
Alcohol	10
Ether	9
Aromatic	8
Alicyclic	8
Aldehyde	8
Ketone	9
Ester	10
Amine	7
Amide	2
Carboxylic acid	6
F	9
Si	N/A
Total	105

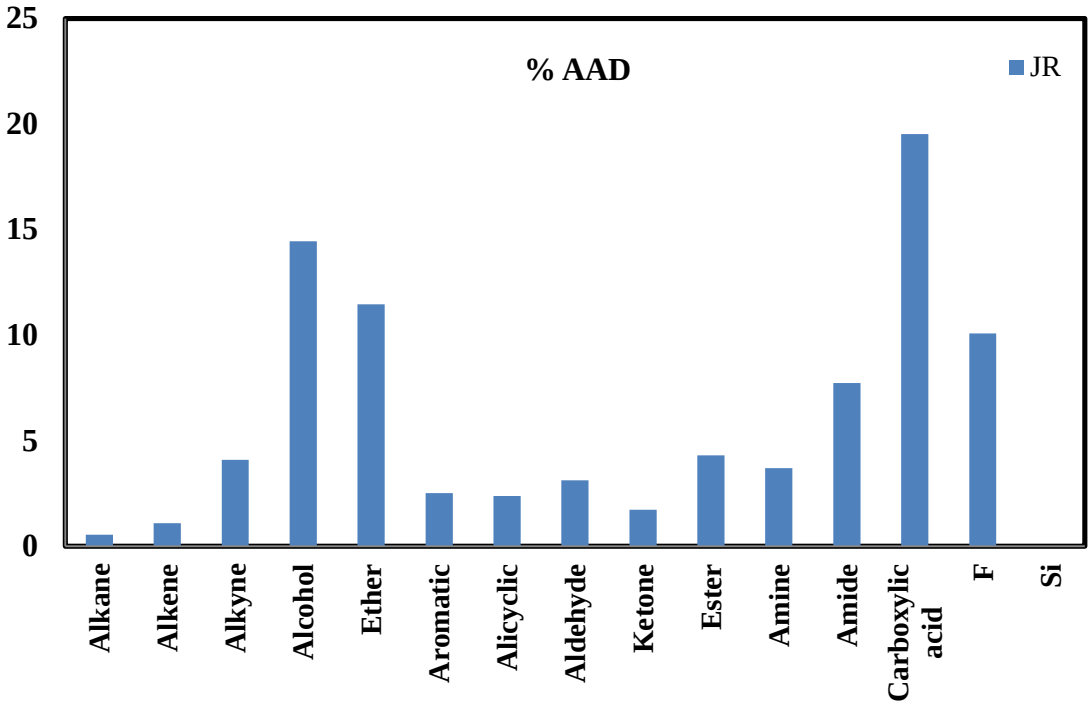

Figure 2.9. AADs for the JR method in the prediction of C_p.

2.2.9 Summary

Based on the results presented in the previous section, it can be concluded that the four GC methods are able to predict most properties of interest in heat transfer with AADs of about 10 % (except viscosity and surface tension). [43] Overall AADs of the four methods are listed in Table 2.9. Based on heat transfer considerations and the results presented in Table 2.9, it was decided to constrain T_b, H_{vap}, and k in the CAMD calculations. As mentioned earlier, organosilicon fluids are an important class of heat transfer fluids due to their low viscosity and wide liquid range (-100 to 250 °C) [38]. Since none of these methods are reliable for organosilicon compounds, it was decided to develop new GC values for thermophysical properties of such compounds.

Table 2.9. Overall AADs (%) for four GC methods.

	MG	CG	JR	WJ
T_m	12.55	9.36	13.37	N/A
T_b	3.91	2.23	5.18	4.27
H_{vap}	14.56	7.67	15.46	9.96
σ	11.76	11.69	16.17	13.60
ρ	9.53	7.37	8.20	8.34
η	23.38	16.45	24.79	N/A
k	9.14	7.65	9.45	9.73
C_p	N/A	N/A	6.19	N/A

2.3 Group Contribution Method for Organosilicon Compounds

The database for organosilicon compounds was expanded to 44 compounds (all liquid at room temperature) by using data from the DIPPR database. The GC methods were evaluated again for the expanded database. The AADs with the expanded database are listed in Table 2.10. [44]

Table 2.10. Evaluation of GC methods for organosilicon compounds.

Property	% AAD	
	MG	WJ
Melting point, T_m	32.16	-
Boiling point, T_b	7.75	-
Critical temperature, T_c	-	6.66
Heat of vaporization, H_{vap}	-	32.44
Surface tension, σ	26.86	76.67
Liquid density, ρ	-	57.56
Thermal conductivity, k	-	16.97
Liquid viscosity, η	-	-
Specific heat, C_p	-	-

New GC values were computed using the expanded database of 44 compounds compiled from the DIPPR database using the same property function as used by Marrero and Gani [37]. Viscosity and surface tension functions were obtained from Conte *et al.* [45] who extended the work of Marrero and Gani [37] and developed GC methods for viscosity and surface tension. Contributions for acentric factor (ω) were computed using the function described by Constantinou *et al.* [46]. Kolska *et al.* [47] recently proposed a GC method for liquid specific heat (C_p) that employs 3 contributions for each group compared to 4 in the JR method [34]. Their method was developed using a larger dataset compared to the JR method and reported an average absolute deviation of 2.5 %. Therefore, contribution values for C_p were obtained using the function used by Kolska *et al*. Only first order groups were used for computing contributions of silicon containing groups. Hence, second and third order groups are not included in equations 2.24 - 2.33.

$$T_m / K = 147.45 \ln\left(\sum_i n_i C_i\right) \tag{2.24}$$

$$T_b / K = 222.543 \ln\left(\sum_i n_i C_i\right) \tag{2.25}$$

$$T_c / K = 231.239 \ln\left(\sum_i n_i C_i\right) \tag{2.26}$$

$$P_c / bar = 5.9827 + \frac{1}{\left(0.108998 + \sum n_i C_i\right)^2} \tag{2.27}$$

$$V_c / cc.mol^{-1} = 7.95 + \left(\sum_i n_i C_i\right) \tag{2.28}$$

$$H_{vap} / kJ.mol^{-1} = 11.733 + \left(\sum_i n_i C_i\right) \tag{2.29}$$

$$\sigma / dynes.cm^{-1} = 19.50525 + \left(\sum_i n_i C_i \right) \tag{2.30}$$

$$\eta / cP = \left(\sum_i n_i C_i \right) \tag{2.31}$$

$$\omega = 0.4085 \left[\ln \left(1.1507 + \sum n_i C_i \right) \right]^{1.9802} \tag{2.32}$$

$$C_p / J.mol^{-1}.K^{-1} = C_{p0} + \sum n_i . C_{pi}$$

(2.33) where, $C_{p0} = 105.94 - 51.94(T/100) + 7.24(T/100)^2$, $C_{pi} = a_i + b_i(T/100) + d_i(T/100)^2$, and a_i, b_i and d_i are contributions of group *i*.

Four new groups were defined for organosilicon compounds: Si, SiH, SiO, and cSiO. The cSiO group represents a SiO group in a cyclic molecule (e.g. octamethylcyclotetrasiloxane has 4 cSiO groups). New group contributions listed in Tables 2.11 were obtained by minimizing average absolute deviations between predicted and DIPPR data using a nonlinear generalized reduced gradient (GRG) solver available with Microsoft Excel. Since the GRG algorithm is likely to find local minima, many initial guesses were tested and the lowest minimum selected. Few other solvers including BARON, LINDOGlobal, and CONOPT available with the General Algebraic Modeling System (GAMS) [48] were also tested. The final solution apparently was not very sensitive to the choice of solver. In addition, contributions of chlorine group (Cl) were also regressed in this work because chlorinated groups defined in Marrero and Gani, Conte *et al.*, Constantinou *et al.* and Kolska *et al*. methods (CH_2Cl, CHCl, CCl, CCl_2, CCl_3) could not be employed in organosilicon compounds as chlorine was attached to

silicon. It was also not practical to define groups such as $SiCl_3$, $SiCl_2$, SiCl, SiHCl due to the limited dataset employed.

Table 2.11. Contributions for silicon containing groups.

Property	Cl	Si	SiH	SiO	cSiO
T_m	0.58261	1.02940	0.43138	-1.27926	-0.40086
T_b	1.09798	1.06775	0.45566	-0.26568	0.05282
T_c	2.31735	1.68949	0.65113	-1.73192	-0.59137
P_c	0.01179	0.02297	0.02061	0.05881	0.02781
V_c	58.35094	95.99811	88.14295	142.11336	104.91564
ω	0.29882	-0.02812	-0.16545	-0.22183	-0.13728
σ	8.92519	-28.88397	-35.29652	-15.74079	-16.14952
H_{vap}	2.22051	10.83634	11.91660	8.59807	8.44296
η	-0.98087	3.31704	4.43649	2.46009	2.81571
C_p - a	40.05049	4.73322	4.47380	4.66013	4.85476
C_p - b	-5.33975	4.20501	3.43194	3.98718	4.56718
C_p - d	0.39714	2.63092	0.32717	1.98178	3.71019

It was observed that average absolute deviations were very high for viscosities of fluids containing OCH_3 and OCH_2 groups. Therefore, contributions of these groups were also regressed and updated from -0.6902 for OCH_3 and 0.6134 for OCH_2 to -0.96427 and 0.00853 respectively. While former values are applicable to all other classes of fluids, latter values should be used for estimating viscosity of organosilicon compounds. In addition, temperature dependent properties (H_{vap}, σ, ρ, k, η, and C_p) were all computed at 298 K and hence the new group contributions are applicable only at 298 K.

The reliability of the method was assessed by comparing *J* values calculated by regressing data sets with random subsets of N data points removed from each set, as suggested by Marrero and Gani [37]. The residual *(J)* is calculated using:

$$J = \sum \frac{\left| X_i - Y_i \right| / X_i}{N} \times 100 \tag{2.34}$$

where X_i and Y_i are the property values of compound *i* estimated using full and partial data sets. Table 2.12 shows that the new group contributions yield significantly lower AADs than existing methods (Table 2.10). In addition, *J* values are comparable with the AAD for most properties indicating that the GCs obtained are reliable. AADs were relatively high for melting point and viscosity. Therefore, the GCs developed in this work must be used judiciously for these properties.

Table 2.12. AADs from DIPPR data using new GCs for silicon containing fluids.

	% AAD	*J*
T_m	21.41	0.51
T_b	3.89	0.14
T_c	3.99	1.02
P_c	7.99	0.57
V_c	3.93	0.38
ω	13.71	6.53
σ	13.41	1.16
H_{vap}	9.15	1.32
η	25.37	0.02
C_p	9.54	0.01

2.4 Conclusions

Property data for a wide variety of organic compounds was compiled from the DIPPR database and used to evaluate estimation capabilities of the Marrerro-Gani, Constantinou-Gani, Joback-Reid, and Wilson-Jaspersen methods. These four methods were critically evaluated and found to provide reasonable estimates of many thermophysical properties of interest in heat transfer applications. AADs of about 10 % were obtained for most properties, with the exception of surface tension and viscosity. As none of these methods were found to be reliable for compounds containing silicon, new group contributions were developed for organosilicon compounds. Heat transfer considerations and availability of reliable estimation methods led to selection of three properties - T_b, H_{vap}, and k - where limits could be applied with confidence in CAMD calculations.

2.5 References

1. Kontogeorgis, G. M. and Gani R. (eds.), *Computer aided property estimation for process and product design*, Computer-Aided Chemical Engineering, Volume 19. 2004. Amsterdam, The Netherlands: Elsevier.

2. Joback, K. G., *Designing molecules possessing desired physical properties*, PhD Thesis, 1989. Massachusetts Institute of Technology, Cambridge, Massachusetts.

3. Gani, R. and O' Connell, *Properties and CAPE: from present uses to future challenges*, Computers and Chemical Engineering, 2000. **25**(1): p. 3-14.

4. Chemical Abstracts Service, http://www.cas.org/newsevents/releases/research120810.html

5. Dortmund Data Bank, http://www.ddbst.com/en/products/DDB-00-Basic-Data.php

6. Solomons, T. W. G. and Fryhle, C. B., *Organic Chemistry*, 7th edition, 2000. New York: John Wiley & Sons, Inc.

7. Fredenslund, A., Jones, R. L., and Prausnitz, J. M., *Group-contribution estimation of activity coefficients in nonideal liquid mixtures*, AIChE Journal, 1975. **21**(6): p. 1086-1099.

8. Rowley, R. L., Wilding, W. V., Oscarson, J. L., Yang, Y., and Giles, N. F., *DIPPR® Data Compilation of Pure Chemical Properties*, 2010. Design Institute for Physical Properties, http://dippr.byu.edu, Brigham Young University, Provo, Utah.

9. Joback, K. G., *A unified approach to physical property estimation using multivariate statistical techniques*, MS Thesis, 1984, Massachusetts Institute of Technology, Cambridge, Massachusetts.

10. Wu, H. S. and Sandler, S. I., *Use of ab initio quantum mechanics calculations in group contribution methods. 1. Theory and the basis for group identifications*, Industrial and Engineering Chemistry Research, 1991. **30**: p. 881-889.

11. Wu, H. S. and Sandler, S. I., *Use of ab initio quantum mechanics calculations in group contribution methods. 1. Test of new groups in UNIFAC*, Industrial and Engineering Chemistry Research, 1991. **30**: p. 889-897.

12. Bader, R. F. W., *Atoms in Molecules: A Quantum Theory*, 1990. Oxford: Oxford University Press.

13. Bader, R. F. W. and Bayles, D., *Properties of atoms in molecules: group additivity*, Journal of Physical Chemistry A, 2000. **104**: p. 5579-5589.

14. Cortes-Guzman, F. and Bader, R. F. W., *Role of functional groups in linear regression analysis of molecular properties*, Journal of Physical Organic Chemistry, 2004. **17**: p. 95-99.

15. Cortes-Guzman, F. and Bader, R. F. W., *Transferability of group energies and satisfaction of the virial theorem*, Chemical Physics Letters, 2003. **379**: p. 183-192.

16. Matta, C. F. and Bader, R. F. W., *An experimentalist's reply to "what is an atom in a molecule"*, Journal of Physical Chemistry: A, 2006. 110: p. 6365-6371.

17. Glasstone, S., *Textbook of Physical Chemistry*, 2nd edition 1946. Van Nostrand: New York.

18. Le Fevre, R. J. W. in Gold, V., (ed.), *Advances in Physical Organic Chemistry*, Vol. 3. 1965. New York: Academic Press.

19. Pascal, P., *Magnochemical studies*, Annales De Chimie Et De Physique, 1910. **19**: p. 5-70.

20. Pascal, P., *The diamagnetic properties of elements following a periodic law*, Comptes Rendus Hebdomadaires Des Séances De l'Académie Des Sciences, 1914. **158**: p. 1895 -1897.

21. Sugden, S., *The variation of surface tension with temperature and some related functions*, Journal of the Chemical Society, 1924. **125**: p. 32-41.

22. Souders, M., Matthews, C. S., and Hurd, C. O., *Relationship of thermodynamic properties to molecular structure. Heat capacities and heat contents of hydrocarbon vapors*, Industrial and Engineering Chemistry, 1949. **41**(5): p.1037-1048.

23. Bremner, J. G. M. and Thomas, G. D., *The standard free energies of formation of gaseous organic compounds - a group method of summation*, Transactions of the Faraday Society, 1947. **44**(4): p. 230-238.

24. Bensen, S. W. and Buss, J. H., *Additivity rules for the estimation of molecular properties. Thermodynamic properties*, Journal of Chemical Physics, 1958, **29**(3): p. 546-572.

25. Ronc, M. and Ratcliff, G. A., *Prediction of excess free energies of liquid mixtures by an analytic group solution model*, Canadian Journal of Chemical Engineering, 1971. **49**(6): p. 825-830.

26. Poling, B. E., Prausnitz, J. M., and O'Connell, J. P., *The Properties of Gases and Liquids*, 5th edition 2004. New York: McGraw-Hill.

27. Riedel L., *Estimation of unknown critical pressures of organic compounds*. Z. Elektrochemistry, 1949. **53**: p. 222-228.

28. Lydersen A. L., *Estimation of critical properties of organic compounds*, University of Wisconsin College of Engineering, Engineering Experimental Station, 1955. Report 3.

29. Guldberg C. M., *About the law of molecular volumes and boiling points*, Journal of Physical Chemistry, 1890, **5**: p. 374.

30. Ambrose D., *Correlation and estimation of vapor-liquid critical properties. I. Critical temperatures of organic compounds*, National Physical Laboratory, 1978, NPL Report. Chem, 92.

31. Ambrose D., *Correlation and estimation of vapor-liquid critical properties. II. Critical pressures and volumes of organic compounds*, National Physical Laboratory, 1979, NPL Report. Chem, 98.

32. Daubert T. E., State-of-the-art-property predictions, Hydrocarbon Processing, 1980. P. 107-112.

33. Fedors R. F., *A relationship between chemical structure and the critical properties*, Chemical Engineering Communications, 1982. **16**: p. 149-151.

34. Joback, K. G. and Reid, R. C., *Estimation of pure component properties from group contributions*, Chemical Engineering Communications, 1987. **57**(16): p. 233-243.

35. Constantinou, L. and Gani, R., *New group contribution method for estimating properties of pure compound*s, AIChE Journal, 1994. **40**(10): p. 1697-1710.

36. Wilson, G. M. and Jasperson. L. V., *Critical constants T_c, P_c, estimation based on zero, first and second order methods*, AIChE Spring Meeting, 1996. New Orleans, LA.

37. Marrero, J. and Gani, R., *Group-contribution based estimation of pure component properties*, Fluid Phase Equilibria, 2001. **183-184**(1): p. 183-208.

38. Organosilicon heat transfer fluid, Syltherm, http://www.dow.com/heattrans/products/synthetic/syltherm.htm

39. Computer Aided Process Engineering Center, *Integrated Computer Aided System*, Department of Chemical and Biochemical Engineering, Technical University of Denmark. http://www.capec.kt.dtu.dk/Software/ICAS-and-its-Tools/ (accessed April 2012).

40. Molecular Knowledge Systems, Inc., *Cranium*, http://www.molknow.com/Cranium/cranium.htm (accessed April 2012).

41. Mavrovouniotis, M. L., *Estimation of properties from conjugate forms of molecular structures: the ABC approach*, Industrial and Engineering Chemistry Research, 1990. **29**(9): p. 1943-1953.

42. Rowley, R. L., Wilding, W. V., Oscarson, J. L., Yang, Y., and Giles, N. F., DIPPR® Data Compilation of Pure Chemical Properties, 2010. Design Institute for Physical Properties, http://dippr.byu.edu, Brigham Young University, Provo, Utah.

43. Warrier, P., Sathyanarayana, A., Patil, D. V., France, S., Joshi, Y., and Teja, A. S., *Novel heat transfer fluids for direct immersion phase change cooling of electronic systems*, International Journal of Heat and Mass Transfer, 2012. **55**: p. 3379–3385.

44. Warrier, P., Sathyanarayana, A., Bazdar, S., Joshi, Y., and Teja, A. S., *Selection and evaluation of organosilicon coolants for direct immersion cooling of electronic systems*, Industrial and Engineering Chemistry Research, 2012. (Submitted).

45. Conte, E., Martinho, A., Matos, H. A., and Gani, R., *Combined group-contribution and atom connectivity index-based methods for estimation of surface tension and viscosity*, Industrial and Engineering Chemistry Research, 2008. **47**: p. 7940-7954.

46. Constantinou, L., Gani, R., and O'Connell, J. P., *Estimation of the acentric factor and the liquid molar volume at 298 K using a new group contribution method*, Fluid Phase Equilibria, 1995. **103**: p. 11-22.

47. Kolska, Z., Kukal, J., Zabransky, M., and Ruzicka, V., *Estimation of the heat capacity of organic liquids as a function of temperature by a three-level group contribution method*, Industrial and Engineering Chemistry Research, 2008. **47**: p. 2075-2085.

48. General Algebraic Modeling System, http://www.gams.com/

CHAPTER 3

DESIGN AND SCREENING OF HEAT TRANSFER FLUIDS

This chapter deals with the application of computer-aided molecular design (CAMD) to identify new heat transfer fluids for direct immersion cooling of electronic systems. New heat transfer fluids were identified using the Integrated Computer Aided Systems (ICAS) software developed by the Computer Aided Process-Product Engineering Center (CAPEC) of the Technical University of Denmark. As organosilicon compounds could not be generated using ICAS, a new CAMD code was also developed in this work for such fluids. The compounds identified using CAMD were screened using a figure of merit (FOM) analysis. Compounds with FOMs greater than those of existing coolant HFE 7200 were selected for further (experimental) evaluation.

3.1 Computer-Aided Molecular Design

Four principle steps are involved in any product design process [1, 2]:

1. Define needs
2. Generate ideas
3. Select most promising ideas
4. Manufacture product

The first step may be considered to be a pre-design or problem formulation step, whereas the last step is a process design step. The second and third steps considered together

represent the CAMD approach and can be restated as follows [2]: "*Given a set of building blocks and a set of target properties, identify a molecule that matches these properties.*" CAMD is thus the reverse of property prediction, where the molecular structure is given and a set of target properties is calculated.

CAMD has shown promise in identifying molecules for specific applications including molecules that would not otherwise be considered if ad hoc approaches are used. [3, 4] Briefly, the CAMD approach involves molecule generation by combining functional groups (or atoms), and the screening of these molecules using structural and thermophysical property constraints. The CAMD approach was first demonstrated in 1983 by Gani and Brignole [5] for the selection of solvents for a separation process using UNIFAC groups. Using 14 groups and constraints of $T_b > 373$ K and MW < 140 they were able to identify 84 promising candidates that were selected based on their solvent power i.e. ratio of infinite dilution activity coefficient in the solvent of the two components to be separated. Their work was extended by Brignole *et al.* [6] by partitioning the molecule generation problem. They classified the groups into terminal groups (groups with one free bond such as -OH) and intermediate groups (more than 1 free bond such as $-CH_2-$). Molecules were generated in two steps in their work. In the first step only combinations of intermediate groups were considered and screened for molecular weight and structural feasibility. Screened intermediate structures were then combined with terminal groups to make the whole molecule. The number of possible combinations that must be evaluated was thus reduced considerably by this partitioning. The extensive development of GC methods since then has resulted in CAMD approach being evaluated for a variety of applications. Several CAMD methods have been

described in the literature, and their application in developing new drugs [7], novel materials [3], benign solvents [8], alternative refrigerants [9, 10], polymers [11, 12], and heat transfer fluids [13, 14] has been outlined. For example, Odele and Macchietto [8] employed mixed-integer non-linear programming (MINLP) for optimal solvent design with GC methods for predicting T_b, T_c, activity coefficients, vapor pressure and C_p. Similarly, Duvedi and Achenie [9] employed MINLP for designing environmentally benign refrigerants using a GC method for ozone depletion potential. A simulated annealing algorithm was presented by Markoulaki and Kokossis [13] for molecular design of solvents and heat transfer fluids. Many of these studies, however, have been concerned with the development of property estimation methods and/or molecular design algorithms. Only a few studies [15, 16] have investigated the performance of the candidates generated in practical situations. For example, Karunanithi *et al.* [15] used MINLP for CAMD of solvents for the crystallization process and experimentally verified the performance of one candidate in the crystallization of ibuprofen. 2-ethoxy ethyl acetate, solvent identified via CAMD, was found to give bigger crystals as well as the desired morphology. Similarly, Chen and Trout [16] observed that solvent identified via CAMD (toluene+diethylether) improved the crystal morphology in crystallization of 2,6-dihydroxybenzoic acid.

The fundamental objective of the CAMD approach is to identify a collection of compounds having specific desired properties. CAMD is used when validated mathematical models for the estimation of all desired properties are available. In this case, a list of candidate molecules can be quickly generated and tested against property constraints. For simpler problems i.e. those involving 10-15 distinct groups, a

combinatorial approach can be used. In this approach, all possible combinations of specified groups are evaluated and are screened for structural feasibility. For example, structural feasibility of saturated compounds can be tested by the following relation based on graph theory [17]:

$$b/2 = n + r - 1 \quad (3.1)$$

where, b is the total number of free bonds, n is the number of groups, and r is the number of rings in the structure. Table 3.1 illustrates the application of equation 3.1 for determining structural feasibility.

Table 3.1. Test for structural feasibility of saturated compounds.

Groups	n	b	r	Equation 3.1	Feasible
CH_2, CH_3	2	3	0	$3/2 \neq 2 + 0 - 1$	No
CH_2, CH	2	5	0	$5/2 \neq 2 + 0 - 1$	No
CH_3, CH_2, OH	3	4	0	$4/2 = 3 + 0 - 1$	Yes
6-CH_2	6	12	1	$12/2 = 6 + 1 - 1$	Yes

Once each collection of groups has been screened for structural feasibility, the groups must be connected together into complete molecular structures. In computational chemistry this procedure is called enumeration because all of the "group isomers" are enumerated. [18] The procedure forms all pairings of bonds, checks that each bond pair is connectable (i.e., that single bonds are paired with single bonds, double bonds with double bonds, etc.), and then checks for duplicated structures. Properties of the candidate molecules are then estimated using group contribution methods, and molecules which fail

to satisfy the property constraints are screened out. As the combinatorial algorithm generates all possible combinations of specified groups, this approach is susceptible to the problem of combinatorial explosion. For example, a CAMD problem involving 10 different groups with a maximum of 10 groups per molecule would generate over a billion group combinations. All of these must be subjected to structural feasibility and property constraints. The advantage of such "generate-and-test" approach is that it evaluates all possible group combinations and, therefore, guarantees finding of the best candidate. However, it cannot be applied for problems involving large number of groups. Optimization methods are, therefore, required for complex CAMD problems.

For complex cases, the molecular design problem can be modeled as a minimization of a single objective function subject to structural and property constraints and is given by [2]:

$$\min f(x,v,\theta) \tag{3.2}$$

$$\varphi_j(x,v,\theta) \leq 0, \qquad j = 1,\ldots.. m_1 \tag{3.3}$$

$$h_i(x,v,\theta) \leq 0, \qquad i = 1,\ldots.. m_2 \tag{3.4}$$

where v is the vector of binary variables that define the molecular structure, x is the vector of continuous variables such as pressure, temperature, and θ is the vector of parameters of property estimation methods. $f(x,v,\theta)$ is the objective function. The CAMD problem defined using equations 3.2 - 3.4 is a nonconvex MINLP. A number of optimization algorithms have been proposed for solving the CAMD problem. For example, Sinha *et al.* [19] and Ostrovsky *et al.* [20] presented a reduced order branch and

bound algorithm that decreases the number of branching variables by using branching functions. A simulated annealing algorithm was employed by Markoulaki and Kokossis [13], whereas a genetic algorithm based approach was proposed by Venkatasubramanian *et al.* [21] and Glen and Payne [22]. However, Patkar and Venkatasubramanian [23] report that such optimization based CAMD approaches cannot guarantee the finding of the target solution.

In order to avoid the problems associated with optimization based methods and combinatorial explosion, Harper *et al.* [24, 25] proposed a hybrid multi-level "generate-and-test" approach. They use the Brignole *et al.* [6] approach of partitioning the molecule generation problem and extended it to four levels. The first level employs a basic group set (UNIFAC groups) and generates all feasible molecular structures. The problem of combinatorial explosion is avoided by defining detailed rules regarding feasibility of intermediate and final molecular structures. The second level takes the results from first level and also evaluates new combinations by including second and third order groups defined by Marrero and Gani [26]. GC methods and corresponding state correlations are employed at both the first and second levels to screen the generated molecules. In level three, the group level molecular information is transformed to atom level information. This conversion allows the use of connectivity indices [27] based methods to be employed for property estimation. In the fourth level, the atomic representations from level three are further refined to three-dimensional representations. This conversion helps in creating further isomer variations (cis/trans, Z/E, anti/gauche, etc.) as well as enables the use of molecular modeling techniques. The four level hybrid CAMD approach can handle large number of groups without getting plagued by combinatorial explosion, and

employs property estimation at different size scales. Therefore, this approach, which has been integrated in ProCAMD module in the ICAS software, was employed in this work for design of new heat transfer fluids.

3.2 Constraints on Thermophysical Properties

Thermophysical properties important for direct immersion phase change cooling of electronic systems include:

- Thermal conductivity (k): A high value of thermal conductivity is essential for efficient heat transfer. Hence, k of new fluids must be greater than those of existing coolants.
- Viscosity (η): A low viscosity is desirable for minimizing pumping power.
- Normal boiling point (T_b): Based on the complementary metal oxide semiconductor technology, chip temperatures need to be maintained below 80 °C. As the focus of this work was on phase change heat transfer, the normal boiling point was constrained to be in the vicinity of 80 °C.
- Melting point (T_m): Melting points of new heat transfer fluids should be comparable with those of currently used coolants.
- Electrical resistivity (ρ_e): As the focus of this work is on direct contact cooling, the fluids have to be dielectric. Therefore, electrical resistivity of new fluids should be comparable with those of current coolants. However, due to lack of estimation methods for ρ_e, this property could not be used as a constraint in CAMD.

- Enthalpy of vaporization (H_{vap}): As the focus of this work is on phase change heat transfer, high enthalpy of vaporization is desired.
- Specific heat (C_p): Specific heat needs to be as high as practicable.

Some of these properties for Novec fluids [28] are listed in Table 3.2, and were used as the basis for developing property constraints.

Table 3.2. Thermophysical properties of some Novec fluids.

	HFE 7100 $C_4F_9OCH_3$	HFE 7200 $C_4F_9OC_2H_5$	HFE 7500 $C_7F_{15}OC_2H_5$
T_b (K)	334	349	401
T_m (K)	138	135	173
η (cP)	0.58	0.60	1.24
H_{vap} (kJ mol^{-1})	28.0	31.4	36.8
k (W m^{-1} K^{-1})	0.069	0.068	0.065
σ (dynes cm^{-1})	13.6	13.6	16.2
C_p (J mol^{-1} K^{-1})	296	322	467

It can be observed from Table 2.9 that among the properties listed above highest AADs are for η and σ. Therefore, constraints cannot be applied on these properties with confidence. Applying all property constraints in the initial design phase is also not practical because too few candidates will be selected in that case. Therefore, it was decided to apply constraints on T_b, H_{vap}, and k as follows [29]:

- $320 \text{ K} \leq T_b \leq 370 \text{ K}$
- $k \geq 0.09 \text{ W m}^{-1} \text{ K}^{-1}$
- $H_{vap} \geq 35 \text{ kJ mol}^{-1}$

3.3 Figure of Merit

The screening of candidates based on property constraints is effective, but can still lead to dozens of candidates for a specific application. Therefore, several FOMs for phase change heat transfer were used to provide additional screens. FOMs are often used to compare the performance of heat transfer equipment in various heat transfer regimes. A FOM represents the relationship among thermophysical properties of the fluid and these relationships are derived from existing heat transfer correlations by grouping all the fluid thermophysical property dependent terms. A higher value of FOM therefore corresponds to better heat transfer characteristics. As the focus of this work was on boiling heat transfer, pool [30] and flow [31, 32] boiling FOMs listed in Table 3.3 were used to screen candidates. Though there are many other heat transfer correlations available in literature such as those by Chen [33] and Klimenko [34], the FOMs mentioned in Table 3.3 provide a reasonable estimate of the heat transfer performance in the boiling regime [35-37]. Table 3.3 shows that the thermal conductivity, enthalpy of vaporization, and viscosity have significant effect on the three FOMs of interest in this work.

FOMs were computed for candidates with thermal conductivity, heat of vaporization, and boiling temperature within the set limits. Candidates with FOMs that were lower than those of existing coolants (allowing for errors in property estimation methods) were screened out. The cut-off values for FOMs were calculated using a 20 % change in viscosity and 10 % change in all other properties. The FOMs for HFE 7200 and

the cut-off values are presented in Table 3.4 [29]. The best fluids were chosen for further evaluation.

Table 3.3. Pool and flow boiling FOMs.

Pool boiling FOM (Rohsenow [30]) =	$\frac{10^3}{\left(\frac{H_{vap}}{C_p}\right)\left(\frac{C_p\eta}{k}\right)^{1.7}\left(\frac{1}{\eta H_{vap}}\sqrt{\frac{\sigma}{g(\rho_l-\rho_v)}}\right)^{0.33}}$
Flow boiling FOM (Lazarek and Black [31]) =	$\frac{10^3 \times k}{\eta^{0.857} H_{vap}{}^{0.714}}$
Flow boiling FOM (Tran [32]) =	$\frac{10^6 \times k}{(\eta H_{vap})^{0.62}}\left(\frac{\rho_v}{\rho_l}\right)^{0.607}$

Table 3.4. FOMs for HFE 7200, and FOM cut-off values for candidate heat transfer fluids.

FOM	HFE 7200	FOM cut-off
Lazarek and Black (L&B)	9.21	13.22
Tran	260.87	311.43
Rohsenow	7.20	13.72

3.4 CAMD - ICAS

The four-level hybrid CAMD approach of Harper and Gani [25] incorporated in the ProCAMD, ICAS software was used in this work to identify new heat transfer fluids.

3.4.1 Molecule Generation

Molecules were generated by combining the following functional groups: alcohol, ketone, ester, ether, and fluorine. Only single and double bonds between groups were allowed. In addition, the maximum number of groups in a molecule was restricted to 10, because boiling points of molecules containing more than 10 groups are likely to be too high. In addition, chlorine, carboxylic acid, aldehydes, phenol, amine, amide functional groups were excluded because of environmental and reactivity concerns. Results of the combinatorial algorithm and application of property constraints are presented in Table 3.5.

Table 3.5. Screened out statistics for CAMD - ICAS.

Constraint	Acyclic	Cyclic	Aromatic
$H_{vap} \geq 35$ kJ mol^{-1}	215 of 18267	285 of 18366	4 of 38470
320 K $\leq T_b \leq$ 370 K	17986 of 18052	17998 of 18081	38466 of 38466
$k \geq 0.09$ W m^{-1} K^{-1}	2 of 66	6 of 83	0 of 0
Selected candidates	64	77	0

A total of 18267 acyclic compounds were designed using the specified groups and groups per molecule constraints out of which 215 were rejected based on the enthalpy of vaporization constraint. Out of the remaining 18052 acyclic compounds, 17986 were rejected based on the boiling point constraint. The thermal conductivity constraint removed 2 of the remaining 66 compounds leaving a total of 64 acyclic compounds that satisfied all three specified property constraints. Similarly, 77 cyclic candidates were selected. However, none of the 38470 aromatic compounds could satisfy all three constraints. Thus, a total of 141 compounds were identified for FOM analysis.

3.4.2 FOM Screening

Properties required to obtain FOMs were calculated using group contribution methods available in the property prediction module (ProPred) in ICAS-11. In addition, the Cranium software, developed by Molecular Knowledge Systems, Inc. NH, was used for calculating vapor densities. Based on FOM analysis, 31 acyclic and 4 cyclic compounds were selected for further evaluation. These compounds are listed in Tables 3.6 and 3.7. [29]

Only 4 out of the selected 35 compounds are available commercially: 1,1,1-trifluorobutan-2-one (#20), methyl 3,3,3-trifluoropropanoate (#22), 4,4,4-trifluorobutan-2-one (#25), and 1-methoxybutane (#28). 1-Methoxybutane is highly flammable and was therefore eliminated from further consideration. Among the 35 newly identified fluids, four fluids were selected for further analysis:

- Commercially available: 1,1,1-trifluorobutan-2-one ($C_4H_5F_3O$) and 4,4,4-trifluorobutan-2-one ($C_4H_5F_3O$)
- For custom synthesis: 1,1,1-trifluoro-3-methylpentane ($C_6H_{11}F_3$) and 1,1,1-trifluoro-3-(2,2,2-trifluoroethoxy)propane ($C_5H_6F_6O$)

A surrogate for 1,1,1-trifluoro-3-(2,2,2-trifluoroethoxy)propane, bis(1,1,1-trifluroethyl)ether ($C_4H_4F_6O$), was also purchased as $C_4H_4F_6O$ was commercially available and its thermophysical properties are very close to those of $C_5H_6F_6O$. If heat transfer experiments with $C_4H_4F_6O$ show improvement over HFE 7200, it becomes highly likely that $C_5H_6F_6O$ will also have superior heat transfer properties.

Table 3.6. Acyclic compounds selected after FOM analysis.

Formula	Name	FOM		
		L & B	Tran	Rohsenow
$C_5H_6F_6$	1,1,1,4,4,4-hexafluoro-2-methylbutane	29.34	571.77	44.26
$C_6H_8F_6$	1,1,1-trifluoro-3-methyl-2-(trifluoromethyl)butane	29.22	621.78	42.03
$C_5H_6F_6$	1,1,1,5,5,5-hexafluoropentane	27.53	533.93	40.74
$C_6H_9F_3$	(E)-6,6,6-trifluorohex-2-ene	25.83	514.50	37.31
$C_6H_8F_6$	1,1,1,5,5,5-hexafluoro-3-methylpentane	26.24	565.44	36.01
$C_7H_{11}F_5$	2,2-difluoro-4-methyl-3-(trifluoromethyl)pentane	25.88	569.35	34.75
$C_6H_9F_5$	1,1,1,5,5-pentafluorohexane	24.45	494.68	33.56
$C_7H_{11}F_3$	4-methyl-3-(trifluoromethyl)pent-1-ene	24.20	522.44	31.67
$C_6H_9F_3$	(E)-1,1,1-trifluoro-3-methylpent-2-ene	22.28	465.67	30.03
$C_6H_9F_3$	6,6,6-trifluorohex-1-ene	22.46	461.31	29.55
$C_6H_{11}F_3$	**1,1,1-trifluoro-3-methylpentane**	**21.83**	**461.31**	**26.87**
$C_4H_7F_3O$	1,1,1-trifluoro-3-methoxypropane	20.33	371.17	26.40
$C_7H_{11}F_3$	(E)-5,5,5-trifluoro-4,4-dimethylpent-2-ene	21.13	481.22	26.04
$C_6H_8F_6$	1,1,1,4,4,4-hexafluoro-2,2-dimethylbutane	20.98	494.18	25.17
$C_6H_9F_3$	5,5,5-trifluoro-2-methylpent-1-ene	19.94	425.40	24.46
$C_6H_9F_5O$	2-(2,2-difluoropropoxy)-1,1,1-trifluoropropane	19.65	435.16	23.18
$C_5H_9F_3O$	1,1,1-trifluoro-3-methoxybutane	19.22	391.49	22.97
$C_5H_6F_6O$	**1,1,1-trifluoro-3-(2,2,2-trifluoroethoxy)propane**	**19.34**	**419.21**	**22.97**
$C_6H_{11}F_3$	1,1,1-trifluorohexane	19.45	417.06	22.63
$C_4H_5F_3O$	**1,1,1-trifluorobutan-2-one**	**16.70**	**328.77**	**22.45**
$C_7H_{11}F_5$	2,2-difluoro-3-methyl-3-(trifluoromethyl)pentane	18.80	455.17	21.21
$C_4H_5F_3O_2$	methyl 3,3,3-trifluoropropanoate	15.83	317.06	20.95
$C_7H_{14}F_2$	3,3-difluoroheptane	18.01	389.37	19.91
$C_7H_{11}F_3$	3-methyl-3-(trifluoromethyl)pent-1-ene	17.38	414.27	18.97
$C_4H_5F_3O$	**4,4,4-trifluorobutan-2-one**	**14.98**	**311.18**	**18.58**
$C_7H_{13}F_3$	1,1,1-trifluoro-2,3,3-trimethylbutane	16.98	406.64	18.08
$C_5H_9F_3O$	3-ethoxy-1,1,1-trifluoropropane	16.30	345.26	17.51
$C_5H_{12}O$	1-methoxybutane	15.86	300.50	16.82
$C_7H_{11}F3$	4,4,4-trifluoro-2,3,3-trimethylbut-1-ene	16.10	394.35	16.74
$C_7H_{13}F_3$	1,1,1-trifluoro-2,2-dimethylpentane	15.10	385.54	14.57
$C_7H_{13}F_3$	1,1,1-trifluoro-2,3-dimethylpentane	14.73	368.63	14.20

Table 3.7. Cyclic compounds selected after FOM analysis.

Formula	Name	FOM		
		L & B	Tran	Rohsenow
$C_8H_{13}F_3$	1,1,2,2-tetramethyl-3-(trifluoromethyl)cyclopropane	17.49	368.43	21.28
$C_7H_{11}F_3$	1,1,2-trimethyl-2-(trifluoromethyl)cyclopropane	15.68	366.73	17.47
C_7H_{12}	(E)-prop-1-en-1-ylcyclobutane	15.16	317.39	17.01
C_6H_9F	1-fluoro-1-methyl-3-methylenecyclobutane	15.10	329.63	13.71

3.5 CAMD for Organosilicon Compounds

As mentioned in Chapter 2, organosilicon fluids are an important class of heat transfer fluids due to their low viscosity and large liquid range. The ICAS software was not reliable for organosilicon compounds and therefore a new CAMD code was developed for such compounds. This code made use of the group contributions discussed in Section 2.3. The new CAMD code employs a combinatorial algorithm (implemented in MATLAB) that generates all possible combinations of specified groups subject to a maximum number of groups per molecule. Unlike the 4 level CAMD approach used in ICAS [25], all possible combinations of specified groups were tested at a single level. Therefore, the new method is susceptible to the problem of combinatorial explosion. Nevertheless, all combinations of groups that satisfy all property constraints were checked for structural feasibility using equation 3.1. Properties of the structurally feasible candidates were then estimated using group contributions developed in this work.

3.5.1 Molecule Generation

Molecules were generated by combining the following groups: CH_3, CH_2, OCH_3, OCH_2, COO, OH, SiH, Si, and SiO. In order to avoid the problem of combinatorial explosion, the number of groups per molecule was restricted to 4 or 5. This was based on the assumption that the boiling point of molecules containing more than 5 or less than 4 groups is likely to be outside the desired range. Overall 7 compounds with 4 groups per molecule and 30 compounds with 5 groups per molecule satisfied both property constraints. Thus a total of 37 compounds were identified for FOM screening.

3.5.2 FOM Screening

Ten compounds with FOMs greater than those of HFE 7200 were identified after FOM screening. Newly identified organosilicon compounds and their calculated FOMs are listed in Table 3.8 [38]. Two of these candidates - dimethoxydimethylsilane and ethyldimethylsilane - were selected for further evaluation because they were commercially available.

Table 3.8. Organosilicon compounds selected after FOM analysis.

Formula	Name	L & B	Tran	Rohsenow
$C_4H_{12}OSi$	ethoxydimethylsilane	18.81	381.05	22.86
$C_3H_{10}OSi$	methoxydimethylsilane	16.15	316.92	18.21
$C_4H_{12}OSi$	ethoxy(methoxy)(methyl)silane	15.44	334.91	17.12
$C_4H_{12}Si$	tetramethylsilane	15.04	325.29	15.65
$C_3H_{10}O_2Si$	dimethoxy(methyl)silane	13.75	302.52	14.50
$C_4H_{12}OSi$	methoxytrimethylsilane	13.13	298.50	13.08
$C_4H_{12}O_3Si$	ethoxydimethoxysilane	13.02	299.99	13.28
$C_3H_{10}O_3Si$	trimethoxysilane	11.86	261.22	11.69
$C_4H_{12}Si$	**ethyldimethylsilane**	**11.58**	**242.75**	**10.87**
$C_4H_{12}O_2Si$	**dimethoxydimethylsilane**	**11.48**	**274.83**	**10.83**

3.6 Computer-Aided Mixture Design

The focus of this exercise was to improve the pool boiling heat transfer properties of HFE 7200 by the addition of a second component that would enhance its thermophysical properties. ProCAMD, ICAS was utilized for design of additives that are miscible with HFE 7200 and would enhance its heat transfer properties.

3.6.1 Molecule Generation

The software was used to generate acyclic compounds with alcohol and ether functional groups as these groups were expected to be miscible with HFE 7200. The groups were: CH_3, CH_2, CH, OH, and OCH_2. In addition, the maximum number of groups in a molecule was limited to 10, with one group being either OH or OCH_2. A total of 46 compounds were generated out of which 7 candidates satisfied all constraints. These compounds are listed in Table 3.9 [14].

Table 3.9. Compounds generated using CAMD mixture design.

Name	H_{vap} (kJ mol^{-1})	T_b (K)	k (W m^{-1} K^{-1})
Ethanol	40.12	330.01	0.1719
Isopropanol	42.65	347.70	0.1535
Propanol	44.77	364.44	0.1645
2-Butanol	45.61	365.52	0.1502
1-Ethoxybutane	**36.49**	**371.91**	**0.1312**
1-Propoxypropane	36.49	371.91	0.1312
1-Isopropoxy-3-methylbutane	36.90	371.46	0.1237

1-Ethoxybutane ($C_4H_9OC_2H_5$) was selected as the candidate for designing mixture formulations with HFE 7200 because of its structural similarity with HFE 7200. In

addition, thermophysical properties of ethoxybutane were also found to be superior to those of HFE 7200.

To compare the CAMD mixture design approach with ad hoc experimental approach, methanol was also chosen as an additive for HFE 7200. Methanol is often used as an additive in heat transfer fluids [39] and it has been shown to be miscible with HFE 7200 [40]. Moreover, methanol has a high thermal conductivity, low viscosity, high heat of vaporization, and a low boiling point. Therefore, the addition of methanol to HFE 7200 was expected to lead to enhanced heat transfer performance. On the other hand, HFE 7200 - methanol mixtures are likely to be highly non-ideal because of the large differences in polarity between the two components.

3.7 Summary

Three approaches were evaluated for designing heat transfer fluids for direct immersion cooling of electronics systems. The candidates designed using CAMD were screened by applying FOM constraints for pool and flow boiling. A total of 52 compounds were shortlisted after FOM analysis. From these 52 fluids, the following 9 fluids were selected for experimental evaluation based on commercial availability and knowledge of synthesis steps:

- 1,1,1-Trifluorobutan-2-one
- 4,4,4-Trifluorobutan-2-one
- 1,1,1-Trifluoro-3-methylpentane
- 1,1,1-Trifluoro-3-(2,2,2-trifluoroethoxy)propane

- Bis(1,1,1-trifluroethyl)ether
- Dimethoxydimethylsilane
- Ethyldimethylsilane
- 1-Ethoxybutane
- Methanol

Among these fluids, 1,1,1-trifluoro-3-methylpentane and 1,1,1-trifluoro-3-(2,2,2-trifluoroethoxy)propane were synthesized in this work and their synthesis is described in the next chapter. The experimental evaluation of thermophysical properties and pool boiling heat transfer performance of these fluids are presented in Chapter 5.

3.8 References

1. Cussler, E. L. and Moggridge, G. D., *Chemical Product Design*, 2001. Cambridge: University Press.

2. Achenie, L. E. K., Gani, R., and Venkatasubramanian, V. (eds), *Computer Aided Molecular Deisgn: Theory and Practice*, Computer-Aided Chemical Engineering, Volume 12, 2003. Amsterdam, The Netherlands: Elsevier.

3. Ng, K. M., Gani, R., and Dam-Johansen, K. (eds.), *Chemical Product Design: Toward a Perspective through Case Studies*, Computer-Aided Chemical Engineering-Volume 23, 2007. Amsterdam, The Netherlands: Elsevier.

4. Charpentier, J. C., *Among the trends for a modern chemical engineering, the third paradigm: the time and length multiscale approach as an efficient tool for process intensification and product design and engineering*, Chemical Engineering Research and Design, 2010. **88**: p. 248-254.

5. Gani, R., and Brignole, E. A., *Molecular design of solvents for liquid extraction based on UNIFAC*, Fluid Phase Equilibria, 1983. **13**: p. 331-340.

6. Brignole, E. A., Bottini, S., and Gani, R., *A strategy for the design and selection of solvents for separation processes*, Fluid Phase Equilibria, 1986. **29**: p. 125-132.

7. Bunin, B. A., Bajorath, J., Siesel, B., and Morales, G., *Chemoinformatics: Theory, Practice, and Products*, 2007. AA Dordrecht, The Netherlands: Elsevier.

8. Odele, O. and Macchietto, S., *Computer aided molecular design: a novel method for optimal solvent selection*, Fluid Phase Equilibria, 1993. **82**: p. 47-54.

9. Duvedi, A. and Achenie, L. E. K., *On the design of environmentally benign refrigerant mixtures: a mathematical programming approach*, Computers and Chemical Engineering, 1997. **21**: p. 915-923.

10. Papadopoulos, A. I., Stijepovic, M., and Linke, P., *On the systematic design and selection of optimal working fluids for organic Rankine cycles*, Applied Thermal Engineering, 2010, **30**(6-7): p. 760-769.

11. Maranas, C. D., *Optimal computer-aided molecular design: a polymer design case stud*y, Industrial and Engineering Chemistry Research, 1996, **35**(10): p. 3403-3414.

12. Satyanarayana, K. C., Abildskov, J., Gani, R., Tsolou, G., and Mavrantzas, V. G., *Computer aided molecular design using multi-scale modeling*, Brazilian Journal of Chemical Engineering, 2010. **27**(3): p. 369-380.

13. Markoulaki E. C. and Kokossis A. C. *On the development of novel chemicals using a systematic synthesis approach. Part 1. Optimization framework*, Chemical Engineering Science, 2000. **55**(13): p. 2529-2546.

14. Warrier, P., Sathyanarayana, A., Joshi, Y., and Teja, A. S., *Screening and evaluation of mixture formulations for electronics thermal management using pool boiling*, IEEE Transactions on Components and Packaging Technology, 2011. **1**: p. 1387-1394.

15. Karunanithi, A. T., Acquah. C., Achenie, L. E. K., Sithambaram, S., Suib, S. L., and Gani, R., *An experimental verification of morphology of ibuprofen crystals from CAMD designed solvent*, Chemical Engineering Science, 2007. **62**(12): p. 3276-3281.

16. Chen, J., and Trout, B. L., *Computer-aided solvent selection for improving the morphology of needle-like crystals: a case study of 2,6-dihydroxybenzoic acid*, Crystal Growth and Design, 2010. **10**(10): p. 4379-4388.

17. Joback, K. G., *Design molecules possessing desired physical properties*, PhD Thesis, Massachusetts Institute of Technology, 1989. Cambridge, Massachusetts.

18. Gray, N. A. B., *Computer-assisted structure elucidation*, 1986. New York: John Wiley & Sons.

19. Sinha, M., Achenie, L. E. K., and Ostrovsky, G. M., *Design of environmentally benign solvents via global optimization*, Computers and Chemical Engineering, 1999. **23**: p. 1381-1394.

20. Ostrovsky, G. M., Achenie, L. E. K., and Sinha, M., *A reduced dimension branch-and-bound algorithm for molecular design*, Computers and Chemical Engineering, 2003. **27**: p. 551-567.

21. Venkatasubramanian, V., Chan, K., and Caruthers, J. M., *Computer-aided molecular design using genetic algorithms*, Computers and Chemical Engineering, 1994. **18**(9): p. 833-844.

22. Glen, R. C. and Payne, A. W. R., *A genetic algorithm for the automated generation of molecules within constraints*, Journal of Computer Aided Molecular Design, 1994. **9**: p. 181-202.

23. Patkar, P. R. and Venkatasubramanian, V., Genetic algorithms based CAMD, in Achenie, L. E. K., Gani, R., and Venkatasubramanian, V. (eds), *Computer Aided Molecular Deisgn: Theory and Practice*, Computer-Aided Chemical Engineering, Volume 12, 2003. Amsterdam, The Netherlands: Elsevier.

24. Harper, P. M., Gani, R., Kolar, P., and Ishikawa, T., *Computer-aided molecular design with combined molecular modeling and group contribution*, Fluid Phase Equilibria, 1999, **158-160**: p. 337–347.

25. Harper, P. M. and Gani, R., *A multi-step and multi-level approach for computer aided molecular design*, Computers and Chemical Engineering, 2000. **24**: p. 677-683.

26. Marrero, J. and Gani, R., *Group-contribution based estimation of pure component properties*, Fluid Phase Equilibria, 2001. **183-184**(1): p. 183-208.

27. Horvath, L., *Molecular design. Chemical structure generation from the properties of pure organic compounds*, Studies in Physical and Theoretical Chemistry Book Series, Volume 75, 1992. Amsterdam, The Netherlands: Elsevier.

28. Properties of Novec fluids from 3M Company, available at: http://multimedia.3m.com/mws/mediawebserver?66666UuZjcFSLXTtnx&y5xz6EVuQEcuZgVs6EVs6E666666-- (accessed April 2012).

29. Warrier, P., Sathyanarayana, A., Patil, D. V., France, S., Joshi, Y., and Teja, A. S., *Novel heat transfer fluids for direct immersion phase change cooling of electronic systems*, International Journal of Heat and Mass Transfer, 2012. **55**: p. 3379–3385.

30. Rohsenow, W. M. A., *Method of correlating heat transfer data for surface boiling of liquids*, Division of Industrial Cooporation, Massachusetts Institute of Technology, Technical Report No. 5, 1951. Cambridge, Massachusetts.

31. Lazarek, G. M. and Black, S. H., *Evaporative heat transfer, pressure drop and critical heat flux in a small vertical tube with R-113*, International Journal of Heat and Mass Transfer, 1982. **25**(7): p. 945-960.

32. Tran, T. N., Wambsganss, M. W., and France, D. M., *Small circular- and rectangular-channel boiling with two refrigerants*, International Journal of Multiphase Flow, 1996. **22**(3): p. 485-498.

33. Chen, T. and Garimella, S. V., *Flow boiling heat transfer to a dielectric coolant in a microchannel heat sink*, IEEE Transactions in Components and Packaging Technology, 2007, **30**: p. 24-31.

34. Klimenko, V. V., *A generalized correlation for two-phase forced flow heat transfer-second assessment*, International Journal of Heat and Mass Transfer, 1990. **33**(10): p. 2073-2088.

35. Liu, D., Garimella, S. V., *Flow boiling heat transfer in microchannels*, Journal of Heat Transfer, 2007. **129**: p. 1321-1332.

36. Riehl, R. R., Seleghim, P., and Ochterbeck, J. M., *Comparison of heat transfer correlations for single- and two-phase microchannel flows for microelectronics cooling*, Sixth Intersociety Conference on Thermal and Thermomechanical Phenomena in Electronic Systems, 1998. p. 409-416.

37. Dhir, V. K., *Boiling heat transfer*, Annual Reviews of Fluid Mechanics, 1998. **30**: p. 365-401.

38. Warrier, P., Sathyanarayana, A., Bazdar, S., Joshi, Y., and Teja, A. S., *Selection and evaluation of organosilicon coolants for direct immersion cooling of electronic systems*, Industrial and Engineering Chemistry Research, 2012. (Submitted).

39. McGillis, W. R., Fitch, J. S., Hamburgen, W. R., and Carey, V. P., *Boiling binary mixtures at sub-atmospheric pressures*, Western Research Laboratory, Technical Note TN-23, January 1992. Palo Alto, California.

40. Flynn, R. M., Milbrath, D. S., Owens, J. G., Vitcak, D. R., and Yanome, H., *Azeotrope-like compositions and their use*, 2001. US Patent 6288018 B1.

CHAPTER 4

SYNTHESIS OF TWO NOVEL HEAT TRANSFER FLUIDS

This chapter describes the synthesis of two new heat transfer fluids - 1,1,1-trifluoro-3-methylpentane ($C_6H_{11}F_3$) and 1,1,1-trifluoro-3-(2,2,2-trifluoroethoxy)propane ($C_5H_5F_6O$). These fluids were selected from a list of 35 candidates generated using the CAMD-ICAS method combined with the application of physical property and FOM constraints.

4.1 Introduction

As mentioned in Section 3.4.2, only 4 of the 35 fluids identified in this work were available commercially. The commercial custom synthesis of several promising candidates was also attempted. Over one hundred custom synthesis companies were contacted, but they could not provide adequate quantities (500 ml) of any of the candidates at a reasonable price (quotes as high as $ 50,000 for 500 ml were received). SynQuest Laboratories Inc., FL agreed to synthesize 100 g of 1,1,1-trifluoro-3-methylpentane for $4,995 with a delivery time of 45 days. However, they were unable to synthesize the compound in 4 months and therefore cancelled the order. After this setback, synthesis was pursued in collaboration with Prof. Stefan France in the School of Chemistry & Biochemistry at the Georgia Institute of Technology. About 50 ml of 1,1,1-trifluoro-3-methylpentane was successfully synthesized [1] by trifluoroethylation of *cis*-2-butene with trichlorotrifluoroethane followed by reductive dechlorination. This

procedure is described by Puy [2]. The synthesis procedure was then given to SynQuest Laboratories Inc., FL and they provided 50 ml more of 1,1,1-trifluoro-3-methylpentane. 1,1,1-trifluoro-3-(2,2,2-trifluoroethoxy)propane was also synthesized in small quantities by Williamson ether synthesis. The following sections describe the synthesis procedures in detail.

4.2 Synthesis of 1,1,1-trifluoro-3-methylpentane

4.2.1 Materials

Trichlorotrifluoroethane (> 99 %) was purchased from Matrix Scientific, SC. *cis*-2-butene, (> 98 %) was purchased from TCI America, OR. *t*-Butanol (> 99%), dichloromethane (> 99.5 %), anhydrous magnesium sulfate (> 99.5 %), and 1 wt. % Pd on carbon were purchased from Sigma Aldrich, MO. Ethanolamine (> 98 %) and cuprous chloride (> 90 %) were purchased from Alfa Aesar, MA. These chemicals were used without any purification in the experiments described below.

4.2.2 Synthesis of 2,2,4-trichloro-1,1,1-trifluoro-3-methylpentane

The first step in the synthesis of 1,1,1-trifluoro-3-methylpentane is the trifluoroethylation of *cis*-2-butene with trichlorotrifluoroethane to produce 2,2,4-trichloro-1,1,1-trifluoro-3-methylpentane ($C_6H_8Cl_3F_3$). The reaction scheme is shown in Figure 4.1.

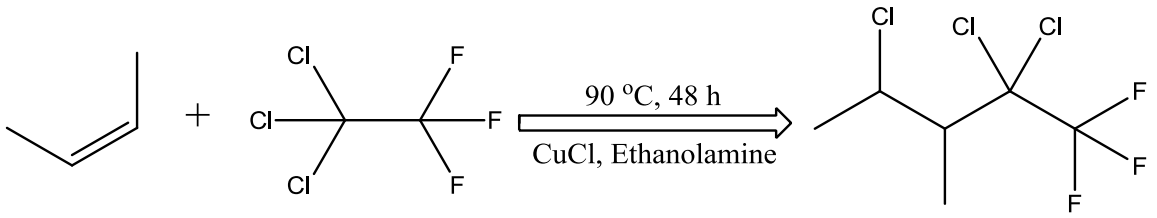

Figure 4.1. Trifluoroethylation of *cis*-2-butene with trichlorotrifluoroethane.

The reaction was carried out in a 300 ml glass pressure vessel (Andrews Glass Company, NJ). *cis*-2-butene (which is a gas at room temperature) was condensed using a dry ice/acetone bath prior to its addition to the reaction mixture. A mixture of 81 g trichlorotrifluoroethane, 13 g *cis*-2-butene, 75 ml *t*-butanol, 1.0 g CuCl catalyst, and 3 g ethanolamine (co-catalyst) was heated in the pressure vessel for 48 h at 90 °C. The pressure vessel was equipped with a pressure gauge and the pressure was monitored as the reaction media was heated. The maximum pressure attained over the 48 h reaction period was about 5 bar. After 48 h, the cooled reaction mixture was poured into 200 ml of de-ionized (DI) water and the lower organic layer was separated. The aqueous layer was extracted twice with 50 ml dichloromethane, and the combined organic layer was washed twice with 100 ml DI water. The organic layer was then dried with anhydrous magnesium sulfate and the volatiles were removed by rotary evaporation. Distillation under vacuum (~0.07 bar) produced 2,2,4-trichloro-1,1,1-trifluoro-3-methylpentane at 80 - 90 °C with a 30 % yield with respect to CF_3CCl_3, i.e. 31 g of $C_6H_8Cl_3F_3$ per 81 g CF_3CCl_3 reacted. ^1H and ^{19}F NMR (Varian Mercury Vx 400) spectra of the product recorded using $CDCl_3$ solvent are presented in Figure 4.2 and 4.3. They match well with those reported by Puy [2] i.e., ^{19}F NMR: -76 and -75.7 ppm and ^1H NMR: 4.8 (1H); 3.0 (1H); 1.6 (3H) and 1.4

(3H) ppm. The slight shift in ^{19}F NMR peaks is because of the different solvent ($CFCCl_3$) used by Puy.

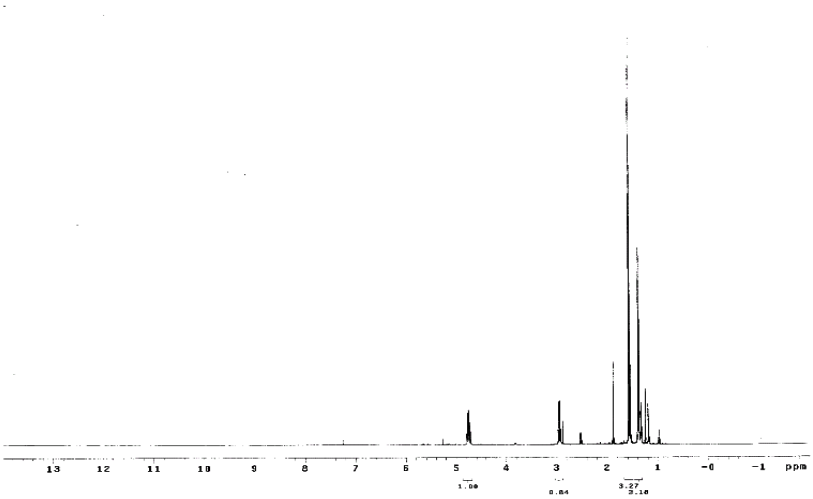

Figure 4.2. ^{1}H NMR of $C_6H_8Cl_3F_3$.

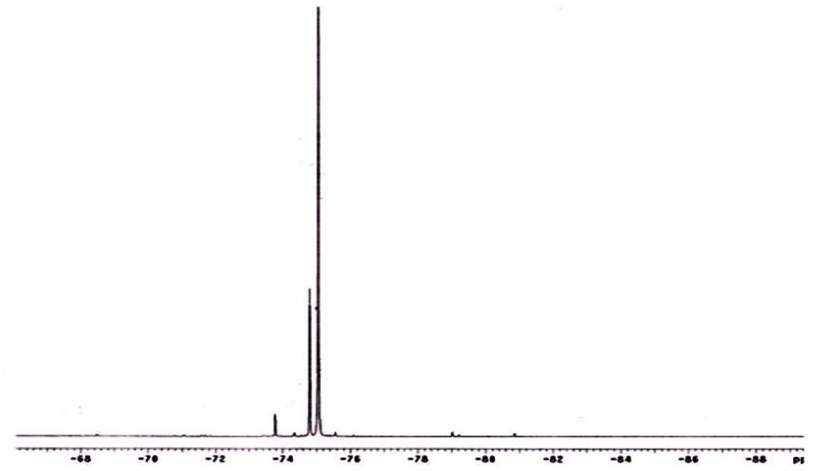

Figure 4.3. ^{19}F NMR of $C_6H_8Cl_3F_3$.

4.2.3 Hydrogenation of 2,2,4-trichloro-1,1,1-trifluoro-3-methylpentane

2,2,4-trichloro-1,1,1-trifluoro-3-methylpentane was hydrogenated over 1 wt. % Pd on carbon (4-8 mesh) at 250 °C to produce the desired compound 1,1,1-trifluoro-3-methylpentane. The reaction scheme is shown in Figure 4.4.

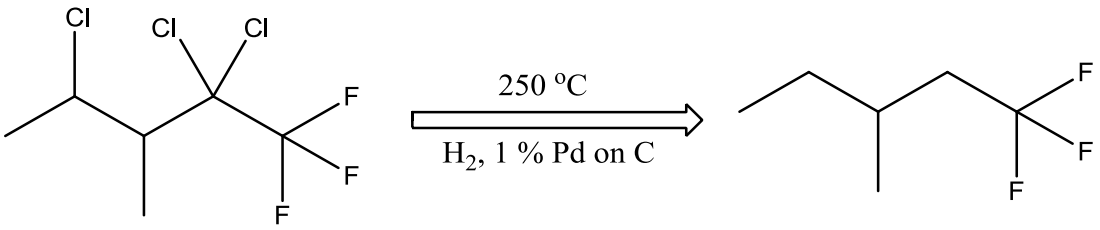

Figure 4.4. Hydrogenation of 2,2,4-trichloro-1,1,1-trifluoro-3-methylpentane.

The hydrogenation reactor was constructed as described by Puy [2] and is shown in Figure 4.5.

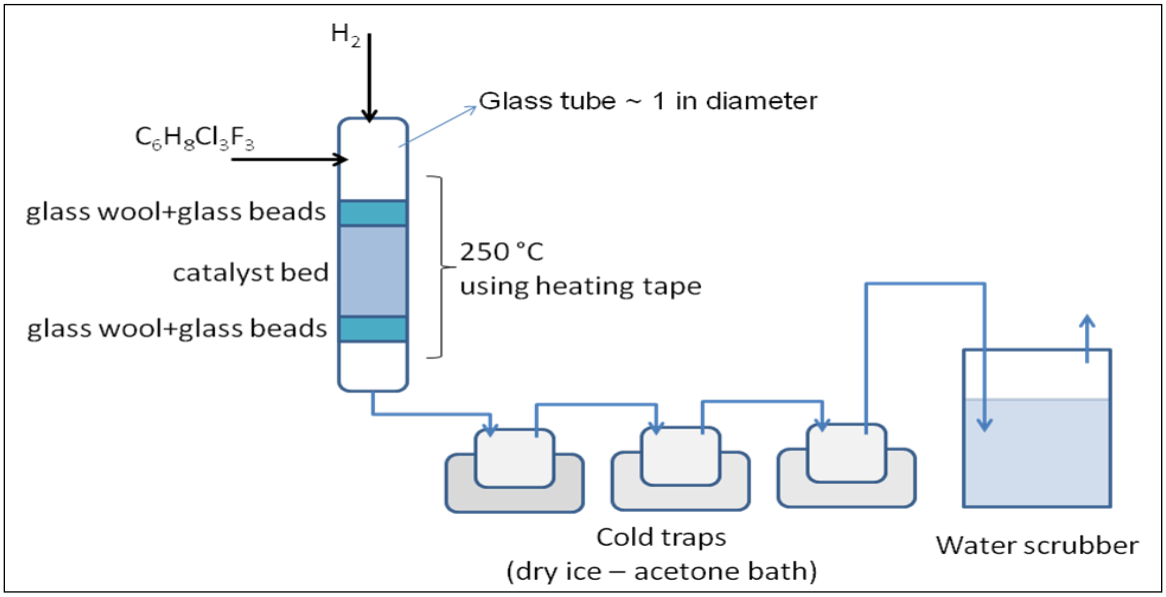

Figure 4.5. Hydrogenation reaction setup.

The reactor was heated using an electrical heating tape wrapped around the outside of the tube. The tube was mounted vertically and packed with glass wool and glass beads in the lower end of the tube, followed by about 15 cc of 1 wt. % Pd on carbon. The remainder of the tube was packed with glass wool and glass beads leaving about 5 cm at the top for the syringe dispensing organic material. The reactor exit was

connected to three dry-ice/acetone baths and a water scrubber. The reactor was heated first with a N_2 purge to 250 °C near the center of the reactor (skin temperature) and then with H_2. $C_6H_8Cl_3F_3$ (31 g) was fed from the top of the reactor by means of a syringe pump at the rate of 5 ml per hour. In order to ensure that an excess of hydrogen was present in the reactor, the hydrogen flow rate was adjusted as necessary after the organic flow was started to maintain a slow bubble rate in the water scrubber. After all the organic material was added, heating was continued at 250 °C with H_2 flow for 30 minutes and with N_2 flow for 30 minutes. The crude product was collected after warming the cold traps. Distillation at room temperature of the crude product gave 1,1,1-trifluoro-3-methylpentane at 60 - 70 °C with a 18 % yield with respect to CF_3CCl_3, i.e. 10.5 g of $C_6H_{11}F_3$ per 81 g of CF_3CCl_3. ^1H and ^{19}F NMR spectra recorded with $CDCl_3$ solvent are presented in Figures 4.6 and 4.7 match well with those reported by Puy [2] i.e., ^1H NMR 1.7-2.3 (3H); 1.15-1.7 (2H); and 0.8-1.15 (6H) ppm and ^{19}F NMR -64.5 ppm.

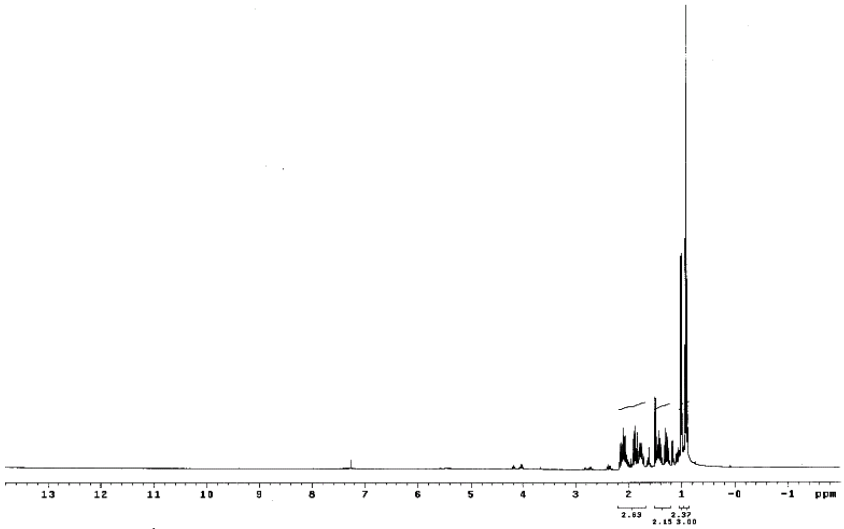

Figure 4.6. ^1H NMR for $C_6H_{11}F_3$.

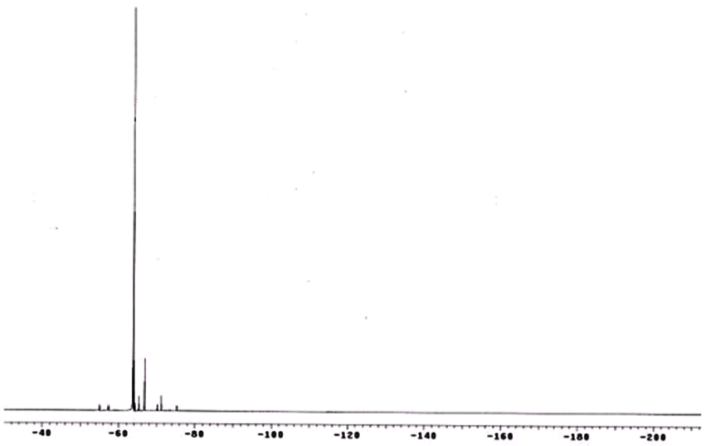

Figure 4.7. ^{19}F NMR for $C_6H_{11}F_3$.

4.3 Synthesis of 1,1,1-trifluoro-3-(2,2,2-trifluoroethoxy)propane

4.3.1 Materials

3-bromo-1,1,1-trifluoropropane (> 99 %) was purchased from Matrix Scientific, SC. 2,2,2-trifluoroethanol (> 99 %) and diethylether (> 99 %) were purchased from Sigma Aldrich, MO. These chemicals were used without any purification in the experiments described below.

4.3.2 Synthesis of 1,1,1-trifluoro-3-(2,2,2-trifluoroethoxy)propane via Williamson ether reaction

1,1,1-trifluoro-3-(2,2,2-trifluoroethoxy)propane ($C_5H_6F_6O$) was synthesized via the Williamson ether reaction between 2,2,2-trifluoroethanol and 3-bromo-1,1,1-trifluoropropane. Following the procedure of Wu and Chen [3], who used the Williamson ether reaction for synthesis of bis(1,1,1-trifluroethyl)ether, the reaction was carried out in near critical water at 250 °C and 50 bar. The reaction scheme is shown in Figure 4.8.

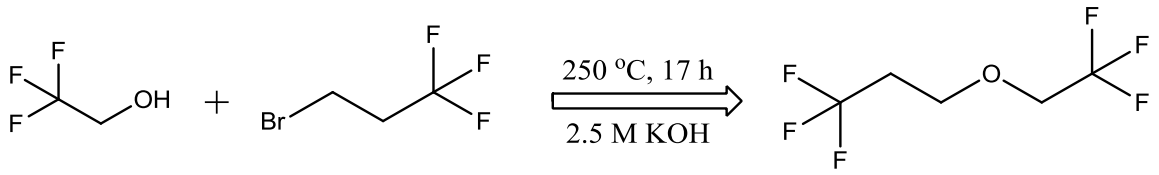

Figure 4.8. Reaction scheme for synthesis of 1,1,1-trifluoro-3-(2,2,2-trifluoroethoxy)propane.

The reaction was carried out in a Parr high pressure autoclave by adding 30 g of 3-bromo-1,1,1-trifluoropropane, 14.6 g of KOH dissolved in 45 ml of DI water, and 42.4 g of 2,2,2-trifluoroethanol. The reactor was closed tightly and heated to 250 °C. After 17 h, the reaction medium was collected and the organic layer was extracted twice by adding 30 ml diethylether. The aqueous layer was washed twice with 15 ml diethylether. The combined organic layer was then dried with anhydrous magnesium sulfate and the volatiles were removed by rotary evaporation. Distillation at ambient pressure, produced $C_5H_6F_6O$ at 80 - 90 °C with a 24 % yield with respect to 3-bromo-1,1,1-trifluoropropane, i.e. 8.2 g of $C_5H_6F_6O$ per 30 g of $C_3H_4F_3Br$. ^1H NMR spectra recorded using $CDCl_3$ solvent and GC-MS results are presented in Figures 4.9 and 4.10 respectively.

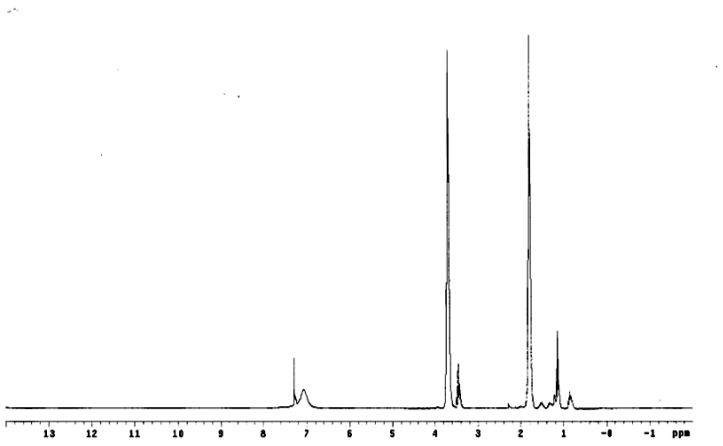

Figure 4.9. ^1H NMR for $C_5H_6F_6O$.

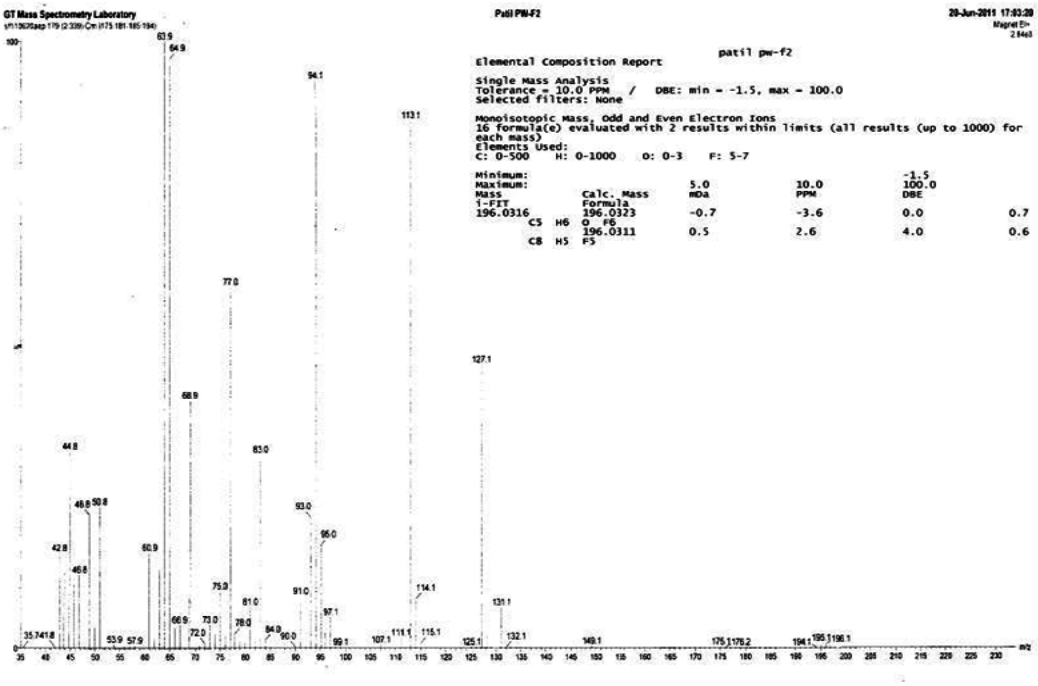

Figure 4.10. GC-MS for $C_5H_6F_6O$.

4.4 Conclusions

1,1,1-trifluoro-3-methylpentane ($C_6H_{11}F_3$) and 1,1,1-trifluoro-3-(2,2,2-trifluoroethoxy)propane ($C_5H_6F_6O$) were synthesized in this work. About 50 ml of $C_6H_{11}F_3$ was synthesized by trifluoroethylation of *cis*-2-butene with trichlorotrifluoroethane followed by hydrogenation. Although the synthesis proved difficult to scale-up, sufficient quantities were obtained for property measurements and feasibility studies. A small quantity (~ 8 g) of $C_5H_6F_6O$ was synthesized using the Williamson ether reaction between 2,2,2-trifluoroethanol and 3-bromo-1,1,1-trifluoropropane.

4.5 References

1. Warrier, P., Sathyanarayana, A., Patil, D. V., France, S., Joshi, Y., and Teja, A. S., *Novel heat transfer fluids for direct immersion phase change cooling of electronic systems*, International Journal of Heat and Mass Transfer, 2012. **55**: p. 3379-3385.

2. Puy, M. V. D., *Trifluoroethylation of olefins with trichlorotrifluoroethane*, Journal of Fluorine Chemistry, 1993. **61**: p. 133-140.

3. Wu, K. and Chen, Q. -Y., *Synthesis of trifluoroethyl ethers from 2,2,2-triflurorethyl chloride (HCFC-133a) in high temperature aqueous medium*, Journal of Fluorine Chemistry, 2002. **113**: p. 79-83.

CHAPTER 5

THERMOPHYSICAL PROPERTIES AND HEAT TRANSFER PERFORMANCE OF NEW HEAT TRANSFER FLUIDS

This chapter discusses the experimental evaluation of the properties and performance of newly identified heat transfer fluids and their mixtures. The fluids were characterized via measurements of their density, viscosity, thermal conductivity, and electrical resistivity. The heat transfer performance of the fluids during pool boiling was evaluated via measurements of critical heat flux and incipience superheat. To ascertain whether rectification of the mixtures occurred during pool boiling, vapor-liquid equilibria were predicted using regular solution theory and the COSMO-RS method. A rough hard-sphere correlation was also developed for transport properties of mixtures of HFE 7200 with methanol and 1-ethoxybutane.

5.1 Materials

Chemicals used in the investigation are listed in Table 5.1 along with their purity and supplier. These chemicals were used without further purification.

Table 5.1. Chemicals, purity, and supplier information.

Name	Formula	Purity (mol %)	Supplier
HFE7200	$C_6H_5F_9O$	98	3M Company, MN
Dimethoxydimethylsilane	$C_4H_{12}O_2Si$	99.5	Sigma Aldrich, MO
Ethyldimethylsilane	$C_4H_{12}Si$	98	Sigma Aldrich, MO
1-ethoxybutane	$C_6H_{14}O$	98	Sigma Aldrich, MO
1,1,1-trifluoro-2-butanone	$C_4H_5F_3O$	95	SynQuest Labs, FL
Bis(2,2,2-trifluoroethyl)ether	$C_4H_4F_6O$	99	SynQuest Labs, FL
4,4,4-trifluoro-2-butanone	$C_4H_5F_3O$	97	Matrix Scientific, SC
1,1,1-trifluoro-3-methylpentane	$C_6H_{11}F_3$	90	Synthesized in this work + SynQuest Labs, FL
Methanol	CH_4O	99.9	Fisher Scientific, PA

5.2 Thermophysical Properties

5.2.1 Methods

5.2.1.1 Viscosity

Viscosities (η) were measured using a size 25 Cannon-Fenske viscometer (Cannon Instrument Company, PA). The instrument was factory calibrated using viscosity standard fluids I.50 and N1.0 and was reported to be capable of measuring viscosities with a maximum uncertainty of 0.16 % for fluids having a kinematic viscosity less than 10 cSt. The calibration was validated by measuring the viscosity of de-ionized (DI) water [1] (0.913 cSt at 23 °C) and compared with the literature value of 0.9122 cSt [2]. The two values agree within 0.16 % which is within the uncertainty of the instrument. Each value reported in this work represents an average of three measurements.

5.2.1.2 Density

Densities (ρ) were measured using a 25 ml glass pycnometer as described by Marsh [1] with an estimated uncertainty of ±1 kg m^{-3}. DI water was again used as a reference fluid to validate the measurement and its density at 22 °C was measured as 996.06 kg m^{-3} which agrees with the literature value of 997 kg m^{-3} [2].

5.2.1.3 Electrical Resistivity

Electrical resistivities (ρ_e) were measured by impedance spectroscopy using an Agilent 4284A LCR impedance meter. The impedance meter consists of two parallel plate Pt electrodes immersed in the liquid to be tested which is contained in a Teflon cell. The cell constant was obtained by measuring the resistance of three standard KCl solutions (0.01 M, 0.1 M, and 1 M) and plotting the real part of the impedance as a function of the reciprocal of the square root of frequency and extrapolating it to infinite frequency [3]. The electrical resistivity (ρ_e) was obtained by dividing the solution resistance by the cell constant. HFE 7200 was used as the reference fluid, and therefore these measurements of electrical resistivity should be used for comparison purposes only. The electrical resistivity of HFE 7200 obtained using this technique was 6.45×10^7 Ω-cm which matches reasonably well with the reported value of 10^8 Ω-cm [4]. Electrical resistivity was measured only for mixtures of methanol and 1-ethoxybutane with HFE 7200, as the other fluids (fluorocarbons and organosilicon fluids) are known to be dielectric.

5.2.1.4 Thermal Conductivity

Thermal conductivities were measured using a transient hot-wire method that employed a mercury-filled glass capillary suspended in the liquid. The temperature change of the mercury "wire" as it was being heated was computed from its changing resistance with time. The thermal conductivity was then calculated from an analytic solution of Fourier's equation for a linear heat source of infinite length in an infinite medium. Observation of a linear relationship between the temperature change of the wire and the natural log of time was used to confirm that the primary mode of heat transfer during the measurement was conduction. Corrections to the temperature were included for the insulating layer around the wire, the finite dimensions of the wire, the finite volume of the fluid, and heat loss due to radiation. Finally, a calibration was performed with a reference fluid to obtain an effective wire length in order to account for the non-uniform capillary thickness and end effects. In the present study, water and dimethyl phthalate were the reference fluids used for the calibration. Each thermal conductivity value reported in this work represents an average of 5 measurements with an error estimate of ± 2 %. Additional details of the method can be found in Bleazard and Teja [5] and Diguilio and Teja [6].

Measurement using the transient hot-wire method require about 75 ml of fluid. Since this quantity was not available in the case of $C_6H_{11}F3$, a KD2-pro thermal conductivity meter (Decagon Devices Inc., WA) was used for this fluid. A thermal conductivity measurement with the KD2-pro instrument requires only about 20 ml of fluid. However, thermal conductivity measurements of low viscosity fluids (η < 1 cP) using KD2-pro are subject to systematic errors associated with natural convection. To account for these errors, the instrument was calibrated using measurements on twelve

fluids with kinematic viscosity (ν) ranging from 3.8×10^{-7} m^2 s^{-1} to 1.26×10^{-5} m^2 s^{-1}. Corrections were applied based on these measurements as follows [7]:

$$\frac{(k-k_{obs})}{k}\times100 = -7.569\frac{\beta}{\nu^2} - 3.191 \tag{5.1}$$

where k is the corrected thermal conductivity of the fluid, k_{obs} is the observed thermal conductivity value using the KD2-pro instrument, and β is the coefficient of volumetric expansion. The uncertainty in thermal conductivity measurements after correcting for natural convection was estimated to be 6 %. DI water was again used to validate the measurements and its thermal conductivity at 299.4 K was measured as 0.5819 W m^{-1} K^{-1} which agrees within 6 % with the literature value of 0.61 W m^{-1} K^{-1} [2]. The measurements were repeated three times and an average value is reported.

5.2.2 Properties of Pure Fluids

Results of the thermophysical property measurements for pure fluids, HFE 7200, 1,1,1-trifluoro-3-methylpentane, bis(2,2,2-trifluoroethyl)ether, 1,1,1-trifluoro-2-butanone, 4,4,4-trifluoro-2-butanone, dimethoxydimethylsilane, and ethyldimethylsilane are presented in Table 5.2. As this data was not included in the dataset used for development of GC methods, GC estimates are also listed in Table 5.2 to provide further validation of the GC method. It can be observed that GC estimates are in reasonable agreement with the measured data, except in the case of viscosity. This, therefore, validates the decision to use constraints based on the thermal conductivity and not viscosity to screen candidates.

Table 5.2. Thermophysical properties of new heat transfer fluids.

	ρ (g cc^{-1})		η (cP)		k (W m^{-1} K^{-1})	
	Exp	GC	Exp	GC	Exp	GC
HFE 7200	1.417	1.627	0.607	0.210	0.066	0.081
$C_6H_{11}F_3$	0.973	0.896	0.350	0.250	0.089	0.106
$C_4H_4F_6O$	1.396	1.312	0.560	0.270	0.083	0.092
111-$C_4H_5F_3O$	1.137	1.016	0.367	0.320	0.091	0.112
444-$C_4H_5F_3O$	1.222	0.985	0.765	0.370	0.119	0.115
$C_4H_{12}SiO_2$	0.857	0.862	0.341	0.452	0.115	0.126
$C_4H_{12}Si$	0.668	0.753	0.249	0.446	0.109	0.119

5.2.3 Properties of Mixture Formulations

Tables 5.3 and 5.4 list measured values for density, viscosity, thermal conductivity, and electrical resistivity for the mixtures of HFE 7200 with methanol and 1-ethoxybutane. Thermal conductivities of HFE 7200 and 1-ethoxybutane were also measured as a function of temperature for development of rough hard-sphere correlations are listed in Tables 5.5 and 5.6 respectively.

Table 5.3. Measured properties of HFE 7200 + methanol mixtures.

Methanol % (w/w)	ρ_l (kg m^{-3})	η (cP)	k (W m^{-1} K^{-1})	ρ_e (Ω-cm)
0	1417.0	0.6065	0.0662	6.45×10^{7}
10	1357.0	0.6034	0.0729	2.23×10^{6}
20	1294.4	0.6802	0.0794	4.97×10^{5}
40	1058.4	0.6089	0.0948	3.44×10^{5}
60	946.5	0.5710	0.1108	3.30×10^{5}
80	852.6	0.5495	0.1326	2.22×10^{5}
100	791.8	0.5463	0.1999	2.79×10^{5}

Table 5.4. Measured properties of HFE 7200 + 1-ethoxybutane mixtures.

1-ethoxybutane % (w/w)	ρ_l (kg m^{-3})	η (cP)	k (W m^{-1} K^{-1})	ρ_e (Ω-cm)
0	1417.0	0.6065	0.0662	6.45×10^{7}
10	1293.4	0.5458	0.0664	3.62×10^{8}
20	1187.4	0.5042	0.0707	2.55×10^{8}
40	1024.9	0.4379	0.0774	4.52×10^{8}
60	907.4	0.4077	0.0921	3.91×10^{8}
80	813.7	0.3970	0.1085	4.13×10^{8}
100	743.0	0.3868	0.1258	4.91×10^{8}

Table 5.5. Thermal conductivity of HFE 7200 as a function of temperature.

T (K)	k (W m^{-1} K^{-1})
278.8	0.0712
300.6	0.0644
314.1	0.0616
328.3	0.0590
344.1	0.0563

Table 5.6. Thermal conductivity of ethoxybutane as a function of temperature.

T (K)	k (W m^{-1} K^{-1})
299.62	0.1250
312.17	0.1229
333.39	0.1017
354.63	0.0949

5.2.4 Rough Hard-Sphere Correlations for Mixture Transport Properties

The rough hard sphere expressions for the reduced viscosity (η^*) and reduced thermal conductivity (k^*) as functions of the reduced molar volume ($V_r = V/V_0$) are as follows [8-14]:

$$\log(\eta^*/ R_\eta) = 1.0945 - 9.26324\ V_r^{-1} + 71.0385\ V_r^{-2} - 301.9012\ V_r^{-3} + 797.69\ V_r^{-4} - 1221.977\ V_r^{-5} + 987.5574\ V_r^{-6} - 319.4636\ V_r^{-7} \quad (5.2)$$

$$\log(k^*/ R_k) = 1.0655 - 3.538\ V_r^{-1} + 12.120\ V_r^{-2} - 12.469\ V_r^{-3} + 4.562\ V_r^{-4} \quad (5.3)$$

These equations were used to correlate the viscosity and thermal conductivity of n-alkanes, alkanols, aromatic hydrocarbons, and refrigerants, using empirical expressions for the parameters (V_0, R_η, and R_k). Teja *et al.* [15] and Bleazard and Teja [16] showed that the viscosity and thermal conductivity of 58 polar liquids could be correlated using equations 5.2 and 5.3 if V_0, R_η and R_k are expressed as follows:

$$R_\eta = A_0 \quad (5.4)$$

$$V_0 = B_0 + B_1 / T \quad (5.5)$$

$$R_k = C_0 + C_1\ T \quad (5.6)$$

The five coefficients (A_0, B_0, B_1, C_0, C_1) in equations 5.4 - 5.6 were obtained by simultaneously fitting viscosity and thermal conductivity data for 58 polar liquids. The liquids studied included diols, disulfides, amines, carboxylic acids, alcohol-ethers, pyridines, ethanolates and polyethylene glycols. Transport properties of these 58 liquids

were correlated within experimental error at temperatures between 293 and 423 K. The parameters were found to exhibit regular trends for series of diols, carboxylic acids, ethanolates and polyethylene glycols. Recently, Sun and Teja [17] proposed further generalizations for the RHS parameters in order to correlate the viscosity and thermal conductivity of n-alkanes, 1-alkanols, alkanediols, benzene, toluene, and refrigerants.

Equations 5.2 and 5.3 can be extended to mixtures using mole fraction averaged mixture parameters [15] (V_0, R_η, and R_k). These mixing rules have been shown to work well for thermal conductivity, although they were less satisfactory for viscosity. Sun and Teja [18] incorporated binary interaction parameters in these mixing rules and were able to successfully correlate the thermal conductivity and viscosity of aqueous solutions of glycols. In the present work, modified versions of their mixing rules were used as follows:

$$V_{0,mix} = x_1^2 V_{0,1} + 2x_1 x_2 V_{0,12} + x_2^2 V_{0,2} \tag{5.7}$$

$$V_{0,12} = \frac{\left(V_{0,1}^{\ 1/3} + V_{0,2}^{\ 1/3}\right)^3}{8} \tag{5.8}$$

$$R_{\eta,mix} = x_1^2 R_{\eta 1} + 2x_1 x_2 R_{\eta 12} + x_2^2 R_{\eta 2} \tag{5.9}$$

$$R_{\eta 12} = \left(R_{\eta 1} R_{\eta 2}\right)^{1/2} \left(1 - K_\eta\right) \tag{5.10}$$

$$R_{k,mix} = x_1^2 R_{k1} + 2x_1 x_2 R_{k12} + x_2^2 R_{k2} \tag{5.11}$$

$$R_{k12} = \left(R_{k1} R_{k2}\right)^{1/2} \left(1 - K_k\right) \tag{5.12}$$

Here, K_η and K_k are adjustable parameters that account for any non-linear dependence of the viscosity and thermal conductivity, respectively.

RHS parameters for pure fluids required in equations 5.7 - 5.12 were calculated from the density, viscosity, and thermal conductivity vs. temperature data obtained from literature [2, 4, 19] or measured in this work. Literature correlations are given below:

Methanol [2]:

$$\rho / kmol.m^{-3} = \frac{2.3267}{0.27073^{[1+(1-T/5124)]^{0.24713}}} \tag{5.13}$$

$$\eta / Pa.s = \exp\left[-25.317 + 1789.2/(T) + 2.069\ln(T)\right] \tag{5.14}$$

$$k / W.m^{-1}.K^{-1} = 0.2837 - 0.000281T \tag{5.15}$$

Ethoxybutane [2]:

$$\rho / g.cm^{-3} = 0.26107 / 0.26506^{[1-T/531]^{0.28570}} \tag{5.16}$$

$$\eta / Pa.s = \exp\left[-25.317 + 1789.2/T + 2.069\ln(T)\right] \tag{5.17}$$

HFE 7200 [4, 19]:

$$\rho / g.cm^{-3} = 1.4811 - 0.0023026.\left[T - 273.15\right] \tag{5.18}$$

$$\eta / cP = -1.363 \times 10^{-5}.T^3 + 1.226 \times 10^{-2} T^2 - 3.685T + 370.25 \quad (5.19)$$

RHS coefficients and regression statistics are presented in Table 5.7.

Table 5.7. Coefficients for the RHS parameters for pure fluids.

	$B_0 \times 10^5$	$B_1 \times 10^3$	R_η	C_0	$C_1 \times 10^3$	AAD - η	AAD - k
Ethoxybutane	6.3041	6.4810	1.5151	3.4823	-3.4476	1.07	2.26
Methanol	0.0326	5.9965	3.3976	-0.9370	7.9504	1.01	0.26
HFE 7200	4.9303	17.3975	2.3055	0.4939	7.8426	0.49	2.57

Mixture data were correlated using RHS parameters from Table 5.7 and mixing rules given in equations 5.7 - 5.12. HFE 7200 + 1-ethoxybutane data could be correlated reasonably well without any adjustable parameters (K_k and K_η = 0). Average absolute deviations were 7.72 % for thermal conductivity and 4.55 % for viscosity. The fit could be improved with K_k = 0.1755 and K_η = 0.0937. HFE 7200 + methanol mixtures, on the other hand, required the use of adjustable parameters to obtain reasonable fits of the data. This is not surprising because of the significant difference in polarities between the two compounds. Highly nonlinear viscosity-composition behavior has also been reported for mixtures of methanol with toluene and benzene. [20] In addition, the dynamic and kinematic viscosities of HFE 7200 + methanol mixtures exhibit unusual behavior as can be seen in Figure 5.1. The sudden increase in viscosity at low mass fractions could be due to a change of phase, as has been observed in mixtures of methanol with hexane and cyclohexane. [21] However, no phase separation was observed in HFE 7200 + methanol mixtures at 298 ±2 K over a period of one week.

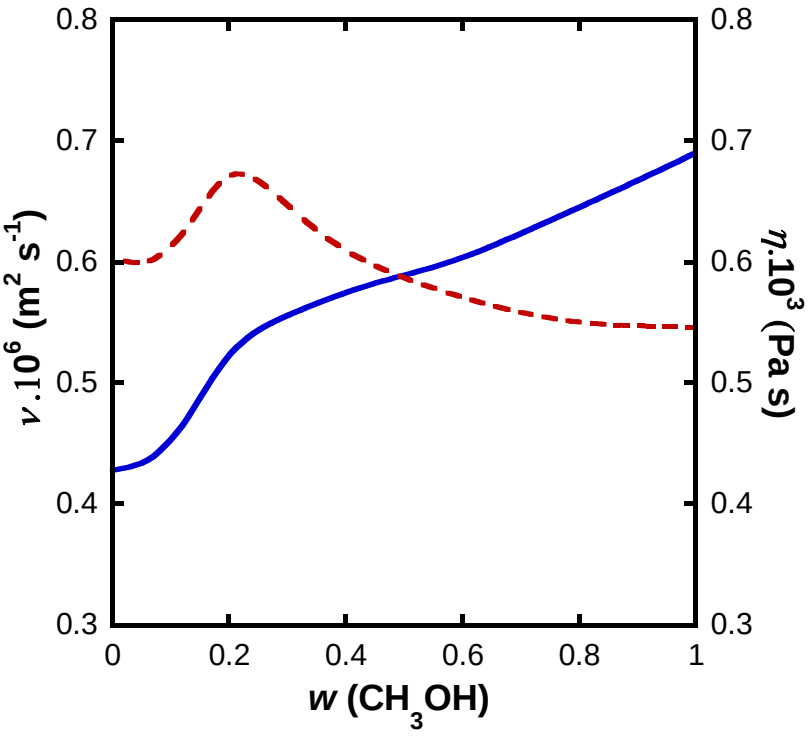

Figure 5.1. Kinematic viscosity (ν, blue solid line) and dynamic viscosity (η, brown dashed line) of HFE 7200 + methanol mixtures as a function of methanol weight fraction (w). [22]

Assuming no phase separation, average absolute deviations between calculated and experimental were 15.83 % in the case of thermal conductivity and 11.46 % in the case of without the use of adjustable parameters. The best fit was obtained with K_k = 0.3146 and K_η = -0.2451 as shown in Tables 5.8 and 5.9. However, average absolute deviations were still about 10 %, suggesting that further investigation of phase separation in this system may be warranted [22].

Table 5.8. RHS correlations for HFE 7200 + ethoxybutane mixtures.

Ethoxybutane (wt. %)	$\lvert(k_{expt} - k_{calc} / k_{expt})\rvert \times 100$		$\lvert(\eta_{expt} - \eta_{calc} / \eta_{expt})\rvert \times 100$	
	$K_k = 0$	$K_k = 0.1755$	$K_\eta = 0$	$K_\eta = 0.0937$
10	6.20	0.00	2.60	0.34
20	7.57	1.29	1.71	2.58
40	13.15	3.75	4.78	0.00
60	8.66	2.17	7.43	3.74
80	2.99	0.09	6.22	4.32
Average	7.72	1.46	4.55	2.19

Table 5.9. RHS correlations for HFE 7200 + methanol mixtures.

Methanol (wt. %)	$\lvert(k_{expt} - k_{calc} / k_{expt})\rvert \times 100$		$\lvert(\eta_{expt} - \eta_{calc} / \eta_{expt})\rvert \times 100$	
	$K_k = 0$	$K_k = 0.3146$	$K_\eta = 0$	$K_\eta = -0.2451$
10	3.28	12.25	3.11	8.74
20	17.89	0.00	9.09	0.00
40	11.92	0.49	21.55	17.19
60	22.52	15.44	13.91	11.43
80	23.56	20.51	9.67	8.61
Average	15.83	9.74	11.46	9.19

5.3 Pool Boiling Experimental Setup

Pool boiling experiments were performed by Mr. Aravind Sathyanarayana in Prof. Yogendra Joshi's laboratory in the G. W. Woodruff School of Mechanical Engineering at the Georgia Institute of Technology. The schematic of their pool boiling setup is shown in Figure 5.2. The setup consisted of a flip-chip packaged silicon thermal test chip (Figure 5.3) that was immersed in a jacketed transparent beaker containing the test liquid. The beaker was fitted with a Teflon block for mounting the chip and also included a

water-cooled coil to condense the boiling vapor. Two types of test chips were used during this work: (i) chip with grooves (70 μm wide and 70 μm deep with a pitch of 0.25 mm) cut into silicon and coated with 4 μm thick copper (Figure 5.4) and (ii) nanostructured chip with 20 μm height and 200 nm diameter copper nanowire array on the surface (Figure 5.5). The structured surfaces on the test chips were expected to increase CHF and decrease incipience superheat, relative to a bare substrate [23]. Details of the chip fabrication, packaging, and test set-up can be found in Im *et al.* [23, 24]. The setup was designed with features that included easy changeability of samples, visual access, and low heat loss, and to allow pool boiling tests to be performed at different temperatures and pressures. It should be noted here that the small heater size makes the pool boiling heat transfer performance size dependent. Therefore, results from this study should not be compared with those involving "infinite" heater arrangements, but should be used only to compare the relative pool boiling performance of pure HFE 7200 with that of its mixtures using the same setup. Since all experiments were performed on the same substrate, differences in the incipience superheat, critical heat flux, and figure of merit can be attributed to differences in fluid properties.

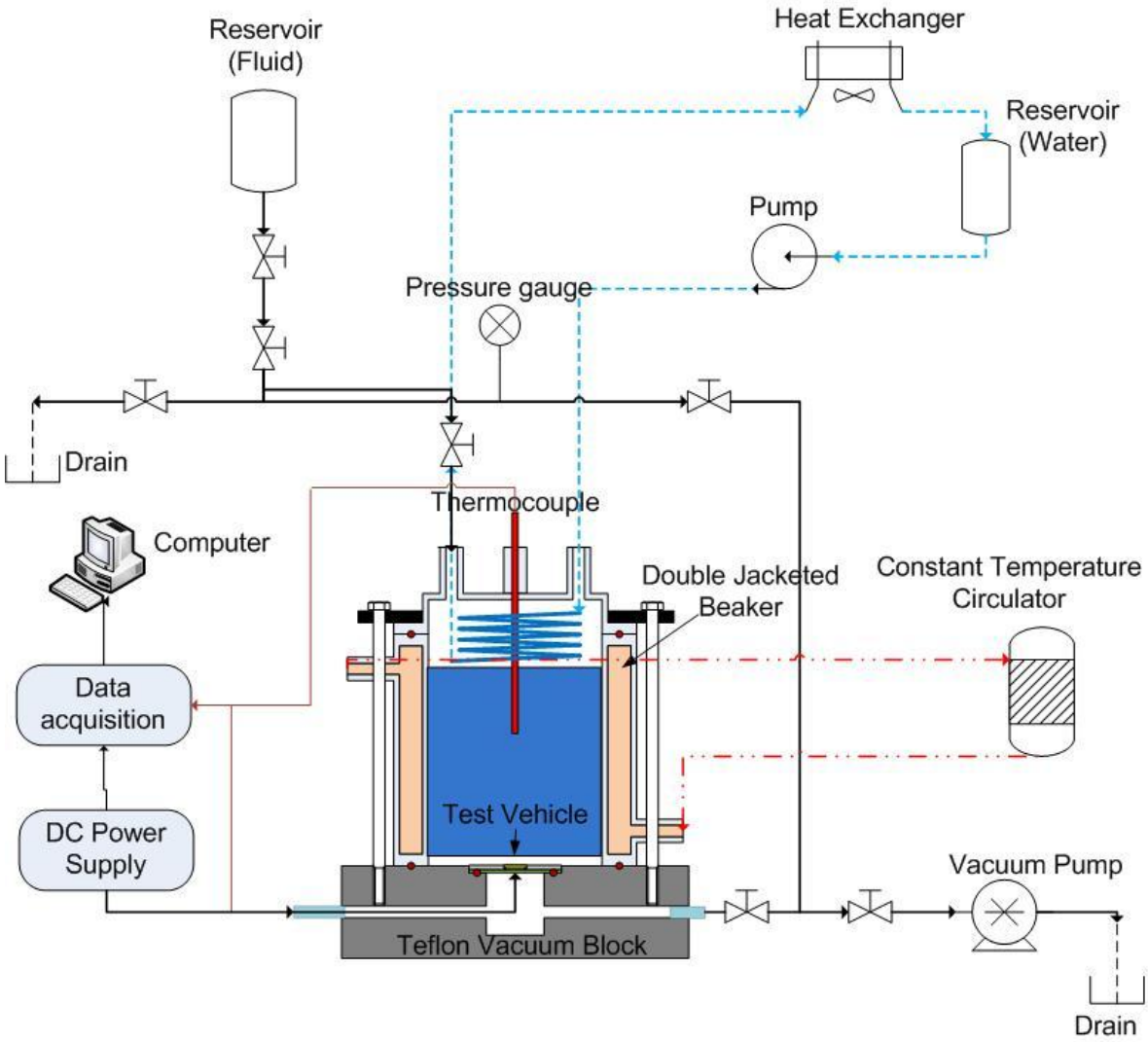

Figure 5.2. Schematic of the pool boiling setup. [25]

Experiments were conducted under saturation conditions at atmospheric pressure. Before starting each experiment, the fluid was degassed by boiling vigorously for 1 hour. After degassing, an experiment was begun by supplying power to the test chip using an Agilent E3645A power supply (0 – 60 V and 0 – 1.3 A).

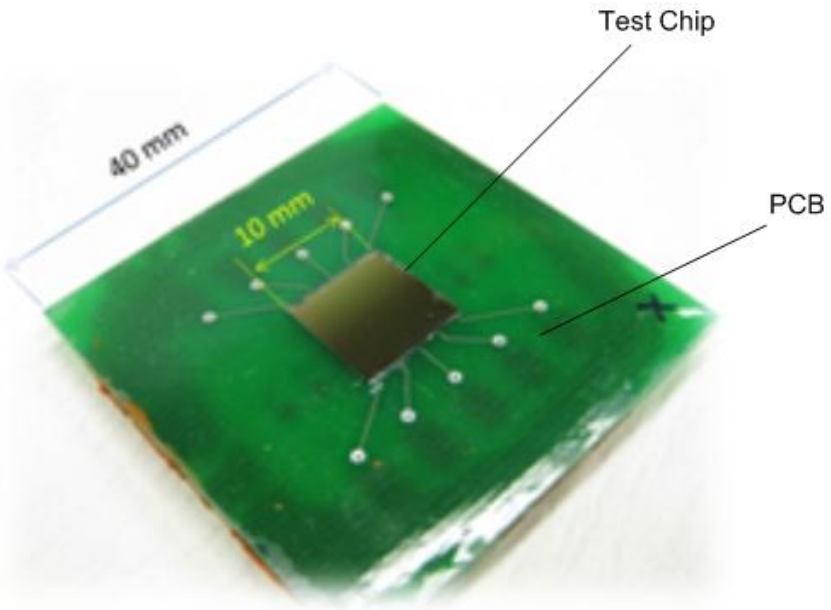

Figure 5.3. Test chip package. [7]

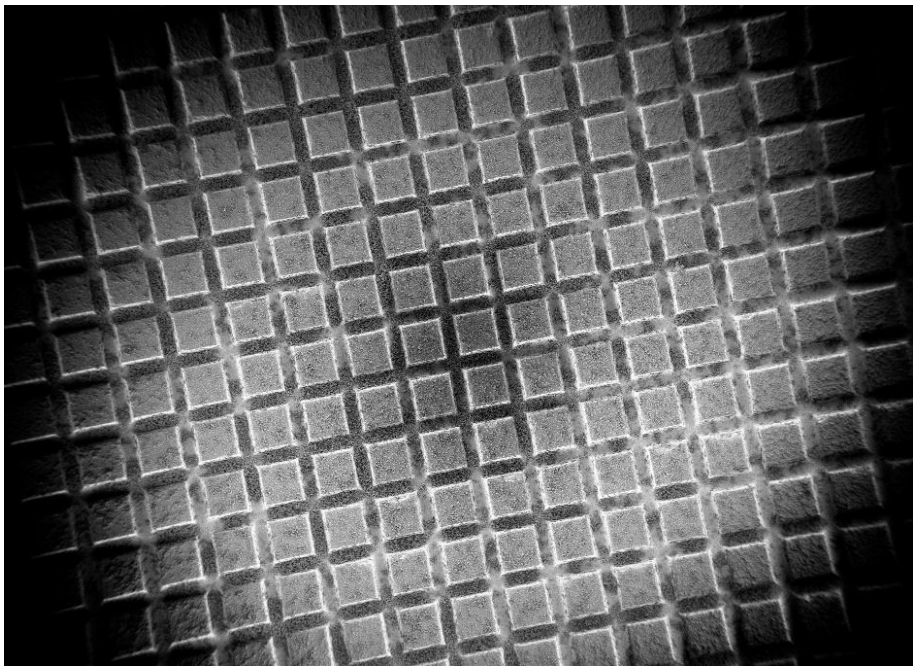

Figure 5.4. Chip surface with copper grooves. [7]

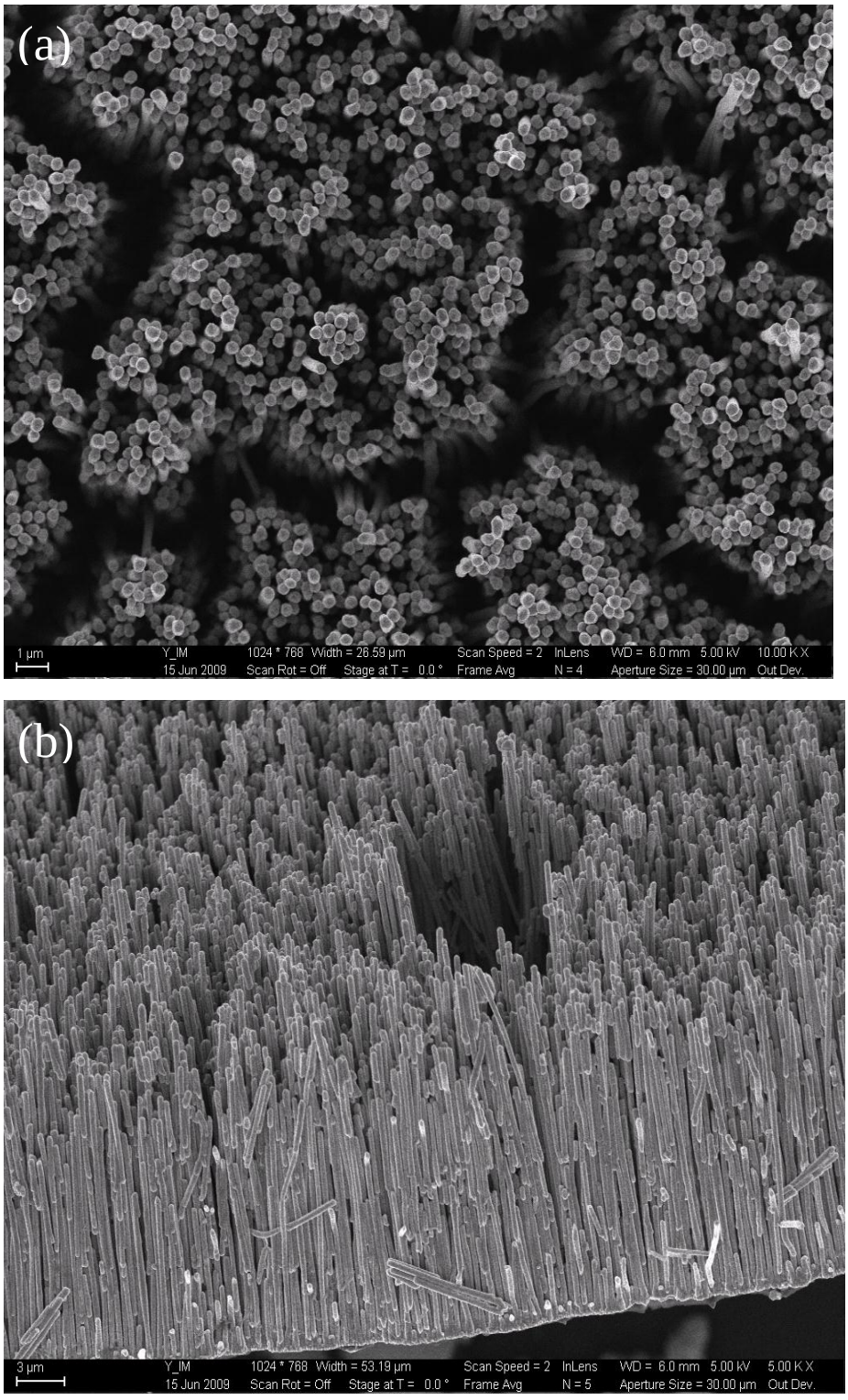

Figure 5.10. Copper nanowires on test chip (a) side view (b) top view. [26]

A platinum resistive thermal device (Pt RTD) fabricated on the back side of the chip was used to measure the chip temperature. Simultaneous heating and temperature

sensing capability were provided by the platinum resistor (shown in Figure 5.6). The heater was calibrated over the entire operating range of the experiment (see Figure 5.7) and the test chip was placed on the heater and shielded from the surroundings by enclosing it in a chamber. The chip was intially at room temperature, which was recorded together with the resistance at this temperature. The hot plate heater temperature was then set to 80 °C, 130 °C, and 180 °C in different runs. The temperature and resistance of the Pt resistor were recorded in each of these runs.

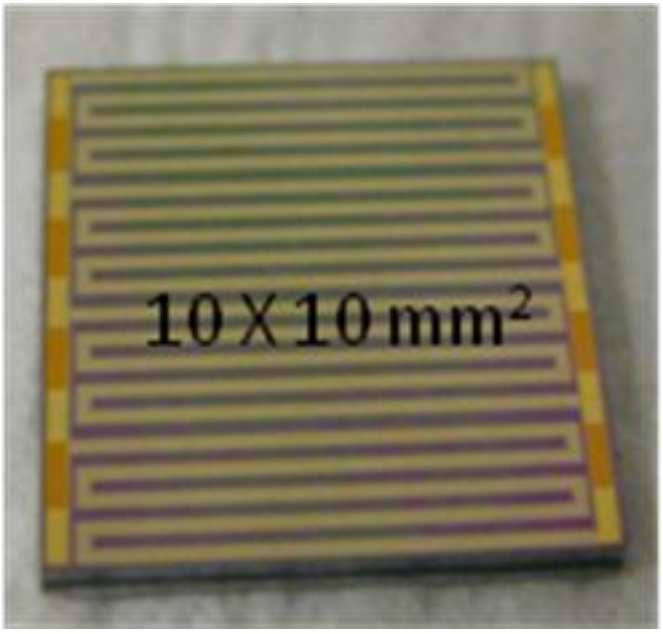

Figure 5.11. Platinum RTD to heat and sense the chip temperature. [26]

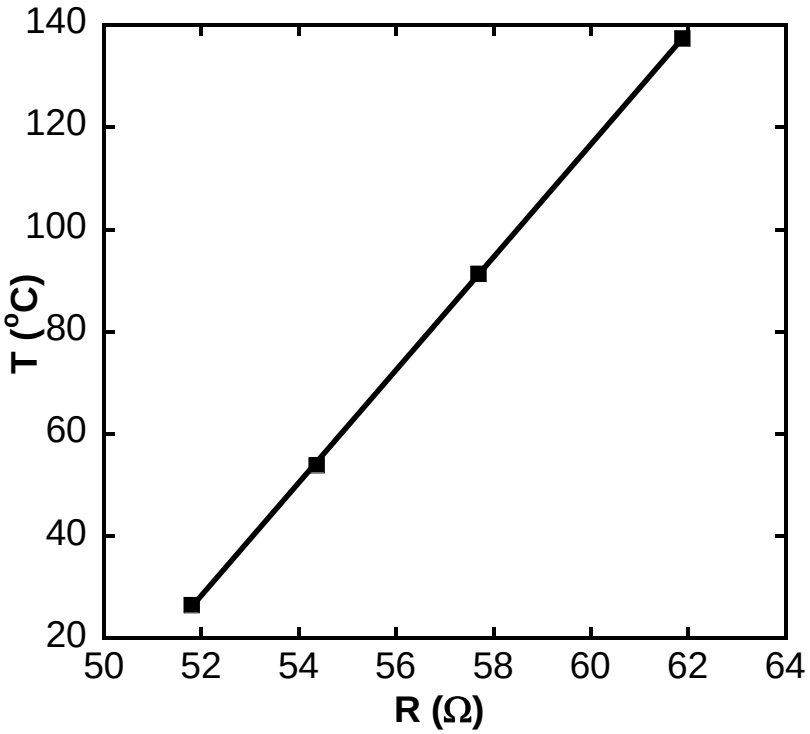

Figure 5.7. Calibration curve for Pt resistor, T (°C) = 11.137R - 552.73. [26]

At each power input, data were recorded once the temperature reading of the test surface reached a steady state (temperature variation less than 0.5 K, achieved within 3-5 minutes). Since the actual test conditions were different from the calibrated conditions of the heater, a corresponding offset was input to rectify the error in the calibrated data. To estimate the offset, the temperature value calculated from the resistance was subtracted from the actual temperature measured using a thermocouple immersed in the liquid bath. The same offset was then used for all the temperature readings of the test surface. An average of at least five readings were taken at each power input at steady state. The uncertainty in the heat flux measurements was estimated from uncertainties in the voltage and current of the DC power supply, and the uncertainty in the measurement of chip surface area following the approach of Kline and McClintock [27]. It was estimated to be 1.6 %. The uncertainty in the wall temperature was estimated from uncertainties in the

resistance and the temperature-resistance calibration curve and was estimated to be 0.77 %.

5.4 Vapor-Liquid Equilibria

Difficulties in custom synthesis and high cost of some of the newly identified coolants prohibited evaluation of pool boiling heat transfer characteristics of pure fluids. Therefore, heat transfer experiments were performed for mixture formulations of newly identified fluids with current coolant HFE 7200. Vapor-liquid equilibria (VLE) play an important role in pool boiling heat transfer of mixtures as the preferential evaporation of the low boiling component can have detrimental effects on heat transfer performance [28]. The deterioration in heat transfer is directly proportional to the difference between dew point and bubble point. The existence of azeotropes is preferred since azeotropes behave as pure fluids and there is no preferential evaporation during pool boiling.

VLE of binary mixtures were evaluated using regular solution theory [29]. Due to significant difference in polarities, VLE of HFE 7200 + methanol mixture were evaluated using COSMO-RS [30]. The results are shown in Figures 5.8 - 5.12. It can be observed that differences between the dew and bubble point are very small for mixtures of new fluids (except methanol) with HFE 7200 for low mole fractions (< ~ 0.3) of the first component. As pool boiling experiments were performed at low concentrations of the new fluids, detrimental effects due to preferential evaporation are likely to be insignificant. Figure 5.12 shows that HFE 7200 + methanol mixtures form a minimum boiling azeotrope at 0.49 mole fraction methanol. Hence, pool boiling experiments were performed at this composition.

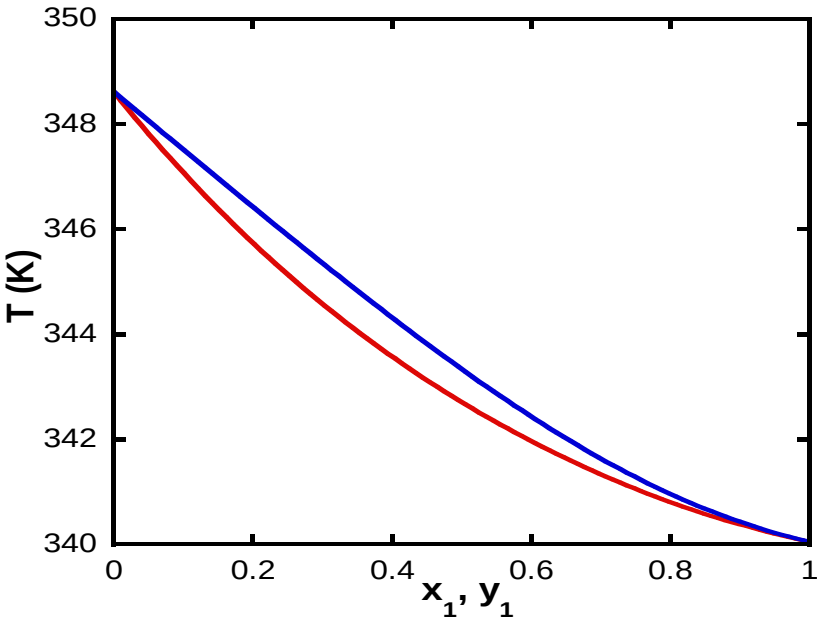

Figure 5.8. VLE for $C_6H_{11}F_3$ (1) + HFE 7200 (2) mixture at 1 atm.

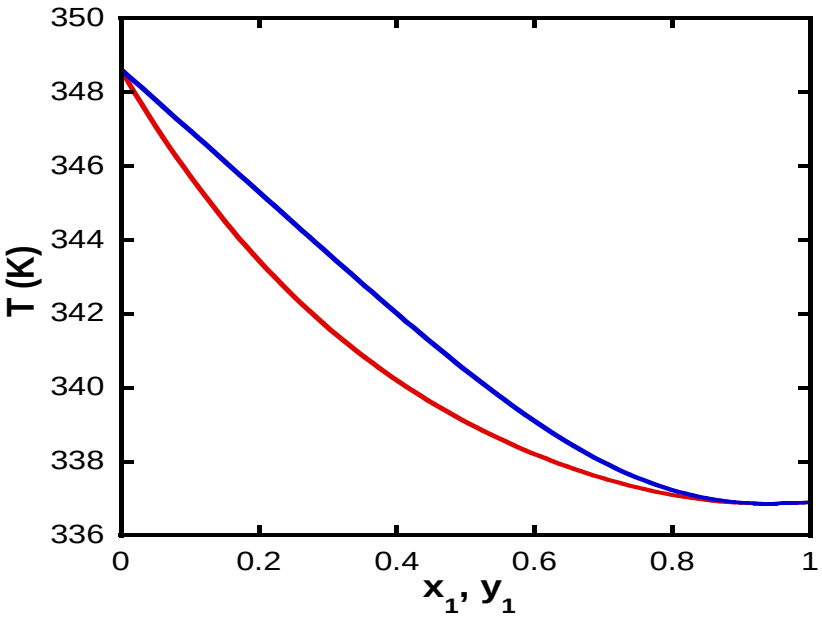

Figure 5.9. VLE for $C_4H_4F_6O$ (1) + HFE 7200 (2) mixture at 1 atm.

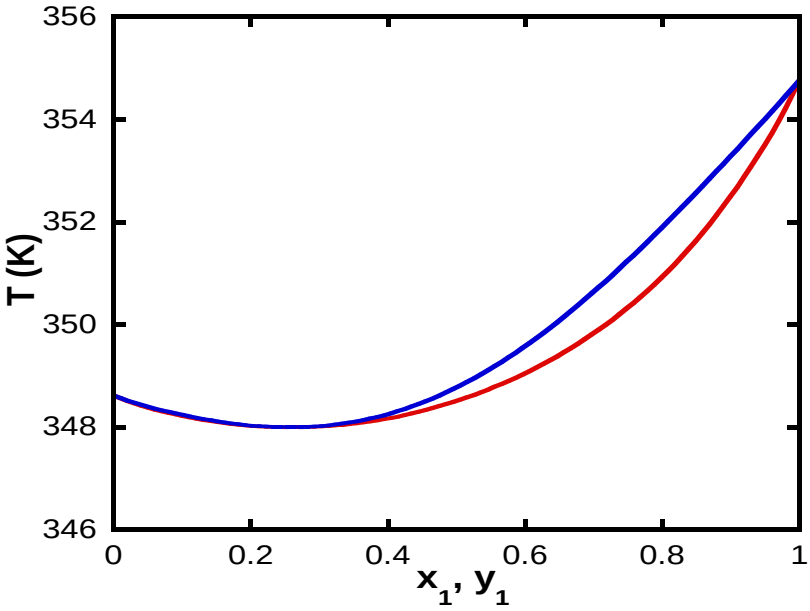

Figure 5.10. VLE for dimethoxydimethyl silane (1) + HFE 7200 (2) mixture at 1 atm.

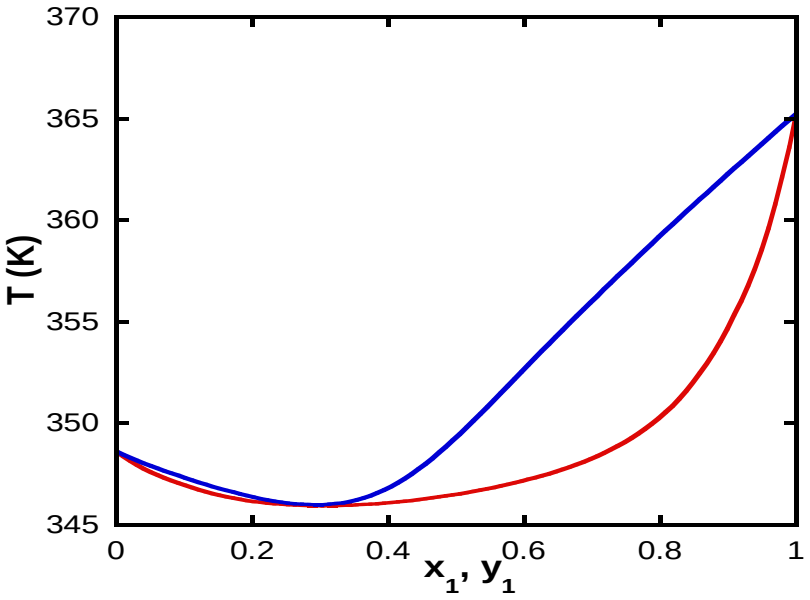

Figure 5.11. VLE for ethoxybutane (1) + HFE 7200 (2) mixture at 1 atm.

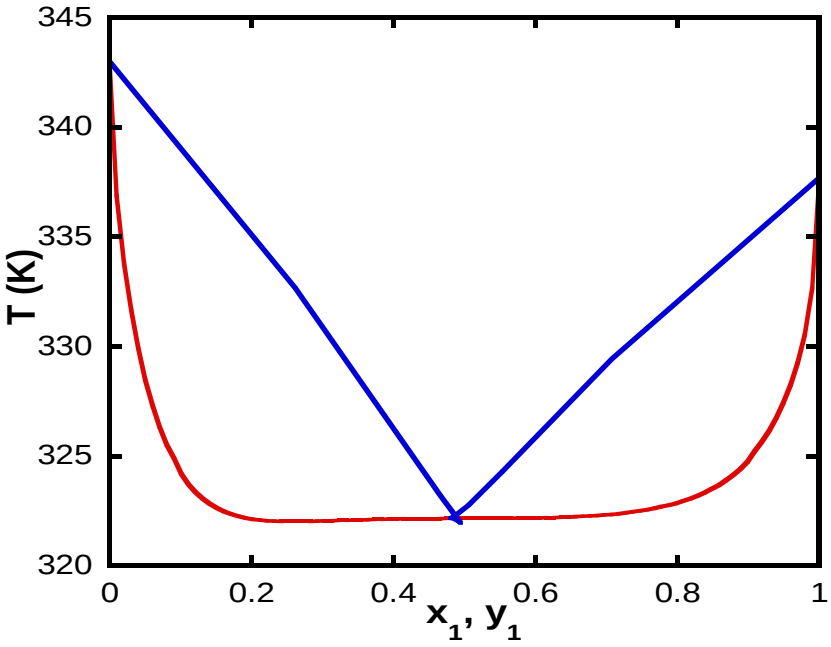

Figure 5.12. VLE for methanol + HFE 7200 mixture at 1 atm predicted using COSMO-RS.

5.5 Pool Boiling Heat Transfer Characteristics

Nucleate boiling is a very efficient mode of heat transfer and is employed in energy conversion and heat exchange systems, and in cooling of high energy density electronic components [31]. As phase change occurs over a small temperature gradient, boiling heat transfer coefficients are often orders of magnitude greater than conduction and convection heat transfer modes. In pool boiling, the heated surface is submerged in a body of stagnant liquid as opposed to flow boiling where liquid flows over the surface by external means. Natural convection and buoyancy effects thus play crucial roles in pool boiling.

A typical pool boiling curve is shown in Figure 5.13 where wall heat flux is plotted against wall superheat (wall temperature minus saturation temperature of the liquid). The pool boiling heat transfer regime of interest is the nucleate boiling regime

that lies between boiling incipience, where there is an initial generation of vapor bubbles from nucleation sites, and the critical heat flux (CHF), where nucleate boiling heat transfer attains its maximum value. The pool boiling curve can be characterized by the wall superheat required for boiling incipience (ΔT_{incip}), and CHF. [31] Incipience superheat determines the wall temperature at which the heat transfer regime shifts from convection to nucleate boiling. Low ΔT_{incip} are, therefore, preferred in boiling heat transfer because the wall temperature can then be maintained close to saturation temperature of the fluid. CHF determines the maximum heat flux that can be removed for a given system (fluid, heater geometry, pressure) and, therefore, should be as high as possible.

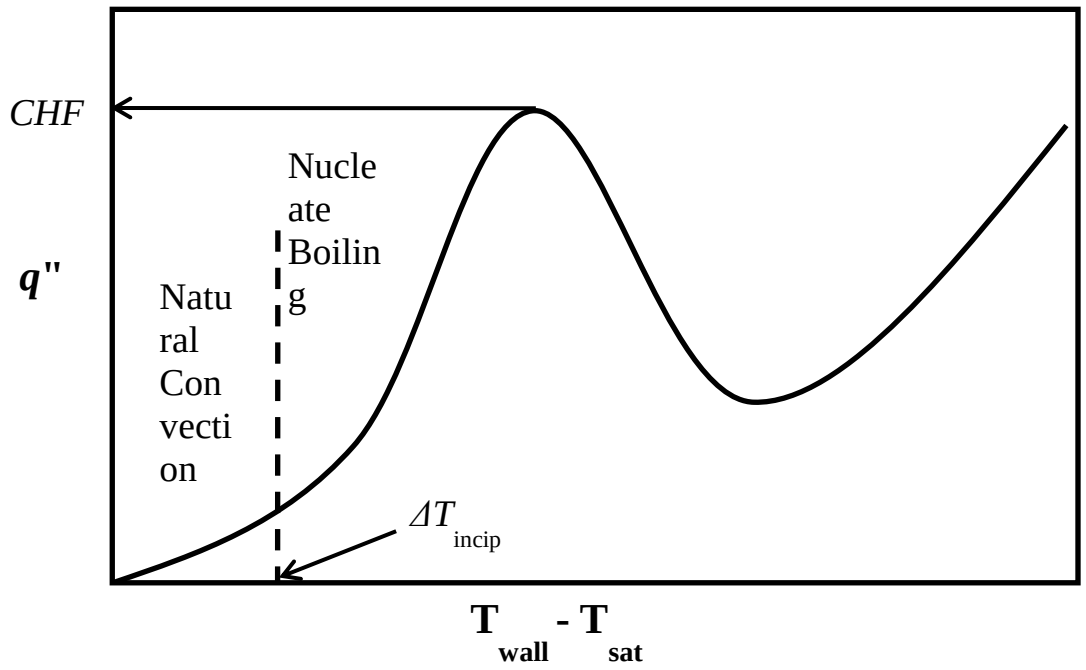

Figure 5.13. Typical pool boiling curve.

Liquids with low surface tensions (e.g. fluorocarbons) wet the surface well. In such liquids, a delay in the onset of nucleation is observed. A sudden inception of a large

number of cavities at a certain wall superheat causes a reduction in the surface temperature, while the heat flux remains constant [31].

5.5.1 Fluids Identified Using CAMD - ICAS

5.5.1.1 HFE 7200 + 1,1,1-trifluoro-3-methylpentane

Pool boiling curves for pure HFE 7200 and HFE 7200 + 7 wt. % 1,1,1-trifluoro-3-methylpentane ($C_6H_{11}F_3$) are shown in Figure 5.14. These experiments were performed on a chip surface with Cu grooves. The enhancement in critical heat flux (CHF) for this fluid mixture over pure HFE 7200 was 6.9 %, whereas the wall superheat for the onset of nucleate boiling was similar for both pure HFE 7200 and the mixture of $C_6H_{11}F_3$ and HFE 7200. This suggests that the addition of larger amounts of $C_6H_{11}F_3$ is likely to lead to further improvements in CHF. Therefore, the heat transfer performance of pure $C_6H_{11}F_3$ is likely to be significantly better than that of HFE 7200 in electronics cooling applications [7].

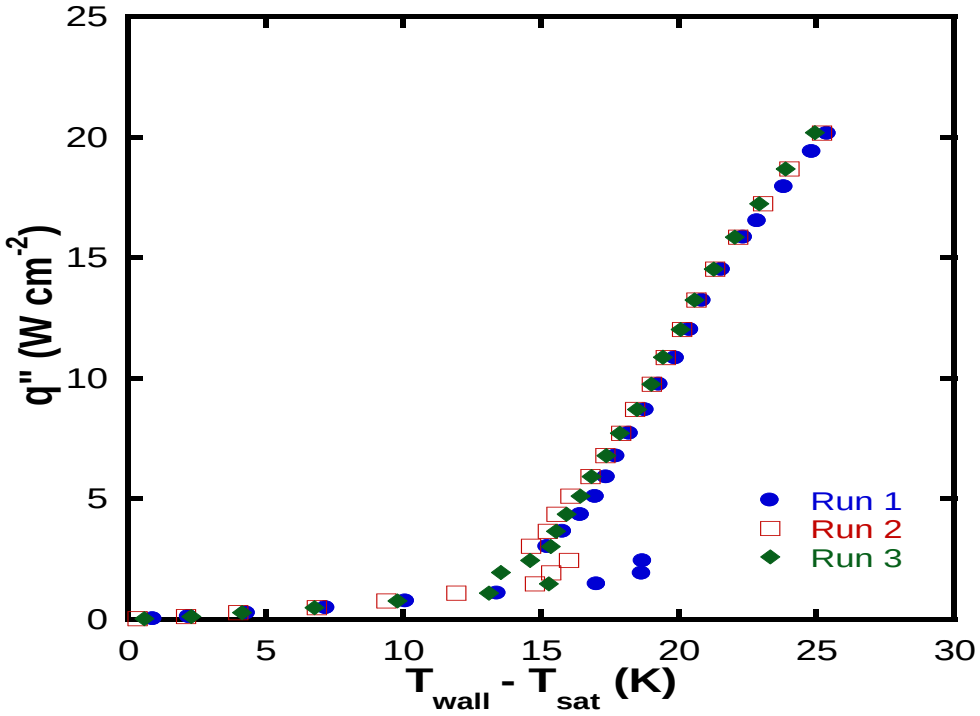

5.14 (a) HFE 7200

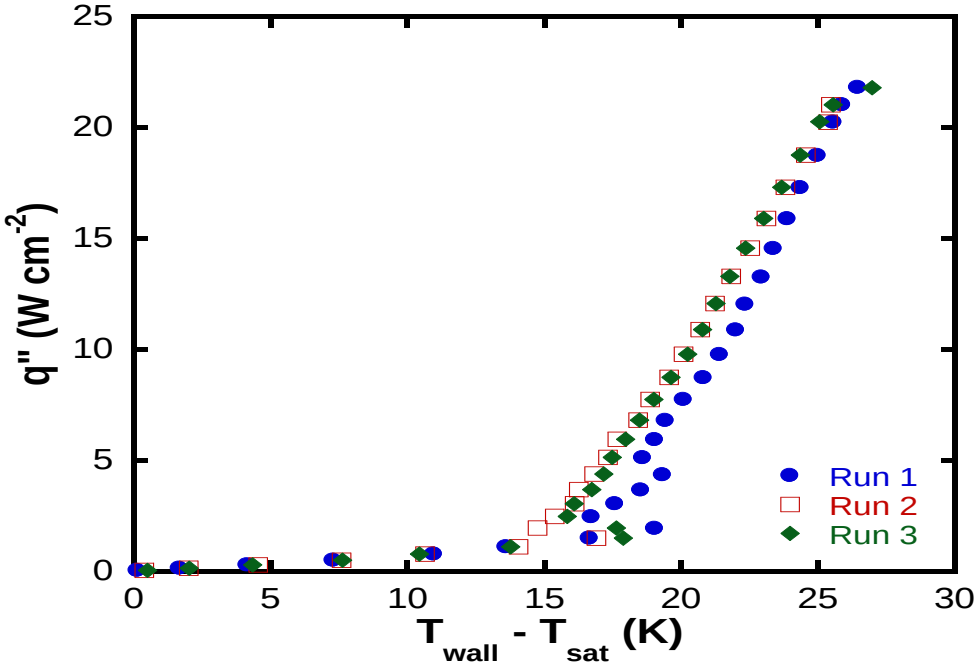

5.14 (b) HFE 7200 + 7 wt. % $C_6H_{11}F_3$

Figure 5.14. Pool boiling curve for (a) HFE 7200 and (b) HFE 7200 + 7 wt. % $C_6H_{11}F_3$ mixture. [7]

5.5.1.2 HFE 7200 + bis(2,2,2-trifluoroethyl)ether

Bis(2,2,2-trifluoroethyl)ether ($C_4H_4F_6O$) was used as a surrogate for 1,1,1-trifluoro-3-(2,2,2-trifluoroethoxy)propane ($C_5H_5F_6O$) which could not be synthesized in sufficient quantities for experimental evaluation. Pool boiling experiments for a mixture of HFE 7200 + 10 wt. % $C_4H_4F_6O$ were performed on a chip surface with Cu grooves and are shown in Figure 5.15 for pure HFE 7200 and its mixture with $C_4H_4F_6O$. It was observed that the addition of 10 wt. % bis(2,2,2-trifluoroethyl)ether resulted in 8.4 % increase in CHF over that of pure HFE 7200 without significant increase in incipience superheat [32]. Given the similarity in chemical structure and close thermophysical property values, 1,1,1-trifluoro-3-(2,2,2-trifluoroethoxy)propane is also expected to better heat transfer performance than HFE 7200.

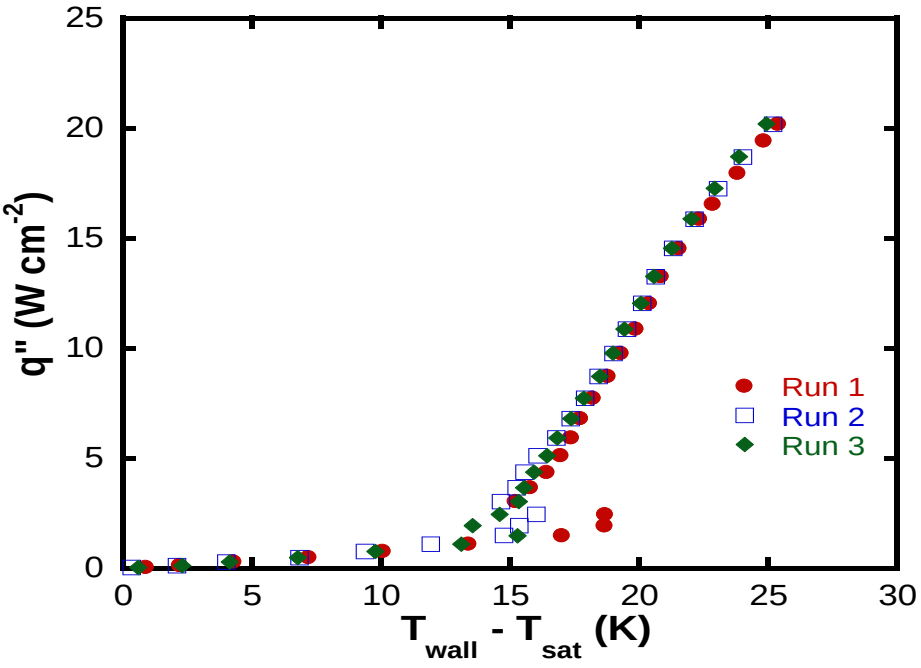

5.15 (a) HFE 7200

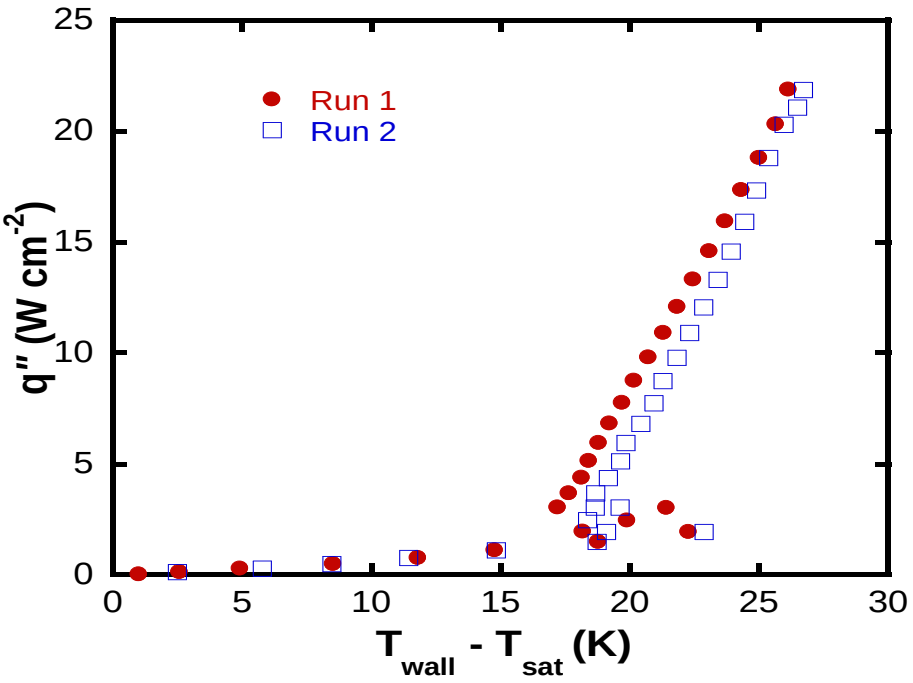

5.15 (b) HFE 7200 + 10 wt. % $C_4H_4F_6O$

Figure 5.15. Pool boiling curve for (a) HFE 7200 and (b) HFE 7200 + 10 wt. % $C_4H_4F_6O$ mixture. [32]

5.5.2 Fluids Identified Using CAMD of Organosilicon Compounds

Pool boiling curves for pure HFE 7200 and a mixture of dimethoxydimethylsilane ($C_4H_{12}O_2Si$) and HFE 7200 (10:90 w/w) are shown in Figure 5.16 [33]. These experiments were also performed on the test surface with Cu grooves. The CHF of pure HFE 7200 was found to be 16.9 W cm^{-2} whereas that for the dimethoxydimethylsilane + HFE 7200 mixture was 19.9 W cm^{-2}, an enhancement of 17.8 %. In addition, the incipience temperature of the mixture was found to be lower than that of pure HFE 7200. The results indicate that addition of dimethoxydimethylsilane to HFE 7200 improves heat transfer performance, although it should be added that the incipience temperature for Run 1 was higher than for Run 2 in both pure HFE 7200 and the mixture. This could be because of vapor trapped in the cavities after Run 1. As Run 2 is performed immediately

after Run 1, the trapped vapor lowers the wall superheat required for activating nucleation sites.

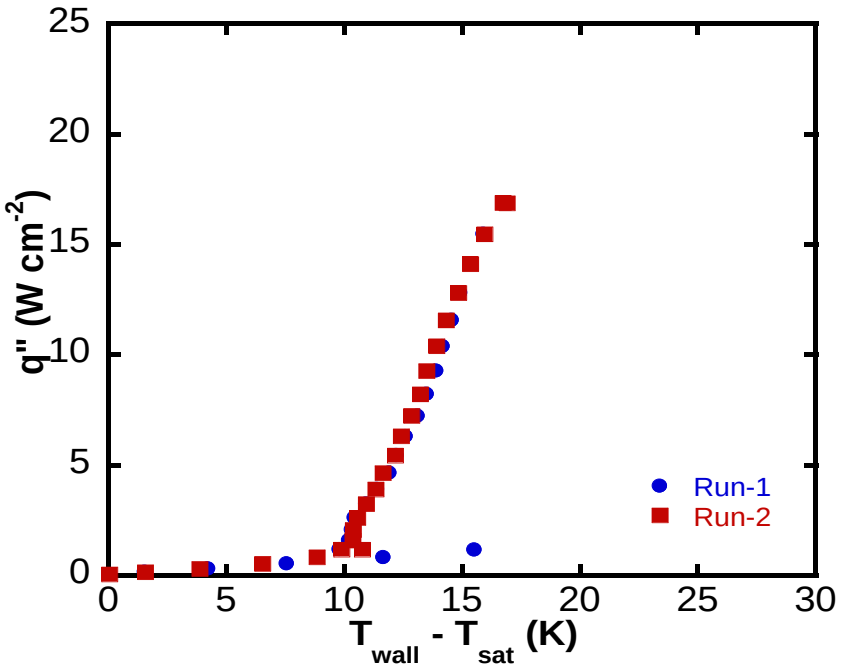

5.16 (a) HFE 7200

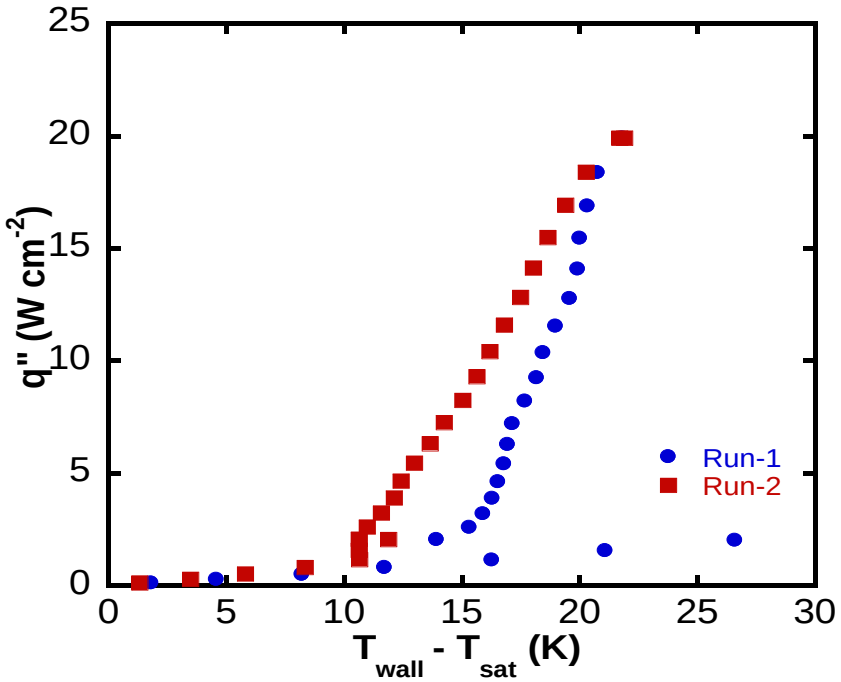

5.16 (b) HFE 7200 + 10 wt. % dimethoxydimethylsilane

Figure 5.16. Pool boiling curves for (a) HFE 7200 and (b) HFE 7200 + 10 wt. % dimethoxydimethylsilane mixture. [33]

5.5.3 Fluids Identified as Additives for HFE 7200

Boiling curves for pure HFE 7200 and its mixtures with methanol (10:90 w/w) and ethoxybutane (10:90 w/w) on the chip surface with a Cu nanowire array are shown in Figure 5.17 [11]. CHF values for both mixtures are higher than that for pure HFE 7200. The addition of methanol increased incipience superheat by about 10 K. Ethoxybutane, on the other hand, had very little effect on the incipience superheat. Based on the experimental results presented above, ethoxybutane appears to be a better candidate for designing mixture formulations with HFE 7200 for pool boiling applications.

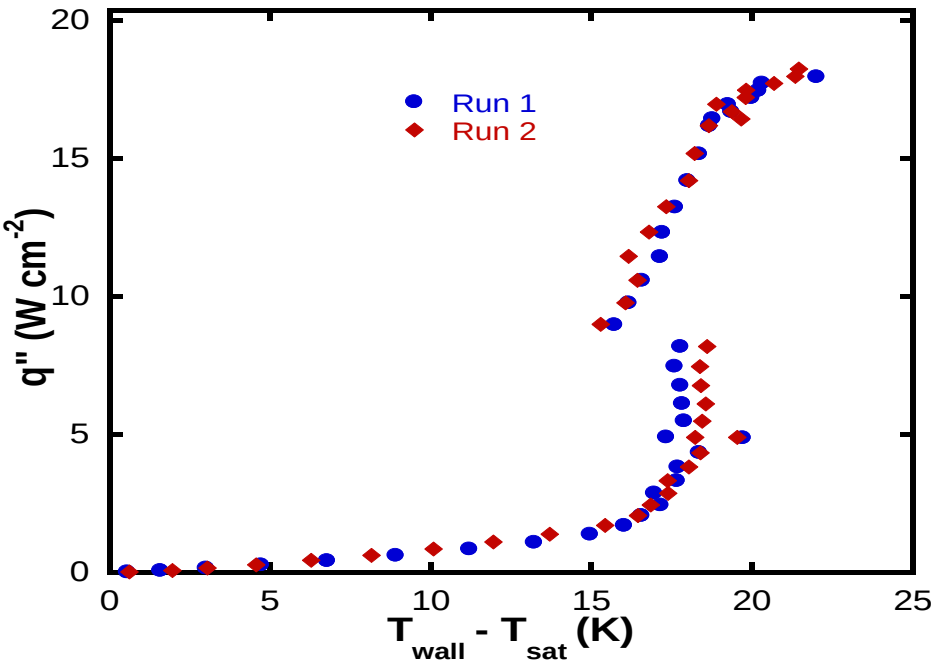

5.17 (a) HFE 7200

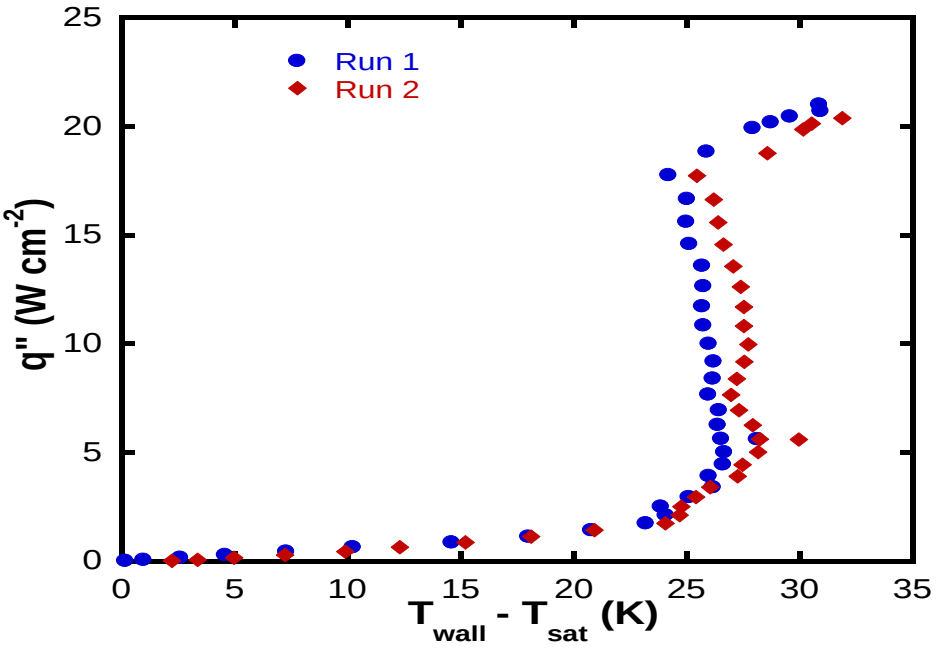

5.17 (b) HFE 7200 + 10 wt. % methanol.

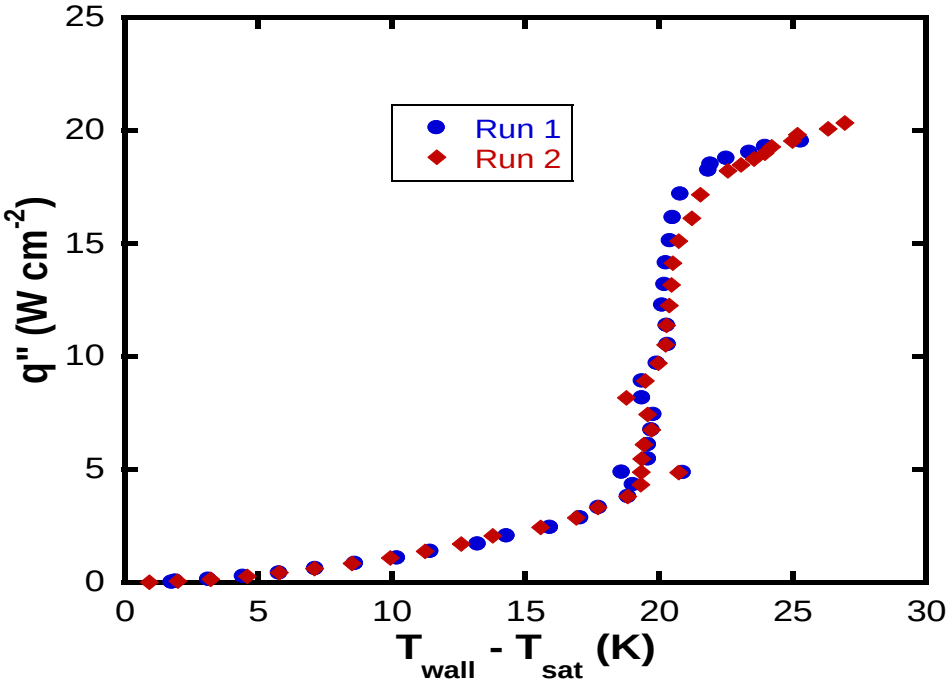

5.17 (c) HFE 7200 + 10 wt. % ethoxybutane.

Figure 5.17. Pool boiling curves for (a) HFE 7200 (b) HFE 7200 + 10 wt. % methanol mixture, and (c) HFE 7200 + 10 wt. % ethoxybutane mixture. [26]

The increase in CHF over that of pure HFE 7200 upon addition of newly identified fluids is listed in Table 5.10. It can be observed that all fluids evaluated in this

work exhibit higher CHF than pure HFE 7200. Therefore, fluorinated fluids ($C_6H_{11}F_3$, $C_4H_4F_6O$, and $C_5H_6F_6O$) identified using CAMD can be used for direct immersion cooling of electronic systems as pure fluids. Organosilicon fluid ($C_4H_{12}O_2Si$) and ethoxybutane may be used for designing mixture formulations with existing or newly identified coolants. However, commercial development may require further investigations with respect to optimal composition and chemical compatibility of the mixture with electronic components.

Table 5.10. Increase in CHF over HFE 7200 for fluids identified in this work.

Fluid	Concentration (wt. %)	Increase in CHF (%)
$C_6H_{11}F_3$	7	6.9
$C_4H_4F_6O$	10	8.4
$C_4H_{12}O_2Si$	10	20.1
CH_3OH	10	24.0
$C_4H_9OC_2H_5$	10	13.9

This work has thus provided the experimental verification that heat transfer fluids identified using CAMD have superior heat transfer performance than current coolants. It should be noted that the fluids evaluated in this work are not the top ranked candidates based on their FOM (see Tables 3.5-3.8). Therefore, top ranked candidates are likely to exhibit superior heat transfer properties.

5.6 Conclusions

Density, viscosity, thermal conductivity, electrical resistivity, and pool boiling heat transfer performances of newly identified fluids are reported in this chapter, as are

VLE and a rough hard-sphere correlation for transport properties of mixtures. Finally, pool boiling heat transfer studies show that new fluids identified in this work have superior heat transfer properties than existing coolant HFE 7200.

5.7 References

1. Marsh, K. N. (ed.), *Recommended reference materials for the realization of physicochemical properties*, 1987. Boston: Blackwell Scientific Publications.

2. Rowley, R. L., Wilding, W. V., Oscarson, J. L., Yang, Y., and Giles, N. F., *DIPPR® Data Compilation of Pure Chemical Properties*, 2010. Design Institute for Physical Properties, http://dippr.byu.edu, Brigham Young University, Provo, Utah.

3. Levitin G. and Hess, D. W., *Ionic conductivity of elevated pressure $TMAHCO_3/MeOH/CO_2$ mixtures*, Electrochemical and Solid State Letters, 2005. **8**(1): p. G23-G26.

4. Properties of HFE 7200 from 3M company, available at: http://multimedia.3m.com/mws/mediawebserver?66666UuZjcFSLXTtnx&y5xz6EVuQEcuZgVs6EVs6E666666-- (accessed April 2012).

5. Bleazard J. G. and Teja, A. S., *Thermal conductivity of electrically conducting liquids by the transient hot-wire method*, Journal of Chemical and Engineering Data, 1995. **40**: p. 732-737.

6. Diguilio R. and Teja, A. S., *Thermal conductivity of poly(ethylene glycols) and their binary mixtures*, Journal of Chemical and Engineering Data, 1990. **35**(2): p. 117-121.

7. Warrier, P., Sathyanarayana, A., Patil, D. V., France, S., Joshi, Y., and Teja, A. S., *Novel heat transfer fluids for direct immersion phase change cooling of electronic systems*, International Journal of Heat and Mass Transfer, 2012. **55**: p. 3379–3385.

8. Chandler, D., *Rough hard sphere theory of the self-diffusion constant for molecular liquids*, Journal of Chemical Physics, 1975. **62**: p. 1358-1363.

9. Dymond, J. H., *Hard-sphere theories of transport properties*, Quarterly Reviews of the Chemical Society, 1985. **3**: 317-356.

10. Dymond, J. H., *Corrections to Enskog Theory for Viscosity and Thermal Conductivity*, Physica, 1987, **144B**: p. 267-276.

11. Assael, M. J., Dymond, J. H., Papadaki, M., and Patterson, P. M., *Correlation and prediction of dense fluid transport coefficients. I. n-Alkane*s, International Journal of Thermophysics, 1992. **13**: p. 269-281.

12. Assael, M. J., Dymond, J. H., and Polimatidou, S. K., *Correlation and prediction of dense fluid transport coefficients. IV. n-Alkanols*, International Journal of Thermophysics, 1994. **15**: p. 189-201.

13. Assael, M. J., Dymond, J. H., and Polimatidou, S. K., *Correlation and prediction of dense fluid transport coefficients. V. Aromatic Hydrocarbons*, International Journal of Thermophysics, 1992. **13**: p. 895-905.

14. Assael, M. J., Dymond, J. H., and Polimatidou, S. K., *Correlation and prediction of dense fluid transport coefficients*, International Journal of Thermophysics, 1995. **16**: p. 761-772.

15. Teja, A. S., Smith, R. L., King, R. K., and Sun, T. F., *Correlation and prediction of the transport properties of refrigerants using two modified rough hard-sphere models*, International Journal of Thermophysics, 1999. **20**: 149-161.

16. Bleazard, J. G., and Teja, A. S., *Extension of the Rough Hard-Sphere Theory for Transport Properties to Polar Liquids*, Industrial and Engineering Chemistry Research, 1996. **35**: 2453-2459.

17. Sun, T., and Teja, A. S., *Correlation and prediction of the viscosity and thermal conductivity of dense fluids*, Journal of Chemical and Engineering Data, 2009. **54**: p. 2527-2531.

18. Sun, T., and Teja, A.S., *Density, viscosity and thermal conductivity of aqueous solutions of propylene glycol, dipropylene glycol, and tripropylene glycol between 290 K and 460 K*. Journal of Chemical and Engineering Data, 2004. **49**: p. 1311-1317.

19. 3M Novec HFE7200 datasheet. http://multimedia.3m.com/mws/mediawebserver?mwsId=SSSSSu7zK1fslxtU4Y_G5x_Gev7qe17zHvTSevTSeSSSSSS-- (accessed April 2012).

20. Qunfang, L., and Yu-Chun, H., *Correlation of viscosity of binary liquid mixtures*, Fluid Phase Equilibria, 1999. **154**: p. 153-163.

21. Brunet, J. and Gubbins, K. E., *Viscosity of binary liquid mixtures near the critical mixing point*, Transactions of the Faraday Society, 1969. **65**: 1255-1266.

22. Warrier, P., and Teja, A. S., *Density, viscosity, and thermal conductivity of mixtures of 1-ethoxy-1,1,2,2,3,3,4,4,4-nonafluorobutane (HFE 7200) with methanol and 1-ethoxybutane*, Journal of Chemical and Engineering Data, 2011. **56**: p. 4291-4294.

23. Im, Y., *Copper nanowire and flower-like CuO nanostructure surfaces for enhanced boiling*, PhD Thesis, 2009. Daejeon, South Korea: Department of Mechanical Engineering, Korea Advanced Institute of Science and Technology.

24. Im, Y., Joshi, Y., Dietz, C., and Lee, S. S., *Enhanced boiling of a dielectric liquid on copper nanowire surfaces*, International Journal of Micro-Nano Scale Transport, 2010. **1**: p. 79-96.

25. Sathyanarayana, A., Warrier, P., Joshi, Y., and Teja, A. S., *Saturated and subcooled pool boiling of HFE 7200 mixtures on a copper nanowire surface*, Frontiers in Heat and Mass Transfer, 2011. **2**: p. 043007.

26. Warrier, P., Sathyanarayana, A., Joshi, Y., and Teja, A. S., *Screening and evaluation of mixture formulations for electronics thermal management using pool boiling*, IEEE Transactions on Components and Packaging Technology, 2011. **1**: p. 1387-1394.

27. Kline, S. J. and McClintock, F. A., *Describing uncertainties in single-sample experiments*, Mechanical Engineering, 1953. **75**: p. 3-8.

28. Nahra Z. and Nass, E., *Heat transfer in pool boiling of binary and ternary non-azeotropic mixtures*, Heat and Mass Transfer, 2009. **45**(7): p. 951-958.

29. Prausnitz, J. M., Lichtenthaler, R. M., and De Azevedo, E. G., *Molecular thermodynamics of fluid-phase equilibria*, 1998. New Jersey: Prentice Hall.

30. Klamt, A., *COSMO-RS: from quantum chemistry to fluid phase thermodynamics and drug design*, 2005. Elsevier, The Netherlands.

31. Dhir, V. K., *Boiling heat transfer*, Annual Reviews of Fluid Mechanics, 1998. **30**: p. 365-401.

32. Sathyanarayana, A., Warrier, P., Im, Y., Joshi, Y., and Teja, A. S., *Pool boiling of HFE 7200 - $C_4H_4F_6O$ mixture on hybrid micro-nano structured surface*, ASME Journal of Nanotechnology in Engineering and Medicine, 2012. (Submitted)

33. Warrier, P., Sathyanarayana, A., Bazdar, S., Joshi, Y., and Teja, A. S., *Selection and evaluation of organosilicon coolants for direct immersion cooling of electronic systems*, Industrial and Engineering Chemistry Research, 2012. (Submitted).

CHAPTER 6

GLOBAL WARMING POTENTIAL OF NEW COOLANTS

In this chapter, a new group contribution (GC) method for estimating radiative forcing (RF) of fluorocarbons is described. The method is used to calculate the global warming potential (GWP) of newly identified heat transfer fluids for direct immersion cooling of electronics. Validation of the GC method is provided by comparing GC estimates of RF for 5 coolants with measurements of RF using FT-IR spectroscopy. Finally, GWP estimates for 33 new coolants and existing coolants are presented.

6.1 Introduction

Hydrofluorocarbons (HFC), perfluorocarbons (PFC), and hydrofluoroethers (HFE) are increasingly being used to replace chlorofluorocarbon (CFC) and hydrochlorofluorocarbon (HCFC) in refrigeration, and in other applications. [1] It is estimated that the effect of these fluorocarbons and fluoroethers on global warming will increase significantly in the coming years because of such substitutions. [2] There is, therefore, much interest in identifying environmentally benign alternatives to these fluoro-compounds for heat transfer applications. Tables 3.5 and 3.6 show that most fluids identified in this work as candidates for direct immersion cooling of electronics are fluorinated. [3] It is therefore very important to assess the climate impact of these fluids before considering them for further evaluation. Here, a new method for estimation of the GWP of these fluids is outlined and comparisons with the GWP of currently used

coolants are shown. The calculation of GWP employs values of radiative forcing (RF), reaction rate constant involving the OH radical (k_{OH}), and atmospheric lifetime (τ) of the fluid. A new GC method is therefore presented for estimating RF based on published RF data for over 75 fluorocarbons. The method was validated by comparison with new measurements of RF using FT-IR spectroscopy. Calculation of k_{OH} was done using the updated Kwok-Atkinson method [4] employed in the EPI 4.10 (Estimation Programs Interface) [5] available from US EPA.

6.2 Group Contribution Method for Radiative Forcing

Radiative forcing (RF) is generally used to assess the impact that a compound can have on climate change and is quantified by the rate of energy change per unit area of the globe measured at the tropopause. [6] RF is directly proportional to the global annual mean temperature change at the Earth's surface. Hence greenhouse gases (CO_2, CH_4, fluorocarbons, etc.) with positive RF values are associated with an increase in the Earth's mean temperature and cause global warming. Greenhouse gases absorb strongly in the atmospheric window (1500 cm^{-1} - 500 cm^{-1}) and prevent outgoing terrestrial radiation from escaping the Earth's atmosphere. As the frequency of the vibrational stretching mode of the C-F bond occurs in the atmospheric window, fluorocarbons tend to have large RF values. For greenhouse gases, RF is calculated for a 1 ppbv increase in the concentration of the gas in the troposphere. The existing methods for predicting RF of greenhouse gases include quantum chemical method that predicts IR spectra using density functional theory [7, 8] and structure-activity relations [9]. Both methods report average absolute deviations of about 25 % from experimental values. Moreover,

structure-activity relationships [9] are available only for fluoroethers. As the absorption spectrum of a molecule depends on the constituting functional groups, it is hypothesized that RF can be expressed by a mathematical function comprising contributions of each group towards RF. To estimate the contribution of each group, RF data on fluorocarbons were compiled and regressed. Data for over 75 fluorocarbons was compiled from various sources [6-14] and checked for consistency before being employed in the development of the GC estimation method. Group contributions C_i were obtained by regression of the evaluated data using the following function:

$$RF = \sum_i n_i C_i \tag{6.1}$$

In equation 6.1, n_i is the number of times that group *i* appears in the molecule, and C_i is the contribution that group *i* makes to RF. Selection of groups was based on *ab initio* molecular orbital calculations by Wu and Sandler [15] who used such calculations to obtain theoretically defined functional groups. Higher order groups such as $CH_xCl_yF_z$ were not considered in this work because of the limited dataset employed. An additional contribution was included for fluorine bonded to a carbon that is also bonded to an oxygen atom (labeled as F(O)). This was based on the study by Bera *et al.* [16] who pointed out that such proximity of fluorine and oxygen results in larger IR intensities for C-F stretches. GC values (C_i) were obtained by minimizing the average absolute deviation (AAD) between predicted and literature values of RF using a nonlinear generalized reduced gradient (GRG) solver. As the GRG algorithm often finds local minima, many initial guesses were tested and the lowest minimum was selected. The reliability of the method was assessed by comparing *J* values calculated by regressing

data sets with random subsets of N data points removed from each set, as suggested by Marrero and Gani [17]. The residual (J) was calculated as follows:

$$J = \sum \frac{\left| X_i - Y_i \right| / X_i}{N} \times 100 \tag{6.2}$$

where, X_i and Y_i are property values of compound i estimated using full and partial data sets.

6.3 Estimation of k_{OH}, τ, and GWP

The overall impact of a compound on climate is evaluated in terms of global warming potential (GWP) that considers both the RF value of the compound and its atmospheric lifetime (τ). GWP is defined by IPCC [6] as the time-integrated global mean RF of a pulse emission of 1 kg of compound i relative to that of 1 kg of the reference gas CO_2 and is given by:

$$GWP_i = \frac{RF_i \int_0^{TH} \exp\left(-t/\tau_i\right) \Big/ MW_i}{AGWP_{CO2}^{TH} / MW_{CO2}} \tag{6.3}$$

where, TH is the time horizon (20, 100, or 500 years), MW is the molecular weight (g/mol), and $AGWP_{CO2}^{TH}$ is the absolute GWP of CO_2 over the chosen time horizon. In this work, 0.235, 0.768, and 2.459 W year m^{-2} $ppmv^{-1}$ were used for time horizons of 20, 100, and 500 years respectively for $AGWP_{CO2}^{TH}$. [7] It should however be noted that $AGWP_{CO2}$ values can vary up to 20 % depending on the models used to calculate the RF and response function of CO_2.

The atmospheric lifetime (τ) of a compound depends on its reactivity with the atmospheric OH radical (OH·). Reaction with atmospheric OH· can proceed via 4 possible pathways: abstraction of an H atom from C-H and O-H bonds; addition of OH· to double and triple bonds between 2 carbon atoms; OH· addition to aromatic rings; and interaction of OH· with N, S, and P atoms. [4] The reaction rate constant with OH· or k_{OH} (cm^3 molecule $^{-1}$ s^{-1}) at 298 K was estimated using the updated Kwok-Atkinson method employed in EPI 4.10 software [5]. Kwok and Atkinson [4] have reported that the method can predict k_{OH} values within a factor of 2 of experimental values for many compounds. τ (years) was calculated with reference to that of CH_3CCl_3 using the following relation:

$$\tau = \tau_{CH3CCl3} \times \frac{k_{OH-CH3CCl3}}{k_{OH}} \tag{6.4}$$

Values of τ and k_{OH} for CH_3CCl_3used in this work were 6.7×10^{-15} cm^3 molecule $^{-1}$ s^{-1} and 5.7 years respectively. [7]

6.4 Experimental

6.4.1 Materials

HFE 7200 (> 98 %) and PF 5060 (> 98 %) were purchased from 3M company, MN. 1,1,1-trifluoro-2-butanone (> 95 %) and 1,1,1-trifluoro-3-methylpentane (> 90 %) were purchased from SynQuest Labs, FL. 4,4,4-trifluoro-2-butanone (> 97 %) was purchased from Matrix Scientific, SC, USA. These fluids were used without further purification.

6.4.2 ATR FT-IR

FT-IR spectra were recorded with a Shimadzu IR Prestige-21 FT-IR spectrophotometer using the heated golden attenuated total reflectance (ATR) accessory (Specac Ltd., RI, USA). The ATR accessory employs a type IIa diamond optical crystal and ZnSe focusing lenses. All measurements were performed at room temperature at a resolution of 0.5 cm^{-1}. It should be noted that the average tropospheric temperature of 277 K should be used for evaluating RF and k_{OH}. However, because of the very weak dependence of RF and k_{OH} on temperature, the differences in RF and k_{OH} values between 277 K and 298 K are likely to be negligible. [8] Following the work of Elrod [18], the FT-IR absorbance spectrum in the atmospheric window (500 cm^{-1} to 1500 cm^{-1}) was divided into one hundred 10 cm^{-1} intervals. The RF (W m^{-2}) for a 1 ppbv increase was then calculated using the narrow band model of Pinnock *et al.* [13] as follows:

$$RF = \sum_{i=0}^{100} \sigma_i F_i^{\sigma} \tag{6.5}$$

where σ_i (cm^2 $molecule^{-1}$ cm^{-1}) is the integrated absorption cross section over each 10 cm^{-1} interval and F_i^{σ} in units of W m^{-2} $(cm^{-1})^{-1}$ $(cm^2$ $molecule^{-1})^{-1}$ is the RF per unit cross section per inverse centimeter for the spectral interval *i* for the average Earth sky. The integrated absorption cross section (σ) was calculated for each interval using the Beer-Lambert law [19]:

$$\sigma = 3.82 \times 10^{-21} \frac{A}{d_e C} \tag{6.6}$$

where A (cm^{-1}) is the integrated absorption data for the 10 cm^{-1} interval, d_e (cm) is the effective distance travelled by the evanescent wave in ATR FT-IR that corresponds to the path length in transmission IR, and C is the molar concentration of the sample. d_e was

calculated by taking an average of the distances travelled by the part of evanescent wave that is parallel ($d_{e,p}$) and the part perpendicular ($d_{e,s}$) to the plane of incidence. [20] $d_{e,p}$and $d_{e,s}$ were calculated using following equations:

$$d_{e,s} = \frac{(n_2/n_1)\lambda_1 \cos\theta}{\pi\left(1-(n_2/n_1)^2\right)\left(\sin^2\theta-(n_2/n_1)^2\right)^{1/2}} \tag{6.7}$$

$$d_{e,p} = \frac{(n_2/n_1)\lambda_1 \cos\theta\left(2\sin^2\theta-(n_2/n_1)^2\right)}{\pi\left(1-(n_2/n_1)^2\right)\left(\sin^2\theta-(n_2/n_1)^2\right)^{1/2}\left[\left(1+(n_2/n_1)^2\right)\sin^2\theta-(n_2/n_1)^2\right]} \tag{6.8}$$

where n_1 and n_2 are refractive indices of the optical crystal and sample respectively, λ_1 is the wavelength of the incident radiation, and θ is the incident angle. Refractive indices for the newly identified fluid were calculated using a correlation employed in the property prediction package (ProPred) of the ICAS11 software obtained from Computer Aided Process-Product Engineering Center, Technical University of Denmark.

6.5 Results and Discussion

6.5.1 Group Contribution Method

GC values (C_i) for RF obtained by regression are shown in Table 6.1. The AAD between literature and estimated values was 11.37 %. This compares favorably with existing methods that employ density functional theory to predict IR spectra (AAD of 14 - 25 %) [7, 8] or structure-activity relationship (AAD of 25 %) [9]. Predicted RF values are plotted against literature values in Figure 6.1. It can be seen that most of the data points lie along the diagonal. The highest errors (~ 70 %) occur in the case of the two

hydrofluoroethers HFE 7100 and HFE 7200. The next highest deviations (~ 40 %) were observed for CFCs containing one C atom. For other fluorocarbons, the GC method appears to be in very good agreement with the literature. In addition, the residual *J* value (equation 6.2) for this problem was 1.81 % confirming the reliability of the GC method.

Table 6.1. Group contributions for RF.

Group	C_i
CF_3	0.14319
CF_2	0.08332
CF	0.09840
F	0.13844
CHF_2	0.11804
CH_2F	0.03461
CHF	0.05962
O	0.07318
F(O)	0.02723
Cl	0.02875

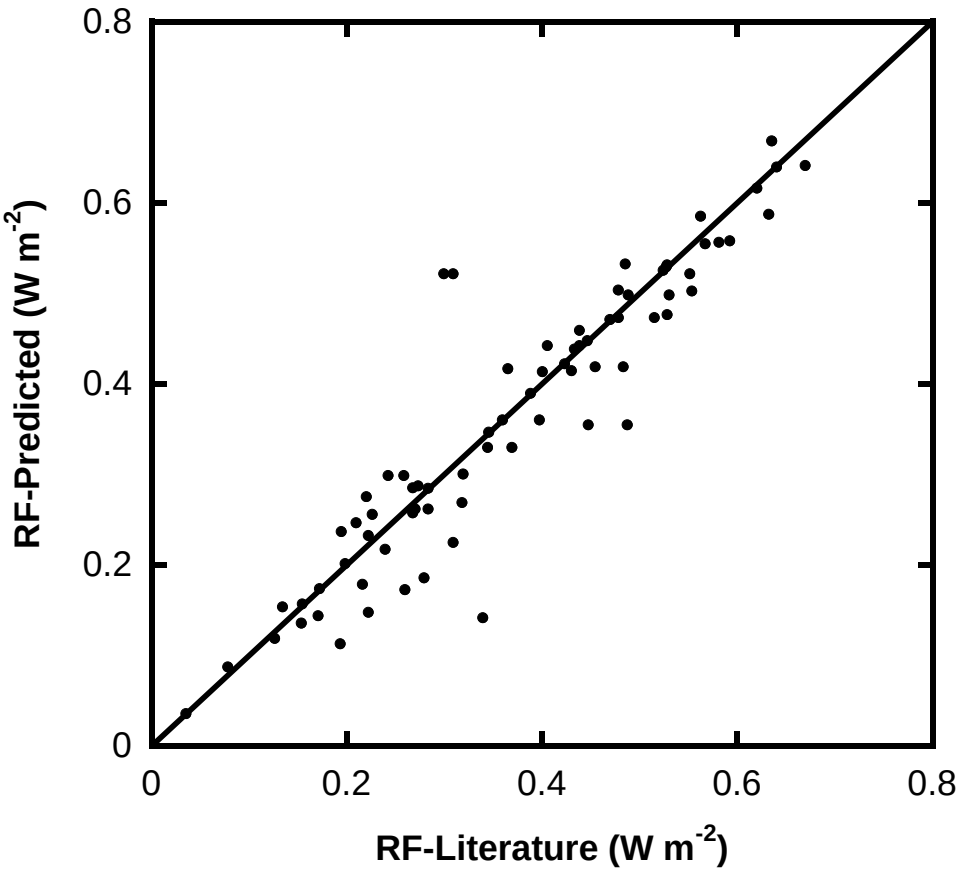

Figure 6.1. Comparison of predicted and literature RF values.

6.5.2 Estimated RF, k_{OH}, τ, GWP

Estimated RF (equation 6.1 and Table 6.1), k_{OH}, τ (equation 6.4), and GWP (equation 6.3) for 33 newly identified coolants are listed in Tables 6.2 and 6.3. It can be observed that only 2 of the 33 new coolants have RF greater than or equal to that of HFE 7200 (see Table 6.3). Moreover, GWP values of all new coolants are lower than that of HFE 7200. Hence the impact on climate of these fluids is likely to be less than that of HFE 7200.

Table 6.2. Estimated RF, k_{OH}, and τ of newly identified heat transfer fluids.

Compound	RF ($W\ m^{-2}$)	$k_{OH} \times 10^{12}$ ($cm^3\ molec.^{-1}\ s^{-1}$)	τ (years)
1,1,1,4,4,4-hexafluoro-2-methylbutane	0.2864	0.418	0.0913
1,1,1-trifluoro-3-methyl-2-(trifluoromethyl)butane	0.2864	2.733	0.0139
1,1,1,5,5,5-hexafluoropentane	0.2864	1.576	0.0242
(E)-6,6,6-trifluorohex-2-ene	0.1432	57.766	0.0006
1,1,1,5,5,5-hexafluoro-3-methylpentane	0.2864	3.265	0.0117
2,2-difluoro-4-methyl-3-(trifluoromethyl)pentane	0.2612	2.726	0.0140
1,1,1,5,5-pentafluorohexane	0.2612	1.518	0.0251
4-methyl-3-(trifluoromethyl)pent-1-ene	0.1432	29.190	0.0013
(E)-1,1,1-trifluoro-3-methylpent-2-ene	0.1432	67.281	0.0006
6,6,6-trifluorohex-1-ene	0.1432	28.943	0.0013
1,1,1-trifluoro-3-methylpentane	0.1432	4.500	0.0085
1,1,1-trifluoro-3-methoxypropane	0.2164	8.070	0.0047
(E)-5,5,5-trifluoro-4,4-dimethylpent-2-ene	0.1432	56.871	0.0007
1,1,1,4,4,4-hexafluoro-2,2-dimethylbutane	0.2864	0.416	0.0918
5,5,5-trifluoro-2-methylpent-1-ene	0.1432	52.766	0.0007
2-(2,2-difluoropropoxy)-1,1,1-trifluoropropane	0.2997	0.286	0.1337
1,1,1-trifluoro-3-methoxybutane	0.2164	15.634	0.0024
1,1,1-trifluoro-3-(2,2,2-trifluoroethoxy)propane	0.3596	1.498	0.0255
1,1,1-trifluorohexane	0.1432	4.224	0.0090
1,1,1-trifluorobutan-2-one	0.2249	0.633	0.0603
2,2-difluoro-3-methyl-3-(trifluoromethyl)pentane	0.2265	1.486	0.0257
methyl 3,3,3-trifluoropropanoate	0.1432	0.238	0.1603
3,3-difluoroheptane	0.0833	2.934	0.0130
3-methyl-3-(trifluoromethyl)pent-1-ene	0.1432	27.783	0.0014
4,4,4-trifluorobutan-2-one	0.1432	0.152	0.2517
1,1,1-trifluoro-2,3,3-trimethylbutane	0.1432	0.839	0.0455
3-ethoxy-1,1,1-trifluoropropane	0.2164	13.413	0.0028
4,4,4-trifluoro-2,3,3-trimethylbut-1-ene	0.1432	51.871	0.0007
1,1,1-trifluoro-2,2-dimethylpentane	0.1432	3.064	0.0125
1,1,1-trifluoro-2,3-dimethylpentane	0.1432	4.755	0.0080
1,1,2,2-tetramethyl-3-(trifluoromethyl)cyclopropane	0.1432	0.673	0.0567
1,1,2-trimethyl-2-(trifluoromethyl)cyclopropane	0.1432	0.530	0.0720
1-fluoro-1-methyl-3-methylenecyclobutane	0.1384	52.059	0.0007

Table 6.3. Estimated GWP of newly identified heat transfer fluids.

Compound	GWP (W year m^{-2} $ppbv^{-1}$)		
	TH_{20}	TH_{100}	TH_{500}
1,1,1,4,4,4-hexafluoro-2-methylbutane	27.18	8.32	2.60
1,1,1-trifluoro-3-methyl-2-(trifluoromethyl)butane	3.86	1.18	0.37
1,1,1,5,5,5-hexafluoropentane	7.21	2.20	0.69
(E)-6,6,6-trifluorohex-2-ene	0.13	0.04	0.01
1,1,1,5,5,5-hexafluoro-3-methylpentane	3.23	0.99	0.31
2,2-difluoro-4-methyl-3-(trifluoromethyl)pentane	3.60	1.10	0.34
1,1,1,5,5-pentafluorohexane	6.99	2.14	0.67
4-methyl-3-(trifluoromethyl)pent-1-ene	0.23	0.07	0.02
(E)-1,1,1-trifluoro-3-methylpent-2-ene	0.11	0.03	0.01
6,6,6-trifluorohex-1-ene	0.26	0.08	0.02
1,1,1-trifluoro-3-methylpentane	1.62	0.50	0.15
1,1,1-trifluoro-3-methoxypropane	1.49	0.46	0.14
(E)-5,5,5-trifluoro-4,4-dimethylpent-2-ene	0.12	0.04	0.01
1,1,1,4,4,4-hexafluoro-2,2-dimethylbutane	25.35	7.76	2.42
5,5,5-trifluoro-2-methylpent-1-ene	0.14	0.04	0.01
2-(2,2-difluoropropoxy)-1,1,1-trifluoropropane	39.05	11.95	3.73
1,1,1-trifluoro-3-methoxybutane	0.69	0.21	0.07
1,1,1-trifluoro-3-(2,2,2-trifluoroethoxy)propane	8.75	2.68	0.84
1,1,1-trifluorohexane	1.73	0.53	0.16
1,1,1-trifluorobutan-2-one	20.14	6.16	1.92
2,2-difluoro-3-methyl-3-(trifluoromethyl)pentane	5.73	1.75	0.55
methyl 3,3,3-trifluoropropanoate	30.25	9.26	2.89
3,3-difluoroheptane	1.49	0.46	0.14
3-methyl-3-(trifluoromethyl)pent-1-ene	0.24	0.07	0.02
4,4,4-trifluorobutan-2-one	53.53	16.38	5.11
1,1,1-trifluoro-2,3,3-trimethylbutane	7.92	2.42	0.76
3-ethoxy-1,1,1-trifluoropropane	0.81	0.25	0.08
4,4,4-trifluoro-2,3,3-trimethylbut-1-ene	0.13	0.04	0.01
1,1,1-trifluoro-2,2-dimethylpentane	2.17	0.66	0.21
1,1,1-trifluoro-2,3-dimethylpentane	1.39	0.43	0.13
1,1,2,2-tetramethyl-3-(trifluoromethyl)cyclopropane	9.15	2.80	0.87
1,1,2-trimethyl-2-(trifluoromethyl)cyclopropane	12.69	3.88	1.21
1-fluoro-1-methyl-3-methylenecyclobutane	0.19	0.06	0.02

6.5.3 RF from FT-IR Spectroscopy

FT-IR spectra of HFE 7200 and PF 5060, as well as those of 3 new coolants (1,1,1-trifluoro-2-butanone, 4,4,4-trifluoro-2-butanone, 1,1,1-trifluoro-3-methylpentane) are presented in Figures 6.2-6.6. In Table 6.4, calculated values of RF (see equations 6.5-6.8) and GWP (see equation 6.3) for HFE 7200 and PF 5060 are compared with literature values [6] in order to validate the experimental analysis. Table 6.4 confirms that RF and GWP values from ATR FT-IR spectroscopy are in good agreement with values reported in the literature. The experimentally determined RF values are compared with GC estimates in Table 6.5. Note that GC estimates are not reported for the two ketones because the C=O group contribution could not be regressed due to lack of published data on this class of compounds.

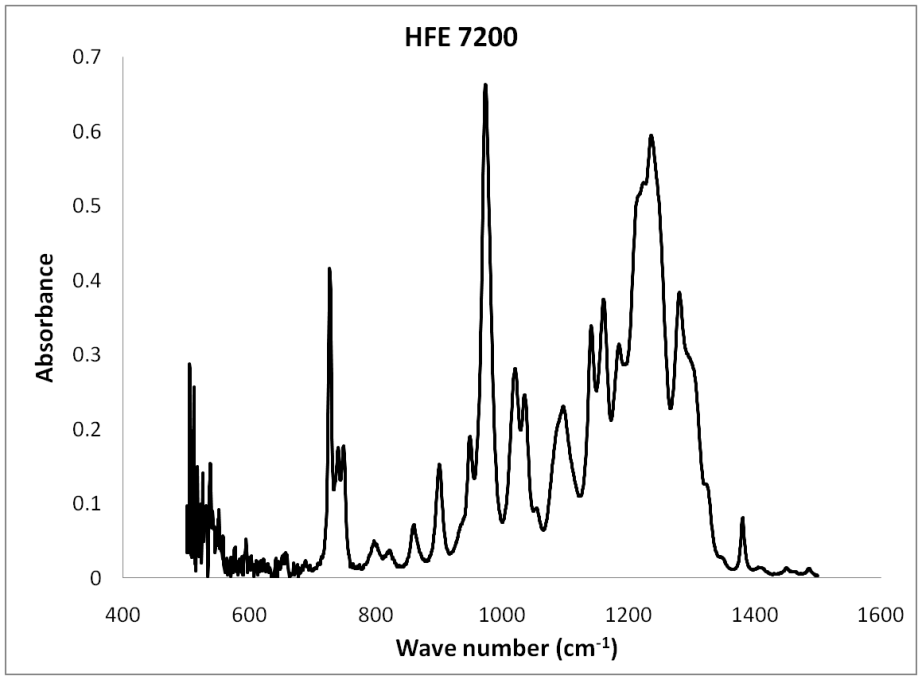

Figure 6.2. FT-IR spectra of HFE 7200.

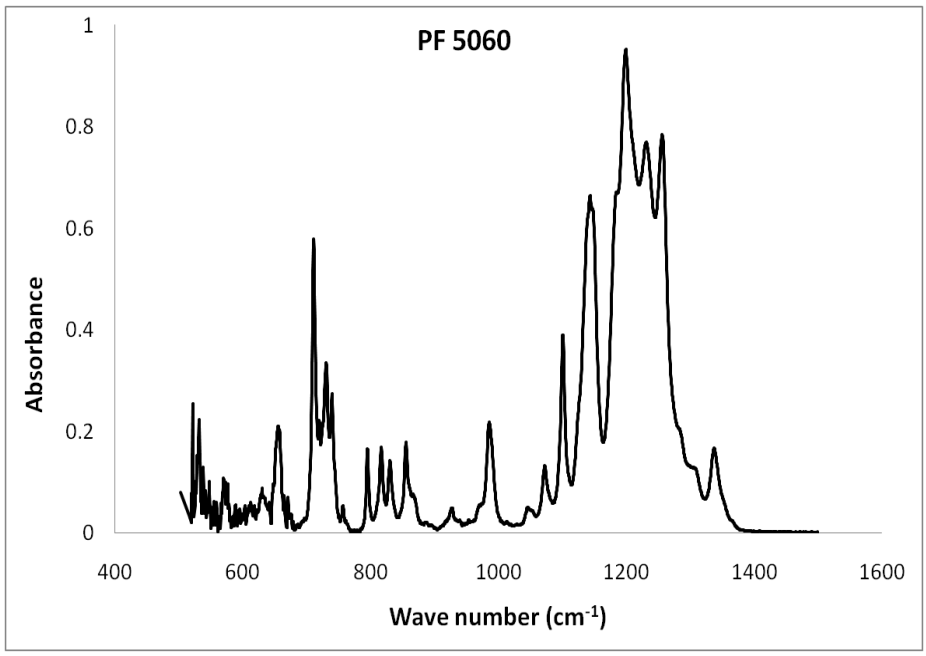

Figure 6.3. FT-IR spectra of PF 5060.

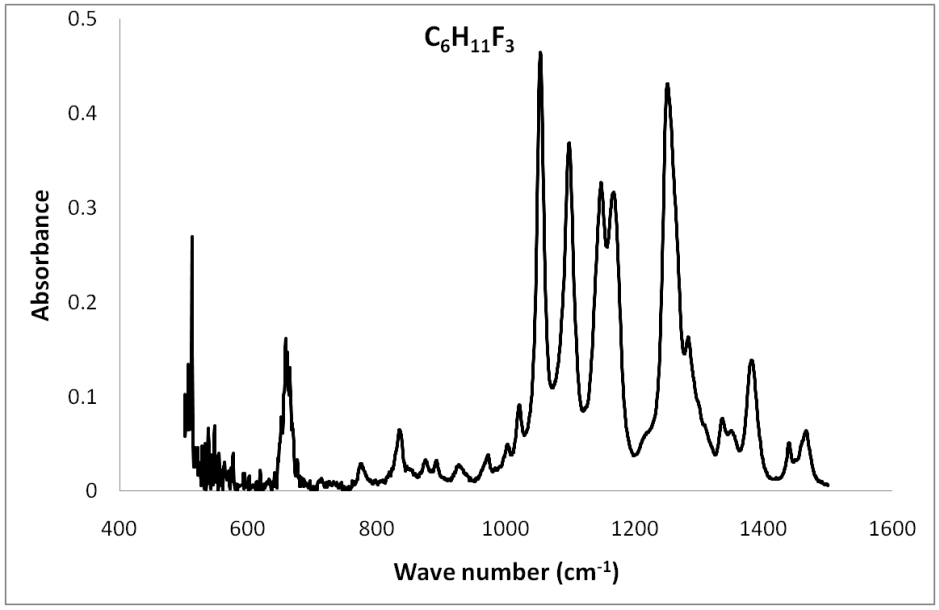

Figure 6.4. FT-IR spectra of 1,1,1-trifluoro-3-methylpentane.

.

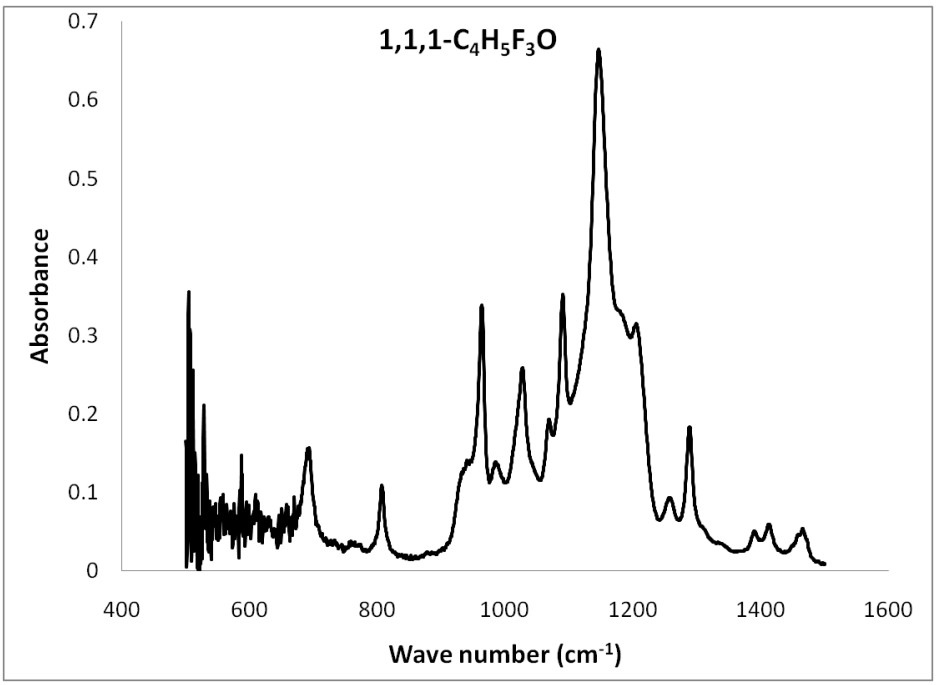

Figure 6.5. FT-IR spectra of 1,1,1-trifluoro-2-butanone.

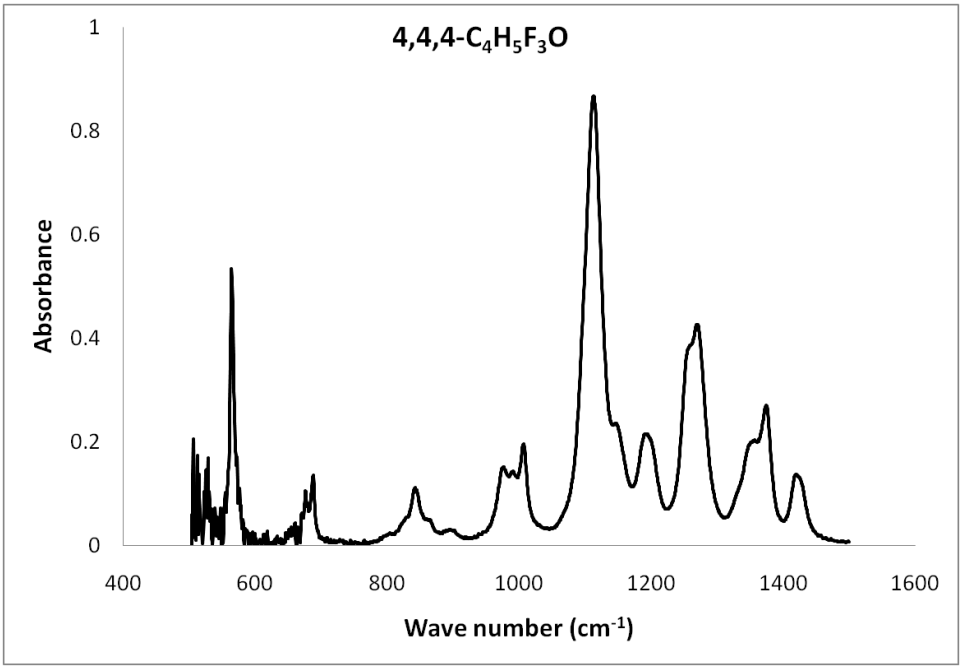

Figure 6.6. FT-IR spectra of 4,4,4-trifluoro-2-butanone.

Table 6.4. Comparison of experimentally estimated RF and GWP with literature values.

	RF (W m^{-2})		τ (years) [6]	GWP - TH_{100} (W year m^{-2} $ppbv^{-1}$)	
	FT-IR	Lit.[17]		Calc.	Lit.[6]
HFE 7200	0.2245	0.3	0.77	37	59
PF 5060	0.5724	0.49	3200	9552	9300

Table 6.5. Experimentally determined RF and GWP of new fluids.

	RF (W m^{-2})		τ (years)	GWP-Calc. (W year m^{-2} $ppbv^{-1}$)		
	FT-IR	GC		TH_{20}	TH_{100}	TH_{500}
$C_6H_{11}F_3$	0.1041	0.1432	0.008	1.18	0.36	0.11
1,1,1-$C_4H_5F_3O$	0.1066	NA	0.060	9.55	2.92	0.91
4,4,4-$C_4H_5F_3O$	0.0854	NA	0.252	31.92	9.77	3.05

6.6 Conclusions

A new GC method is presented for estimating RF of fluorocarbons. The method compares favorably with existing density functional theory based methods. The GC method was validated for five fluids with experimental determination of radiative forcing using FT-IR spectroscopy. Finally, the method was used to calculate GWP of newly identified heat transfer fluids. Only 2 of the 33 new fluids exhibited RF values greater than those of HFE 7200. Moreover, GWP values of all new fluids were lower than those of HFE 7200. Hence these fluids can be considered as potential replacements for HFEs and PFEs for electronics cooling. The group contribution method developed in this work should be useful in designing new fluorocarbons as it facilitates the use of quantitative environmental constraints in CAMD.

6.7 References

1. Bivens, D. B. and Minor, B. H, *Fluoroethers and other next generation fluids*, International Journal of Refrigeration, 1998. **21**(7): p. 567–576.

2. Velders, G. J. M., Fahey, D. W., Daniel, J. S., McFarland, M., and Anderson, S. O., *The large contribution of projected HFC emissions of future climate forcing*, Proceedings of the National Academy of Sciences U.S.A., 2009. **106**: p. 10949-10954.

3. Warrier, P., Sathyanarayana, A., Patil, D. V., France, S., Joshi, Y., and Teja, A. S., *Novel heat transfer fluids for direct immersion phase change cooling of electronic systems*, International Journal of Heat and Mass Transfer, 2012. **55**: p. 3379–3385.

4. Kwok, E. S. C. and Atkinson, R., *Estimation of hydroxyl radical reaction rate constants for gas-phase organic compounds using a structure-activity relationship: an update*, Atmospheric Environment, 1995. **29**(14): p. 1685-1695.

5. US EPA. *Estimation Programs Interface Suite*™ for Microsoft® Windows, v 4.10, United States Environmental Protection Agency, Washington, DC, USA, 2012

6. Forster, P., et al. *Changes in atmospheric constituents and in radiative forcing*. In Solomon, S., Qin, D., Manning, M., Chen, Z., Marquis, M., Averyt, K. B., Tignor, M., and Miller, H. L., (eds.), Climate Change 2007: The Physical Science Basis. Contribution of Working Group I to the Fourth Assessment Report of the Intergovernmental Panel on Climate Change, 2007, New York: Cambridge University Press.

7. Blowers, P., Moline, D. M., Tetrault, K. F., Wheeler, R. R., and Tuchawena, S. L., *Global warming potential of hydrofluoroethers*, Environmental Science and Technology, 2008. **42**: p. 1301-1307.

8. Blowers, P., Tetrault, K. F., and Trujillo-Morehead, Y., *Global warming potential predictions for hydrofluoroethers with two carbon atoms*, Theoretical Chemistry Accounts: Theory, Computation, and Modeling, 2008. **119**: p. 369-381.

9. Young, C. J., Hurley, M. D., Wallington, T. J., and Mabury, S. A., *Molecular structure and radiative efficiency of fluorinated ethers: A structure-activity relationship*, Journal of Geophysical Research, 2008. **113**: D24301.

10. Naik, V., Jain, A. K., Patten, K. O., and Wuebbles, D. J., *Consistent sets of atmospheric lifetimes and radiative forcings on climate for CFC replacements: HCFCs and HFCs*, Journal of Geophysical Research, 2000. **105**(D5): p. 6903-6914.

11. Jain, A. K., Briegleb, B. P., Minschwaner, K., and Wuebbles, D. J., *Radiative forcings and global warming potentials of 39 greenhouse gases*, Journal of Geophysical Research, 2000. **105**(D16): p. 20773-20790.

12. Sihra, K., Hurley, M. D., Shine, K. P., and Wallington, T. J., *Updated radiative forcing estimates of 65 halocarbons and nonmethane hydrocarbons*, Journal of Geophysical Research, 2001. **106**(D17): p. 20493-20505.

13. Pinnock, S., Hurley, M. D., Shine, K. P., Wallington, T. J., and Smyth, T. J., *Radiative forcing of climate by hydrochlorofluorocarbons and hydrofluorocarbons*, Journal of Geophysical Research, 1995. **100**(D11): p. 23227-23238.

14. Calm, J. M. and Hourahan, G. C., *Refrigerant data update*, HPAC Engineering, 2007. **January**: p. 50-64.

15. Wu, H. S. and Sandler, S. I., *Use of ab initio quantum mechanics calculations in group contribution methods. 1. Theory and the basis for group identifications*, Industrial and Engineering Chemistry Research, 1991. **30**: p. 881-889.

16. Bera, P. P., Francisco, J. S., and Lee, T. J., *Design strategies to minimize the radiative efficiency of global warming molecules*, Proceedings of the National Academy of Sciences U.S.A., 2010. **107**(20): p. 9049-9054.

17. Marrero, J. and Gani, R., *Group-contribution based estimation of pure component properties*, Fluid Phase Equilibria, 2001. **183-184**(1): p. 183-208.

18. Elrod, M. J., Greenhouse warming potentials from the infrared spectroscopy of atmospheric gases, Journal of Chemical Education, 1999. **76**(12): p. 1702-1705.

19. Lakowicz, J. R., *Principles of Fluorescence Spectroscopy*, 2006. New York: Springer.

20. Harrick, N. J. and Carlson, A. I., *Internal reflection spectroscopy: validity of effective thickness equations*, Applied Optics, 1971. **10**(1): p. 19-23.

CHAPTER 7

NANOFLUIDS

It has been suggested that the thermal conductivity (and hence, heat transfer performance) of coolants can be enhanced significantly by the addition of nanoparticles to the liquid coolants. This chapter reviews experimental data and models for the thermal conductivity of nanoparticle suspensions and examines the effect of the properties of the two phases on the effective thermal conductivity of the heterogeneous system. A modified geometric mean model is presented for the effective thermal conductivity of nanofluids that takes into account the temperature dependence of the thermal conductivities of the individual phases, as well as the size dependence of the thermal conductivity of the dispersed phase. Application of this model is demonstrated by calculating the thermal conductivity of nanofluids over a wide range of particle sizes, particle volume fractions, and temperatures. The model can also be used to validate experimental thermal conductivity data for nanofluids and confirm the size dependence of the thermal conductivity of nanoparticles. Finally, the rheological properties of nanofluids are discussed and experimental evaluation of the effects of particle concentration, temperature and shear rate are presented for bentonite nanofluids.

7.1 Introduction

The properties of heterogeneous mixtures containing micro- and macro-scale particles have been studied for over 100 years. [1, 2] These studies have shown that the

effective thermal conductivity of particle dispersions depends on the thermal conductivity of the two phases that comprise the dispersion, in proportion to the volume fraction of each phase. However, more recent work by Choi [3] and Eastman *et al.* [4] has shown that dispersions of nanoparticles (i.e. nanofluids) exhibit unusual behavior with respect to properties such as the thermal conductivity, viscosity, and refractive index. For example, Eastman *et al.* [4] describe a 40 % enhancement in the thermal conductivity of ethylene glycol with the addition of 0.3 % (v/v) Cu nanoparticles. 150 % enhancement in the thermal conductivity of synthetic oil was observed by Choi *et al.* [5] upon addition of 1 % (v/v) carbon nanotubes. These enhancements in the thermal conductivity are much higher than those predicted for dispersions of micro- and macro-scale particles [1]. As a result, it has been suggested that nanofluids be considered as heat transfer fluids for thermal management applications, as well as in areas such as optics [6], enhanced mass transport [7, 8] and solar heat collection [9, 10]. The focus of the present work is on the behavior of nanofluid thermal conductivity and its correlation/prediction using fundamental models.

Many of these studies on nanofluids [11] have reported large increases in the thermal conductivity of the heterogeneous system over that of the base liquid. However, a few studies [12, 13] have also produced seemingly conflicting results, particularly with respect to the effect of particle size. A number of mechanisms have also been proposed [11, 14] to account for the magnitude of the enhancement in the thermal conductivity. These mechanisms have included Brownian motion of particles to create a microconvective effect, the ordering of liquid molecules at the solid interface to enhance conduction, and the clustering of nanoparticles to form pathways of lower thermal

resistance. However, models for the thermal conductivity based on one or more of these mechanisms have generally proved ineffective in predicting the thermal conductivity of nanofluids. Thus, fundamental questions remain with respect to the mechanism of thermal conduction in nanofluids as well as the particle size dependence of the thermal conductivity. This work compiles literature data on the thermal conductivity of nanofluids containing solid semiconductor, insulator, and metallic particles and critically examines published models for their prediction. On the basis of this evaluation, a model for thermal transport in such nanofluids is proposed and its predictive capabilities are evaluated.

7.2 Thermal Conductivity of Liquids and Solids

7.2.1 Thermal Conductivity of Liquids

As nanofluids are composite materials consisting of a solid discrete phase and a liquid continuous phase, the behavior of their thermal conductivity can best be understood by first considering the behavior of the individual phases. Thermal conductivities of liquids range from about 0.06 W m^{-1} K^{-1} for fluorocarbons to about 0.6 W m^{-1} K^{-1} for water, with nonpolar liquids generally exhibiting lower thermal conductivities than polar liquids. The thermal conductivity vs. temperature behaviors for typical polar (water) and nonpolar (*n*-decane) fluids are illustrated in Figure 7.1. The thermal conductivity of nonpolar liquids decreases monotonically with increasing temperature due to thermal expansion of the liquid. [15] On the other hand, associating liquids such as water and ethylene glycol display a maximum in their thermal conductivity vs. temperature behavior [16, 17] due to changes in the hydrogen bonding

network with temperature. At low temperatures, some of the energy being transferred is stored in hydrogen bonds as they form a network, leading to a lower thermal conductivity. As the temperature increases, less energy is captured by the hydrogen bonding network, leading to increased thermal conductivity. This phenomenon competes with the typical decrease in thermal conductivity with temperature due to thermal expansion and results in a maximum in the thermal conductivity - temperature behavior of the fluid.

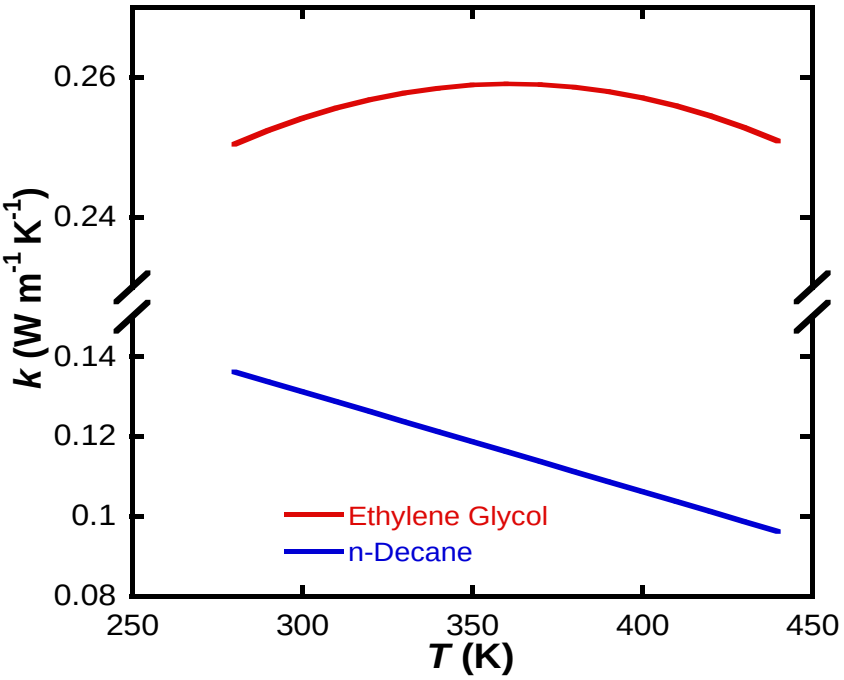

Figure 7.1. Thermal conductivity vs. temperature behavior of ethylene glycol and *n*-decane.

7.2.2 Thermal Conductivity of Solids

Heat is conducted in metallic solids by free electrons, and in semiconductors and insulators by lattice waves. As thermal conduction by electrons is more effective than

conduction by phonons, the thermal conductivity of metals is generally an order of magnitude greater than that of insulators. The thermal conductivity also depends on the structure of the solid. For example, amorphous carbon has a thermal conductivity of 1.6 W m^{-1} K^{-1}, but diamond and carbon nanotubes can exhibit [18-20] thermal conductivities as high as 900 and 2000 W m^{-1} K^{-1} respectively. Crystalline solids typically conduct heat more readily than amorphous solids and, therefore, their thermal conductivities are higher than those of amorphous solids. The mechanism of heat transport differs significantly between metals and semiconductors and insulators and is discussed in following subsections.

7.2.2.1 Thermal Conductivity of Insulators and Semiconductors

In the case of insulators and semiconductors, energy is propagated through the crystal lattice by phonon waves. [21] If the atoms could oscillate harmonically, the velocity of these phonon waves would be the speed of sound in a crystal. However, anharmonicity is observed [22] due to higher order interactions among atoms, and leads to a change in the direction of the phonon wave (or phonon scattering). Phonon scattering can be divided into elastic phonon scattering, where phonon momentum is conserved, and inelastic scattering, where it is not. Inelastic scattering creates resistance to thermal transport and lowers the thermal conductivity. Scattering can result from collisions of phonons with each other (Umklapp scattering) or defects in the crystal structure such as impurities and grain boundaries. Thermal conductivities of semiconductor solids [23] generally increase and then decrease with temperature due to these competing phenomena.

The effect of size of the solid particle on the thermal conductivity has received considerable attention recently. A number of studies [24-26] have focused on thermal conduction in nanoscale semiconductor thin films, and concluded that thermal conductivities of submicron films decrease as the thickness of the film decreases. Indeed, Liu and Asheghi [26] reported that the out-of-plane thermal conductivity of a silicon film of thickness 20 nm was nearly an order of magnitude smaller than the thermal conductivity of bulk silicon. They suggested that phonon scattering at the interface of the solid must become the dominant source of thermal resistance in solid nanomaterials because of their large specific surface area. A less substantial decrease of the in-plane thermal conductivity (~ 10 % at 300 K) was observed by Yu *et al.* [27] in a superlattice with a periodic structure of 70 nm.

Phonon-interface scattering is not as well understood as other phonon scattering processes (such as boundary scattering or phonon-phonon scattering), and it is seldom incorporated into models for the thermal conductivity of solids. This could be one reason [28] why most methods are unable to predict the reduced thermal conductivity of nanostructured materials. Ziambaras and Hyldgaard [29] examined the thermal conductivity of nanoscale films and wires using the Boltzmann transport equation with phonon-interface scattering and found that the axial thermal conductivity of a wire is less than the in-plane thermal conductivity of a film of the same thickness. They suggested that this effect is similar to Knudsen diffusion, and is caused by confinement of the phonon wave when the phonon mean free path is of the same order as the thickness of the nanomaterial. Nanowires, which are confined in two dimensions, are therefore expected to exhibit a lower thermal conductivity than nanofilms, which are only confined in one

dimension. Li *et al.* [30] demonstrated this phenomenon when they measured axial heat conduction in silicon nanowires. They reported that the axial thermal conductivity of a 22 nm diameter silicon nanowire was approximately 6 W m^{-1} K^{-1}, while the out-of-plane thermal conductivity for a 20-nm-thick silicon film was about 22 W m^{-1} K^{-1}. The nanowire value is more than two orders of magnitude lower than the bulk thermal conductivity of silicon (237 W m^{-1} K^{-1}).

Semiconductor nanoparticles should exhibit an even lower thermal conductivity than nanowires or nanofilms, because nanoparticles are confined in three dimensions. Fang *et al.* [31] used molecular dynamic simulations to estimate the thermal conductivity of silicon nanoparticles and reported that the thermal conductivity of particles smaller than 8 nm was about 2 W m^{-1} K^{-1}. In contrast, the thermal conductivity of bulk silicon is 237 W m^{-1} K^{-1} as noted previously. These results have yet to be confirmed experimentally, although it seems clear that the thermal conductivity of semiconductor or insulator particles must decrease with particle size when the particle size approaches the mean free path of phonons in the solid. The studies described above imply that the contribution of the particle thermal conductivity to the effective thermal conductivity of a solid dispersion should also decrease as the size of the dispersed particles approaches the phonon mean free path.

Liang and Li [32] recently proposed a phenomenological theory for the size dependence of the thermal conductivity of semiconductors and insulators by taking into account the intrinsic size effect on phonon velocity, mean free path, and surface scattering. An advantage of their model is that the same equation can be used for thin

films, nanowires, and nanoparticles. According to Liang and Li, the thermal conductivity of a nanostructure is given by:

$$\frac{k_p(L)}{k_b} = p\exp\left(-\frac{l_0}{L}\right)\left[\exp\left(\frac{1-A}{L/L_0-1}\right)\right]^{3/2} \tag{7.1}$$

where $k_p(L)$ is the thermal conductivity of the nanostructure of characteristic size L, k_b is the thermal conductivity of the bulk material, l_0 is the phonon mean free path at room temperature, and L_0 is the critical size when almost all atoms of the crystal are located on its surface. L_0 may be obtained from:

$$L_0 = 2(3\text{-}n)\sigma \tag{7.2}$$

where σ is the atomic / molecular diameter, and n = 0, 1, and 2 for nanoparticles, nanowires, and thin films, respectively. Parameter A depends on the bulk vibrational entropy of melting S_v as follows:

$$A = 1 + (2/3)\, S_v / R \tag{7.3}$$

where R is the universal gas constant. For III-V and II-VI compounds, $S_v = H_m/T_m$ - R where H_m is the enthalpy of melting and T_m is the bulk melting point. For molecular crystals [33], $S_v \approx S_m = H_m/T_m$. The adjustable parameter p ($0 < p \leq 1$) in equation 7.1 provides a measure of surface roughness.

Liang and Li [32] successfully equation 7.1 to thin films and nanowires, but could not validate the equation for nanoparticles because of lack of experimental data. In this

work, equations 7.1-7.3 and the physical parameters given in Table 7.1 [34] were used to calculate the thermal conductivity of semiconductor and insulator nanoparticles. The phonon mean free path l_0 was calculated using the kinetic theory expression:

$$k = \frac{1}{3} \rho \, C_v \, v_a \, l_o \tag{7.4}$$

where ρ is the density, C_v is the specific heat, and v_a is the average phonon velocity. Bulk values of the properties of the material at 300 K were used to obtain l_0. The average phonon velocity v_a was calculated using [23]:

$$\frac{3}{v_a^3} = \frac{1}{v_l^3} + \frac{2}{v_t^3} \tag{7.5}$$

where v_l is the velocity of the longitudinal wave and v_t is the velocity of the (two) transverse waves in the material of interest. Crystal structure and lattice constants were obtained from Bragg *et al.* [35] and Yang *et al.* [36]. For molecular crystals, σ was calculated from nearest-neighbor separation of molecules in the molecular lattice. [37] Jiang *et al.* [38] pointed out that the entropy of melting is not sensitive to σ, especially when L/ σ is large (L > 4 nm, and σ < 0.5 nm). Table 7.2 compares calculated phonon mean free paths for several oxides with published values and confirms that the kinetic theory expression provides reasonable estimates of l_0. Calculated thermal conductivities of several semiconductors and insulators are plotted in Figure 7.2. It can be seen that the effective thermal conductivity of these materials attains its bulk value at particle sizes of about 100 nm.

Table 7.1. Characteristic constants for equations 7.1 - 7.5.

	k_b (W $m^{-1}K^{-1}$)	ρ (kg m^{-3})	C_p (J mol^{-1} K^{-1})	v_a (m s^{-1})	l_0 (nm)	H_m (kJ mol^{-1})	T_m (K)	σ (nm)
Si	236.8	2330	19.99	6351	41	50.55	1685	0.235
α-Al_2O_3	40	3970	78.96	6763	5.77	55.12	2345	0.238
TiO_2 (Rutile)	8.4	4230	54.76	5568	1.56	44.67	2116	0.147
CeO_2	10.4	7650	61.53	6052	2.18	87.18	2673	0.382
CuO	77	6310	42.26	5000	13.78	11.79	1719	0.195
Fe_3O_4	7	5170	143.37	2500	2.56	137.94	1870	0.595
SiO_2	1.34	2650	44.57	3863	0.58	8.78	1996	0.245
ZnO	29	5610	40.21	3159	9.94	18.69	2248	0.162
α-SiC	490	3220	26.74	7893	86.73	3.18	2973	0.153
Diamond	900	3510	6.57	13826	104.81	104.6	4093	0.155

Table 7.2. Calculated phonon mean free path l_0 (nm) at 298 K for some insulators.

	Literature value	Equation 7.4
Al_2O_3	5.08 [106]	5.77
SiO_2	0.6 [106]	0.58
SiC	69.05 [107]	86.73

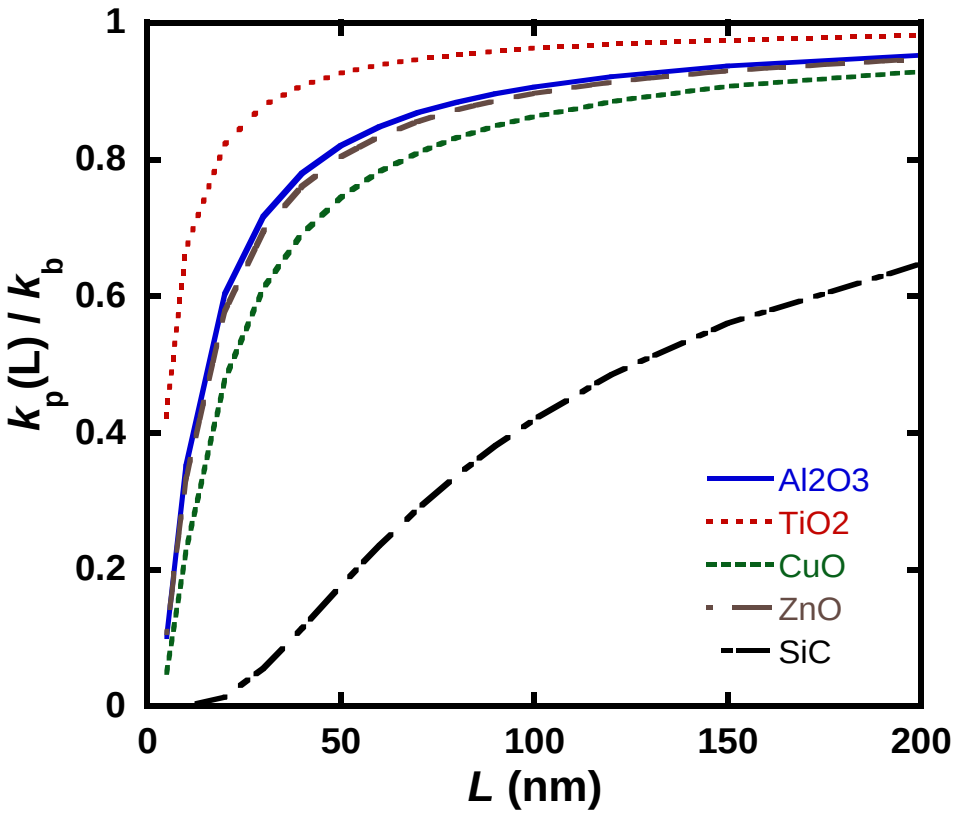

Figure 7.2. Thermal conductivity of semiconductors and insulators calculated using equation 7.1.

7.2.2.2 Thermal Conductivity of Metals

The kinetic theory expression for the thermal conductivity k_b of bulk metals is given by [23]:

$$k_b = \frac{1}{3}\rho C_{v,e} v_F \lambda_{e,b} \tag{7.6}$$

where ρ is the mass of electrons per unit volume, $C_{v,e}$ is the volumetric specific heat of electrons, v_F is the Fermi velocity and $\lambda_{e,b}$ is the mean free path of electrons in the bulk material. Upon substituting for ρ and $C_{v,e}$, equation 7.6 can be expressed as:

$$k_b = \frac{k_B^2 \pi^2 n_e T \lambda_{e,b}}{3 m_e v_F} \tag{7.7}$$

where k_B is the Boltzmann constant, T is the temperature and n_e and m_e are the number of free electrons per atom and the mass of an electron, respectively. These values are presented in Table 7.3 for silver, copper and gold [23, 39]. Equation 7.7 can be used to calculate the mean free path of electrons in the solid $\lambda_{e,b}$ if the bulk thermal conductivity and Fermi energy are known.

Table 7.3. Properties of metals at 298 K.

	k_b (W m^{-1}K^{-1})	μ_F (eV)	$n_e \times 10^{28}$ (m^{-3})	$\lambda_{e,b}$ (nm)
Silver	424	5.5	5.85	49.10
Copper	398	7.0	8.45	35.97
Gold	315	5.5	5.90	36.14

As particle size (L) becomes of the same order as the electron mean free path, boundary or interface scattering will lead to a decrease in particle thermal conductivity. When $L << \lambda_{e,b}$, the thermal conductivity of the particle $k_p(L)$ can be expressed as [23]:

$$\frac{k_p(L)}{k_b} = \frac{\lambda_{e,P}}{\lambda_{e,b}} = \frac{1}{Kn} \tag{7.8}$$

where Kn = $\lambda_{e,b}$ / L is the Knudsen number. When L is of the same order as $\lambda_{e,b}$, the effective mean free path of the electron in the particle can be calculated using the following relation:

$$\frac{1}{\lambda_{e,P}} = \frac{1}{\lambda_{e,b}} + \frac{1}{L} \tag{7.9}$$

This leads to the following relationship for the thermal conductivity of the particle [23]:

$$\frac{k_p(L)}{k_b} = \frac{\lambda_{e,P}}{\lambda_{e,b}} = \frac{1}{1+Kn} \tag{7.10}$$

Equations 7.8 and 7.10 relate the thermal conductivity of metallic nanoparticles to their characteristic size, which is illustrated in Figure 7.3 for copper and silver nanoparticles. The thermal conductivities of silver and copper nanoparticles shown in Figure 7.3 were calculated using equation 7.8 when Kn > 5, and equation 7.10 when Kn < 1. In the intermediate region (1 < Kn < 5), the thermal conductivity was obtained by interpolation. Although no data are available to validate these calculations, the measurements of Nath and Chopra [40] for the thermal conductivity of thin films of copper (also plotted in Figure 7.3) clearly show a decrease in the thermal conductivity as the thickness of the film decreases. It is expected that metallic nanoparticles will exhibit similar trends with size.

The studies described above imply that the contribution of the particle thermal conductivity to the effective thermal conductivity of a solid dispersion should also decrease as the size of the dispersed particles approaches the phonon mean free path. The following sections review data and models related to the thermal conductivity of dispersions of solid particles in liquids.

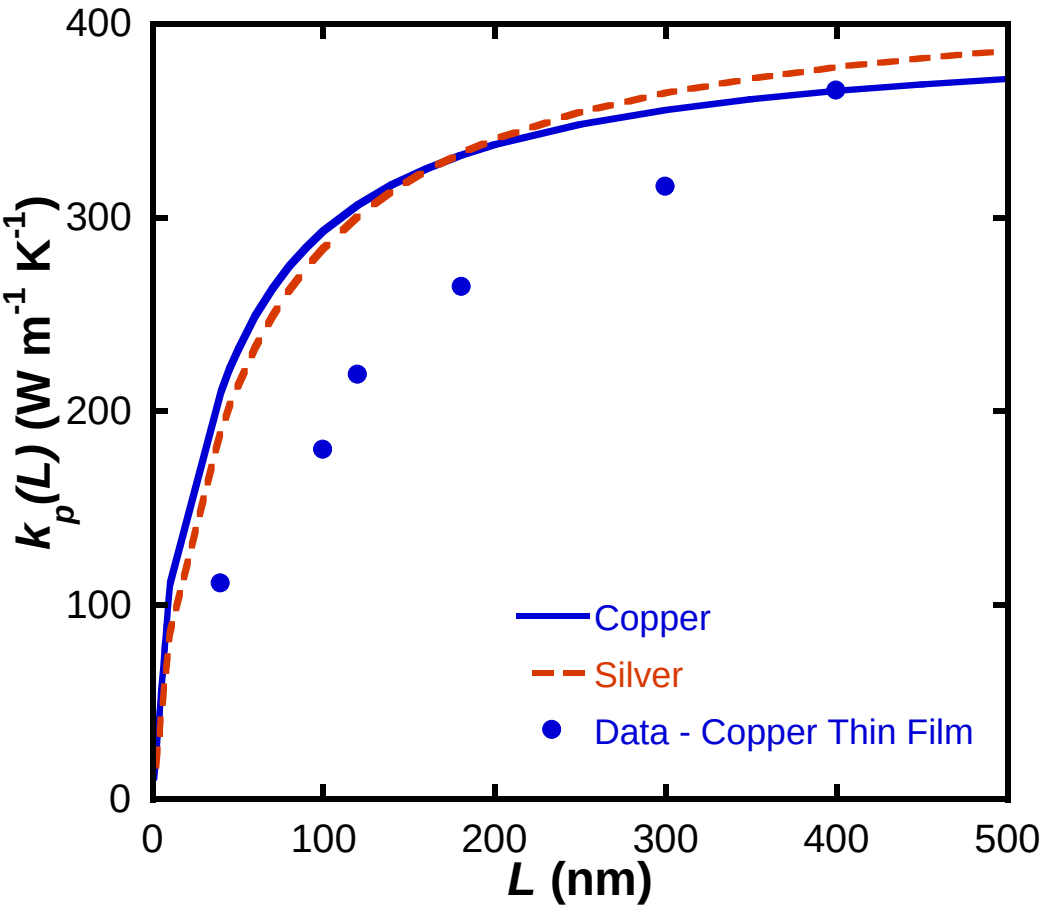

Figure 7.3. Thermal conductivity of copper and silver nanoparticles calculated using equations 7.8 and 7.10. Data points are for copper thin films [40].

7.3 Data Discussion

Although there have been numerous studies related to the transport properties of microparticle suspensions, only two are mentioned here because their conclusions relate directly to the behavior of nanoparticle suspensions. Shin and Lee [41] reported that the effective thermal conductivity of 10 % (v/v) dispersions of micron-sized polyethylene and polypropylene particles in mixtures of silicon oil and kerosene was about 13 % greater than the thermal conductivity of the base fluid. Moreover, they found a linear relationship between the effective thermal conductivity of the heterogeneous system and

the volume fraction of particles. Turian *et al.* [42] measured the thermal conductivity of a number of fluids containing as much as 50 % (v/v) of dispersed coal, glass, gypsum, or silica particles and reported modest increases in the thermal conductivity. For example, they observed an 18 % increase in the thermal conductivity in an aqueous dispersion containing 12 % (v/v) silica particles. In addition, a linear relationship between the thermal conductivity and particle volume fraction was observed, although there was a change in slope at about 0.1 volume fraction.

Fluids containing dispersed nanoparticles have been extensively studied since Choi [3] reported that heat transfer in liquids could be considerably enhanced by the addition of metallic nanoparticles. Thus, Eastman *et al.* [4] found that the addition of 0.3 % (v/v) copper nanoparticles to ethylene glycol resulted in an increase of 40 % in the thermal conductivity of the liquid, although about 1 % (v/v) thioglycolic acid was also added to the liquid to aid in dispersing the nanoparticles. Jana *et al.* [43] measured the thermal conductivity of a similar nanofluid, except that the base fluid was water containing laurate salt as a dispersant. They obtained a 70 % thermal conductivity enhancement when 0.3 % (v/v) copper nanoparticles were added to water. These large enhancements were attributed to increased transport resulting from the large surface area of the particles. Equally large thermal conductivity enhancements have been reported when metal oxides are added to liquids. An early study by Eastman *et al.* [44] reported that an aqueous nanofluid containing 5 % (v/v) copper oxide nanoparticles exhibited a thermal conductivity that was 60 % greater than that of water, and another aqueous nanofluid containing 5 % (v/v) alumina nanoparticles exhibited a thermal conductivity that was 40 % greater than that of water. More recent studies, however, have reported

more modest enhancements [45-48] in similar nanofluids. It should also be added here that differences in reported values of the enhancement are quite common in the nanofluid literature. On the other hand, extremely large enhancements have been reported when carbon nanotubes are dispersed in liquids. According to Yang *et al.* [49], the addition of 0.35 % (v/v) of multiwalled carbon nanotubes (MWCNT) to poly(α-olefin) oil results in a 200 % thermal conductivity enhancement; whereas, Choi *et al.* [20] have stated that a 150 % thermal conductivity enhancement is obtained when 1 % (v/v) MWCNT are added to poly(α-olefin) oil. It is clear from these studies that there is a significant increase in the thermal conductivity when solid particles are added to liquids, although the magnitude of the enhancement is not yet established. The enhancement is, however, proportional to the thermal conductivity of the dispersed particles.

7.3.1 Effect of Volume Fraction

Most studies of nanofluids have reported a linear relationship between the effective thermal conductivity and volume fraction of particles (as shown in Figure 7.4), although a few studies [53, 54] have also reported a change in slope when volume fractions are very small. The magnitudes of the reported enhancements in dilute systems have ranged from unusually high [4, 43, 55, 56] to negligibly small [47, 57].

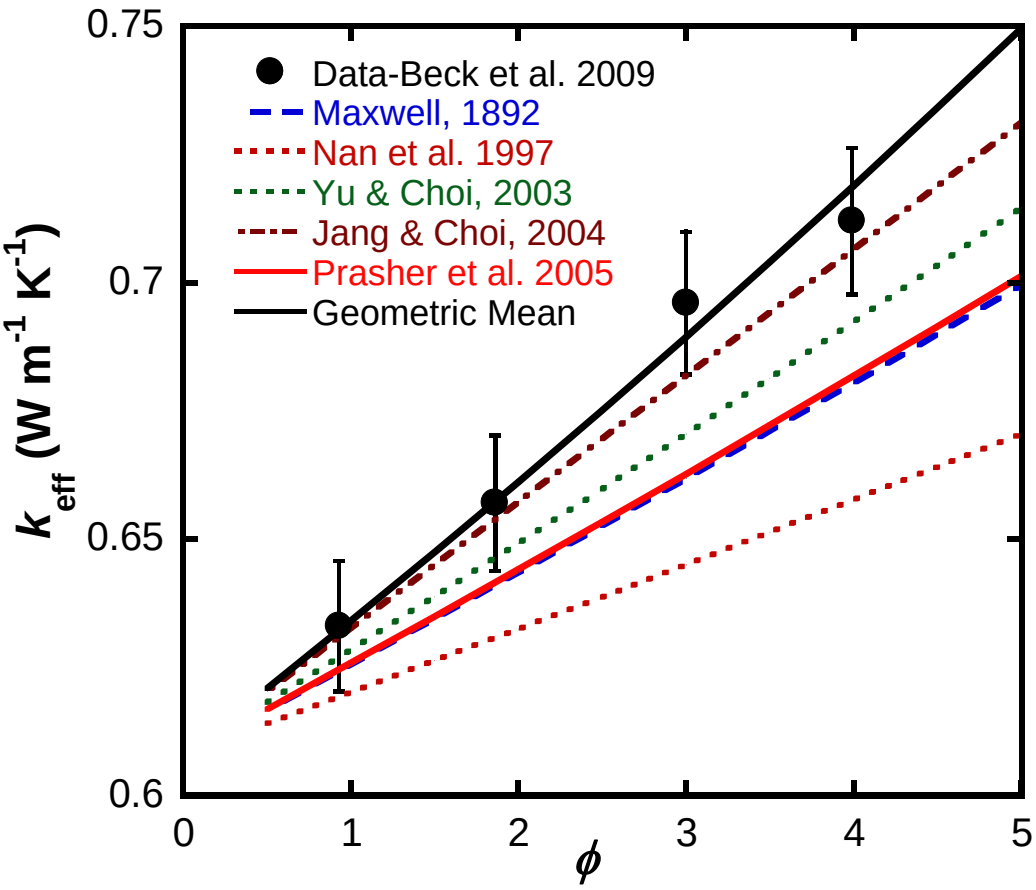

Figure 7.4. Thermal conductivity of an aqueous nanofluid containing 71 nm diameter alumina particles as a function of volume fraction. Data of Beck *et al.* [50].

7.3.2 Effect of Particle Size

The particle-size dependence of the thermal conductivity of dispersions has received considerable attention because of the widely held view that increasing surface to volume ratios must lead to enhanced heat transfer (and hence higher thermal conductivity) as the particle size decreases. Thus, Kim *et al.* [13] reported that enhancements obtained when 10 nm titania particles are dispersed in ethylene glycol are about twice those obtained when 70 nm particles are dispersed in the same fluid at the same volume fraction. Li and Peterson [58] also reported that enhancements in aqueous

alumina nanofluids were 8 % higher for 36 nm particles than for 47 nm particles. On the other hand, Xie *et al.* [12] reported that the thermal conductivity enhancement in alumina nanofluids exhibits a maximum at particle sizes between 12 and 304 nm. More recently, Beck *et al.* [50, 59] reported that the thermal conductivity of alumina nanofluids decreases with particle size below about 50 nm. This behavior is consistent with a decrease in the thermal conductivity of alumina particles with decreasing particle size.

7.3.3 Effect of Temperature

Das *et al.* [60] measured the thermal conductivity of aluminum and copper oxide nanofluids in water at temperatures between 293 and 323 K and concluded that the thermal conductivity of nanofluids increases with temperature. In contrast, Yang and Han [61] studied dispersions of Bi_2Te_3 nanorods in perfluorohexane and reported a decrease in the effective thermal conductivity as the temperature increased from 278 to 323 K. As noted previously, the thermal conductivity of nonpolar liquids generally decreases monotonically with increasing temperature [15], whereas that of associating liquids such as water generally exhibits a maximum in the thermal conductivity vs. temperature behavior. [16, 17] In the case of water, the maximum occurs at ~ 404 K. As many of the measurements on aqueous nanofluids have been made at temperatures below 400 K, they are in the region where the thermal conductivity of water increases with temperature. Also, as the volume fraction of particles in nanofluids is generally small, it is likely that the thermal conductivity of nanofluids is dominated by the thermal conductivity of the base fluid. To confirm this hypothesis, Beck *et al.* [62] measured the thermal conductivity of ethylene glycol-based alumina nanofluids at temperature ranging from 298 to 411 K

and found that the thermal conductivity vs. temperature behavior of the nanofluid follows closely that of the base fluid (ethylene glycol in this case). This behavior is shown in Figure 7.5 and has also been validated [59] when the base fluid is water or a mixture of water and ethylene glycol.

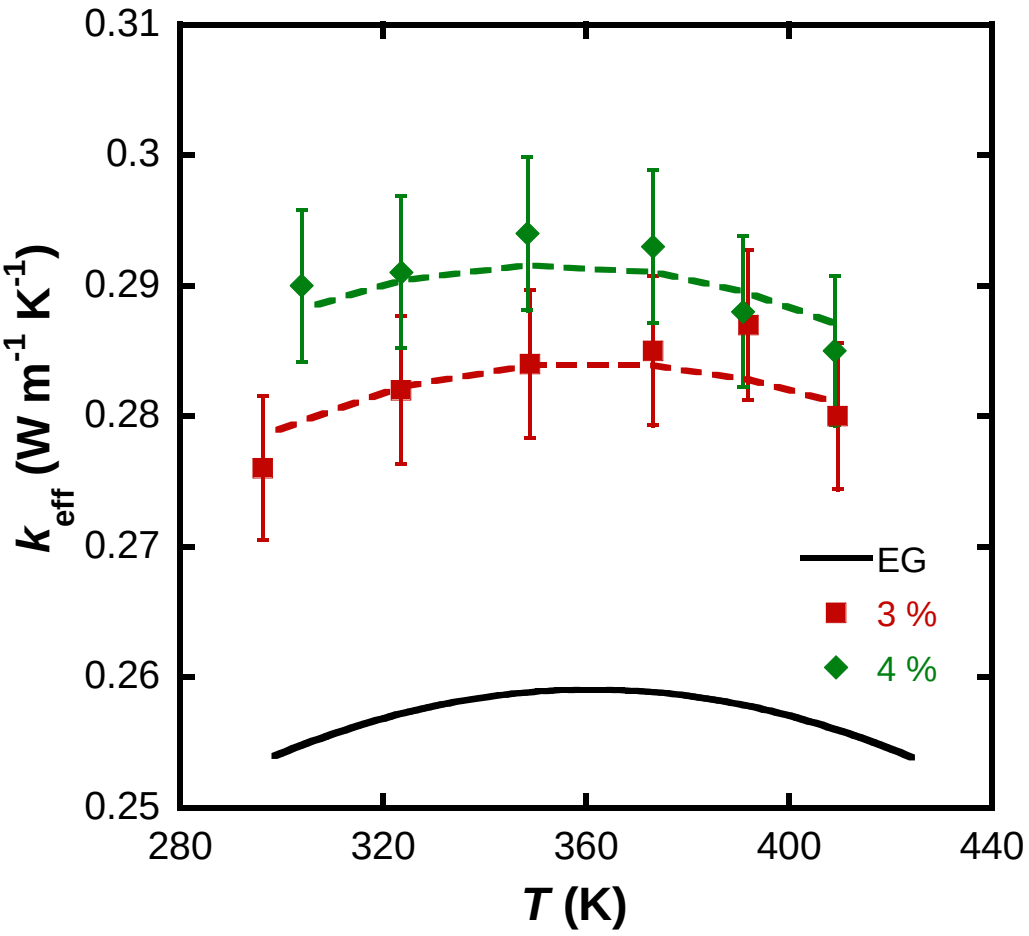

Figure 7.5. Thermal conductivity – temperature behavior of alumina nanofluids in ethylene glycol. Experimental data of Beck *et al.* [62]. The dashed lines represent fits of the nanofluid data.

7.3.4 Effect of the Particle to Fluid Thermal Conductivity Ratio α

Xie *et al.* [63] measured the thermal conductivity of 60 nm alumina particles dispersed in different base fluids, and found larger enhancements when values of α (=

k_p/k_l) were large. For example, the enhancement for alumina in pump oil (α = 326) was about 40 %, whereas that for alumina in water (α = 75) was about 23 %. Similar trends have been noted [60, 64-67] in nanofluids with the same base fluid but containing different nanoparticles. Also, some of the largest thermal conductivity enhancements have been observed in nanofluids containing highly thermally conductive particles such as copper [4], carbon nanotubes [20] and diamond [19].

7.3.5 Effect of Particle Surface Charge

Lee *et al.* [68] varied the pH of the solution before dispersing nanoparticles and observed greater thermal conductivity enhancement in acidic and basic solutions, and a lower enhancement at neutral pH values. They concluded that surface charges increase the stability of the dispersion leading to an increased thermal conductivity.

7.3.6 Effect of Particle Surface Charge

Wright *et al.* [69] studied the thermal conductivity of dilute nanofluids containing 0.01-0.02 % nickel-coated single walled carbon nanotubes (SWCNT) within a magnetic field. They observed greater thermal conductivity enhancement when the magnetic field was applied, which suggests that the nanotubes aligned to form conductive paths within the fluid. Hong *et al.* [70] and Wensel *et al.* [71] observed similar behavior in dilute nanofluids containing both iron oxide and SWCNTs. However, the thermal conductivity decreased after some time in the magnetic field due to agglomeration and settling of particles.

7.3.7 Summary of Findings

The following trends may be discerned from the studies outlined in the preceding paragraphs:

i. The addition of solid particles to liquids generally leads to a change in the effective thermal conductivity of nanofluids, in proportion to the amount (volume fraction) of particles added, and to the thermal conductivity of the solid particles.
ii. Thermal conductivity enhancements in the case of dilute nanofluids are generally less than 25 %, although a few studies have reported much larger enhancements.
iii. The temperature dependence of the effective thermal conductivity of nanofluids conforms closely to that of the base fluid.
iv. The effective thermal conductivity decreases with decreasing size of dispersed particles, when particles are very small.
v. The stability of the suspension and particle aggregation affects the thermal conductivity of nanofluids, although the magnitude of these effects has not been determined quantitatively.

The following paragraphs describe models for the effective thermal conductivity of dispersions and examine their applicability in light of these trends.

7.4 Model Evaluation

7.4.1 Models for Microparticle Dispersions

Maxwell [1] derived the following relationship for the thermal conductivity of dilute suspensions of spherical particles:

$$\frac{k_{eff}}{k_l} = 1 + \frac{3(\alpha - 1)\phi}{(\alpha + 2) - (\alpha - 1)\phi} \tag{7.11}$$

where k_{eff} is the effective thermal conductivity of the dispersion, α is the ratio (k_p/k_l) of thermal conductivity of the particle to that of the fluid, and ϕ is the particle volume fraction. The model is applicable to uniform dispersions of spherical particles when there are no particle interactions. Rayleigh [72] extended the Maxwell model to concentrated dispersions by considering spheres or cylinders arranged in a cubic lattice, whereas Hamilton and Crosser [2] proposed an extension that included an empirical factor n to account for the shape of particles as follows:

$$\frac{k_{eff}}{k_l} = 1 + \frac{n(\alpha - 1)\phi}{(\alpha + n - 1) - (\alpha - 1)\phi} \tag{7.12}$$

In equation 7.12, $n = 3/\psi$ and ψ is the sphericity of the particle. A second order extension of the Maxwell model was proposed by Jeffrey [73] by considering the effect of interactions between pairs of spheres. Models based on the effective medium theory were proposed by Progelhof *et al.* [74] and Landauer [75]. Maxwell type models generally imply an effective thermal conductivity that increases with the volume fraction of particles, is dependent mostly on the thermal conductivity of the base liquid, and is 0-15 % greater than that of the base liquid when $\phi < 0.05$. Turian *et al.* [42] demonstrated that these models, including those proposed by Maxwell [1], Jeffrey [73] and Progelhof *et al.* [74] are able to fit experimental data for dilute suspensions within 2 % when $0.4 < \alpha < 2.4$. Agreement with experiment becomes less satisfactory as α and ϕ increase. Note that

increasing ϕ often leads to particle aggregation and this cannot be accounted for by these models.

Krischer [76] considered an array of elements of specific resistance distributed in a matrix, and obtained:

$$k_{eff} = \left[\frac{1-f}{(1-\phi)k_l + \phi k_P} + f\left(\frac{1-\phi}{k_l} + \frac{\phi}{k_P} \right) \right]^{-1} \tag{7.13}$$

where f is an empirical factor equivalent to the fraction of parallel resistances in a rectangular array of elements. This model can be used to determine upper and lower bounds for the thermal conductivity of a heterogeneous system, with $f = 0$ signifying that all particles are arranged in series (creating a high thermal conductivity pathway) and $f = 1$ signifying that all particles are arranged in parallel (creating a low thermal conductivity arrangement). The actual value of f must be obtained by experiment. Tsao [77] developed a similar model by considering different geometries of the discrete phase, whereas Hashin and Shtrikman [78] derived more restrictive bounds using the variational theorem. Their bounds may be expressed as:

$$1 + \frac{3\phi(\alpha-1)}{\alpha+2-\phi(\alpha-1)} \leq \frac{k_{eff}}{k_l} \leq \alpha\left[1 - \frac{3(\alpha-1)(1-\varphi)}{3\alpha-\phi(\alpha-1)} \right] \tag{7.14}$$

In equation 7.14, the lower bound is the Maxwell limit. The upper bound implies an effective thermal conductivity that is higher than the Maxwell limit when particle aggregation is significant.

Turian *et al.* [42] noted that the upper and lower bounds of the Krischer model are equal to the volume-fraction-weighted arithmetic and harmonic means of the thermal conductivities of the two phases. The geometric mean of the two thermal conductivities falls between these bounds and also falls within the more restrictive Hashin - Shtrikman bounds when $\alpha > 5$. Turian *et al.* therefore used the volume fraction weighted geometric mean of the thermal conductivities of the individual phases defined by:

$$\frac{k_{eff}}{k_l} = \alpha^{\phi} \tag{7.15}$$

to calculate thermal conductivities of their suspensions. They found that the Maxwell model was able to fit data within 14.3 %, whereas equation 7.15 could predict data within 5.7 % of experimental values when $3.5 < \alpha < 70$. When $70 < \alpha < 200$, the average deviation was 26.3 % for the Maxwell equation and 9.9 % for equation 7.15. Turian *et al.* concluded that equation 7.15 provides good estimates of the effective thermal conductivity for particle suspensions when $\alpha > 3.5$. It should be added here that particle sizes in their suspensions were relatively large (of the order of microns).

Similar "mixture models" for the effective thermal conductivity of composites have also been proposed [79, 80]. These models may be summarized as follows:

$$\left(k_{eff}\right)^n = \phi \left(k_p\right)^n + \left(1-\phi\right)\left(k_l\right)^n \qquad -1 < n < 1 \tag{7.16}$$

When $n = 1$, equation 7.16 reduces to the arithmetic mean of the thermal conductivities of the two materials, and provides a good representation for conduction in materials arranged in parallel. Similarly, when $n = -1$, equation 7.16 reduces to the harmonic mean

of the two thermal conductivities, and provides a representation for conduction in materials arranged in series. Finally, for *n* approaching zero, equation 7.16 reduces to the geometric mean of the thermal conductivities of the two materials. As discussed previously, Turian *et al.* [42] have shown that the geometric mean works well in heterogeneous suspensions of micron-sized particles. Their conclusions agree with those of Prasher *et al.* [81] who suggested further that particle aggregation would result in thermal conductivity enhancements that are greater than those predicted by the Maxwell equation. None of these models, however, include any particle size dependence.

7.4.2 Nanofluid Models

Several mechanistic models for heat transport in nanofluids have been proposed to account for thermal conductivities that exceed values predicted by the Maxwell equation. These models are discussed below.

Yu and Choi [52] proposed a contribution to the thermal conductivity of nanofluids from an ordered liquid layer at the solid–liquid interface. This ordered layer is assumed to have a higher thermal conductivity than the bulk liquid, leading to an effective thermal conductivity given by:

$$\frac{k_{eff}}{k_l} = \frac{k_{pe} + 2k_l + 2\left(1+\beta_l\right)^3\left(k_{pe} - k_l\right)\phi}{k_{pe} + 2k_l - \left(1+\beta_l\right)^3\left(k_{pe} - k_l\right)\phi} \tag{7.17}$$

where β_l is the ratio of the ordered liquid layer thickness to the nanoparticle radius, and k_{pe} is the effective thermal conductivity of the particle defined by:

$$k_{pe} = \frac{\left[2(1-\gamma) + (1+\beta_l)^3(1+2\gamma)\right]\ \gamma}{(1+\beta_l)^3(1+2\gamma) - (1-\gamma)}\ k_p \tag{7.18}$$

Here, γ is the ratio of the thermal conductivity of the ordered liquid layer to that of the solid particle. Similar models based on an effective particle size that includes the surrounding ordered liquid layer have been proposed by others [82-87]. These models imply an inverse relationship of the effective thermal conductivity with particle size, and generally treat the thickness and thermal conductivity of the ordered liquid layer as adjustable parameters. However, values of the ordered layer thickness obtained by fitting data were found [84] to be between 1 - 3 nm, and the thermal conductivity of the ordered layer was reported [52, 85] to be about 5-10 times the thermal conductivity of the base fluid. In contrast, Li *et al.* [88] and Evans *et al.* [89] used MD simulations to estimate an ordered layer thickness of about 0.5 nm, and an ordered layer thermal conductivity of crystalline water to be about three times that of liquid water. Neither of these values is in agreement with that obtained by fitting data. Moreover, use of values from MD simulations leads to enhancements that are about the same as those predicted by the Maxwell equation, except when particle diameters are less than 5 nm.

A number of models attribute the enhanced thermal conductivity of nanofluids to a local microscale convective effect created by Brownian motion of particles. As an example, the Jang and Choi [90] equation combines contributions from the liquid, suspended particles, and Brownian motion of the particles to obtain:

$$\frac{k_{eff}}{k_l} = (1-\phi) + \varepsilon\,\alpha\,\phi + \phi\,C_1\,\frac{d_f}{d}\,\mathrm{Re}^2\,\mathrm{Pr} \tag{7.19}$$

where ε is a constant related to the interfacial thermal resistance, C_1 is a proportionality constant, d_f is the diameter of a fluid molecule, d is the particle diameter, and *Re* and *Pr* are the Reynolds the Prandtl numbers, respectively, based on the properties of the fluid. However, it has been demonstrated [42] that a linear combination of the individual thermal conductivity contributions is a poor predictor of the effective thermal conductivity of heterogeneous systems. This has led some researchers [91-95] to incorporate Brownian motion based particle size dependence directly into conventional thermal conductivity models for heterogeneous systems. For instance, Xuan *et al.* [94] included the microconvective effect of the dynamic particles in the Maxwell equation to obtain:

$$\frac{k_{eff}}{k_l} = \frac{\alpha + 2 + 2\phi(\alpha - 1)}{\alpha + 2 - \phi(\alpha - 1)} + \frac{18\phi H A k T}{\pi^2 \rho d^6 k_l} \tau \tag{7.20}$$

where H is the overall heat transfer coefficient between the particle and the fluid, A is the corresponding heat transfer area, and τ is a comprehensive relaxation time constant. The heat transfer area is proportional to the square of the diameter, leading to an effective thermal conductivity that is inversely proportional to the fourth power of the particle diameter. Such strong inverse dependence on particle size has not been demonstrated experimentally. In addition, equation 7.20 reduces to the Maxwell equation with increasing particle size, and cannot therefore account for thermal conductivities that are greater than the Maxwell limit.

Models that incorporate an interfacial thermal resistance into the Maxwell equation have been published by Nan *et al.* [51] and others. The interfacial thermal

resistance is related to the different rates of transport in the two phases that lead to a temperature discontinuity at the solid-liquid interface. The interfacial resistance is sometimes referred to as the Kapitza resistance [96] and includes the effects of phonon scattering at the interface, as well as other phenomena that create resistance to heat transport such as poor contact between the phases. For spheres, the Nan *et al.* model can be written as follows:

$$\frac{k_{eff}}{k_l} = \frac{\alpha(1+2\chi) + 2 + 2\,\phi\left[\alpha(1-\chi)-1\right]}{\alpha\,(1+2\chi) + 2 - \phi\left[\alpha(1-\chi)-1\right]} \tag{7.21}$$

where $\chi = R_B\, k_l / d$ and R_B is the interfacial thermal resistance. Equation 7.21 reduces to the Maxwell equation when $\chi << 1$ and is thus incapable of representing enhancements that are greater than those predicted by the Maxwell equation. However, it correctly predicts a decrease in effective thermal conductivity with particle size.

Another type of model takes account of particle aggregation in nanofluids and was proposed by Prasher *et al.* [81]. Their model assumes that particle aggregates form conductive pathways in the fluid resulting in enhancements that are greater than those predicted by the Maxwell model. However, the model requires information on aggregate size, as well as the fraction of particles forming conductive pathways. These quantities are seldom available, although the hypothesis that particle clustering enhances conduction in suspensions is supported by numerical simulations and molecular dynamics studies [97-99].

Figure 7.6 displays a comparison of thermal conductivity predictions from various models and their relationship with particle diameter. With the exception of the Nan et al. model, all models described above predict an inverse relationship between nanofluid thermal conductivity and particle size. The models therefore predict an increase in the effective thermal conductivity as the particle size decreases. As noted previously, the thermal conductivity of thin films and nanowires decreases with decreasing size [29] and this trend should be more pronounced in nanoparticles due to confinement of phonon waves in all three dimensions. Recent experimental data [50, 59, 100, 101] confirm such a trend. Thus, none of the above models are able to correctly predict both the size-dependence of the effective thermal conductivity and enhancements that are greater than the Maxwell limit.

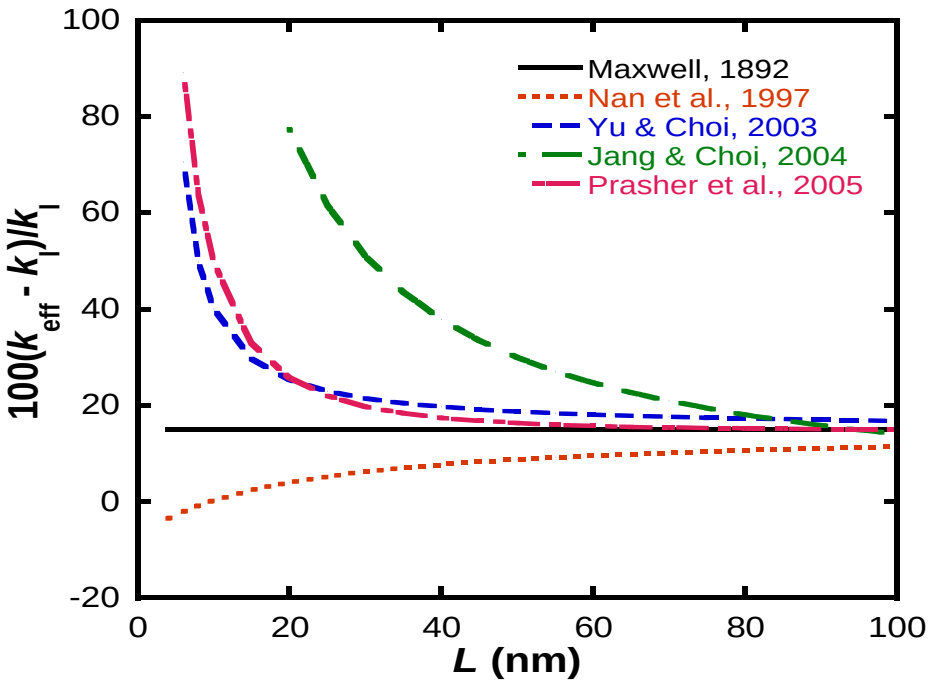

Figure 7.6. Calculated thermal conductivity enhancement as a function of particle size for an aqueous nanofluid containing 5 % (v/v) alumina at room temperature from several models.

7.5 Modified Geometric Mean Model

All published models for the thermal conductivity of nanofluids predict a linear dependence of the enhancement on particle volume fraction, which is confirmed by published data. However, as shown in Figure 7.4, the magnitude of the thermal conductivity is not necessarily predicted well by all models. In addition, the dependence with respect to temperature and particle size is not represented adequately by many of these models. The Nan *et al.* [51] model reproduces the general trends of thermal conductivity data with particle volume fraction, temperature, and particle diameter. However, the model reduces to the Maxwell model at large particle sizes and cannot therefore reproduce enhancements that are greater than those predicted by the Maxwell model.

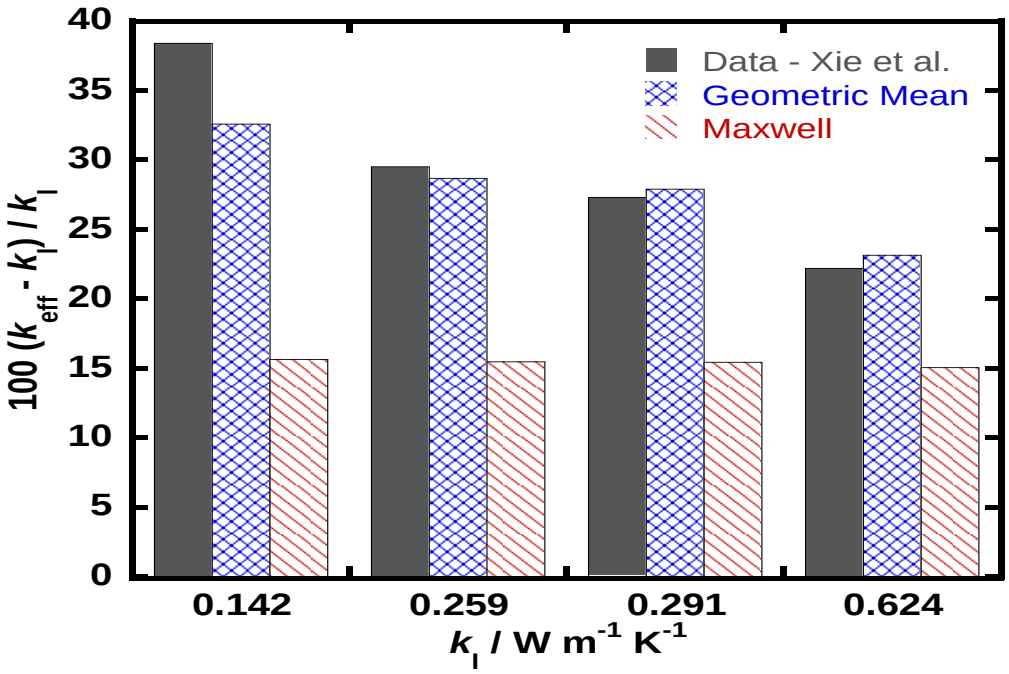

Figure 7.7. The thermal conductivity of 5 % (v/v) alumina in pump oil, ethylene glycol, glycerol, and water. Data of Xie *et al.* [63] and predictions of Maxwell [1] and geometric mean [42] models.

Figure 7.7 compares predictions of the geometric mean and Maxwell models with experimental data on nanofluids containing alumina particles larger than 50 nm. The predictions of the geometric mean model are within 2 % of experimental values irrespective of the base fluid (pump oil, ethylene glycol, glycerol, or water). It would therefore appear that the geometric mean is capable of predicting the limiting value of the thermal conductivity of alumina nanofluids. However, the geometric mean model does not explicitly include any particle size dependence.

The size-dependent thermal conductivity from equations 7.1, 7.8, and 7.10 was incorporated into the volume fraction weighted geometric mean to obtain a modified geometric mean model as follows [34, 102]:

$$\frac{k_{eff}(L,T,\varphi)}{k_l(T)} = \left[\frac{k_p(L,T)}{k_l(T)}\right]^{\varphi} \tag{7.22}$$

where $k_p(L,T)$ is the size dependent thermal conductivity of the nanoparticle. The following section will discuss the applicability of modified geometric mean model for nanofluids containing metallic and insulator nanoparticles.

7.6 Evaluation of Modified Geometric Mean Model

7.6.1 Nanofluid Containing Semiconductor or Insulator Particles

The modified geometric mean model was evaluated using data on alumina, ceria, and titania nanofluids. The material properties required to calculate the size dependent thermal conductivity of alumina, ceria, and titania nanoparticles are listed in Table 7.1.

Figure 7.8 compares the predictions of modified geometric mean model (equations 7.1 and 7.22) with the experimental data for alumina nanofluids [50, 59]. Equation 7.22 was fitted by minimizing the average absolute deviation in k_{eff} with p as the adjustable parameter. Optimized values for each particle size are as follows: 8 nm, p=0.12; 12 nm, p=0.21; 16 nm, p=0.28; 71, 245, and 282 nm, p=1. In order to ascertain if the values of p obtained are physically realistic, the relation [32] $p = 1 - 10\ \eta/L$ was used to calculate the surface roughness η. The surface roughness was found to be less than 10 % of the particle size in all cases, which appears to be reasonable. Figure 7.9 shows predictions of the thermal conductivity of alumina nanofluids in water and ethylene glycol using equation 7.22. A single value of p was used for each particle size irrespective of the base fluid or temperature. For example, for 12 nm alumina particles, a value of p = 0.28 was obtained by fitting the nanofluid data of 12 nm alumina particles in water as well as in ethylene glycol. As observed for alumina nanofluids, equation 7.22 is able to predict the decrease in thermal conductivity of ceria nanofluids [100] with decreasing particle size. The average absolute deviation from the experimental values is 2.85 %.

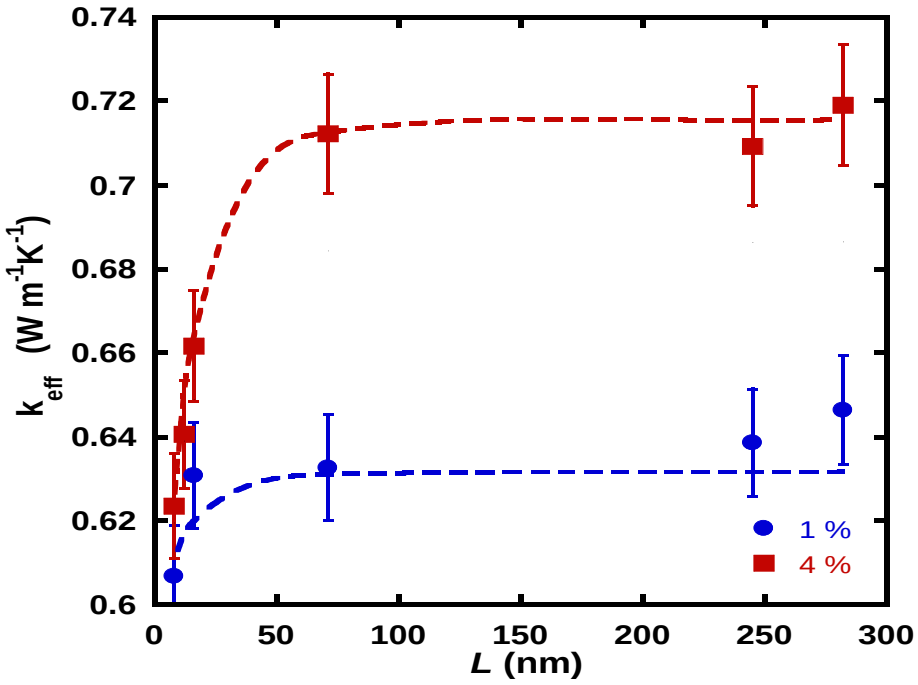

Figure 7.8. Thermal conductivity of aqueous nanofluids containing 1 and 4 % (v/v) alumina particles at room temperature. Points represent experimental values of Beck *et al.* [50]. Dashed lines represent calculations using equations 7.1 and 7.22.

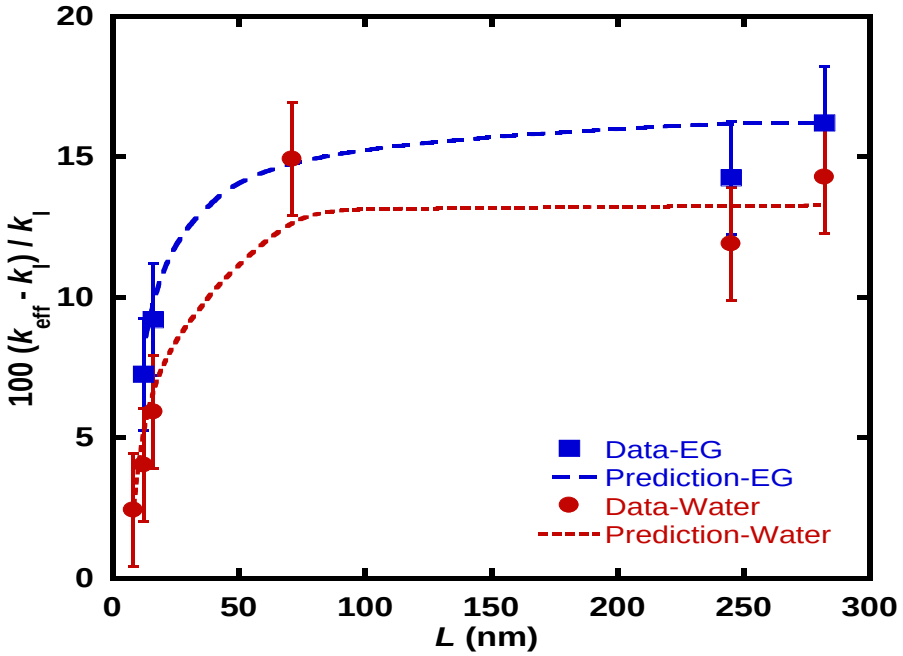

Figure 7.9. Thermal conductivity enhancement in water and ethylene glycol based nanofluids containing 3 % (v/v) alumina particles at 298 K as a function of particle size. Dashed lines represent equation 7.22 using the same values of *p* as in Figure 7.8.

Variation in thermal conductivity of solids enables us to tailor particles that exhibit a thermal conductivity that is lower than that of common liquids, and to design nanofluids that exhibit negative thermal conductivity enhancement or a decrease in the effective thermal conductivity of the dispersion compared with that of the base liquid. This was experimentally demonstrated by Teja *et al.* [103] for nanofluids containing 2 nm titania particles dispersed in ethylene glycol+water mixture. None of the models discussed in Section 7.4 could have predicted this behavior as none considers the size effect on intrinsic thermal conductivity of particles. It can be observed from Figure 7.10 that modified geometric mean model is able to correctly predict the decrease in thermal conductivity of fluid upon addition of nanoparticles with only one value of adjustable parameter p (= 0.41).

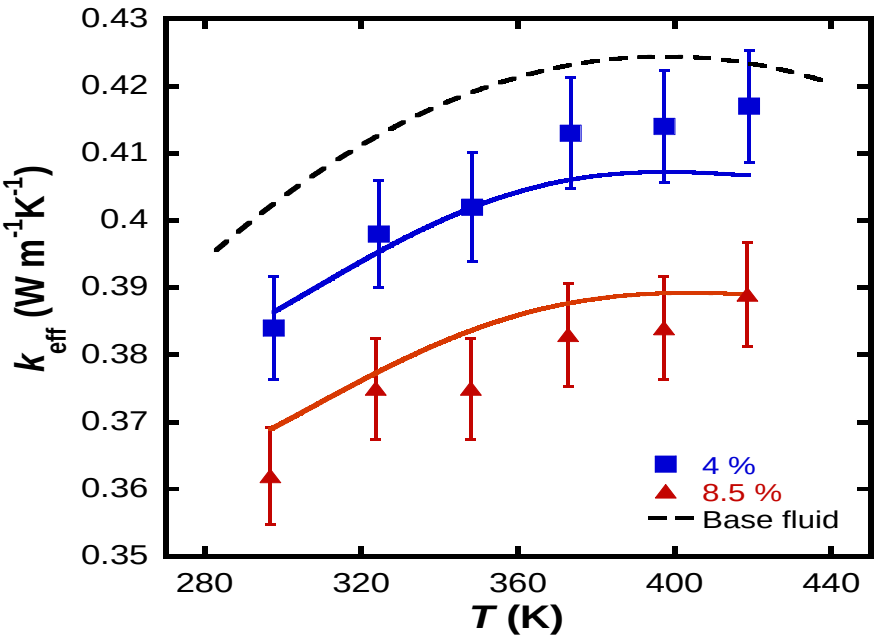

Figure 7.10. Thermal conductivity of 2 nm titania nanoparticles dispersed in ethylene glycol + water mixture. The data points are from Teja *et al.* [103]. Solid lines are predictions using the modified geometric mean model with p = 0.41.

Tables 7.4 - 7.12 list average deviations between experimental thermal conductivities of several nanofluids and calculated values using equations 7.1 and 7.22. In the case of alumina nanofluids, comparisons are also shown with the Nan *et al.* model (equation 7.21). Because of lack of published data on interfacial thermal resistance, the Nan *et al*. model could not be evaluated for other nanofluids. Optimized values of *p* were obtained by minimizing the average absolute deviation between experimental and predicted values and are also given in Table 7.4. Thermal conductivities of the base fluids were obtained by fitting literature data [16, 17]. Thermal conductivities of the solids were assumed to be independent of temperature within the temperature ranges encountered in this study.

Table 7.4. Comparing the geometric mean (GM), modified geometric mean (mGM), and Nan *et al.* models with experimental data for alumina nanofluids.

Data Reference	Particle size (nm)	Fluid	T (K)	AAD (%)			
				Nan *et al.* model [51]	GM	mGM	mGM (*p*)
44	33	Water	298	11.03	3.2	3.87	3.87 (1)
108	35	Water	298	5.46	2.76	2.09	0.47 (0.54)
66	38.4	Water	298	2.28	5.55	4.98	0.19 (0.18)
	38.4	EG	298	3.81	5.64	5.04	0.58 (0.18)
65	28	Water	298	8.17	4.71	3.39	2.52 (0.75)
	28	EG	298	15.8	3.74	2.68	2.36 (0.75)
12, 63	60.4	Water	298	8.79	1.32	1.56	1.56 (1)
	12.4-302	EG	298	7.29	4.39	3.39	1.48 (0. 3)
60	38.4	Water	294-324	6.88	3.61	3.56	3.52 (0.86)
109	13-182	Water	294-344	6.69	4.36	4.46	4.46 (1)
64	36	Water	301-309	7.97	13.54	12.53	6.47 (0.14)
45-47	20	Water	283-323	5.74	20.32	16.48	2.14 (0.09)
13	38	Water	298	1.57	2.09	1.83	0.16 (0.24)
	38	EG	298	2.85	3.42	3.02	0.15 (0.24)
58	36 and 47	Water	302-310	5.19	4.11	3.89	3.48 0.54)
48	11-40	Water	296-333	4.59	14.89	12.13	1.93 (0.13)
	11-40	EG	296-333	4.06	15.43	12.98	2.11 (0.13)
104, 110	48	Water	298	2.53	0.61	0.71	0.71 (1)
111	45	Water	298	1.76	4.62	1.45	0.69 (0.63)
	45	EG	298	7.38	1.04	6.97	5.75 (0.63)

Table 7.5. Comparing the geometric mean (GM), and modified geometric mean (mGM) models with experimental data for titania nanofluids.

Data Reference	Particle Size (nm)	Fluid	T (K)	AAD (%)	
				GM	mGM (*p*)
53	15	Water	298	11.02	11.55 (1)
13	10-79	Water	298	1.16	1.46 (1)
	10-79	EG	298	1.76	2.05 (1)
104	25	Water	298	9.54	9.62 (1)
112	26	Water	291-338	0.78	0.76 (1)
45	40	Water	283-313	0.66	0.49 (0.93)
103	2	Water+EG	297-421	33.12	2.99 (0.07)
113	21	Water	288-308	1.13	1.09 (0.92)

Table 7.6. Comparing the geometric mean (GM), and modified geometric mean (mGM) models with experimental data for ceria nanofluids.

Data Reference	Particle Size (nm)	Fluid	T (K)	AAD (%)	
				GM	mGM (*p*)
100	12 and 74	Water	298	3.17	2.85 (1)

Table 7.7. Comparing the geometric mean (GM), and modified geometric mean (mGM) models with experimental data for copper oxide nanofluids.

Data Reference	Particle size (nm)	Fluid	T (K)	AAD (%)	
				GM	mGM (p)
44	36	Water	298	13.59	14.61 (1)
108	36	Water	298	0.85	0.83 (0.94)
66	23.6	Water	298	6.94	0.99 (0.22)
	23.6	EG	298	3.03	2.37 (0.22)
65	23	Water	298	17.38	2.61 (0.14)
	23	EG	298	32.77	2.37 (0.14)
60	28.6	Water	294-324	8.38	8.99 (1)
114	12	Water	298	0.84	0.4 (1)
67	33	Water	298	0.13	0.58 (1)
	33	EG	298	3.03	3.47 (1)
68	25	Water	298	6.89	6.95 (1)
64	29	Water	302-309	14.59	16.43 (1)
115	29	EG	298	4.47	0.62 (0.37)
45, 46	33	Water	283-303	8.03	0.88 (0.19)

Table 7.8. Comparing the geometric mean (GM), and modified geometric mean (mGM) models with experimental data for silicon dioxide nanofluids.

Data Reference	Particle size (nm)	Fluid	T (K)	AAD (%)	
				GM	mGM (p)
67	12	Water	298	2.37	3.52 (1)
19	20	Water	298	1.09	2.82 (1)
	23	Water	298	1.95	2.55 (1)
112	23	EG	298	2.04	2.64 (1)
	23	Ethanol	298	2.32	2.92 (1)

Table 7.9. Comparing the geometric mean (GM), and modified geometric mean (mGM) models with experimental data for iron oxide nanofluids.

Data Reference	Particle size (nm)	Fluid	T (K)	AAD (%)	
				GM	mGM (p)
54	10	Water	298	18.82	28.31 (1)

Table 7.10. Comparing the geometric mean (GM), and modified geometric mean (mGM) models with experimental data for zinc oxide nanofluids.

Data Reference	Particle size (nm)	Fluid	T (K)	AAD (%)	
				GM	mGM (p)
13	10-60	Water	298	1.77	2.20 (0.32)
	30 and 60	EG	298	2.77	2.93 (0.32)

Table 7.11. Comparing the geometric mean (GM), and modified geometric mean (mGM) models with experimental data for diamond nanofluids.

Data Reference	Particle size (nm)	Fluid	T (K)	AAD (%)	
				GM	mGM (p)
19	40	EG	298	17.11	18.29 (1)
105	10	Water+EG	298	1.95	14.19 (1)

Table 7.12. Comparing the geometric mean (GM), and modified geometric mean (mGM) models with experimental data for silicon carbide nanofluids.

Data Reference	Particle size (nm)	Fluid	T (K)	AAD (%)	
				GM	mGM (p)
116	26 and 900	Water	277	11.51	5.78 (0.03)
	26 and 900	EG	277	13.57	4.31 (0.03)
117	130	Water	296-343	4.27	0.71 (0.13)

Tables 7.4 - 7.12 show that deviations between experimental and predicted thermal conductivities using the modified geometric mean model are generally less than ±3 %. Deviations greater than ±3 % occur when the reported experimental value is unusually high, or when the effect of particle size or temperature is not in agreement with the experimental trends noted above. For example, Li [64] reported a linear increase in thermal conductivity with temperature for alumina nanofluids and also ignored the temperature dependence of the thermal conductivity of their base fluids when calculating their enhancements. Hence, deviations between experimental and calculated values in Table 7.4 for the Li data are greater than 3 %. In Table 7.5, large deviations were obtained in fitting the Mursheed [53] and Yoo [104] data because the reported enhancements of 14 - 18 % are unusually high for nanofluids containing 1 % (v/v) titania particles. This is also true for the Zhu *et al.* [54] data for iron oxide nanofluids in Table 7.9. Zhu *et al.* obtained enhancements of 15 - 30 % in the case of 0.5 - 1.5 % (v/v) iron oxide nanofluids and attributed these high values to alignment of iron oxide nanoparticles. In addition, they also reported a nonlinear dependence of thermal conductivity on particle volume fraction for these nanofluids, which is unusual. In the case of diamond nanofluids (Table 7.11), predictions of the modified geometric mean

model appear to be poor because the phonon mean free path for diamond (104.81 nm) is an order of magnitude larger than its particle size (10 nm) [105]. It appears that the Liang and Li equation may not be applicable in this case because the equation does not account for quantum size effects [23]. For most nanofluids containing semiconductor or insulator particles, however, the modified geometric mean model provides good estimates of the effective thermal conductivity without any adjustable parameters. If roughness must be accounted for, then one parameter can be included in the model and optimized using data for one base fluid. Thermal conductivities for other base fluids, particle sizes, and temperatures may then be predicted.

7.6.2 Nanofluid Containing Metallic Particles

Literature data for nanofluids containing metallic nanoparticles were compiled and fitted using equation 7.16 with and without considering the size dependence of the thermal conductivity of the particles. Table 7.13 lists our results for the two cases. Equation 7.16 is able to fit the literature data for nanofluids containing metallic particles reasonably well. However, values of n required to fit the data are higher than expected, and increase when the size dependence is considered. High values of n appear to be related to unusually large thermal conductivity enhancements. For example, enhancements of 80 % were reported for 0.3 % (v/v) copper nanoparticles [43] in water, and 10 % enhancements were reported for as little as 0.005 % (v/v) gold nanoparticles in water [119]. By contrast, Jana *et al*. [43] report 35 % enhancement in the thermal conductivity of nanofluids containing 0.8 % (v/v) carbon nanotubes (CNT). Since the thermal conductivity of CNT is about an order of magnitude higher than that of copper or

gold, we would expect nanofluids containing copper or gold particles to exhibit lower enhancements than nanofluids containing CNTs, or for nanofluids containing CNTs to exhibit much larger enhancements than nanofluids containing copper or gold. Clearly, there are inconsistencies in the literature data. This is also apparent in the results of Li *et al*. [121] for 0.5 % (v/v) copper particles in ethylene glycol (EG). Their work reports an increase in the thermal conductivity enhancement from about 10 % to about 45 % when the temperature increases from 10 to 50 °C, but shows no increase in the thermal conductivity of EG with temperature. Finally, it should be noted that many of these experiments employed very low volume fractions of nanoparticles. As a result, it is often difficult to separate size effects in these studies. Therefore, the thermal conductivity of nanofluids containing relatively higher volume fractions of metallic nanoparticles was measured in this work.

Table 7.13. Evaluation of the modified geometric mean thermal conductivity model for nanofluids containing metallic particles.

Particle	Fluid	φ / % v/v	T / K	L / nm	Data Ref.	Size Indep.		Size Dep.	
						AAD %	n	AAD %	n
Ag	Water	1-4 $\times 10^{-1}$	298	15	[19]	0.40	0.38	0.40	0.55
Ag+ citrate	Water	1 $\times 10^{-3}$	303-333	70	[119]	2.99	1.00	3.25	1.00
Cu	EG	1-3 $\times 10^{-1}$	298	10	[4]	5.24	0.60	5.40	0.82
Cu	Water	2.5-7.5	298	100	[120]	2.15	0.06	2.10	0.08
Cu	PFTE	2-25 $\times 10^{-1}$	298	26	[121]	3.47	0.14	3.45	0.19
Cu	EG	3-5 $\times 10^{-1}$	278-323	7.5	[122]	7.07	0.39	6.75	0.61
Cu	Water	5-30 $\times 10^{-2}$	298	42.5	[43]	1.61	0.81	1.56	0.92
Cu	Water	2-9 $\times 10^{-3}$	298	25	[113]	6.27	0.77	6.24	0.93
Au+ thiolate	Toluene	5-11 $\times 10^{-3}$	299-333	3.5	[119]	0.77	0.81	2.60	1.00
Au+ citrate	Water	1.3-2.6 $\times 10^{-3}$	303-333	15	[119]	5.19	1.00	5.25	1.00

PFTE = Perfluorotriethylamine

7.2.2.1 Experimental

Silver nanoparticles of sizes 20 nm, 30-50 nm, and 80 nm, loaded with 0.3 wt. % polyvinylpyrrolidone (PVP), were purchased from Nanostructured and Amorphous Materials, Inc. (Los Alamos, NM) and dispersed in ethylene glycol to make nanofluids. The particle sizes were chosen to span sizes below and above the mean free path of electrons in silver. SEM/TEM images of the particles provided by the vendor are shown in Figure 7.11 and appear to show significant aggregation of the 20 nm particles. Nanofluids were prepared by dispersing pre-weighed quantities of nanoparticles into

ethylene glycol. The samples were subjected to ultrasonic processing to obtain dispersions. The nanofluid dispersions remained stable without any noticeable settling for over 2 hours after processing.

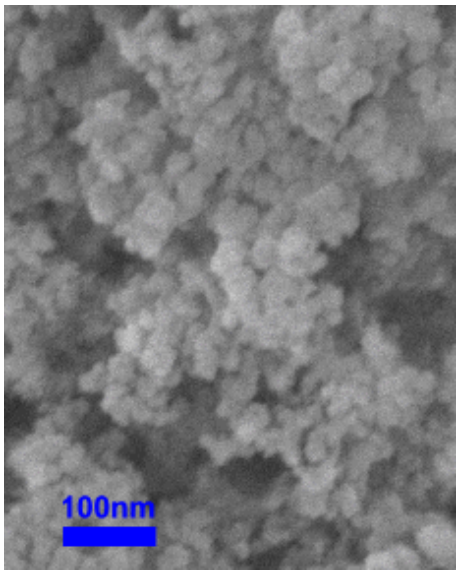

(a) 20 nm

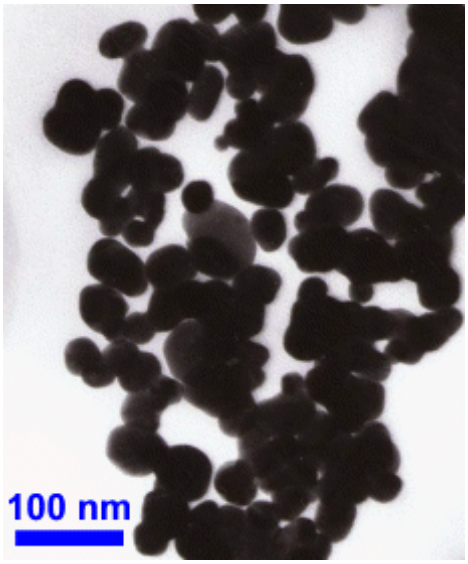

(b) 30-50 nm

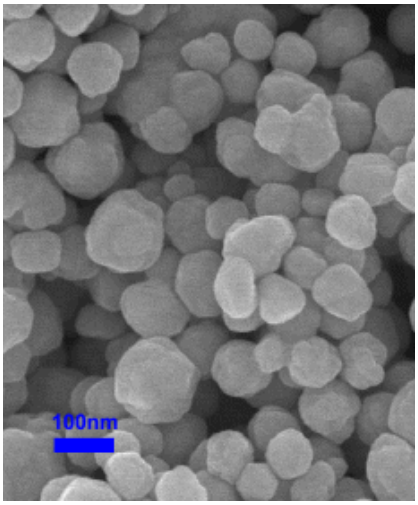

(c) 80 nm

Figure 7.11. SEM/ TEM images of the silver nanoparticles provided by Nanostructured and Amorphous Materials, Inc. (Los Alamos, NM).

The thermal conductivity of each nanofluid was measured using the transient hot-wire method as described in Section 5.2.1.4. The experiment was performed five times for each sample and condition, and a data point reported in this work thus represents an average of 5 measurements with an estimated error of ± 2 %.

Table 7.14. Thermal conductivity of nanofluids consisting of silver nanoparticles dispersed in ethylene glycol.

T (K)	φ (% v/v)	d (nm)	k_P (W m^{-1} K^{-1})	k_{eff} (Wm^{-1}K^{-1})	Standard deviation in k_{eff}
299.3	1	20	123.49	0.2700	0.0052
299.9	1	30-50	191.32	0.2701	0.0025
298.4	1	80	263.50	0.2798	0.0023
300.8	2	20	123.49	0.3048	0.0029
300.9	2	30-50	191.32	0.2907	0.0023
300.5	2	80	263.50	0.3089	0.0033

Table 7.14 presents measured values of the thermal conductivity enhancement for silver nanofluids. As noted previously, each data point represents the average of five measurements at a specific concentration and room temperature. The experimental data along with calculations using equation 7.16 with and without considering the size dependence are presented in Figure 7.12. First, the size dependent model (equation 7.16 + equations 7.8 and 7.10) was used to correlate the data and a value of n = 0.088 was found to give the best fit with an AAD = 2.01 %. Then, the same value of n was used in the size independent model (equation 7.16) and resulted in an AAD = 3.64 %. Figure 7.12 appears to confirm that the thermal conductivity of the nanofluid decreases with decreasing particle size, although the results are not conclusive. This could be due to the

higher than expected thermal conductivity of nanofluids containing 20 nm silver particles resulting from aggregation (Figure 7.11a). Since the dry 20 nm particles were highly aggregated when purchased, it is likely that they are aggregated in the dispersion despite being subjected to sonication. In an aggregated structure, a fraction of the particles form a conductive pathway which could results in enhanced conduction [97]. This is supported by numerical simulations and molecular dynamics studies [98-100]. On the other hand, the value of $n = 0.088$ obtained by fitting data implies that the extent of aggregation was probably small and most particles were randomly dispersed in the fluid. Values of n close to ±1 in Table 7.13, obtained by fitting literature data, do not appear to be physically reasonable because they imply series (-1) or parallel (+1) alignment of particles.

The results are in agreement with our previous work on nanofluids containing semiconductor or insulator particles, and appear to confirm that the thermal conductivity of silver nanofluids decreases with decreasing particle size.

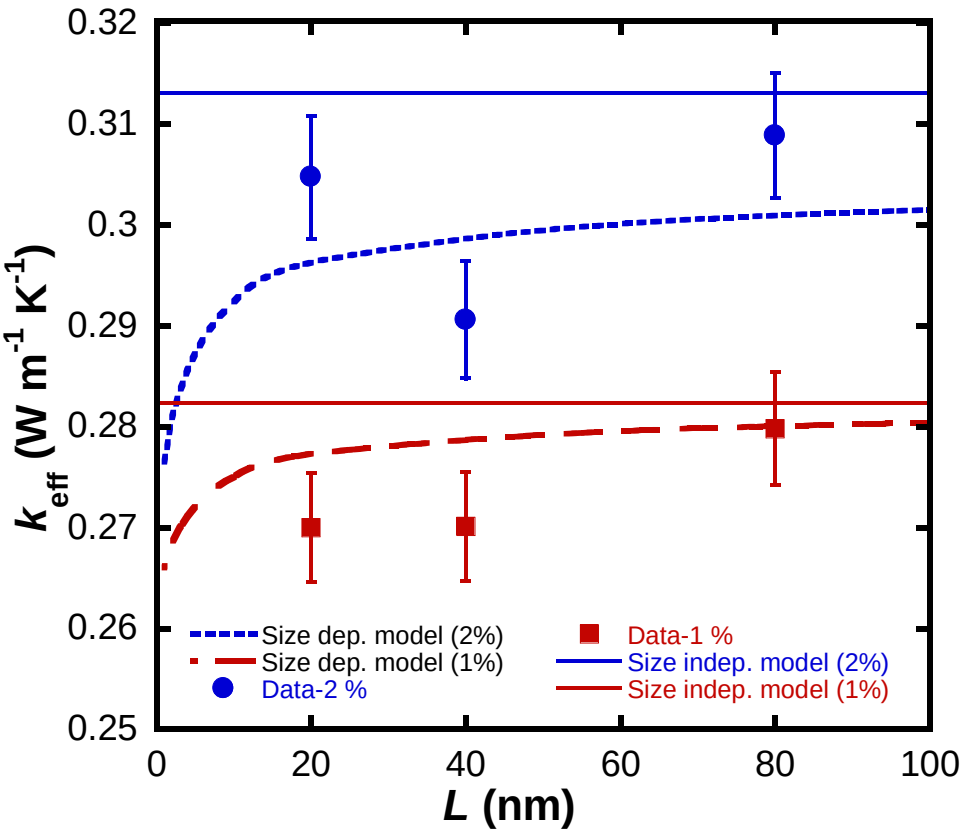

Figure 7.12. Effect of particle size on the thermal conductivity of nanofluids containing silver nanoparticles. Points represent experimental data of this work. Dashed and solid lines represent calculated values assuming size dependence and without size dependence.

7.7 Nanofluid Viscosity

As discussed in previous sections, most studies in nanofluids have focused on thermal properties of nanofluids where it is apparent that addition of nanoparticles results in an enhancement in the thermal conductivity of nanofluids. Very few studies have investigated the rheological properties of nanofluids, although any increase in viscosity is likely to adversely affect pumping of nanofluids.

7.7.1 Data Discussion

As noted above, the few available studies of the rheological characteristics of nanofluids show that viscosity increases with the addition of particles, and with increasing particle volume fraction. Although the base fluids in all studies were Newtonian, these studies [126-131] report that nanofluids exhibit non-Newtonian shear thinning behavior. A few studies [132, 133] also report Newtonian behavior at low particle concentrations. As observed for thermal conductivity, the temperature behavior of nanofluid viscosity appears to follow that of the base fluids and shows a decrease in viscosity with increasing temperature [126, 130, 134]. The effect of particle size on nanofluid viscosity was studied by Chang *et al.* [135], Kang *et al.* [19], Zhao *et al.* [136] and others. The viscosity of nanofluids was found to increase with decreasing particle size. Zhao *et al.* [136] observed that for particle sizes below ~ 20 nm, the ratio of aggregate size to particle diameter increased significantly resulting in nonlinear increase in viscosity with decreasing particle size. Unlike thermal conductivity, the nanofluid viscosity studies appear to agree with each other qualitatively. The discrepancies in the magnitude of the increase can be attributed to the method of nanofluid preparation and stabilization technique used.

7.7.2 Viscosity Models

Einstein [137] investigated the viscosity of colloidal dispersions and developed the following equation for very dilute dispersions of hard spheres:

$$\eta = \eta_0 (1 + [\eta]\phi) \tag{7.23}$$

where η is the viscosity of the dispersion, η_0 is the viscosity of the base fluid, ϕ is the volume fraction and [η] is the intrinsic viscosity of the suspension. For hard spheres, [η] = 2.5. Einstein's model works well for dilute suspensions (ϕ < 0.01). For concentrated suspensions, the model was extended by Batchelor [138] as follows:

$$\eta_r = \frac{\eta}{\eta_0} = 1 + [\eta]\phi + k_H([\eta]\phi)^2 \tag{7.24}$$

where k_H is the Huggins constant and accounts for interparticle interactions.

A semi-empirical relationship for the viscosity covering the full range of particle volume fraction was obtained by Krieger and Dougherty [139, 140]:

$$\eta_r = \left(1 - \frac{\phi_a}{\phi_m}\right)^{-[\eta]\phi_m} \tag{7.25}$$

where $\phi_a = \phi / \phi_{ma}$ and ϕ_{ma} is the packing fraction of the aggregates and ϕ_m is the maximum particle packing fraction. For power law fluids with consistency index D,

$$\phi_a = \phi\left(\frac{a_a}{a}\right)^{3-D} \tag{7.26}$$

where a_a/a is the ratio of the effective radii of the aggregate to that of primary particle. ϕ_m generally varies from 0.495 to 0.54 under quiescent conditions, and is approximately 0.605 at high shear rates [141].

The Krieger and Dougherty model is widely used as it covers the entire range of particle concentrations. However, aggregation alone cannot describe the rheological

properties of nanofluids [142]. This has led many researchers to develop nanofluid viscosity models drawing parallels with the nanofluid thermal conductivity. For example, Avsec and Oblak [143] modified the Taylor series expansion of Einstein's model by incorporating liquid layering as follows:

$$\eta_r = 1 + 2.5\phi_e + (2.5\phi_e)^2 + (2.5\phi_e)^3 + (2.5\phi_e)^4 + \ldots \tag{7.27}$$

where, ϕ_e is the effective volume fraction of the particles and is expressed as:

$$\phi_e = \phi\left(1 + \frac{h}{r}\right)^3 \tag{7.28}$$

where, h is the thickness of the nanolayer and r is the particle radius.

A Brownian motion based model was developed by Masoumi *et al.* [144] and is given as:

$$\eta = \eta_0 + \frac{\rho_p V_B d_p^2}{72C\delta} \tag{7.29}$$

where, ρ_p is the particle density, δ is the average interparticle separation, d_p is the particle diameter, V_B is the Brownian velocity, and C is the correction factor given by:

$$C = \frac{(c_1 d_p + c_2)\phi + (c_3 d_p + c_4)}{\eta_0} \tag{7.30}$$

The Brownian velocity is given by:

$$V_B = \frac{1}{d_p}\sqrt{\frac{18k_BT}{\pi\rho_p d_p}} \tag{7.31}$$

where, k_B is the Boltzmann constant and T is the temperature. Here, c_1 - c_4 are adjustable parameters subject to constraint $\phi < (c_1 d_p + c_2)/ (c_3 d_p + c_4)$.

The models discussed above only describe the behavior of nanofluid viscosity with temperature and particle concentration and do not depend on shear rate. As nanofluids generally display shear thinning behavior [126-131], their rheological behavior can be modeled using the power law expression:

$$\eta = K\gamma^{n-1} \tag{7.32}$$

where K is the consistency index and n is the flow behavior index with $n = 1$, >1, and < 1 for Newtonian, shear thickening, and shear thinning fluids respectively. There is a lack of reliable models that can describe the rheological behavior of nanofluids as a function of temperature, particle concentration, as well as shear rate. For this reason, nanofluid viscosities are often correlated using the power law model with different values of K and n for different volume fractions.

The following section discusses the experimental evaluation of nanofluids made by dispersing bentonite clay nanoparticles in pentadecane.

7.7.3 Rheological Characteristics of Bentonite-Pentadecane Nanofluids

7.7.3.1 Experimental

Bentonite particles were purchased from Sigma-Aldrich (WI, USA). Their average particle size and porosity were found to be 15.7 nm and 12.2 %, respectively using a Micromeritics TriStar II 3020 surface are analyzer. Nitrogen adsorption isotherms were measured at 77 K. Before the measurement, the sample was degassed at 458 K under vacuum for 24 h. Pentadecane (> 99 %) was purchased from Sigma Aldrich, MO. Nanofluids were prepared by dispersing pre-weighed quantities of bentonite into pentadecane. The samples were subjected to ultrasonic agitation to break up any aggregates. The rheological characteristics were studied using Anton Paar MCR 300 rheometer equipped with concentric cylinder (CC17) geometry.

7.7.3.2 Effect of Temperature

The viscosities of nanofluids consisting of 1 - 4 % (v/v) bentonite particles dispersed in pentadecane were measured as a function of temperature at a shear rate of 10 s^{-1}. Table 7.15 lists the measured viscosity of pure pentadecane and four nanofluids. Figure 7.13 illustrates the viscosity-temperature behavior of pentadecane and 1 % and 4 % bentonite nanofluids. It can be observed that the viscosity-temperature behavior of nanofluids follows that of the base fluid.

Table 7.15. Viscosity of bentonite nanofluids as a function of temperature.

T (°C)	η_0 (mPa·s)	η (mPa·s)							
		T (°C)	1 %	T (°C)	2 %	T (°C)	3 %	T (°C)	4 %
20.0	2.85	20.0	5.67	20.0	25.2	19.9	42.0	20.0	193.0
22.3	2.87	22.2	5.46	22.2	24.0	22.2	40.0	22.3	182.0
28.6	2.76	27.9	5.24	28.0	23.6	27.9	39.1	28.6	175.0
34.8	2.53	33.5	4.9	33.6	23.1	33.6	38.1	34.7	165.0
40.6	2.32	38.9	4.66	39.0	22.6	39.0	36.5	40.4	152.0
46.1	2.12	44.2	4.57	44.3	23.3	44.4	34.7	45.8	137.0
51.3	1.92	49.4	4.14	49.5	20.5	49.7	32.5	50.8	114.0
56.2	1.79	54.3	3.32	54.5	17.8	54.7	30.9	55.7	94.2
60.9	1.66	59.1	2.89	59.2	15.3	59.6	26.1	60.4	80.3
65.5	1.53	63.6	2.50	63.8	14.8	64.3	22.7	64.9	72.0
69.9	1.42	68.0	2.27	68.2	13.7	68.8	20.1	69.2	69.7
74.1	1.31	72.2	2.07	72.4	12.6	73.0	19.0	73.3	70.5
78.1	1.22	76.2	1.93	76.4	10.4	77.1	18.8	77.4	68.1
81.9	1.14	80.0	1.82	80.3	8.39	81.0	17.1	81.2	67.4
85.1	1.10	83.5	1.73	83.8	6.66	84.4	16.3	84.6	67.8

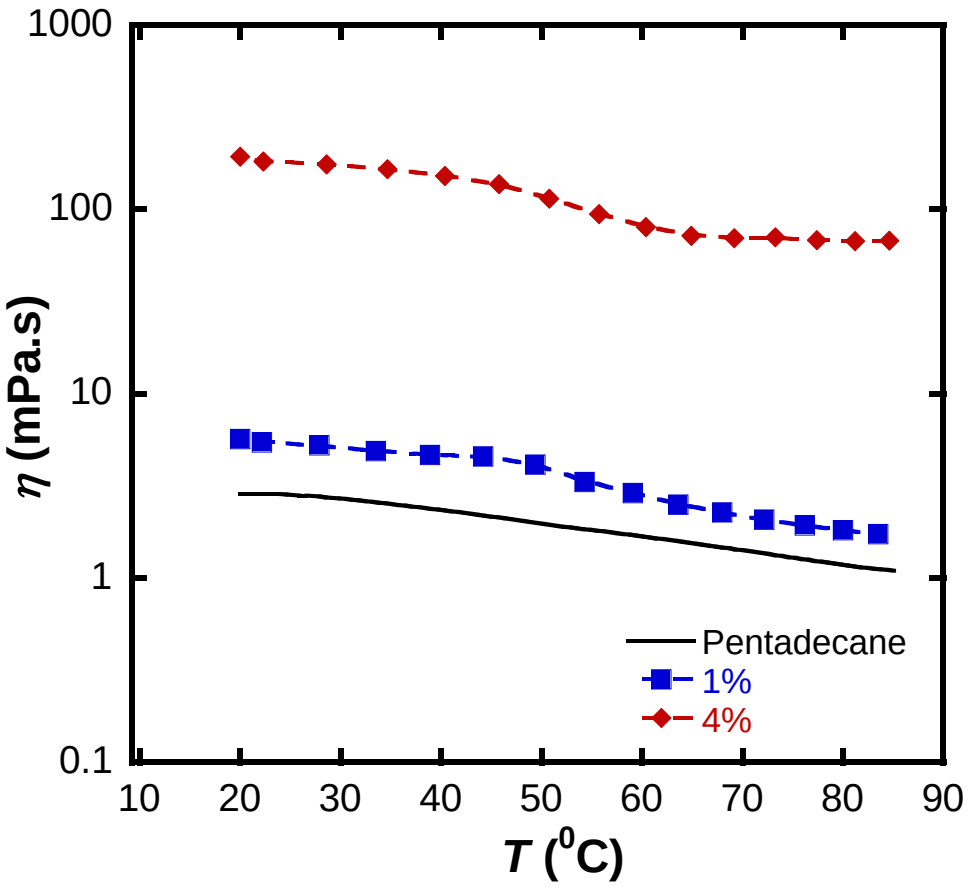

Figure 7.13. Effect of temperature on the viscosity of bentonite nanofluid.

7.7.3.3 Effect of Shear Rate

Viscosities of four nanofluids were measured as a function of shear rate at 20 and 100 °C. Table 7.16 lists the measured shear viscosities of the pure fluid and four nanofluids over a shear rate of 1 - 100 s^{-1}. Figure 7.14 illustrates the viscosity-shear rate behavior of 1 % and 4 % bentonite nanofluids at 20 and 100 °C. It can be observed from the figure that the nanofluids display shear thinning behavior.

Table 7.16. Effect of shear rate on viscosity of bentonite nanofluids.

Shear Rate (s^{-1})	1 %		2 %		3 %		4 %	
	20 °C	100 °C	20 °C	100 °C	20 °C	100 °C	20 °C	100 °C
1	39.3	10.5	77.6	17.2	129.0	54.7	330.0	184.0
2.15	30.9	2.8	37.1	11.9	115.0	269.0	240.0	105.0
4.64	25.8	1.6	20.5	7.3	95.0	180.0	256.0	71.4
10	18.5	1.2	11.1	8.5	63.3	70.4	179.0	86.6
21.5	8.6	1.1	7.6	5.3	29.9	35.6	103.0	41.5
46.4	5.2	1.0	6.5	2.6	17.3	16.5	56.8	27.1
100	4.4	1.1	5.5	1.8	12.1	8.88	33.4	10.8

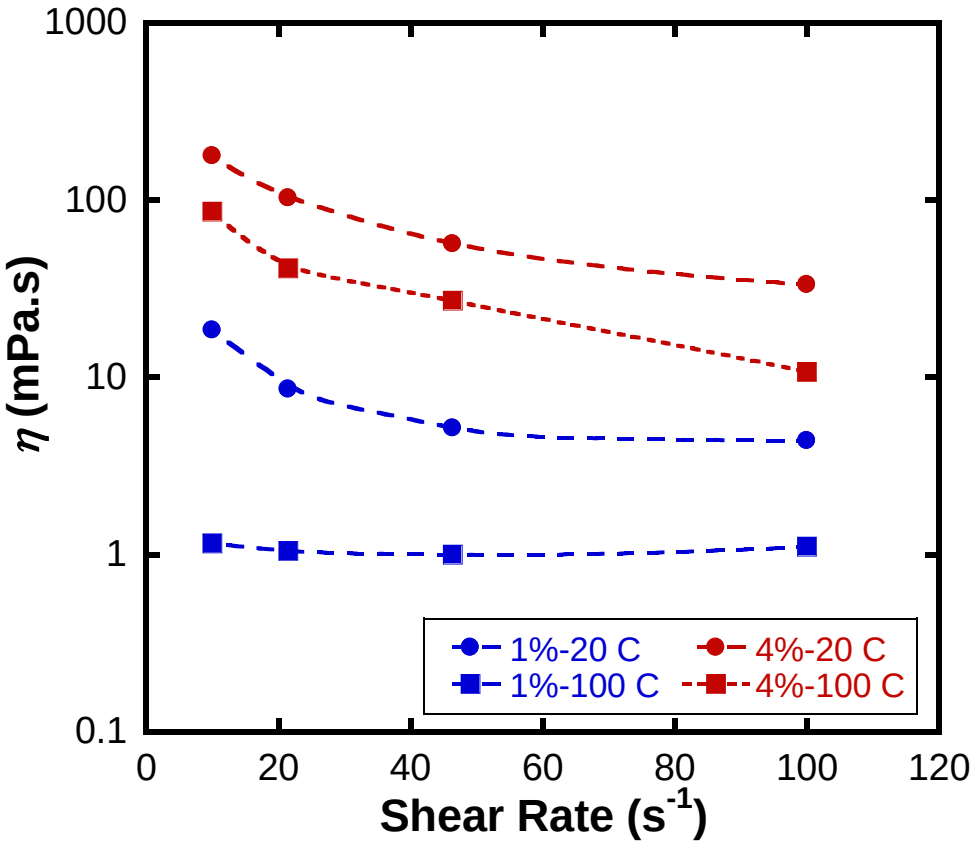

Figure 7.14. Shear rate vs. viscosity for bentonite nanofluid at 20 and 100 °C.

7.7.3.4 Effect of Particle Concentration

The effect of particle concentration on the viscosity of bentonite nanofluids is shown in Figure 7.15 for 20 and 50 °C. At lower concentrations ($\phi < 3$ %), the viscosity appears to be increasing linearly with particle volume fraction. However, it increases nonlinearly at higher volume fractions.

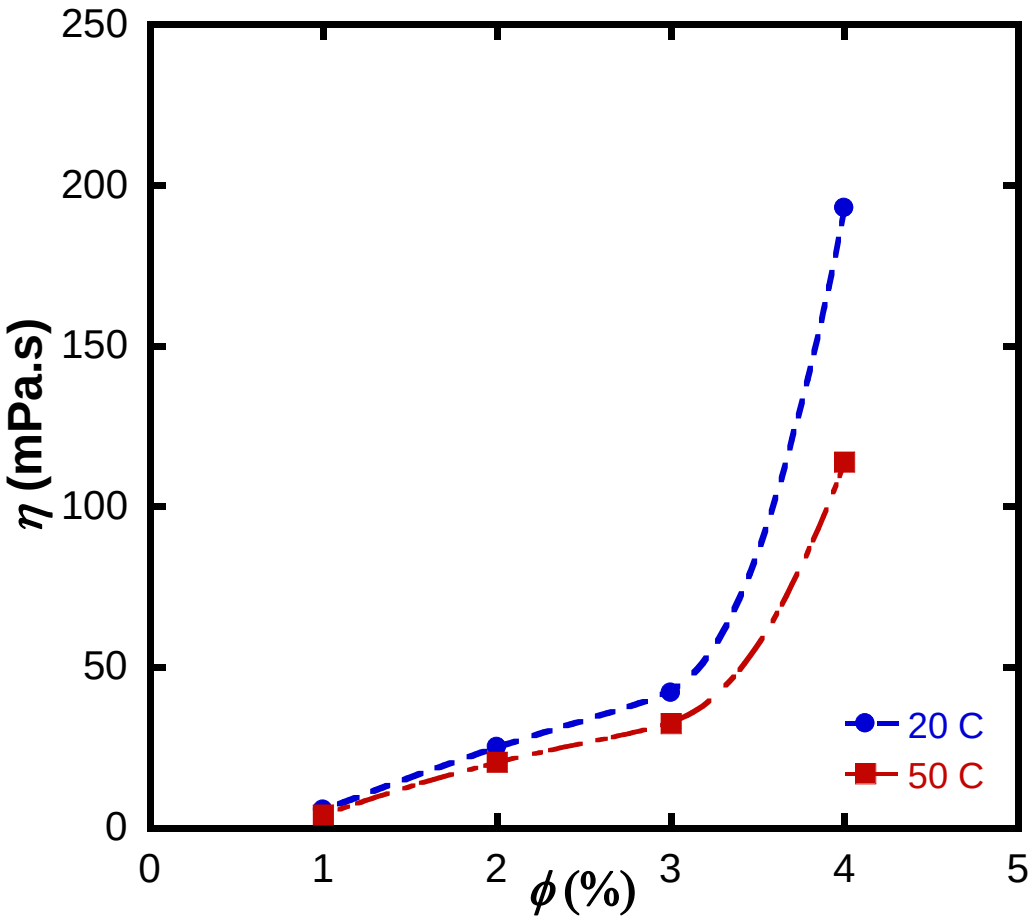

Figure 7.15. Effect of particle concentration on viscosity of bentonite nanofluid.

The rheological properties of bentonite nanofluid were correlated using the power law model as described in the previous section. The values of K and n are reported for each volume fraction in Table 7.17. As viscosity vs. temperature behavior of the nanofluid follows the behavior of the base fluid, the temperature effect was embedded in these calculations by fitting the relative viscosity ($\eta/\ \eta_0$) to obtain K and n. It can be

observed from Table 7.17 that power law model is able to describe the viscosity of bentonite nanofluids with reasonable accuracy.

Table 7.17. Effect of shear rate on viscosity of bentonite nanofluids.

ϕ (%)	K	n	% AAD
1	2.100	0.946	10.39
2	40.184	0.343	25.23
3	52.996	0.452	19.00
4	300.821	0.295	16.01

Figures 7.13 - 7.15 show that the viscosity of bentonite nanofluid increases by 1 or 2 orders of magnitude whereas the thermal conductivity enhancement is probably about 25 % as discussed previously. This raises serious questions regarding the use of nanofluids for practical heat transfer applications. Using Nusselt number and pressure drop for a fully developed flow inside a tube, Prasher *et al.* [145] concluded that nanofluids will not be beneficial if the increase in viscosity is more than 4 times the increase in thermal conductivity. A more restrictive limit was obtained by Escher *et al.* [146] using a coefficient-of-performance analysis for a microchannel heat sink. Escher *et al.* reported severe deterioration in the heat sink performance when the increase in viscosity was greater than the increase in thermal conductivity. A figure of merit analysis (Table 3.1) reveals that a 30 % increase in thermal conductivity and an order of magnitude increase in viscosity would decrease the L&B, Tran, and Rohsenow FOMs by 82, 69, and 93 % respectively. There are, therefore, significant design challenges in the use of nanofluids particularly with respect to minimizing viscosity while maximizing thermal conductivity enhancement. The fundamental insight obtained in this work with

respect to effects of temperature and particle size should help in the design of nanofluids for commercial use.

7.8 Conclusions

A critical review of the experimental data and models for the thermal conductivity of nanofluids is presented with particular emphasis on the effect of particle size. A modified geometric mean model was developed that takes into account the temperature dependence of the thermal conductivities of the individual phases, as well as the size dependence of the thermal conductivity of the dispersed phase. Applications of this model were demonstrated for nanofluids containing insulator, semiconductor, and metallic particles over a wide range of particle sizes, particle volume fractions, and temperatures. The model can be used to validate experimental thermal conductivity data for nanofluids and confirm the size dependence of the thermal conductivity of nanoparticles. The rheological properties of nanofluids were also discussed and experimental evaluation of the effects of particle concentration, temperature, and shear rate was presented for bentonite nanofluids. The significant increase in viscosity in the case of bentonite nanofluids indicates that the addition of nanoparticles may not be useful for electronics cooling applications.

7.9 References

1. Maxwell, J. C., *A Treatise on Electricity and Magnetism*, 3rd edition, Vol. II., 1892. London: Oxford University Press.

2. Hamilton, R. L. and Crosser, O. K., *Thermal conductivity of heterogeneous two-component systems*. Industrial & Engineering Chemistry Fundamentals, 1962. **1**: p. 187-191.

3. Choi, S. U. S., *Enhancing thermal conductivity of fluids with nanoparticles*. 1995. In: Siginer, D. A. and Wang, H. P. (eds.) Developments and applications of non-Newtonian flows, New York: ASME-FED **231**: p. 99-105.

4. Eastman, J. A., Choi, S. U. S., Li, S., Yu, W., and Thompson, L. J., *Anomalously increased effective thermal conductivities of ethylene glycol-based nanofluids containing copper nanoparticles*, Applied Physics Letters, 2001. **78**: p. 718-720.

5. Choi, S. U. S., Zhang, Z. G., Yu, W., Lockwood, F. E., and Grulke, E. A., *Anomalous thermal conductivity enhancement in nanotube suspensions*, Applied Physics Letters, 2001, **79**: p. 2252-2254.

6. Taylor, R. A., Phelan, P. E., Otanicar, T. P., Adrian, R., and Prasher, R., *Nanofluid optical property characterization: towards efficient direct absorption solar collectors*, Nanoscale Research Letters, 2011. **6**(1): p. 225.

7. Fang, X., Xuan, Y., and Li, Q., *Experimental investigation on enhanced mass transfer in nanofluids*, Applied Physics Letters, 2009. **95**(20): p. 203108.

8. Veilleux J. and Coulombe, S., *A dispersion model of enhanced mass diffusion in nanofluids*, Chemical Engineering Science, 2011. **66**(11): p. 2377-2384.

9. Tyagi, H., Phelan, P. E., and Prasher, R., *Predicted efficiency of a low-temperature nanofluid-based direct absorption solar collector*, Journal of Solar Energy Engineering, 2009. **131**(4): p. 041004.

10. Taylor, R. A., Phelan, P. E., Otanicar, T. P., Walker, C. A., Nguyen, M., Trimble, S., and Prasher, R., *Applicability of nanofluids in high flux solar collectors*, Journal of Renewable and Sustainable Energy, 2011. **3**(2): p. 023104.

11. Das, S. K., Choi, S. U. S., Yu, W., and Pradeep T., *Nanofluids Science and Technology*, 2008. New Jersey: John Wiley & Sons, Inc.

12. Xie, H. Q., Wang, J. C., Xi, T. G., Liu, Y., Ai, F., and Wu, Q. *Thermal conductivity enhancement of suspensions containing nanosized alumina particles*, Journal of Applied Physics, 2002. **91**: p. 4568-4572.

13. Kim, S. H., Choi, S. R., and Kim, D., *Thermal conductivity of metal-oxide nanofluids: particle size dependence and effect of laser irradiation*, ASME Journal of Heat Transfer, 2007. **129**: p. 298-307.

14. Keblinski, P., Phillpot, S. R., Choi, S. U. S., and Eastman, J. A., *Mechanisms of heat flow in suspensions of nano-sized particles (nanofluids)*, International Journal of Heat and Mass Transfer, 2002. **45**: p. 855-863.

15. Bird, R. B., Stewart, W. E., and Lightfoot, E. N. *Transport Phenomena*. 2002. New York: John Wiley & Sons, Inc.

16. Meyer, C. A., (ed.) *ASME Steam Tables: Thermodynamic and Transport Properties of Steam*. 1993. New York: American Society of Mechanical Engineers.

17. Diguilio, R. and Teja, A. S., *Thermal conductivity of poly(ethylene glycols) and their binary mixtures*, Journal of Chemical and Engineering Data, 1990. **35**: p. 117-121.

18. Dean, J. A., *Lange's Handbook of Chemistry*, 14th edition, 1992. New York: McGraw-Hill, Inc.

19. Kang, H. U., Kim, S. H., Oh, J. M., *Estimation of thermal conductivity of nanofluid using experimental effective particle volume*. Experimental Heat Transfer, 2006. **19**: p. 181-191.

20. Choi, S. U. S., Zhang, Z. G., Yu, W., Lockwood, F. E., Grulke, E. A., *Anomalous thermal conductivity enhancement in nanotube suspensions*. Applied Physics Letters, 2001. **79**: p. 2252-2254.

21. Tien, C. -L., Majumdar, A., and Gerner, F. M. (eds.) *Microscale Energy Transport*. 1998. Washington D.C.: Taylor & Francis.

22. Tien, C. -L. (ed.) *Annual Review of Heat Transfer*. Vol. 7. 1996. New York: Begell House, Inc.

23. Zhang, Z. M., *Nano/Microscale Heat Transfer*. 2007. McGraw Hill Professional: Nanoscience and Nanotechnology Series.

24. Ju, Y. S., *Phonon heat transport in silicon nanostructures*, Applied Physics Letters, 2005. **87**(15): p. 153106.

25. Behkam, B., Yang, Y. Z., and Asheghi, M., *Thermal property measurement of thin aluminum oxide layers for giant magnetoresistive (GMR) head applications*, International Journal of Heat and Mass Transfer, 2005. **48**: p. 2023-2031.

26. Liu, W. and Asheghi, M., *Phonon-boundary scattering in ultrathin single-crystal silicon layers*, Applied Physics Letters, 2004. **84**: p. 3819-3821.

27. Yu, X. Y., Chen, G., Verma, A., Smith, J. S., *Temperature dependence of thermophysical properties of GAAS/ALAS periodic structure*, Applied Physics Letters, 1995; **67**: p. 3554-3556.

28. Cahill, D. G., Ford, W. K., Goodson, K. E., Mahan, G. D., Majumdar, A., Maris, H. J., Merlin, R., and Phillpot, S. R. *Nanoscale thermal transport*, Journal of Applied Physics, 2003. **93**: p. 793-818.

29. Ziambaras, E. and Hyldgaard, P., *Phonon Knudsen flow in nanostructured semiconductor systems*, Journal of Applied Physics, 2006, **99**: p. 054303.

30. Li, D. Y., Wu, Y. Y., Kim, P., Shi, L., Yang, P. D., and Majumdar, A., *Thermal conductivity of individual silicon nanowires*, Applied Physics Letters, 2003; **83**: p. 2934-2936.

31. Fang, K. C., Weng, C. I., and Ju, S. P., *An investigation into the structural features and thermal conductivity of silicon nanoparticles using molecular dynamics simulations*, Nanotechnology, 2006. **17**: p. 3909-3914.

32. Liang, L. H. and Li, B., *Size-dependent thermal conductivity of nanoscale semiconducting systems*, Physical Review B, 2006. **73**: p. 153303.

33. Zhang, Z., Zhao, M., and Jiang, Q., *Melting temperatures of semiconductor nanocrystals in the mesoscopic size range*, Semiconductor Science and Technology, 2001. **16**: p. L33-L35.

34. Warrier, P., Yuan, Y., Beck, M. P., and Teja, A. S. *Heat transfer in nanoparticle suspensions: modeling the thermal conductivity of nanofluids*, AIChE Journal, 2010. **56**(12): p. 3243-3256.

35. Bragg, L., Claringbull, G. F., and Taylor, W. H., *Crystal Structure of Minerals*. 1965. New York: Cornell University Press.

36. Yang, Z., Woo, T. K., Baudin, M., and Hermansson, K., *Atomic and electronic structure of unreduced and reduced CeO_2 surfaces: a first-principles study*, Journal of Chemical Physics, 2004. **120**: p. 7741-7749.

37. Wen, Z., Zhao, M., and Jiang, Q., *The melting temperature of molecular nanocrystals at the lower bound of the mesoscopic size range*, Journal of Physics: Condensed Matter, 2000, **12**: p. 8819-8824.

38. Jiang, Q., Shi, H. X., and Zhao, M., *Melting thermodynamics of organic nanocrystals*, Journal of Chemical Physics, 1999. **111**: p. 2176-2180.

39. Warrier, P. and Teja, A. S., *Effect of particle size on the thermal conductivity of nanofluids containing metallic nanoparticles*, Nanoscale Research Letters, 2011. **6**: p. 247.

40. Nath, P. and Chopra, K. L., *Thermal conductivity of copper films*, Thin Solid Films, 1974. **20**(1): p. 53-62.

41. Shin, S. and Lee, S. H., *Thermal conductivity of suspensions in shear flow fields*, International Journal of Heat and Mass Transfer, 2000. **43**: p. 4275-4284.

42. Turian, R. M., Sung, D. J., and Hsu, F. L., *Thermal conductivity of granular coals, coal-water mixtures and multi-solid/liquid suspensions*, Fuel, 1991. **70**: p. 1157-1172.

43. Jana, S., Salehi-Khojin, A., and Zhong, W. H., *Enhancement of fluid thermal conductivity by the addition of single and hybrid nano-additives*, Thermochimica Acta, 2007. **462**(1-2): p. 45-55.

44. Eastman, J. A., Choi, S. U. S., Li, S., Thompson, L. J., and Lee, S., *Enhanced thermal conductivity through the development of nanofluids*, Materials Research Society Symposium Proceedings (Nanophase and Nanocomposite Materials II), 1997. **457**: p. 3-11.

45. Zhang, X., Gu, H., and Fujii, M., *Effective thermal conductivity and thermal diffusivity of nanofluids containing spherical and cylindrical nanoparticles*, Experimental Thermal and Fluid Science, 2007. **31**: p. 593-599.

46. Zhang, X., Gu, H., and Fujii, M., *Experimental study on the effective thermal conductivity and thermal diffusivity of nanofluids*, International Journal of Thermophysics, 2006. **27**: p. 569-580.

47. Zhang, X., Gu, H., Fujii, M., *Effective thermal conductivity and thermal diffusivity of nanofluids containing spherical and cylindrical nanoparticles*, Journal of Applied Physics, 2006. **100**: p. 044325.

48. Timofeeva, E. V., Gavrilov, A. N., McCloskey, J. M., Tolmachev, Y. V., Sprunt, S., Lopatina, L. M., and Selinger, J. V., *Thermal conductivity and particle agglomeration in alumina nanofluids: experiment and theory*, Physical Review E, 2007, **76**: p. 061203.

49. Yang, Y., Grulke, E. A., Zhang, Z. G., and Wu, G. F., *Thermal and rheological properties of carbon nanotube-in-oil dispersions*, Journal of Applied Physics, 2006. **99**: p. 114307.

50. Beck, M. P., Yuan,Y., Warrier, P., and Teja, A. S., *The effect of particle size on the thermal conductivity of nanofluids*, Journal of Nanoparticle Research, 2009. **11**: p. 1129-1136.

51. Nan, C. W., Birringer, R., Clarke, D. R., and Gleiter, H., *Effective thermal conductivity of particulate composites with interfacial thermal resistance*, Journal of Applied Physics, 1997. **81**: p. 6692-6699.

52. Yu, W. and Choi, S. U. S., *The role of interfacial layers in the enhanced thermal conductivity of nanofluids: a renovated Maxwell model*, Journal of Nanoparticle Research, 2003. **5**: p. 167-171.

53. Murshed, S. M. S., Leong, K. C., and Yang, C., *Enhanced thermal conductivity of TiO_2-water based nanofluids*, International Journal of Thermal Sciences, 2005. **44**: p. 367–373.

54. Zhu, H. T., Zhang, C. Y., Liu, S. Q., Tang, Y. M., and Yin, Y. S., *Effects of nanoparticle clustering and alignment on thermal conductivities of Fe_3O_4 aqueous nanofluids*, Applied Physics Letters, 2006. **89**: p. 023123.

55. Liu, M. S., Lin, M. C. C., Tsai, C. Y., and Wang, C. C., *Enhancement of thermal conductivity with Cu for nanofluids using chemical reduction method*, International Journal of Heat and Mass Transfer, 2006. **49**: p. 3028-3033.

56. Ceylan, A., Jastrzembski, K., and Shah, S. I., *Enhanced solubility of Ag-Cu nanoparticles and their thermal transport properties*, Metallurgical and Materials Transactions A, 2006. **37**: p. 2033-2038.

57. Putnam, S. A., Cahill, D. G., Braun, P. V., Ge, Z. B., and Shimmin, R. G., *Thermal conductivity of nanoparticle suspensions*, Journal of Applied Physics, 2006. **99**: p. 084308.

58. Li, C. H., Peterson, G. P., *The effect of particle size on the effective thermal conductivity of Al_2O_3-water nanofluids*, Journal of Applied Physics, 2007. **101**: p. 044312.

59. Beck, M. P., Yuan,Y., Warrier, P., and Teja, A. S. *The thermal conductivity of alumina nanofluids in water, ethylene glycol, and ethylene glycol + water mixtures*, Journal of Nanoparticle Research, 2010. **12**: p. 1469-1477.

60. Das, S. K., Putra, N., Thiesen, P., and Roetzel, W., *Temperature dependence of thermal conductivity enhancement for nanofluids*, ASME Journal of Heat Transfer, 2003. **125**: p. 567-574.

61. Yang, B. and Han, Z. H., *Temperature-dependent thermal conductivity of nanorod based nanofluids*, Applied Physics Letters, 2006. **89**: p. 083111.

62. Beck, M. P., Sun, T., and Teja, A. S., *The thermal conductivity of alumina nanoparticles dispersed in ethylene glycol*, Fluid Phase Equilibria, 2007. **260**: p. 275-278.

63. Xie, H. Q., Wang, J. C., Xi, T. G., Liu, Y., and Ai, F., *Dependence of the thermal conductivity of nanoparticle-fluid mixture on the base fluid*, Journal of Material Science Letters, 2002. **21**: p. 1469-1471.

64. Li, C. H. and Peterson, G. P., *Experimental investigation of temperature and volume fraction variations on the effective thermal conductivity of nanoparticle suspensions (nanofluids).* Journal of Applied Physics, 2006. **99**: p. 084314.

65. Wang, X. W., Xu, X. F., and Choi, S. U. S., *Thermal conductivity of nanoparticle-fluid mixture*, Journal of Thermophysics and Heat Transfer, 1999. **13**: p. 474-480.

66. Lee, S., Choi, S. U. S., Li, S., Eastman, J. A., *Measuring thermal conductivity of fluids containing oxide nanoparticles*, ASME Journal of Heat Transfer, 1999. **121**: p. 280-289.

67. Hwang, Y. J., Ahn, Y. C., Shin, H. S., Lee, C. G., Kim, G. T., Park, H. S., and Lee, J. K., *Investigation on characteristics of thermal conductivity enhancement of nanofluids*, Current Applied Physics, 2006. **6**: p. 1068-1071.

68. Lee, D., Kim, J. W., and Kim, B. G., *A new parameter to control heat transport in nanofluids: surface charge state of the particle in suspension*, Journal of Physical Chemistry B, 2006. **110**: p. 4323-4328.

69. Wright, B., Thomas, D., Hong, H., Groven, L., Puszynski, J., Duke, E., Ye, X., and Jin, S., *Magnetic field enhanced thermal conductivity in heat transfer nanofluids containing Ni coated single wall carbon nanotubes*, Applied Physics Letters, 2007. **91**: p. 173116.

70. Hong, H. P., Wright, B., Wensel, J., Jin, S. H., Ye, X. R., and Roy, W., *Enhanced thermal conductivity by the magnetic field in heat transfer nanofluids containing carbon nanotube*, Synthetic Metals, 2007. **157**: p. 437-440.

71. Wensel, J., Wright, B., Thomas, D., Douglas, W., Mannhalter, B., Cross, W., Hong, H. P., Kellar, J., Smith, P., and Roy, W., *Enhanced thermal conductivity by aggregation in heat transfer nanofluids containing metal oxide nanoparticles and carbon nanotubes*, Applied Physics Letters, 2008. **92**: p. 023110.

72. Rayleigh, L., *On the influence of obstacles arranged in rectangular order upon the properties of a medium*, Philosophical Magazine, 1892. **34**: p. 481-502.

73. Jeffrey, D. J., *Conduction through a random suspension of spheres*, Proceedings of the Royal Society (London) A, 1973. **335**: p. 355-367.

74. Progelhof, R. C., Throne, J. L., and Ruetsch, R. R., *Methods for predicting thermal conductivity of composite systems*, Polymer Engineering & Science, 1976. **16**: p. 615-625.

75. Landauer, R., *The electrical resistance of binary metallic mixtures*, Journal of Applied Physics, 1952. **23**: p. 779-784.

76. Krischer, O., *Die Wissenschaftlichen Grundlagen der Trocknungstechnik* (*The Scientific Fundamentals of Drying Technology*) 2nd edition, 1963. Berlin: Springer-Verlag.

77. Tsao, G. T. N., *Thermal conductivity of 2-phase materials*, Industrial & Engineering Chemistry, 1961. **53**: p. 395-397.

78. Hashin, Z. and Shtrikman, S., *A variational approach to the theory of the effective magnetic permeability of multiphase materials*, Journal of Applied Physics, 1962. 33: p. 3125.

79. Nielsen, L. E., *Predicting the Properties of Mixtures: Mixing Rules in Science and Technology*, 1978. New York: Mercer Dekker.

80. Nan, C. W., *Physics of inhomogeneous inorganic materials*, Progress in Material Science, 1993. **37**: p. 1-117.

81. Prasher, R., Evans, W., Meakin, P., Fish, J., Phelan, P., and Keblinski, P., *Effect of aggregation on thermal conduction in colloidal nanofluids*. Applied Physics Letters, 2006. **89**: p. 143119.

82. Yu, W. and Choi, S. U. S., *The role of interfacial layers in the enhanced thermal conductivity of nanofluids: a renovated Hamilton-Crosser model*, Journal of Nanoparticle Research, 2004. **6**: p. 355-361.

83. Xie, H. Q., Fujii, M., and Zhang, X., *Effect of interfacial nanolayer on the effective thermal conductivity of nanoparticle-fluid mixture*, International Journal of Heat and Mass Transfer, 2005. **48**: p. 2926-2932.

84. Xue, Q. Z., *Model for thermal conductivity of carbon nanotube based composites*, Physica B, 2005. **368**: p. 302-307.

85. Leong, K. C., Yang, C., and Murshed, S. M. S., *A model for the thermal conductivity of nanofluids - the effect of interfacial layer*, Journal of Nanoparticle Research, 2006. **8**: p. 245-254.

86. Feng, Y. J., Yu, B. M., Xu, P., Zou, M. Q., *The effective thermal conductivity of nanofluids based on the nanolayer and the aggregation of nanoparticles*, Journal of Physics D: Applied Physics, 2007. **40**: p. 3164-3171.

87. Lee, D., *Thermophysical properties of interfacial layer in nanofluids*, Langmuir, 2007. **23**: p. 6011-6018.

88. Li, L., Zhang, Y. W., Ma, H. B., and Yang, M., *An investigation of molecular layering at the liquid-solid interface in nanofluids by molecular dynamics simulation*, Physics Letters A, 2008. **372**: p. 4541-4544.

89. Evans, W., Fish, J., Keblinski, P., *Thermal conductivity of ordered molecular water*, Journal of Chemical Physics, 2007. **126**: p. 154504.

90. Jang, S. P. and Choi, S. U. S., *Role of Brownian motion in the enhanced thermal conductivity of nanofluids*, Applied Physics Letters, 2004, **84**: p. 4316-4318.

91. Koo, J. and Kleinstreuer, C., *A new thermal conductivity model for nanofluids*, Journal of Nanoparticle Research, 2004. **6**: p. 577-588.

92. Prasher, R., Bhattacharya, P., and Phelan, P. E., *Thermal conductivity of nanoscale colloidal solutions (nanofluids)*, Physical Review Letters, 2005. **94**: p. 025901.

93. Ren, Y., Xie, H., and Cai, A., *Effective thermal conductivity of nanofluids containing spherical nanoparticles*, Journal of Physics D: Applied Physics, 2005. **38**: p. 3958-3961.

94. Xuan, Y. M., Li, Q., Zhang, X., and Fujii, M., *Stochastic thermal transport of nanoparticle suspensions*, Journal of Applied Physics, 2006. **100**: p. 043507.

95. Prakash, M., and Giannelis, E. P., *Mechanism of heat transport in nanofluids*, Journal of Computer Aided Materials Design, 2007. **14**: p. 109-117.

96. Swartz, E. T. and Pohl, R. O., *Thermal boundary resistance*, Reviews of Modern Physics, 1989. **61**: 605-668.

97. Prasher, R., Evans, W., Meakin, P., Fish, J., Phelan, P., and Keblinski, P., *Effect of aggregation on thermal conduction in colloidal nanofluids*, Applied Physics Letters, 2006. **89**: p. 143119.

98. Kumar, S., and Murthy, J. Y., *A numerical technique for computing effective thermal conductivity of fluid-particle mixtures*, Numerical Heat Transfer Part B, 2005. **47**: p. 555-572.

99. Gao, L. and Zhou, X. F., *Differential effective medium theory for thermal conductivity in nanofluids*, Physics Letters A, 2006. **348**: p. 355-360

100. Beck, M. P., Yuan, Y., Warrier, P., and Teja, A. S., *Thermal conductivity of aqueous nanofluids containing ceria nanoparticles*, Journal of Applied Physics, 2010. **107**: p. 066101.

101. Shalkevich, N., Escher, W., Burgi, T., Michel, B., Si-Ahmed, L., and Poulikakos, D., *On the thermal conductivity of gold nanoparticle colloids*, Langmuir, 2010. **26** (2): p. 663-670.

102. Warrier, P. and Teja, A. S., *Effect of particle size on the thermal conductivity of nanofluids containing metallic nanoparticles*, Nanoscale Research Letters, 2011. **6**: p. 247.

103. Teja, A. S., Beck, M. P., Yuan, Y., and Warrier, P., *The limiting behavior of the thermal conductivity of nanoparticles and nanofluids*, Journal of Applied Physics, 2010. **107**: p. 114319.

104. Yoo, D. H., Hong, K. S., and Yang, H. S., *Study of thermal conductivity of nanofluids for the application of heat transfer fluids*, Thermochimica Acta, 2007. **455**: p. 66-69.

105. Xie, H., Yu, W., and Li, Y., *Thermal performance enhancement in nanofluids containing diamond nanoparticles*, Journal of Physics D: Applied Physics, 2009. **42**: p. 095413.

106. Kaviany, M., *Principles of Heat Transfer*, 2002. New York: Wiley-Interscience.

107. Watari, K., Nakano, H., Sato, K., Urabe, K., Ishizaki, K., Cao, S., and Mori, K., *Effect of grain boundaries on thermal conductivity of silicon carbide ceramic at 5 to 1300 K*, Journal of American Ceramic Society, 2003. **86**: p. 1812-1814.

108. Eastman, J. A., Choi, S. U. S., Li, S., Soyez, G., Thompson, L. J., and DiMelfi, R. J., *Novel thermal properties of nanostructured materials*, Material Science Forum, 1999. **312-314**: p. 629-634.

109. Chon, C. H., Kihm, K. D., Lee, S. P., Choi, S. U. S., *Empirical correlation finding the role of temperature and particle size for nanofluid (Al_2O_3) thermal conductivity enhancement*, Applied Physics Letters, 2005. **87**: p. 53107.

110. Yoo, D. H., Hong, K. S., Hong, T. E., Eastman, J. A., and Yang, H. S., *Thermal conductivity of Al_2O_3/water nanofluids*, Journal of Korean Physics Society, 2007. **51**: p. S84–S87.

111. Oh, D. K., Jain, A., Eaton, J. K., Goodson, K. E., and Lee, J. S., *Thermal conductivity measurement and sedimentation detection of aluminum oxide nanofluids by using the 3 omega method*, International Journal of Heat and Fluid Flow, 2008. **29**: p. 1456–1461.

112. Wang, Z. L., Tang, D. W., Liu, S., Zheng, X. H., and Araki, N., *Thermal-conductivity and thermal-diffusivity measurements of nanofluids by 3 omega method and mechanism analysis of heat transport*, International Journal of Thermophysics, 2007. **28**: p. 1255–1268.

113. Li, X. F., Zhu, D. S., Wang, X. J., Wang, N., Gao, J. W., and Li, H., *Thermal conductivity enhancement dependent pH and chemical surfactant for Cu-H_2O nanofluids*, Thermochimica Acta, 2008. **469**(1-2): p. 98-103.

114. Wongwises, S. and Duangthongsuk, W., *Measurement of temperature dependent thermal conductivity and viscosity of TiO_2-water nanofluids*, Experimental Thermal and Fluid Science, 2009. **33**: p. 706-714.

115. Kwak, K. and Kim, C., *Viscosity and thermal conductivity of copper oxide nanofluid dispersed in ethylene glycol*, Korea-Australia Rheology Journal, 2005. **17**: p. 35-40.

116. Liu, M. S., Lin, M. C., Huang, I. T., and Wang, C. C., *Enhancement of thermal conductivity with CuO for nanofluids*, Chemical Engineering & Technology, 2006. **29**: p. 72-77.

117. Xie, H. Q., Wang, J. C., Xi, T. G., Liu, Y., and Ai, F., *Thermal conductivity of suspension containing SiC particles*, Journal of Material Science Letters, 2002. **21**: p. 193-195.

118. Singh, D., Timofeeva, W., Yu, W., Routbort, J., Smith, D., and Lopez-Cepero, J. M., *An investigation of silicon carbide-water nanofluid for heat transfer applications*, Journal of Applied Physics, 2009. **105**: p. 064306.

119. Patel, H. E., Das, S. K. Sundararajan, T., Nair, A. S., George, B., and Pradeep, T., *Thermal conductivities of naked and monolayer protected metal nanoparticle based nanofluids: Manifestation of anomalous enhancement and chemical effects*, Applied Physics Letters, 2003. **83**(14): p. 2931.

120. Xuan, Y. and Li, Q., *Heat transfer enhancement of nanofluids*, International Journal of Heat and Fluid Flow, 2000. **21**: p. 58-64.

121. Li, Q. and Xuan, Y., *Enhanced heat transfer behaviors of new heat carrier for spacecraft thermal management*, Journal of Spacecraft and Rockets, 2006. **43**(3): p. 687-689.

122. Yu, W., Xie, H., Chen, L., and Li, Y., *Investigation on the thermal transport properties of ethylene glycol-based nanofluids containing copper nanoparticles*, Powder Technology, 2010. **197**: 218.

123. Marsh, K. N., (ed.), *Recommended Reference Materials for the Realization of Physicochemical Properties*, 1987, Boston: Blackwell Scientific Publications.

124. Rowley, R. L., Wilding, W. V., Oscarson, J. L., Yang, Y., Giles, N. F., *DIPPR® Data Compilation of Pure Chemical Properties, Design Institute for Physical Properties*. 2011. http://dippr.byu.edu, Brigham Young University, Provo, Utah.

125. Bleazard, J. G., and Teja, A. S., *Thermal conductivity of electrically conducting liquids by the transient hot-wire method*, Journal of Chemical and Engineering Data, 1995, **40**(4): p. 732-737.

126. Teipel, U., and Förter-Barth, U., *Rheology of nano-scale aluminum suspensions*, Propellants, Explosives, Pyrotechnics, 2001, **26**(6): p. 268-272.

127. Tseng, W. J. and Wu, C.H., *Aggregation, rheology and electrophoretic packing structure of aqueous Al_2O_3 nanoparticle suspensions*, Acta Materialia, 2002. **50**(15): 3757-3766.

128. Kulkarni, D. P., Das, D. K., Chukwu, G. A., *Temperature dependent rheological property of copper oxide nanoparticles suspension (nanofluid)*, Journal of Nanoscience and Nanotechnology, 2006. **6**(4): p. 1150-1154.

129. Lu, K., *Rheological behavior of carbon nanotube-alumina nanoparticle dispersion systems*, Powder Technology, 2007. **177**(3): p. 154-161.

130. Chen, H., Ding, Y., Lapkin, A., and Fan, X., *Rheological behavior of ethylene glycol-titanate nanotube nanofluids*, Journal of Nanoparticle Research, 2009. **11**(6): p. 1513-1520.

131. Phuoc, T. X., and Massoudi, M., *Experimental observations of the effects of shear rates and particle concentration on the viscosity of Fe_2O_3-deionized water nanofluids*, International Journal of Thermal Sciences, 2009. **48**(7): p. 1294-1301.

132. Xie, H., Chen, L., and Wu, Q., *Measurements of the viscosity of suspensions (nanofluids) containing nanosized Al_2O_3 particles*, High Temperatures-High Pressures, 2008. **37**: p. 127–135.

133. Yu, W., Xie, H. Q., Chen, L. F. and Li, Y., *Investigation of thermal conductivity and viscosity of ethylene glycol based ZnO nanofluid*, Thermochimica Acta, 2009. **491**(1-2): p. 92–96.

134. Duangthongsuk, W. and Wongwises, S., *Measurement of temperature-dependent thermal conductivity and viscosity of TiO_2–water nanofluids*, Experimental Thermal and Fluid Science, 2009, **33**(4): p. 706-714.

135. Chang, H., Jwo, C. S., Lo, C. H., Tsung, T. T., Kao, M. J., and Lin, H. M., *Rheology of CuO nanoparticle suspension prepared by ASNSS*, Reviews on Advanced Material Science, 2005. **10**(2): p. 128-132.

136. Zhao, J. F., Luo, Z. Y., Ni, M. J., Cen, K. F., *Dependence of nanofluid viscosity on particle size and pH value*, Chinese Physics Letters, 2009. **26**(6): p. 066202.

137. Einstein A., *Eine neue bestimmung der molekuldimensionen*, Annals of Physics, 1906, **19**: 289.

138. Batchelor G. K., *The effect of Brownian motion on the bulk stress in the suspension of spherical particles*, Journal of Fluid Mechanics, 1977. **83**: p. 97-117.

139. Krieger I. M. and Dougherty T. J., *A mechanism for non-Newtonian flow in suspensions of rigid spheres*, Transactions of the Society of Rheology, 1959. **3**: p. 137-152.

140. Wang L. Q. (ed.), *Advances in Transport Phenomena*, Vol. 1, 2009. Berlin: Springer-Verlag.

141. Chen, H., Ding, Y., and Tan, C. *Rheological behavior of nanofluids*, New Journal of Physics, 2007. **9**: p. 367.

142. Nwosu, P. N., Meyer, J. P., and Mohsen, S., *Parametric analysis of viscosity models for nanofluids*. Proceedings of the ASME 2012 3rd Micro/Nanoscale Heat & Mass Transfer International Conference, Atlanta, Georgia, USA. MNHMT2012-75314.

143. Avsec J. and Oblak M., *The calculation of thermal conductivity, viscosity and thermodynamic properties for nanofluids on the basis of statistical nanomechanics*, International Journal of Heat and Mass Transfer, 2007. **50**: p. 4331-4341.

144. Masoumi N., Sohrabi N., and Behzadmehr A., *A new model for calculating the effective viscosity of nanofluids*, Journal of Physics D: Applied Physics, 2009. **42**(1-6): p. 055501.

145. Prasher, R., Song, D., Wang, J., and Phelan, P., *Measurements of nanofluid viscosity and its implications for thermal applications*, Applied Physics Letters, 2008. **89**: p. 133108.

146. Escher, W., Brunschwiler, T., Shalkevich, T., Burgi, T., Michel, B., and Poulikakos, D., *On the cooling of electronics with nanofluids*, Journal of Heat Transfer, 2011. **133**: p. 051401.

CHAPTER 8

CONCLUSIONS AND RECOMMENDATIONS

8.1 Conclusions

New heat transfer fluids for direct immersion phase change cooling of electronic systems were identified using CAMD methods combined with physical property and FOM constraints. As the success of this approach depends on the availability and accuracy of property estimation methods, the predictive capabilities of four GC methods (Marrerro-Gani, Constantinou-Gani, Joback-Reid, and Wilson-Jasperson) were critically evaluated with respect to properties needed in heat transfer calculations. Average absolute deviations of about 10 % were obtained for most properties, with the exception of surface tension and viscosity. None of the methods were found to be reliable for compounds containing silicon, and new group contributions were therefore developed for these compounds.

A total of 52 new heat transfer fluids were identified by applying constraints on normal boiling point, thermal conductivity, and enthalpy of vaporization, as well as FOM constraints for pool and flow boiling. Nine fluids were selected for experimental evaluation based on commercial availability and knowledge of synthesis steps. Two of these fluids, 1,1,1-trifluoro-3-methylpentane and 1,1,1-trifluoro-3-(2,2,2-trifluoroethoxy)propane, were synthesized in this work and the remaining 7 fluids were purchased.

Thermophysical property measurements and pool boiling heat transfer experiments were performed with the 9 newly identified fluids and their mixtures with HFE 7200. The new fluids exhibited superior heat transfer properties when compared with HFE 7200. The climate impact of new fluids containing fluorine was investigated by evaluating their GWP. This required the development of a new GC method for RF of fluorocarbons. The method was validated for five fluids with experimental determination of radiative forcing using FT-IR spectroscopy. Only 2 of the 33 new fluorinated fluids exhibited RF values greater than those of HFE 7200. Moreover, GWP values of all new fluids were lower than those of HFE 7200. Hence these fluids can be considered as potential replacements for HFEs for electronics cooling.

Heat transfer fluids obtained by dispersing small amounts of solid nanoparticles in liquids (nanofluids) were also investigated. As there is significant disagreement in the literature regarding the mechanism of heat transport in nanofluids, experimental data and models for the thermal conductivity of nanofluids were critically reviewed. A modified geometric mean model was developed that takes into account the temperature dependence of the thermal conductivities of the individual phases, as well as the size dependence of the thermal conductivity of the dispersed phase. The model can be used to validate experimental thermal conductivity data for nanofluids and confirm the size dependence of the thermal conductivity of nanoparticles. The rheological properties of nanofluids were also measured and a significant increase in the viscosity was noted. It was concluded that the addition of nanoparticles to existing heat transfer fluids is not promising for enhancing the properties of these fluids.

8.2 Recommendations for Future Work

8.2.1 GC Methods

As observed in Chapter 2, liquid viscosity could not be predicted reliably using published GC methods especially for fluorinated compounds. As viscosity significantly influences heat transfer, it will be useful to develop new methods for estimating liquid viscosity. It was shown in Chapter 5, that rough hard-sphere theory was able to capture the nonlinear viscosity composition behavior without any adjustable parameters. Thus, GC methods could be developed for rough hard-sphere parameters. Rough hard-sphere theory may provide a basis to combine GC methods with a fundamental molecular level theory.

Wu and Sandler [1, 2] have used quantum mechanical calculations to identify theoretically defined groups. Their calculations, however, were performed at a low level of theory (Hartree-Fock) and used a relatively small basis set (6-31G**). In addition, 6-31G** basis set does not include diffuse functions which are necessary for electronegative atoms (such as fluorine) and anions. Their approach should be reexamined using density functional theory and post Hartree-Fock methods (configuration interaction, coupled cluster) with larger basis sets such as 6-311++G** and aug-cc-pCVQZ that include diffuse functions. [3]

8.2.2 CAMD of Organosilicon Compounds

CAMD of organosilicon compounds performed in this work was restricted to a maximum of 5 groups per molecule. This was done to avoid the problem of

combinatorial explosion. A CAMD algorithm similar to the 4 level approach used by Harper *et al.* [4] could be developed. In addition, the GC values developed in this work are applicable at 298 K only. The GCs should be updated to capture the temperature behavior by compiling more temperature dependent data.

8.2.3 Scale Up of Synthesis

This work has provided the proof-of-concept that CAMD can be used to design new heat transfer fluids. Therefore, top ranked candidates from the FOM analysis should also be synthesized and evaluated. As experimental evaluation requires about 500 ml of the fluid, the synthesis should be scaled up so that experiments could be performed with pure fluids.

It would also be interesting to see if the feasibility of synthesis could be incorporated at the CAMD phase. This problem could be approached by combining the retrosynthesis algorithm incorporated in the Logic and Heuristics Applied to Synthetic Analysis (LHASA) software [5] with the CAMD algorithm.

8.2.4 Experimental Evaluation

Vapor-liquid equilibria (VLE) of fluid mixtures play a significant role in phase change heat transfer. In this work, VLE was predicted using regular solution theory and COSMO-RS. Experimental VLE measurements for newly identified fluids and fluid mixtures should be performed to validate the predictions.

8.2.5 Nanofluids

In light of the findings of this work, a fundamental study evaluating the effects of different parameters on convective and phase change heat transfer in nanofluids [6-8] should be performed. In addition, strategies for nanofluid preparation as well as their detailed characterization must be strictly defined so that experimental results of one group can be verified by other groups.

8.3 References

1. Wu, H. S. and Sandler, S. I., *Use of ab initio quantum mechanics calculations in group contribution methods. 1. Theory and the basis for group identifications*, Industrial and Engineering Chemistry Research, 1991. **30**: p. 881-889.

2. Wu, H. S. and Sandler, S. I., *Use of ab initio quantum mechanics calculations in group contribution methods. 2. Test of new groups in UNIFAC*, Industrial and Engineering Chemistry Research, 1991. **30**: p. 889-897.

3. Jensen, F., *Introduction to computational chemistry*, 2007. West Sussex, England, John Wiley & Sons Ltd.

4. Harper, P. M., Gani, R., Kolar, P., and Ishikawa, T., *Computer-aided molecular design with combined molecular modeling and group contribution*, Fluid Phase Equilibria, 1999, **158-160**: p. 337-347.

5. Logic and Heuristics Applied to Synthetic Analysis (LHASA), available at: http://lhasa.harvard.edu/

6. You, S. M., Kim, J. H., and Kim, K. H., *Effect of nanoparticles on critical heat flux of water in pool boiling heat transfer*, Applied Physics Letters, 2003. **83**: p. 3374-3376

7. Vassallo, P., Kumar, R., and D'Amico, S., *Pool boiling heat transfer experiments in silica–water nano-fluids*, International Journal of Heat and Mass Transfer, 2004. **47**: p. 407-411.

8. Daungthongsuk, W. and Wongwises, S., *A critical review of convective heat transfer in nanofluids*, Renewable and Sustainable Energy Reviews, 2007. **11**: p. 797-817.

APPENDIX A

FLUIDS FOR AIRCRAFT COOLING - PROJECT FOR AIRFORCE RESEARCH LABORATORY

A.1 Aircraft Systems

The following constraints were provided by the Air Force Research Lab (AFRL):

Phase Change Cooling:

- $400 > T_b > 500$ K

Single Phase Convection:

- $T_m < 240$ K
- $T_b > 500$ K
- $k > 0.15$ W m^{-1} K^{-1}

The ProCAMD (ICAS-11) software was used with the above constraints to generate the following candidates. Two of these fluids were selected by AFRL for further investigation.

A.1.1 Single Phase Convection

Groups used: alcohol, ketone, aldehyde, acid, ester, ether, amine, amide, phenol, and compounds containing F, Cl, and Br. Selected compounds are listed in Tables A.1 and A.2.

Table A.1. Properties of fluids for single phase convection cooling in aircrafts.

	T_m	T_b	H_{vap}
	K	K	kJ mol^{-1}
Diethyl propylmalonate	255.66	509.76	52.98
1-Octanol 3-chloro acetate	248.45	518.59	50.48
4-chloro-3-isopropylpentan-2-yl acetate	242.5	494.14	45.48
Nitric acid decyl ester	252.86	524.16	56.86
3-methylpentan-2-yl 3-chlorobutanoate	242.55	512.89	49.04
2,3-dichloro-N-ethyl-N-isopropylbutan-1-amine	233.31	502.66	44.93
2-hydroxy-4-methylpentan-3-yl propionate	260.52	501.94	56.41
isopropyl 2-(ethyl(2-methoxy-2-oxoethyl)amino)acetate	263.16	527.42	57.1
6-chloro-2,5-dimethylhexan-3-ol	256.66	490.36	52.88
ethyl 2-(ethyl(2-methoxy-2-oxoethyl)amino)acetate	258.43	518.42	55.89
3-isopropyl-1,2,4,5-tetramethylbenzene	250.94	504.78	44.11
2,3-diethyl-1,4,5-trimethylbenzene	243.38	517.17	44.24
1-fluoro-2-isopropyl-3,4,5,6-tetramethylbenzene	262.73	504.26	44.12

Table A.2. Properties of fluids at 298 K for single phase convection cooling in aircrafts.

	σ	ρ	k	η	C_p
	dynes cm^{-1}	g cc^{-1}	W m^{-1} K^{-1}	cP	J mol^{-1} K^{-1}
Diethyl propylmalonate	32.14	1.0691	0.1162	3.529	398.03
1-Octanol 3-chloro acetate	30.22	1.1083	0.117	2.782	379.216
4-chloro-3-isopropylpentan-2-yl acetate	25.64	1.0579	0.1124	2.723	365.38
Nitric acid decyl ester	NA	1.399	0.1244	3.68	NA
3-methylpentan-2-yl 3-chlorobutanoate	29.56	1.1171	0.1153	2.743	369.994
2,3-dichloro-N-ethyl-N-isopropylbutan-1-amine	30.58	1.0092	0.1118	1.75	347.743
2-hydroxy-4-methylpentan-3-yl propionate	28.6	1.1575	0.1243	7.24	403.08
isopropyl 2-(ethyl(2-methoxy-2-oxoethyl)amino)acetate	36.67	1.0914	0.1145	NA	428.91
6-chloro-2,5-dimethylhexan-3-ol	28.83	1.1037	0.1242	7.4	349.402
ethyl 2-(ethyl(2-methoxy-2-oxoethyl)amino)acetate	37.73	1.0472	0.1173	NA	267.4
3-isopropyl-1,2,4,5-tetramethylbenzene	29.32	0.8515	0.1207	1.36	345.702
2,3-diethyl-1,4,5-trimethylbenzene	24.82	0.8831	0.1239	1.37	NA
1-fluoro-2-isopropyl-3,4,5,6-tetramethylbenzene	27.47	0.9176	0.1154	0.8	NA

A.1.2 Phase Change Cooling

Groups used: alcohol, ketone, aldehyde, acid, ester, ether, amine, amide, phenol, and compounds containing F, Cl, and Br. Selected compounds are listed in Tables A.3 and A.4.

Table A.3. Propertied of fluids for phase change cooling in aircrafts.

	T_m	T_b	H_{vap}
	K	K	kJ mol^{-1}
3,3-difluoro-3-(propionyloxy)propanoic hypofluorous anhydride	246.54	467.82	44.22
1,1-difluoroethyl methyl succinate	294.8	483.01	47.12
(2-fluoroacetoxy)methyl propionate	249.84	473.19	44.29
methyl 3-fluoro-3-(2-fluoroacetoxy)butanoate	314.28	501.64	NA
methylene dipropionate	222.5	469.2	47.49
aniline	285.21	463.11	42.28

Table A.4. Properties of fluids at 298 K for phase change cooling in aircrafts.

	σ	ρ	k	η	C_p
	dynes cm^{-1}	g cc^{-1}	W m^{-1} K^{-1}	cP	J mol^{-1} K^{-1}
3,3-difluoro-3-(propionyloxy)propanoic hypofluorous anhydride	NA	1.693	0.1131	1.31	306.91
1,1-difluoroethyl methyl succinate	NA	1.6423	0.1173	0.98	323.32
(2-fluoroacetoxy)methyl propionate	NA	1.4558	0.1256	1.55	289.86
methyl 3-fluoro-3-(2-fluoroacetoxy)butanoate	NA	1.4131	0.1136	NA	323.32
methylene dipropionate	29.95	1.1106	0.1226	1.96	301.588
aniline	38.38	1.023	0.1525	2.75	174.14

APPENDIX B

SOLAR THERMAL ENERGY STORAGE

Solar energy is one the cleanest forms of energy available and it is estimated that 30 min of solar radiation falling on the earth is equal to the world energy demand for one year [1]. However, due to its intermittent availability, seasonal variability, and low energy density, solar energy has not yet been commercialized on a large scale [2]. Use of efficient solar heat collectors can mitigate the problem of low energy density. In this regard, parabolic trough collectors are the most mature solar technology in solar heat collection, and can generate heat at temperatures up to 400 °C [1]. For continuous supply of energy, solar collectors must transfer this heat to a fluid flowing through the collector. The solar energy thus collected is carried from the circulating fluid either directly to hot water, space conditioning equipment, or to a thermal energy storage tank from which energy can be drawn for use at night and/or cloudy days. Energy storage is considered to be one of the most critical factors in the advancement of solar energy systems [3].

Direct storage using a heat transfer fluid as the storage medium represents the simplest path forward since it eliminates a heat exchange step and avoids inefficiencies of transferring heat to the storage medium [2]. One of the goals for future solar energy storage systems is to develop heat transfer fluids as thermal storage media that allow operating temperatures greater than 400 °C combined with lower limits around 0°C [4]. Current heat transfer fluids VP-1^{TM} (eutectic mixture of biphenyl and diphenyl oxide), room temperature ionic liquids (imidazolium family), and nitrate salts (HITEC-XL)

cannot satisfy both these property constraints. Thus, development of heat transfer fluids with broad liquid range and high heat capacity will be of immense benefit.

B.1 Literature Search

Following fluids listed in Table B.1 were identified following a search in DIPPR property database. Table B.2 compares properties of 1 of these fluids with currently used fluid.

Table B.1. Fluids for solar thermal storage identified by literature search.

	T_m (°C)	T_b (°C)
cis-9-octadecenoic acid	13	360
Hexamethyltetracosane (Squalene)	-38	350
Dibutyl decanedioate	-10	345
Tetraethyl pentamine	-40	340
Dibutyl 1,2-phthalate	-35	340
Tri-o-tolyl phosphate	11	410
O,O-Diethyl O-(4-nitrophenyl)phosphorothioate (Parathion)	6	345
Di-(2-ethylhexyl)-o-phthalate	-50	384
Bis-(2-ethylhexyl)-o-phthalate	-52	384
Bis[3-(triethoxysilyl)propyl]disulfide	-3	458

Table B.2. Properties of existing fluids for solar thermal storage.

Compound	T_m (K)	T_b (K)	ρ (g cc^{-1})	k (W m^{-1} K^{-1})	η (cP)	H_{vap} (kJ mol^{-1})	C_p (J mol^{-1} K^{-1})	σ (dynes cm^{-1})
$C_{18}H_{42}O_6S_2Si_2$	270	731	1.022	0.20	2.6*	103.20	617.66	34.4
Biphenyl	321	533	1.013	0.125	-	46	238.94	35.16
Diphenyl oxide	299	532	1.08	0.122	3.8	51	268.14	44.9

* - at 330 K

B.2 CAMD

Constraints

- $T_b > 700$ K and $T_m < 280$ K

Groups

- CH_3, CH_2, CH, C, CH_2=CH, CH=CH, CH_2=C, CH=C, C=C, ACH, AC, $ACCH_3$, $ACCH_2$, ACCH, CH_2=C=CH
- Maximum number of groups per molecule = 30

Screened Out Statistics

	Acyclic	Cyclic	Aromatic
T_m	3731 of 5349	2861 of 4689	566429 of 595349
T_b	1618 of 1618	1828 of 1828	28915 of 28920
Selected	0	0	5

Candidates

As the number of groups per molecule is extremely large, the software was not able to connect the groups to form a molecular structure. The combinations of groups generated are given below:

1) 13 - CH_3, 10 - CH, 1 - CH2=CH, 4 – $ACCH_3$, 2 - ACCH (T_m = 278.6 K , T_b = 700.0 K)
2) 10 - CH_3, 6 - CH, 2 - AC, 6 – $ACCH_3$, 2 - ACCH (T_m = 276.4 K , T_b = 702.1 K)
3) 10 - CH_3, 1 - CH_2, 6 - CH, 1 - ACH, 2 - AC, 5 – $ACCH_3$, 2 - ACCH (T_m = 280.0 K , T_b = 701.3 K)
4) 11 - CH_3, 7 - CH, 1 - ACH, 2 - AC, 5 - $ACCH_3$, 2 - ACCH (T_m = 279.3 K , T_b = 705.1 K)
5) 12 - CH_3, 8 - CH, 3 - ACH, 2 - AC, 3 – $ACCH_3$, 2 - ACCH (T_m = 279.5 K , T_b = 701.3 K)

B.3 References

1. Kalogirou, S. A., *Solar thermal collectors and applications*, Progress in Energy and Combustion Science, 2004, **30**: p: 231-295.

2. Tester, J. W., Drake, E. M., Driscoll, M. J., Golay, M.W., and Peters W.A., *Sustainable energy: choosing among option*s, 2005, Cambridge: M.I.T Press.

3. Moens, L., Blake D. M., Rudnicki, D. L., and Hale, M.J., *Advanced thermal storage fluids for solar parabolic trough systems*, Journal of Solar Energy Engineering, 2003, **125**(1): p. 112-116.

4. Moens, L. and Blake D. M., *Advanced heat transfer and thermal storage fluids*, DOE Solar Energy Technologies, 2005, **NREL/CP-510-37083**: p. 1-2.

APPENDIX C

DATA USED FOR EVALUATION OF GC METHODS

Table C.1. Melting point.

Compound	T_m - Lit. (K)	T_m - Pred. (K)		
		MG	CG	JR
Nonane	219.66	169.24	205.00	190.69
Undecane	247.57	191.07	227.85	213.23
Butane	134.86	94.14	104.62	134.34
Tetradecane	279.01	218.75	254.71	247.04
Tridecane	267.76	210.09	246.52	235.77
Chloroethane	136.75	142.05	136.78	141.72
Chloroform	209.63	206.79	N/A	175.29
1-Chloropropane	150.20	155.57	159.08	152.99
Decane	243.51	180.56	217.06	201.96
Nonadecane	305.04	255.75	288.04	303.39
Acetylene	192.40	N/A	N/A	99.64
1-Butene	87.80	103.08	91.73	132.58
cis-2-Butene	134.26	131.61	114.40	129.26
trans-2-Butene	167.62	131.61	114.40	129.26
1-Decene	206.90	185.60	212.94	200.20
Ethylene	104.00	N/A	N/A	113.36
1-Heptene	154.12	150.04	169.31	166.39
1-Hexene	133.39	135.98	149.35	155.12
Methyl acetylene	170.45	158.15	151.16	170.04
Propylene	87.90	96.22	87.90	121.31
1-Butyne	147.43	170.32	170.80	181.31
1-Decyne	229.15	227.67	244.17	248.93
1-Heptyne	192.22	201.76	213.92	215.12
3-Hexyne	170.05	202.38	257.52	262.98
1-Hexyne	141.25	192.01	201.46	203.85
2-Hexyne	183.65	202.38	257.52	262.98
3-Methyl-1-butyne	183.45	178.82	169.50	177.58
1-Nonyne	223.15	219.53	235.04	237.66
1-Octyne	193.55	210.91	225.02	226.39
2-Pentyne	163.83	192.66	249.55	251.71
Benzyl alcohol	257.85	280.98	248.81	255.39

Table C.1 Continued.

1-Butanol	183.85	212.95	196.88	195.16
2-Butanol	158.45	193.27	170.00	180.16
1-Decanol	280.05	257.86	257.74	262.78
Ethanol	159.05	194.33	164.57	172.62
1-Heptanol	239.15	237.11	231.76	228.97
2-Heptanol	220.00	220.58	213.40	213.97
1-Hexanol	228.55	229.49	221.40	217.70
2-Hexanol	223.00	212.02	200.87	202.70
Methanol	175.47	184.05	N/A	161.35
Anisole	235.65	235.23	240.54	216.80
Benzyl ethyl ether	275.65	250.45	238.73	239.34
Dibutyl ether	175.30	185.62	208.01	201.65
Diethyl ether	156.85	136.01	139.98	156.57
Diphenyl ether	300.03	299.09	N/A	299.57
Ethylhexyl ether	180.00	185.62	208.01	201.65
Ethylisopropyl ether	140.00	146.66	138.22	152.84
Ethylpropyl ether	145.65	150.06	161.66	167.84
Tetrahydrofuran	164.65	191.41	212.48	176.05
Methylbutyl ether	157.48	152.56	186.26	167.84
Benzene	278.68	185.39	222.77	170.78
Propylbenzene	173.55	203.79	226.64	217.11
p-Dichlorobenzene	326.14	281.67	248.68	255.66
Biphenyl	342.20	321.25	277.98	277.34
m-Xylene	225.30	194.33	231.60	218.36
Butylbenzene	185.30	212.82	236.51	228.38
Chlorobenzene	227.95	226.40	236.54	213.22
Cumene	177.14	199.35	192.41	202.11
m-Dichlorobenzene	248.39	241.64	248.68	255.66
Ethylbenzene	178.20	194.18	215.72	205.84
Cyclobutane	182.48	121.50	133.96	153.00
Cyclohexane	279.69	181.28	200.95	168.50
Cyclohexene	169.67	183.59	197.78	169.26
Cyclopentane	179.31	154.40	170.92	160.75
Cyclopentene	138.13	157.16	166.64	161.51
Cyclopropane	145.59	79.08	145.79	145.25
Ethylcyclohexane	161.84	178.83	166.94	186.80
Ethylcyclopentane	134.71	151.45	122.14	179.05
Propenylcyclohexene	199.00	218.72	231.76	210.51
1,1-Dimethylcyclohexane	239.66	229.97	222.33	210.70

Table C.1 Continued.

Propionaldehyde	170.00	203.13	177.93	165.07
Acetaldehyde	150.15	193.47	N/A	153.80
Butyraldehyde	176.75	212.20	193.37	176.34
Decanal	267.15	257.30	255.82	243.96
Formaldehyde	181.15	N/A	N/A	119.76
Heptanal	229.80	236.47	229.28	210.15
Hexanal	217.15	228.81	218.65	198.88
Nonanal	255.15	250.68	247.71	232.69
Octanal	246.00	243.74	238.91	221.42
Pentanal	182.00	220.74	206.79	187.61
Acetone	178.45	191.07	171.62	173.00
Benzophenone	321.35	310.35	N/A	338.54
Cyclohexanone	242.00	265.70	251.40	236.72
Ethylisopropyl ketone	204.15	216.90	205.66	191.81
3-Heptanone	234.15	227.19	229.11	218.08
2-Heptanone	238.15	223.84	222.11	218.08
2-Hexanone	217.35	215.48	210.66	206.81
3-Hexanone	217.50	219.02	218.46	206.81
Methylethyl ketone	186.48	197.19	183.03	184.27
Methylisobutyl ketone	189.15	213.30	196.78	191.81
Butyl acetate	199.65	189.51	203.89	199.21
Ethyl acetate	189.60	167.42	174.07	176.67
Ethyl benzoate	238.45	243.42	239.44	259.44
Ethyl butyrate	175.15	185.83	189.08	199.21
Ethyl formate	193.55	160.46	176.70	187.30
Ethyl propionate	199.25	174.92	172.92	187.94
Methyl acetate	175.15	155.00	155.10	165.40
Methyl acrylate	196.32	188.20	175.65	174.91
Methyl benzoate	260.75	236.13	229.87	248.17
Propyl acetate	178.15	178.88	190.06	187.94
Diethanol amine	301.15	285.20	314.70	308.64
Diethyl amine	223.35	181.17	211.87	187.00
Di-isopropyl amine	176.85	218.49	178.23	179.54
Dipropyl amine	210.15	201.42	233.38	209.54
Ethyl amine	192.15	203.28	202.66	195.06
Ethylenediamine	284.29	284.25	284.29	278.32
Diethyl amine	223.35	181.17	211.87	187.00
Isopropyl amine	177.95	224.76	166.57	191.33
Methyl amine	179.69	205.99	N/A	183.79

Table C.1 Continued.

Propyl amine	190.15	212.34	214.98	206.33
Acetamide	354.15	388.15	354.15	244.99
Benzamide	403.00	406.38	374.77	327.76
Formamide	275.70	272.93	N/A	225.79
N-Methyl acetamide	301.15	268.25	N/A	225.66
N,N-Dimethyl formamide	212.72	227.39	N/A	197.54
Acrylic acid	286.15	353.40	264.36	281.91
Benzoic acid	395.52	402.80	395.52	355.17
Acetic acid	289.81	308.44	254.75	272.40
Butyric acid	267.95	317.32	269.40	294.94
Decanoic acid	304.75	341.15	303.84	362.56
2-Ethyl butanoic acid	258.15	257.96	250.98	302.48
2-Ethyl hexanoic acid	155.15	270.32	266.14	325.02
Formic acid	281.55	259.38	N/A	203.35
Heptanoic acid	265.83	329.72	288.06	328.75
Isobutyric acid	227.15	247.73	233.58	279.94
benzotrifluoride	244.14	NA	243.59	198.76
fluorobenzene	230.94	200.99	234.15	183.89
hexafluorobenzene	278.25	260.94	277.43	249.44
perfluoromethylcyclopentane	228.15	229.68	NA	279.82
perfluoro-n-heptane	221.86	189.76	NA	194.53
perfluoro-n-hexane	185.00	184.31	NA	179.66
perfluoro-n-nonane	257.15	200.07	NA	224.27
perfluoro-n-octane	250.00	195.00	NA	209.40
perfluoro-n-pentane	147.51	178.67	NA	164.79
dichlorodiethylsilane	174.10	242.66	NA	NA
dimethyldichlorosilane	197.05	227.61	NA	NA
dimethyldimethoxysilane	193.00	124.54	NA	NA
ethyltrichlorosilane	167.50	258.77	NA	NA
hexamethyldisiloxane	204.93	173.75	NA	NA
methyl trichlorosilane	195.35	252.22	NA	NA
methyl vinyl dichlorosilane	178.15	241.93	NA	NA
trimethoxysilane	159.60	NA	NA	NA
vinyltrichlorosilane	178.35	264.42	NA	NA
octamethyltrisiloxane	187.15	185.41	NA	NA

Table C.2. Normal boiling point.

Compound	T_b - Lit. (K)	T_b - Pred. (K)			
		MG	CG	JR	W
Nonane	423.97	423.2	430.9	405.32	423.2
Undecane	469.08	466.22	472.21	451.08	466.22
Butane	272.65	253.67	263.12	290.92	253.67
Tetradecane	526.73	518.30	521.78	519.72	518.3
Tridecane	508.63	502.25	506.55	496.84	502.25
Chloroethane	285.45	277.87	275.66	282.59	277.87
Chloroform	334.33	351.70	N/A	334.13	351.70
1-Chloropropane	320.00	319.35	319.52	305.47	319.35
Decane	447.30	445.75	452.6	428.2	445.75
Nonadecane	603.05	584.71	584.46	634.12	584.71
Acetylene	-	N/A	N/A	216.40	216.40
1-Butene	266.91	249.56	253.31	287.6	249.56
cis-2-Butene	276.87	267.83	270.42	295.08	267.83
trans-2-Butene	274.03	267.83	270.42	295.08	267.83
1-Decene	443.75	444.02	448.77	424.88	444.02
Ethylene	169.41	N/A	N/A	234.36	234.36
1-Heptene	366.79	367.38	373.57	356.24	367.38
1-Hexene	336.63	334.59	340.77	333.36	334.59
Methyl acetylene	249.94	213.57	241.32	258.16	213.57
Propylene	225.45	199.02	205.90	264.72	199.02
1-Butyne	281.22	267.38	292.28	281.04	267.38
1-Decyne	447.15	451.63	464.64	418.32	451.63
1-Heptyne	372.93	378.05	396.12	349.68	378.05
3-Hexyne	354.35	349.23	372.48	345.68	349.23
1-Hexyne	344.48	346.90	367.00	326.80	346.9
2-Hexyne	357.67	349.23	372.48	345.68	349.23
3-Methyl-1-butyne	302.15	294.09	313.38	303.48	294.09
1-Nonyne	423.85	429.70	444.25	395.44	429.7
1-Octyne	399.35	405.37	421.6	372.56	405.37
2-Pentyne	329.27	313.41	339.49	322.80	313.41
Benzyl alcohol	478.60	472.09	466.67	478.42	472.09
1-Butanol	391.90	381.73	393.90	383.10	381.73
2-Butanol	372.90	357.69	365.52	382.66	357.69
1-Decanol	503.00	508.90	514.63	520.38	508.90
Ethanol	351.44	315.64	330.01	337.34	315.64

Table C.2 Continued.

1-Heptanol	448.60	454.28	463.05	451.74	454.28
2-Heptanol	432.90	437.19	443.24	451.30	437.19
1-Hexanol	429.90	432.62	442.5	428.86	432.62
2-Hexanol	412.40	413.71	420.47	428.42	413.71
Methanol	337.85	273.39	N/A	314.46	273.39
Anisole	426.73	429.32	438.00	408.66	429.32
Benzyl ethyl ether	458.15	457.66	451.52	454.42	457.66
Dibutyl ether	414.15	420.14	425.37	404.86	420.14
Diethyl ether	307.58	294.09	299.32	313.34	294.09
Diphenyl ether	531.46	532.39	N/A	549.74	532.39
Ethylhexyl ether	417.15	420.14	425.37	404.86	420.14
Ethylisopropyl ether	326.15	317.94	319.74	335.78	317.94
Ethylpropyl ether	337.01	332.89	338.82	336.22	332.89
Tetrahydrofuran	339.12	325.54	350.18	337.82	325.54
Methylbutyl ether	343.31	446.55	449.17	449.74	446.55
Benzene	353.24	359.01	351.27	358.38	359.01
Propylbenzene	432.39	440.50	435.12	432.00	440.50
p-Dichlorobenzene	447.21	450.78	448.51	443.2	450.78
Biphenyl	528.15	532.87	516.94	527.32	532.87
m-Xylene	412.27	416.50	415.88	414.10	416.50
Butylbenzene	456.455	461.43	456.40	454.88	461.43
Chlorobenzene	404.87	407.81	405.62	400.79	407.81
Cumene	425.56	425.51	426.38	431.56	425.51
m-Dichlorobenzene	446.23	448.45	448.51	443.20	448.45
Ethylbenzene	409.35	417.38	411.37	409.12	417.38
Cyclobutane	285.66	265.27	285.65	306.60	265.27
Cyclohexane	353.87	355.50	356.78	360.90	355.50
Cyclohexene	356.12	353.31	356.72	360.06	353.31
Cyclopentane	322.40	314.93	320.75	333.75	314.93
Cyclopentene	317.38	312.30	320.68	332.91	312.30
Cyclopropane	240.37	201.25	240.37	279.45	201.25
Ethylcyclohexane	404.94	408.18	405.52	401.99	408.18
Ethylcyclopentane	376.62	376.8	377.69	374.84	376.8
Propenylcyclohexene	431.65	432.80	436.88	437.84	432.8
1,1-Dimethylcyclohexane	392.70	398.68	393.98	402.23	398.68
Propionaldehyde	321.15	314.11	314.71	316.70	314.11
Acetaldehyde	294.00	271.55	269.68	293.82	271.55
Butyraldehyde	347.95	349.83	351.59	339.58	349.83
Decanal	488.15	491.45	492.29	476.86	491.45

Table C.2 Continued.

Formaldehyde	254.05	N/A	N/A	205.68	205.68
Heptanal	425.95	431.72	433.81	408.22	431.72
Hexanal	401.45	407.63	409.9	385.34	407.63
Nonanal	468.15	473.27	474.59	453.98	473.27
Octanal	447.15	453.46	455.22	431.10	453.46
Pentanal	376.15	380.60	382.82	362.46	380.60
Acetone	329.44	306.66	305.37	321.91	306.66
Benzophenone	579.24	607.95	N/A	604.07	607.95
Cyclohexanone	428.58	432.93	433.47	428.72	432.93
Ethylisopropyl ketone	386.55	379.88	399.19	390.11	379.88
3-Heptanone	420.55	417.12	435.97	413.43	417.12
2-Heptanone	424.18	426.66	429.21	413.43	426.66
2-Hexanone	400.70	401.97	404.73	390.55	401.97
3-Hexanone	396.65	391.29	412.32	390.55	391.29
Methylethyl ketone	352.79	342.47	344.67	344.79	342.47
Methylisobutyl ketone	389.15	391.11	391.08	390.11	391.11
Butyl acetate	399.26	402.94	406.04	394.90	402.94
Ethyl acetate	350.21	343.74	346.44	349.14	343.74
Ethyl benzoate	486.55	487.51	486.54	490.22	487.51
Ethyl butyrate	394.65	402.84	398.22	394.90	402.84
Ethyl formate	327.46	317.26	327.17	339.12	317.26
Ethyl propionate	372.25	375.18	369.43	372.02	375.18
Methyl acetate	330.09	306.94	308.52	326.26	306.94
Methyl acrylate	353.35	337.47	341.45	345.82	337.47
Methyl benzoate	472.65	468.99	468.32	467.34	468.99
Propyl acetate	374.65	375.30	378.40	372.02	375.30
Diethanol amine	541.54	516.13	538.54	525.45	516.13
Diethyl amine	328.60	323.95	341.35	341.09	323.95
Di-isopropyl amine	357.05	354.29	348.66	385.97	354.29
Dipropyl amine	382.00	387.93	402.25	386.85	387.93
Ethyl amine	289.73	288.00	286.09	317.69	288.00
Ethylenediamine	390.41	383.03	390.41	390.22	383.03
Diethyl amine	328.60	323.95	341.35	341.09	323.95
Isopropyl amine	304.92	296.48	296.24	340.13	296.48
Methyl amine	266.82	235.45	N/A	294.81	235.45
Propyl amine	321.00	327.79	327.98	340.57	327.79
Acetamide	494.30	445.84	494.3	371.56	445.84
Benzamide	563.15	563.15	574.33	512.64	563.15
Formamide	493.00	338.17	N/A	343.47	338.17

Table C.2 Continued.

N-Methyl acetamide	478.15	395.81	N/A	372.08	395.81
N,N-Dimethyl formamide	425.15	347.78	N/A	329.14	347.78
Acrylic acid	414.15	424.53	414.91	410.23	424.53
Benzoic acid	522.40	517.92	522.40	531.75	517.92
Acetic acid	391.05	397.25	389.42	390.67	397.25
Butyric acid	436.42	445.06	438.97	436.43	445.06
Decanoic acid	543.15	546.84	540.81	573.71	546.84
2-Ethyl butanoic acid	466.95	468.52	468.62	481.75	468.52
2-Ethyl hexanoic acid	500.66	504.21	503.52	527.51	504.21
Formic acid	373.71	362.83	N/A	363.12	362.83
Heptanoic acid	496.15	501.72	496.17	505.07	501.72
Isobutyric acid	427.65	425.87	423.54	435.99	425.87
dichlorodiethylsilane	403.15	410.94	NA	NA	410.94
dimethyldichlorosilane	343.55	354.11	NA	NA	354.11
dimethyldimethoxysilane	354.55	346.70	NA	NA	346.70
ethyltrichlorosilane	371.05	409.23	NA	NA	409.23
hexamethyldisiloxane	373.67	387.64	NA	NA	387.64
methyl trichlorosilane	339.55	382.41	NA	NA	382.41
methyl vinyl dichlorosilane	366.95	384.19	NA	NA	384.19
trimethoxysilane	357.50	349.58	NA	NA	349.58
vinyltrichlorosilane	363.85	409.10	NA	NA	409.10
octamethyltrisiloxane	425.70	458.19	NA	NA	458.19
benzotrifluoride	375.20	385.73	413.44	380.82	385.73
fluorobenzene	357.88	357.14	351.8	362.63	357.14
hexafluorobenzene	353.41	347.55	354.43	383.88	347.55
perfluoromethylcyclopentane	321.15	209.14	332.94	322.49	209.14
perfluoro-n-heptane	355.66	356.12	353.28	325.27	356.12
perfluoro-n-hexane	330.30	331.73	329.80	307.08	331.73
perfluoro-n-nonane	398.45	398.10	393.43	361.65	398.10
perfluoro-n-octane	376.45	378.10	374.34	343.46	378.10
perfluoro-n-pentane	302.40	304.34	303.27	288.89	304.34

Table C.3. Enthalpy of vaporization.

Compound	H_{vap} - Lit. (kJ mol^{-1})	H_{vap} - Pred. (kJ mol-1)			
		MG	CG	JR	W
Nonane	46.18	51.56	47.61	42.78	44.97
Undecane	56.01	61.29	56.91	40.08	53.20
Butane	21.01	27.22	24.36	24.07	18.17
Tetradecane	70.51	75.90	70.86	65.97	64.54
Tridecane	65.82	71.03	66.21	61.10	60.85
Chloroethane	24.08	28.59	24.73	23.23	23.11
Chloroform	31.30	36.93	N/A	30.71	33.71
1-Chloropropane	28.38	33.46	29.38	26.44	28.87
Decane	50.88	56.43	52.26	47.12	49.18
Nonadecane	92.84	100.23	94.11	88.85	82.12
Acetylene	6.84	N/A	N/A	14.23	15.06
1-Butene	20.22	25.75	21.94	23.54	17.79
cis-2-Butene	22.17	26.99	22.29	24.45	20.80
trans-2-Butene	21.39	26.99	22.29	24.45	20.80
1-Decene	48.73	54.95	49.84	46.16	48.80
Ethylene	13.50	N/A	N/A	16.44	17.63
1-Heptene	35.64	40.35	35.89	33.93	35.47
1-Hexene	30.61	35.48	31.24	30.27	30.33
Methyl acetylene	19.13	22.37	18.70	19.70	13.03
Propylene	14.25	21.51	17.59	20.44	9.32
1-Butyne	23.74	27.24	23.35	22.65	21.03
1-Decyne	52.71	56.45	51.25	44.41	50.28
1-Heptyne	36.94	41.84	37.30	32.59	37.48
3-Hexyne	34.02	38.72	35.91	31.24	33.01
1-Hexyne	33.27	36.98	32.65	29.08	32.61
2-Hexyne	34.82	38.72	35.91	31.24	33.01
3-Methyl-1-butyne	26.26	29.61	25.88	25.32	24.49
1-Nonyne	48.15	51.58	46.60	40.26	46.24
1-Octyne	41.74	46.71	41.95	36.32	41.99
2-Pentyne	30.24	33.85	31.26	27.94	27.68
Benzyl alcohol	65.52	70.30	62.03	67.54	58.12
1-Butanol	53.55	55.73	49.42	47.65	46.81
2-Butanol	49.95	53.11	45.61	46.76	41.45
1-Decanol	80.78	84.93	77.32	80.22	67.72
Ethanol	42.55	45.99	40.12	38.36	35.33
1-Heptanol	69.65	70.33	63.37	63.21	56.19

Table C.3 Continued.

2-Heptanol	61.90	67.71	59.56	62.05	52.49
1-Hexanol	63.83	65.46	58.72	57.82	52.08
2-Hexanol	57.89	62.85	54.91	56.74	48.10
Methanol	37.65	41.13	N/A	34.05	28.10
Anisole	46.62	50.69	50.79	42.48	46.37
Benzyl ethyl ether	50.79	55.57	49.10	50.91	50.97
Dibutyl ether	45.18	50.73	45.79	43.81	45.76
Diethyl ether	27.39	31.26	27.19	28.10	25.06
Diphenyl ether	58.62	N/A	N/A	N/A	N/A
Ethylhexyl ether	47.32	50.73	45.79	43.81	45.76
Ethylisopropyl ether	30.01	33.63	29.72	31.13	28.41
Ethylpropyl ether	31.40	36.13	31.84	31.72	31.05
Tetrahydrofuran	31.98	35.14	31.44	31.64	30.19
Methylbutyl ether	32.61	37.65	35.81	31.72	33.62
Benzene	33.76	38.86	31.42	33.51	33.94
Propylbenzene	46.21	51.53	46.27	45.35	46.43
p-Dichlorobenzene	47.95	52.66	46.99	47.16	47.18
Biphenyl	63.09	N/A	72.91	60.35	N/A
m-Xylene	42.71	45.75	42.77	41.92	42.48
Butylbenzene	50.48	56.39	50.92	49.60	50.09
Chlorobenzene	40.77	45.81	39.20	40.08	40.88
Cumene	44.96	48.95	44.68	44.35	43.77
m-Dichlorobenzene	46.37	51.51	46.99	47.16	46.79
Ethylbenzene	42.23	46.66	41.62	41.35	42.63
Cyclobutane	23.39	28.70	25.43	26.53	20.38
Cyclohexane	33.00	37.18	33.82	33.31	32.96
Cyclohexene	33.41	36.96	31.89	33.38	32.74
Cyclopentane	28.39	32.94	29.51	29.92	27.15
Cyclopentene	27.84	32.72	27.58	29.98	26.96
Cyclopropane	16.93	24.46	20.78	23.13	11.36
Ethylcyclohexane	40.66	44.14	40.60	39.08	40.99
Ethylcyclopentane	36.49	39.90	36.28	35.48	35.98
Propenylcyclohexene	46.14	49.45	44.12	45.02	45.08
1,1-Dimethylcyclohexane	37.98	41.79	38.69	38.24	39.33
Propionaldehyde	29.88	33.61	28.50	30.00	30.57
Acetaldehyde	25.49	28.74	23.85	26.48	24.28
Butyraldehyde	33.99	38.47	33.15	33.72	36.00
Decanal	62.15	67.68	61.05	60.58	61.53
Formaldehyde	20.88	N/A	N/A	12.51	12.98

Table C.3 Continued.

Heptanal	46.82	53.07	47.10	46.19	49.73
Hexanal	43.24	48.21	42.45	41.81	45.45
Nonanal	57.04	62.81	56.40	55.59	57.73
Octanal	52.48	57.94	51.75	50.79	53.81
Pentanal	38.88	43.34	37.80	37.65	40.91
Acetone	31.23	30.77	29.94	30.23	28.74
Benzophenone	76.83	N/A	N/A	N/A	N/A
Cyclohexanone	45.19	50.30	45.31	45.22	47.77
Ethylisopropyl ketone	40.25	41.43	42.28	41.00	39.33
3-Heptanone	47.65	48.79	49.05	46.16	45.93
2-Heptanone	47.08	50.45	47.88	46.16	47.80
2-Hexanone	42.91	45.58	43.23	41.84	43.52
3-Hexanone	42.24	43.92	44.40	41.84	41.49
Methylethyl ketone	34.63	35.85	33.93	33.88	34.02
Methylisobutyl ketone	40.65	43.09	41.11	41.00	41.45
Butyl acetate	43.89	50.26	47.60	42.77	44.39
Ethyl acetate	35.67	40.52	38.30	34.65	34.59
Ethyl benzoate	55.75	64.59	63.51	59.22	58.31
Ethyl butyrate	42.63	48.29	42.12	42.77	44.37
Ethyl formate	31.91	36.45	N/A	34.62	31.47
Ethyl propionate	38.86	43.42	37.47	38.60	39.67
Methyl acetate	32.39	35.65	33.65	30.92	28.89
Methyl acrylate	35.25	38.96	32.53	33.92	33.71
Methyl benzoate	55.06	59.72	58.86	54.48	54.88
Propyl acetate	39.53	45.39	42.95	38.60	39.69
Diethanol amine	85.12	91.79	N/A	N/A	94.65
Diethyl amine	31.21	34.78	34.19	33.60	30.31
Di-isopropyl amine	34.66	38.50	N/A	40.04	34.36
Dipropyl amine	40.78	44.52	43.49	41.69	40.67
Ethyl amine	26.80	31.96	25.54	30.11	26.12
Ethylenediamine	45.20	49.13	36.03	45.44	44.31
Diethyl amine	31.21	34.78	34.19	33.60	30.31
Isopropyl amine	28.58	32.11	27.23	33.11	26.41
Methyl amine	23.94	30.81	N/A	26.69	18.23
Propyl amine	30.99	36.83	30.19	33.74	31.96
Acetamide	65.80	N/A	N/A	41.23	N/A
Benzamide	77.21	N/A	N/A	N/A	N/A
Formamide	61.82	42.06	N/A	37.15	39.02
N-Methyl acetamide	59.56	64.04	N/A	41.02	46.07

Table C.3 Continued.

N,N-Dimethyl formamide	46.90	37.07	N/A	32.86	37.37
Acrylic acid	27.97	N/A	56.59	49.48	N/A
Benzoic acid	80.03	N/A	N/A	N/A	N/A
Acetic acid	23.42	N/A	53.99	45.92	N/A
Butyric acid	40.18	N/A	63.29	55.20	N/A
Decanoic acid	88.66	N/A	N/A	N/A	N/A
2-Ethyl butanoic acid	62.17	52.62	70.18	N/A	64.39
2-Ethyl hexanoic acid	76.12	62.36	79.48	N/A	71.98
Formic acid	19.95	52.38	N/A	47.26	51.26
Heptanoic acid	76.05	N/A	77.24	N/A	N/A
Isobutyric acid	35.65	42.76	60.88	54.07	56.39
dichlorodiethylsilane	43.47	NA	NA	NA	42.84
dimethyldichlorosilane	32.11	NA	NA	NA	33.75
dimethyldimethoxysilane	34.68	NA	NA	NA	34.11
ethyltrichlorosilane	36.55	NA	NA	NA	42.49
hexamethyldisiloxane	36.29	NA	NA	NA	39.91
methyl trichlorosilane	29.85	NA	NA	NA	38.30
methyl vinyl dichlorosilane	35.24	NA	NA	NA	38.53
trimethoxysilane	35.61	NA	NA	NA	35.98
vinyltrichlorosilane	34.21	NA	NA	NA	42.53
octamethyltrisiloxane	46.59	NA	NA	NA	55.65
benzotrifluoride	32.76	34.07	31.11	29.70	33.89
fluorobenzene	31.38	31.17	29.93	30.41	31.01
hexafluorobenzene	31.69	32.24	32.27	29.63	30.41
perfluoromethylcyclopentane	27.90	26.79	33.42	11.12	14.09
perfluoro-n-heptane	31.42	29.02	30.88	9.03	30.98
perfluoro-n-hexane	28.79	26.75	28.79	9.74	28.49
perfluoro-n-nonane	36.08	33.56	34.07	7.62	35.34
perfluoro-n-octane	33.68	31.29	32.63	8.33	33.25
perfluoro-n-pentane	26.12	24.47	26.30	10.44	25.75

Table C.4. Surface tension at 298 K.

Compound	σ - Lit. (dynes cm^{-1})	σ - Pred. (dynes cm^{-1})			
		MG	CG	JR	W
Nonane	22.42	20.47	24.23	22.58	23.19
Undecane	24.24	21.51	26.13	24.66	24.98
Butane	11.94	17.86	17.67	17.05	11.76
Tetradecane	26.15	23.07	28.56	27.44	26.95
Tridecane	25.56	22.55	27.79	26.59	26.35
Chloroethane	18.37	23.37	21.95	18.50	20.08
Chloroform	26.70	29.20	N/A	24.66	29.09
1-Chloropropane	21.30	23.89	23.14	19.59	22.69
Decane	23.40	20.99	25.21	23.63	24.16
Nonadecane	28.28	25.68	31.90	N/A	29.67
Acetylene	1.05	N/A	N/A	12.54	16.12
1-Butene	12.03	19.00	16.30	17.09	12.06
cis-2-Butene	13.96	17.12	16.65	17.74	15.03
trans-2-Butene	13.06	17.12	16.65	17.74	15.03
1-Decene	23.68	22.13	24.42	23.50	24.51
Ethylene	N/A	N/A	N/A	13.50	18.21
1-Heptene	19.90	20.57	21.03	20.36	20.98
1-Hexene	17.98	20.04	19.65	19.30	19.04
Methyl acetylene	13.46	N/A	N/A	16.57	9.87
Propylene	6.94	18.54	14.42	15.88	5.39
1-Butyne	16.17	21.25	N/A	17.68	16.20
1-Decyne	25.67	30.95	N/A	23.65	26.11
1-Heptyne	22.19	27.18	N/A	20.69	23.33
3-Hexyne	22.78	24.32	24.60	20.82	22.15
1-Hexyne	20.56	25.51	N/A	19.71	21.80
2-Hexyne	23.93	24.32	24.60	20.82	22.15
3-Methyl-1-butyne	15.70	21.08	N/A	18.23	17.02
1-Nonyne	24.72	29.86	N/A	22.66	25.37
1-Octyne	23.59	28.61	N/A	21.67	24.48
2-Pentyne	22.25	22.63	23.55	20.00	20.05
Benzyl alcohol	38.63	34.79	46.38	60.09	45.90
1-Butanol	24.38	26.65	39.04	43.31	42.52
2-Butanol	22.97	23.08	36.00	41.95	36.25
1-Decanol	28.42	29.78	38.46	50.78	36.99
Ethanol	22.11	25.61	41.85	40.74	42.05
1-Heptanol	26.72	28.21	38.15	47.27	36.74

Table C.4 Continued.

2-Heptanol	25.19	24.64	35.85	45.72	33.67
1-Hexanol	25.96	27.69	38.24	45.95	36.72
2-Hexanol	24.41	24.12	35.74	44.45	33.17
Methanol	22.23	25.09	N/A	39.46	40.63
Anisole	34.98	30.51	34.85	29.58	33.71
Benzyl ethyl ether	32.50	28.30	28.65	31.03	30.93
Dibutyl ether	22.43	21.56	24.13	24.64	25.25
Diethyl ether	16.44	19.48	19.08	20.11	17.58
Diphenyl ether	39.20	44.90	N/A	N/A	N/A
Ethylhexyl ether	21.82	21.56	24.13	24.64	25.25
Ethylisopropyl ether	16.23	18.43	18.89	20.66	18.24
Ethylpropyl ether	19.30	20.00	20.56	21.27	20.53
Tetrahydrofuran	26.55	26.13	25.76	26.01	25.72
Methylbutyl ether	19.59	20.10	23.33	21.27	22.79
Benzene	28.23	27.95	24.39	25.51	26.89
Propylbenzene	28.51	26.68	27.77	27.41	28.09
p-Dichlorobenzene	35.51	36.83	32.49	32.26	32.60
Biphenyl	39.72	39.19	42.10	35.16	N/A
m-Xylene	28.25	28.77	27.88	26.61	27.78
Butylbenzene	28.65	27.20	28.52	28.19	28.27
Chlorobenzene	32.95	32.49	28.70	28.88	30.22
Cumene	27.70	27.08	26.53	26.50	26.09
m-Dichlorobenzene	35.90	37.54	32.49	32.26	32.26
Ethylbenzene	28.60	26.16	26.98	26.68	27.90
Cyclobutane	19.45	22.14	21.51	21.44	16.06
Cyclohexane	24.67	24.13	23.14	23.14	22.49
Cyclohexene	26.04	26.79	22.52	23.88	23.30
Cyclopentane	21.81	23.13	21.97	22.40	20.02
Cyclopentene	22.13	25.79	21.27	23.17	20.92
Cyclopropane	11.70	21.14	20.08	20.17	8.39
Ethylcyclohexane	25.06	23.90	23.75	22.87	23.94
Ethylcyclopentane	23.35	22.90	22.66	22.21	22.42
Propenylcyclohexene	29.06	29.01	25.44	26.21	26.23
1,1-Dimethylcyclohexane	23.67	24.50	22.58	22.60	22.72
Propionaldehyde	21.98	26.99	25.05	25.46	28.80
Acetaldehyde	20.79	26.46	24.28	24.36	26.29
Butyraldehyde	24.97	27.51	25.86	26.55	30.13
Decanal	28.31	30.63	30.30	33.15	32.91
Formaldehyde	27.43	N/A	N/A	12.14	14.55

Table C.4 Continued.

Heptanal	26.55	29.07	28.21	29.82	31.94
Hexanal	26.01	28.55	27.46	28.72	31.51
Nonanal	28.41	30.11	29.63	32.05	32.61
Octanal	27.59	29.59	28.94	30.94	32.29
Pentanal	25.34	28.03	26.67	27.63	30.94
Acetone	23.06	24.19	26.41	24.95	26.37
Benzophenone	43.52	46.43	N/A	N/A	N/A
Cyclohexanone	34.39	23.84	32.76	32.07	36.43
Ethylisopropyl ketone	24.04	22.69	26.87	27.06	25.98
3-Heptanone	25.70	24.78	29.24	28.97	28.63
2-Heptanone	26.14	26.06	28.72	28.97	30.13
2-Hexanone	25.47	25.54	28.01	27.94	29.58
3-Hexanone	25.00	24.26	28.57	27.94	27.83
Methylethyl ketone	23.98	24.50	26.55	25.93	27.80
Methylisobutyl ketone	23.44	23.97	26.31	27.06	27.79
Butyl acetate	24.76	24.82	29.64	27.63	29.50
Ethyl acetate	23.26	23.78	28.45	25.51	27.21
Ethyl benzoate	34.74	32.95	37.91	36.97	37.02
Ethyl butyrate	23.97	24.70	25.99	27.63	29.48
Ethyl formate	23.10	23.56	N/A	29.63	28.39
Ethyl propionate	23.77	24.18	25.04	26.56	28.53
Methyl acetate	24.55	23.25	27.91	24.46	25.12
Methyl acrylate	25.16	25.56	24.70	25.58	27.68
Methyl benzoate	37.26	32.43	37.96	36.26	37.74
Propyl acetate	23.87	24.30	29.04	26.56	28.55
Diethanol amine	49.59	69.22	N/A	N/A	111.23
Diethyl amine	19.19	21.75	24.48	25.12	22.12
Di-isopropyl amine	19.15	18.63	N/A	25.67	20.60
Dipropyl amine	22.24	22.79	26.37	27.35	25.65
Ethyl amine	19.19	24.57	24.43	27.06	25.45
Ethylenediamine	41.90	32.32	35.41	44.58	46.21
Diethyl amine	19.76	21.75	24.48	25.12	22.12
Isopropyl amine	17.42	20.30	21.81	27.17	21.41
Methyl amine	19.44	35.30	N/A	26.17	19.89
Propyl amine	21.40	25.09	25.25	27.96	27.57
Acetamide	46.63	35.61	N/A	40.29	N/A
Benzamide	50.97	45.49	N/A	N/A	N/A
Formamide	57.79	44.95	N/A	41.20	56.78
N-Methyl acetamide	34.00	N/A	N/A	35.67	44.77

Table C.4 Continued.

N,N-Dimethyl formamide	34.43	29.81	N/A	28.47	34.52
Acrylic acid	27.97	27.90	53.52	45.40	N/A
Benzoic acid	43.63	N/A	N/A	N/A	N/A
Acetic acid	27.06	26.24	57.01	44.52	N/A
Butyric acid	26.16	27.28	50.43	45.69	N/A
Decanoic acid	29.68	30.41	N/A	N/A	N/A
2-Ethyl butanoic acid	42.99	26.45	45.95	N/A	50.16
2-Ethyl hexanoic acid	27.37	27.49	44.79	N/A	48.29
Formic acid	37.12	34.73	N/A	63.23	93.86
Heptanoic acid	27.86	28.84	46.75	N/A	N/A
Isobutyric acid	24.55	25.15	48.00	44.18	53.82
dichlorodiethylsilane	13.63	12.42	NA	NA	25.32
dimethyldichlorosilane	19.62	11.38	NA	NA	23.06
dimethyldimethoxysilane	21.81	NA	NA	NA	21.32
ethyltrichlorosilane	22.96	15.35	NA	NA	28.05
hexamethyldisiloxane	15.40	NA	NA	NA	19.62
methyl trichlorosilane	19.54	14.83	NA	NA	27.60
methyl vinyl dichlorosilane	20.94	13.04	NA	NA	25.34
trimethoxysilane	20.02	NA	NA	NA	24.85
vinyltrichlorosilane	22.88	16.49	NA	NA	29.16
octamethyltrisiloxane	16.66	NA	NA	NA	24.06
benzotrifluoride	22.91	24.80	NA	25.13	25.80
fluorobenzene	26.84	27.74	24.33	25.93	26.05
hexafluorobenzene	22.07	26.68	24.16	29.09	22.28
perfluoromethylcyclopentane	12.45	NA	NA	17.61	NA
perfluoro-n-heptane	12.83	19.04	NA	14.43	16.29
perfluoro-n-hexane	11.28	17.93	NA	13.77	14.79
perfluoro-n-nonane	14.66	20.94	NA	15.40	19.02
perfluoro-n-octane	14.01	20.04	NA	14.99	17.68
perfluoro-n-pentane	9.38	16.64	NA	13.05	13.06

Table C.5. Liquid density at 298 K.

Compound	ρ - Lit. (g cc^{-1})	ρ - Pred. (g cc^{-1})			
		MG	CG	JR	W
Nonane	0.7171	0.7643	0.7265	0.7628	0.7334
Undecane	0.7377	0.7979	0.7504	0.7877	0.7663
Butane	0.5734	0.5452	0.6062	0.5782	0.5351
Tetradecane	0.7590	0.8263	0.7815	0.7991	0.8053
Tridecane	0.7507	0.8187	0.7713	0.7984	0.7931
Chloroethane	0.8895	0.7238	0.8496	0.7704	0.8785
Chloroform	1.4832	1.3664	N/A	1.3828	1.5224
1-Chloropropane	0.8849	0.7774	0.8757	0.8235	0.8877
Decane	0.7280	0.7832	0.7390	0.7772	0.7509
Nonadecane	0.7801	0.8525	0.8365	0.7464	0.8657
Acetylene	0.3782	N/A	N/A	0.4071	0.5356
1-Butene	0.5876	N/A	0.6008	0.5815	0.5564
cis-2-Butene	0.6175	0.5620	0.6046	0.5772	0.5915
trans-2-Butene	0.5996	0.5620	0.6046	0.5772	0.5915
1-Decene	0.7384	0.7781	0.7371	0.7849	0.7657
Ethylene	-	N/A	N/A	0.3782	0.5243
1-Heptene	0.6945	0.7015	0.6935	0.7254	0.7061
1-Hexene	0.6693	0.6599	0.6720	0.6908	0.6746
Methyl acetylene	0.6068	N/A	0.6022	0.5361	0.5145
Propylene	0.5058	N/A	0.5372	0.4958	0.4181
1-Butyne	0.6479	0.6100	0.6817	0.6294	0.6258
1-Decyne	0.7633	0.8515	0.8381	0.8306	0.7914
1-Heptyne	0.7289	0.7825	0.7916	0.7767	0.7425
3-Hexyne	0.7183	0.6405	N/A	0.7175	0.7200
1-Hexyne	0.7117	0.7408	0.7665	0.7428	0.7171
2-Hexyne	0.7269	0.6405	N/A	0.7175	0.7200
3-Methyl-1-butyne	0.6602	0.6617	0.7378	0.6887	0.6567
1-Nonyne	0.7540	0.8354	0.8257	0.8183	0.7779
1-Octyne	0.7427	0.8131	0.8107	0.8009	0.7620
2-Pentyne	0.7057	0.5917	N/A	0.6726	0.6854
Benzyl alcohol	1.0414	1.4184	1.2376	1.3610	1.1492
1-Butanol	0.8041	0.9043	0.9006	0.9869	0.9874
2-Butanol	0.8024	0.8699	0.9842	0.9693	0.9432
1-Decanol	0.8209	1.0015	1.0529	1.1851	0.9582
Ethanol	0.7860	0.7413	0.7566	0.7902	0.9464

Table C.5 Continued.

1-Heptanol	0.8211	0.9912	1.0007	1.1314	0.9321
2-Heptanol	0.8145	0.9648	1.0668	1.1080	0.9103
1-Hexanol	0.8160	0.9751	0.9757	1.0963	0.9230
2-Hexanol	0.8108	0.9458	1.0472	1.0743	0.8982
Methanol	0.7897	0.6004	N/A	0.6348	0.9076
Anisole	0.9907	1.0454	0.9309	0.9752	1.0324
Benzyl ethyl ether	0.9453	0.9666	0.9628	0.9902	0.9836
Dibutyl ether	0.7644	0.8424	0.8058	0.8503	0.8227
Diethyl ether	0.7082	0.7002	0.7387	0.7310	0.7218
Diphenyl ether	1.0680	1.0805	N/A	1.1530	1.1113
Ethylhexyl ether	0.7685	0.8424	0.8058	0.8503	0.8227
Ethylisopropyl ether	0.7166	0.7263	0.7693	0.7637	0.7379
Ethylpropyl ether	0.7242	0.7532	0.7630	0.7758	0.7615
Tetrahydrofuran	0.8802	0.8101	0.8907	0.8617	0.9145
Methylbutyl ether	0.7396	0.7857	0.7682	0.7758	0.7827
Benzene	0.8731	0.8222	0.8540	0.8256	0.8753
Propylbenzene	0.8588	0.8819	0.8560	0.8710	0.8711
p-Dichlorobenzene	1.2848	1.2093	N/A	1.2787	1.2980
Biphenyl	1.0219	N/A	1.0130	1.0355	N/A
m-Xylene	0.8603	0.8549	0.8614	0.8346	0.8713
Butylbenzene	0.8572	0.8906	0.8642	0.8806	0.8711
Chlorobenzene	1.1006	1.0363	N/A	1.0747	1.1146
Cumene	0.8592	0.8515	0.8535	0.8581	0.8560
m-Dichlorobenzene	1.2836	1.1855	N/A	1.2787	1.2951
Ethylbenzene	0.8637	0.8677	0.8450	0.8564	0.8722
Cyclobutane	0.6893	N/A	0.6969	0.6698	0.6762
Cyclohexane	0.7733	0.7709	0.7111	0.7760	0.7563
Cyclohexene	0.8064	0.8090	0.7136	0.7918	0.7873
Cyclopentane	0.7414	0.7109	0.7336	0.7338	0.7269
Cyclopentene	0.7667	0.7452	0.7342	0.7469	0.7633
Cyclopropane	0.6023	N/A	0.6072	0.5758	0.5489
Ethylcyclohexane	0.7846	0.7712	0.7381	0.7860	0.7800
Ethylcyclopentane	0.7628	0.7357	0.7734	0.7687	0.7624
Propenylcyclohexene	0.8402	0.8287	0.7585	0.8379	0.8373
1,1-Dimethylcyclohexane	0.7768	0.7832	0.7512	0.7993	0.7701
Propionaldehyde	0.7914	0.6798	0.7557	0.7332	0.8548
Acetaldehyde	0.7745	0.5905	0.6805	0.6386	0.8274
Butyraldehyde	0.7975	0.7452	0.8060	0.8011	0.8710
Decanal	0.8214	0.8867	0.9259	0.9549	0.9218

Table C.5 Continued.

Formaldehyde	0.7332	N/A	N/A	0.5674	0.6952
Heptanal	0.8141	0.8512	0.8865	0.9125	0.9000
Hexanal	0.8098	0.8270	0.8670	0.8862	0.8919
Nonanal	0.8229	0.8793	0.9148	0.9456	0.9146
Octanal	0.8182	0.8680	0.9020	0.9318	0.9074
Pentanal	0.8048	0.7928	0.8412	0.8503	0.8826
Acetone	0.7868	0.6507	0.7429	0.7019	0.8287
Benzophenone	1.1007	N/A	N/A	N/A	N/A
Cyclohexanone	0.9428	0.7893	0.8082	0.9047	1.0039
Ethylisopropyl ketone	0.8063	0.7919	0.7987	0.8363	0.8408
3-Heptanone	0.8143	0.8410	0.9178	0.8747	0.8663
2-Heptanone	0.8119	0.8216	1.0299	0.8747	0.8778
2-Hexanone	0.8070	0.1398	0.9271	0.8492	0.8692
3-Hexanone	0.8103	0.8151	0.7988	0.8492	0.8558
Methylethyl ketone	0.7997	0.7142	0.7464	0.7671	0.8459
Methylisobutyl ketone	0.7964	0.7752	0.8025	0.8363	0.8555
Butyl acetate	0.8761	0.9196	0.9722	0.9352	0.9728
Ethyl acetate	0.8938	0.8611	0.9489	0.8821	0.9746
Ethyl benzoate	1.0423	1.1320	N/A	1.1200	1.1499
Ethyl butyrate	0.8741	0.9279	1.0201	0.9352	0.9726
Ethyl formate	0.9158	0.8459	0.9178	0.9296	1.0180
Ethyl propionate	0.8835	0.9048	1.0299	0.9133	0.9733
Methyl acetate	0.9282	0.8117	0.9271	0.8378	0.9742
Methyl acrylate	0.9489	0.8681	N/A	0.8959	1.0187
Methyl benzoate	1.0840	1.1504	N/A	1.1241	1.1804
Propyl acetate	0.8824	0.8959	0.9628	0.9133	0.9735
Diethanol amine	1.0945	1.5702	N/A	N/A	1.9764
Diethyl amine	0.7030	0.7188	0.7406	0.7523	0.7347
Di-isopropyl amine	0.7132	0.8262	0.8530	0.8106	0.7455
Dipropyl amine	0.7374	0.8100	0.7947	0.8359	0.7899
Ethyl amine	0.6767	N/A	0.6727	0.6197	0.7144
Ethylenediamine	0.8935	0.9082	0.9283	0.9011	0.9896
Diethyl amine	0.7030	0.7188	0.7406	0.7523	0.7347
Isopropyl amine	0.6841	0.6516	N/A	0.7004	0.7093
Methyl amine	0.6554	N/A	N/A	0.4949	0.6250
Propyl amine	0.7141	0.5849	0.7442	0.7091	0.7580
Acetamide	1.0451	N/A	N/A	0.8879	N/A
Benzamide	1.1661	N/A	N/A	N/A	N/A
Formamide	1.1292	0.8200	N/A	0.8274	1.2372

Table C.5 Continued.

N-Methyl acetamide	0.9535	N/A	N/A	0.9233	1.0788
N,N-Dimethyl formamide	0.9446	0.7738	N/A	0.9402	1.0202
Acrylic acid	1.0456	N/A	1.0453	0.9702	N/A
Benzoic acid	1.1773	N/A	N/A	N/A	N/A
Acetic acid	1.0421	N/A	0.9414	0.8836	N/A
Butyric acid	0.9518	N/A	1.0425	1.0079	N/A
Decanoic acid	0.8973	N/A	1.1341	N/A	N/A
2-Ethyl butanoic acid	0.9195	0.9961	1.0545	1.0470	1.2011
2-Ethyl hexanoic acid	0.9021	1.0019	1.0856	N/A	1.1843
Formic acid	1.2139	1.0527	N/A	1.0952	1.7419
Heptanoic acid	0.9145	N/A	1.1080	N/A	N/A
Isobutyric acid	0.9442	0.9592	1.0034	0.9901	1.2464
dichlorodiethylsilane	1.0468	NA	NA	NA	1.1069
dimethyldichlorosilane	1.0650	NA	NA	NA	1.1591
dimethyldimethoxysilane	0.8574	NA	NA	NA	0.9434
ethyltrichlorosilane	1.2257	NA	NA	NA	1.3607
hexamethyldisiloxane	0.7597	NA	NA	NA	0.8740
methyl trichlorosilane	1.2665	NA	NA	NA	1.4336
methyl vinyl dichlorosilane	1.0770	NA	NA	NA	1.1788
trimethoxysilane	0.9506	NA	NA	NA	1.1075
vinyltrichlorosilane	1.2630	NA	NA	NA	1.4227
octamethyltrisiloxane	0.8147	NA	NA	NA	1.0209
benzotrifluoride	1.1812	0.9799	0.9805	1.2333	1.2508
fluorobenzene	1.0194	0.9547	1.0044	0.9727	1.0302
hexafluorobenzene	1.6065	1.5523	1.6267	1.6004	1.6325
perfluoromethylcyclopentane	1.7190	NA	NA	2.1331	NA
perfluoro-n-heptane	1.7273	2.0810	NA	2.0312	1.8703
perfluoro-n-hexane	1.6699	1.9784	NA	1.9865	1.7824
perfluoro-n-nonane	1.7936	2.2289	NA	2.0491	2.0384
perfluoro-n-octane	1.7665	2.1622	NA	2.0517	1.9540
perfluoro-n-pentane	1.6012	1.8441	NA	1.9140	1.6827

Table C.6. Liquid viscosity at 298 K.

Compound	η - Lit. (cP)	η - Pred. (cP)		
		MG	CG	JR
Nonane	0.6613	0.5700	0.6800	0.6800
Undecane	1.0897	0.8700	1.0471	1.0471
Butane	0.1581	0.2000	0.1717	0.1717
Tetradecane	2.0857	1.6400	1.8877	1.8877
Tridecane	1.6952	1.3300	1.5606	1.5606
Chloroethane	0.2560	0.3000	0.1997	0.1997
Chloroform	0.5395	0.7100	0.5900	0.5726
1-Chloropropane	0.3388	0.3700	0.2733	0.2733
Decane	0.8530	0.7000	0.8479	0.8479
Nonadecane	4.6522	4.7400	4.5856	3.9903
Acetylene	0.0816	N/A	N/A	N/A
1-Butene	0.1526	0.1600	0.1527	0.2245
cis-2-Butene	0.1732	0.1500	0.1404	0.1404
trans-2-Butene	0.1733	0.1500	0.1404	0.1404
1-Decene	0.7654	0.5700	0.7704	1.1323
Ethylene	0.0400	N/A	N/A	0.1420
1-Heptene	0.3369	0.3000	0.3797	0.5580
1-Hexene	0.2677	0.2400	0.2895	0.4255
Methyl acetylene	0.1429	0.1800	N/A	N/A
Propylene	0.0804	0.1400	0.1019	0.1498
1-Butyne	0.2033	0.2300	N/A	N/A
1-Decyne	1.2343	0.8100	N/A	N/A
1-Heptyne	0.5358	0.4300	N/A	N/A
3-Hexyne	0.3929	N/A	N/A	N/A
1-Hexyne	0.4784	0.3500	N/A	N/A
2-Hexyne	0.3987	N/A	N/A	N/A
3-Methyl-1-butyne	0.3453	0.2500	N/A	N/A
1-Nonyne	1.0061	0.6500	N/A	N/A
1-Octyne	0.6778	0.5300	N/A	N/A
2-Pentyne	0.2358	N/A	N/A	N/A
Benzyl alcohol	5.2335	5.1700	5.3191	5.3191
1-Butanol	2.5556	2.5000	2.0432	2.0432
2-Butanol	3.0875	1.7700	2.0288	2.0288
1-Decanol	11.3932	8.9400	8.8025	8.8025
Ethanol	1.0805	1.6300	1.0050	1.0050

Table C.6 Continued.

1-Heptanol	5.8391	4.7300	4.5497	4.5497
2-Heptanol	4.0096	3.3400	4.5176	4.5176
1-Hexanol	4.5445	3.8200	3.5589	3.5589
2-Hexanol	4.3026	2.7000	3.5338	3.5338
Methanol	0.5391	1.3200	0.6219	0.6219
Anisole	1.0254	0.9200	0.5837	0.5837
Benzyl ethyl ether	1.2511	1.2700	0.9288	0.9288
Dibutyl ether	0.6833	0.6800	0.6289	0.6289
Diethyl ether	0.2258	0.2900	0.2242	0.2242
Diphenyl ether	3.6873	6.2200	N/A	1.9972
Ethylhexyl ether	0.9177	0.6800	0.6289	0.6289
Ethylisopropyl ether	0.2535	0.3200	0.2976	0.2976
Ethylpropyl ether	0.3015	0.3600	0.2997	0.2997
Tetrahydrofuran	0.4566	0.8300	0.2164	0.5701
Methylbutyl ether	0.3054	0.3400	0.2997	0.2997
Benzene	0.6009	0.5800	0.3960	0.3960
Propylbenzene	0.8040	0.8500	0.8005	0.8005
p-Dichlorobenzene	1.0850	1.0200	1.1182	1.1182
Biphenyl	2.9086	5.9000	1.8327	1.8327
m-Xylene	0.5825	0.6200	0.5818	0.5818
Butylbenzene	0.9669	1.0500	1.0049	1.0049
Chlorobenzene	0.7567	0.7700	0.6990	0.6990
Cumene	0.7390	0.7200	0.7949	0.7949
m-Dichlorobenzene	1.0400	1.0100	1.1182	1.1182
Ethylbenzene	0.6365	0.6900	0.6290	0.6290
Cyclobutane	0.2080	0.7900	0.1644	0.2626
Cyclohexane	0.8956	0.7100	0.3117	0.6289
Cyclohexene	0.6183	0.6400	0.2578	0.5394
Cyclopentane	0.4155	0.7500	0.2311	0.4148
Cyclopentene	0.3319	0.6800	0.1901	0.3540
Cyclopropane	0.1256	0.8400	0.1097	0.1559
Ethylcyclohexane	0.7872	0.8000	0.5214	0.7832
Ethylcyclopentane	0.5358	0.8500	0.4059	0.5424
Propenylcyclohexene	0.5083	0.5900	N/A	0.8932
1,1-Dimethylcyclohexane	0.7765	0.4700	0.6901	N/A
Propionaldehyde	0.3179	0.4100	0.2931	0.2931
Acetaldehyde	0.2125	0.3300	0.1978	0.1978
Butyraldehyde	0.4199	0.5100	0.4090	0.4090
Decanal	1.5446	1.8200	1.7882	1.7882

Table C.6 Continued.

Formaldehyde	0.1423	N/A	N/A	0.2310
Heptanal	0.8634	0.9600	0.9199	0.9199
Hexanal	0.6636	0.7800	0.7179	0.7179
Nonanal	1.3589	1.4700	1.4480	1.4480
Octanal	1.1518	1.1900	1.1611	1.1611
Pentanal	0.5063	0.6300	0.5492	0.5492
Acetone	0.3073	0.3000	0.2998	0.2998
Benzophenone	19.1100	12.5500	N/A	N/A
Cyclohexanone	2.0211	1.3400	0.7139	N/A
Ethylisopropyl ketone	0.5436	0.4600	0.7292	0.7292
3-Heptanone	0.7448	0.6400	0.9411	0.9411
2-Heptanone	0.7522	0.7300	0.9411	0.9411
2-Hexanone	0.5846	0.5900	0.7344	0.7344
3-Hexanone	0.5790	0.5100	0.7344	0.7344
Methylethyl ketone	0.3952	0.3800	0.4184	0.4184
Methylisobutyl ketone	0.5447	0.5200	0.7292	0.7292
Butyl acetate	0.6782	0.6500	0.7446	0.7446
Ethyl acetate	0.4310	0.4300	0.4470	0.4470
Ethyl benzoate	1.9883	2.0000	1.7177	1.7177
Ethyl butyrate	0.6284	0.5500	0.7446	0.7446
Ethyl formate	0.3806	0.3900	N/A	0.3828
Ethyl propionate	0.5039	0.4400	0.5824	0.5824
Methyl acetate	0.3640	0.3500	0.3343	0.3343
Methyl acrylate	0.4603	N/A	0.4025	0.5916
Methyl benzoate	1.8589	1.6200	1.3854	1.3854
Propyl acetate	0.5551	0.5300	0.5824	0.5824
Diethanol amine	559.9072	251.0600	N/A	N/A
Diethyl amine	0.3221	0.4500	N/A	N/A
Di-isopropyl amine	0.3957	0.4000	N/A	N/A
Dipropyl amine	0.5158	0.6900	N/A	N/A
Ethyl amine	0.1943	0.4800	N/A	N/A
Ethylenediamine	1.7158	1.7000	N/A	N/A
Diethyl amine	0.3221	0.4500	N/A	N/A
Isopropyl amine	0.3256	0.3600	N/A	N/A
Methyl amine	0.1764	0.3900	N/A	N/A
Propyl amine	1.6339	0.5900	N/A	N/A
Acetamide	5.0182	N/A	N/A	N/A
Benzamide	25.2657	N/A	N/A	N/A
Formamide	3.3137	1.0000	N/A	N/A

Table C.6 Continued.

N-Methyl acetamide	4.3149	1.5900	N/A	N/A
N,N-Dimethyl formamide	0.8164	0.7900	N/A	N/A
Acrylic acid	1.0913	1.1600	0.9759	0.0714
Benzoic acid	12.7345	0.1800	N/A	N/A
Acetic acid	1.1179	1.1200	0.7851	0.0391
Butyric acid	1.4808	1.7200	1.4554	0.0725
Decanoic acid	8.0494	6.1400	5.0216	N/A
2-Ethyl butanoic acid	2.5980	2.3100	2.4074	0.1072
2-Ethyl hexanoic acid	5.7158	3.5300	3.7766	N/A
Formic acid	1.6151	N/A	N/A	1.7152
Heptanoic acid	3.8562	3.2500	3.0545	N/A
Isobutyric acid	1.2266	1.5300	1.4451	0.0720
dichlorodiethylsilane	0.6359	NA	NA	NA
dimethyldichlorosilane	0.4610	NA	NA	NA
dimethyldimethoxysilane	0.3590	NA	NA	NA
ethyltrichlorosilane	0.4360	NA	NA	NA
hexamethyldisiloxane	0.4816	NA	NA	NA
methyl trichlorosilane	0.4670	NA	NA	NA
methyl vinyl dichlorosilane	0.4930	NA	NA	NA
trimethoxysilane	0.3752	NA	NA	NA
vinyltrichlorosilane	0.4970	NA	NA	NA
octamethyltrisiloxane	0.8291	NA	NA	NA
benzotrifluoride	0.5408	0.5300	NA	NA
fluorobenzene	0.5592	0.5700	NA	NA
hexafluorobenzene	0.8766	0.4900	NA	NA
perfluoromethylcyclopentane	0.5041	NA	NA	NA
perfluoro-n-heptane	0.9171	0.1100	NA	NA
perfluoro-n-hexane	0.6624	0.1100	NA	NA
perfluoro-n-nonane	1.8025	0.1000	NA	NA
perfluoro-n-octane	1.4068	0.1000	NA	NA
perfluoro-n-pentane	0.4659	0.1100	NA	NA

Table C.7. Liquid thermal conductivity at 298 K.

Compound	*k* - Lit. (W m^{-1} K^{-1})	*k* - Lit. (W m^{-1} K^{-1})			
		MG	CG	JR	W
Nonane	0.1303	0.1309	0.1320	0.1272	0.1300
Undecane	0.1338	0.1272	0.1278	0.1251	0.1265
Butane	0.1069	0.1244	0.1285	0.1423	0.1206
Tetradecane	0.1380	0.1213	0.1218	0.1233	0.1220
Tridecane	0.1371	0.1232	0.1237	0.1238	0.1234
Chloroethane	0.1189	0.1309	0.1293	0.1316	0.1296
Chloroform	0.1175	0.1139	N/A	0.1109	0.1143
1-Chloropropane	0.1152	0.1322	0.1326	0.1280	0.1327
Decane	0.1318	0.1291	0.1299	0.1261	0.1282
Nonadecane	0.1467	0.1127	0.1136	0.1202	0.1172
Acetylene	0.0843	N/A	N/A	0.1483	0.1483
1-Butene	0.1172	0.1258	0.1252	0.1433	0.1205
cis-2-Butene	0.1082	0.1338	0.1346	0.1469	0.1326
trans-2-Butene	0.1071	0.1338	0.1346	0.1469	0.1326
1-Decene	0.1303	0.1289	0.1300	0.1257	0.1283
Ethylene	0.0613	N/A	N/A	0.1601	0.1616
1-Heptene	0.1247	0.1334	0.1355	0.1307	0.1335
1-Hexene	0.1206	0.1336	0.1360	0.1336	0.1341
Methyl acetylene	0.1124	0.1278	0.1409	0.1531	0.1103
Propylene	0.1017	0.1113	0.1019	0.1523	0.0825
1-Butyne	0.1186	0.1370	0.1483	0.1431	0.1352
1-Decyne	0.1380	0.1313	0.1340	0.1241	0.1298
1-Heptyne	0.1316	0.1378	0.1428	0.1294	0.1369
3-Hexyne	0.1297	0.1380	0.1460	0.1377	0.1396
1-Hexyne	0.1285	0.1392	0.1458	0.1325	0.1390
2-Hexyne	0.1313	0.1380	0.1460	0.1377	0.1396
3-Methyl-1-butyne	0.1109	0.1330	0.1406	0.1366	0.1328
1-Nonyne	0.1363	0.1336	0.1368	0.1254	0.1321
1-Octyne	0.1340	0.1358	0.1398	0.1271	0.1345
2-Pentyne	0.1277	0.1397	0.1493	0.1434	0.1406
Benzyl alcohol	0.1588	0.1504	0.1477	0.1494	0.1442
1-Butanol	0.1530	0.1583	0.1633	0.1603	0.1593
2-Butanol	0.1363	0.1502	0.1551	0.1596	0.1524
1-Decanol	0.1615	0.1335	0.1357	0.1384	0.1325
Ethanol	0.1681	0.1719	0.1797	0.1829	0.1729

Table C.7 Continued.

1-Heptanol	0.1566	0.1440	0.1469	0.1456	0.1418
2-Heptanol	0.1375	0.1399	0.1432	0.1448	0.1392
1-Hexanol	0.1537	0.1482	0.1516	0.1492	0.1460
2-Hexanol	0.1363	0.1432	0.1470	0.1484	0.1426
Methanol	0.2000	0.1814	N/A	0.2061	0.1782
Anisole	0.1560	0.1383	0.1373	0.1333	0.1363
Benzyl ethyl ether	0.1366	0.1287	0.1280	0.1279	0.1280
Dibutyl ether	0.1279	0.1294	0.1298	0.1260	0.1284
Diethyl ether	0.1282	0.1273	0.1295	0.1350	0.1272
Diphenyl ether	0.1423	0.1224	N/A	0.1232	0.1212
Ethylhexyl ether	0.1217	0.1294	0.1298	0.1260	0.1284
Ethylisopropyl ether	0.1222	0.1252	0.1260	0.1313	0.1258
Ethylpropyl ether	0.1289	0.1306	0.1323	0.1317	0.1307
Tetrahydrofuran	0.1201	0.1394	0.1487	0.1438	0.1402
Methylbutyl ether	0.1316	0.1352	0.1402	0.1317	0.1349
Benzene	0.1433	0.1429	0.1413	0.1433	0.1433
Propylbenzene	0.1279	0.1338	0.1325	0.1316	0.1325
p-Dichlorobenzene	0.1162	0.1191	0.1191	0.1184	0.1183
Biphenyl	0.1454	N/A	0.1255	0.1262	N/A
m-Xylene	0.1303	0.1363	0.1364	0.1357	0.1357
Butylbenzene	0.1274	0.1309	0.1299	0.1291	0.1296
Chlorobenzene	0.1270	0.1285	0.1285	0.1279	0.1284
Cumene	0.1232	0.1297	0.1311	0.1309	0.1304
m-Dichlorobenzene	0.1173	0.1187	0.1191	0.1184	0.1180
Ethylbenzene	0.1289	0.1369	0.1353	0.1347	0.1359
Cyclobutane	0.1211	0.1351	0.1427	0.1517	0.1327
Cyclohexane	0.1235	0.1378	0.1384	0.1393	0.1386
Cyclohexene	0.1317	0.1389	0.1398	0.1406	0.1393
Cyclopentane	0.1263	0.1382	0.1406	0.1447	0.1387
Cyclopentene	0.1350	0.1394	0.1425	0.1464	0.1397
Cyclopropane	0.1166	0.1216	0.1315	0.1616	0.0984
Ethylcyclohexane	0.1166	0.1317	0.1304	0.1304	0.1324
Ethylcyclopentane	0.1169	0.1334	0.1333	0.1334	0.1340
Propenylcyclohexene	0.1227	0.1307	0.1329	0.1309	0.1309
1,1-Dimethylcyclohexane	0.1158	0.1304	0.1287	0.1295	0.1307
Propionaldehyde	0.1602	0.1519	0.1525	0.1536	0.1525
Acetaldehyde	0.1811	0.1551	0.1530	0.1651	0.1527
Butyraldehyde	0.1451	0.1484	0.1496	0.1461	0.1491
Decanal	0.1442	0.1298	0.1307	0.1290	0.1297

Table C.7 Continued.

Formaldehyde	0.1796	N/A	N/A	0.1158	0.1161
Heptanal	0.1375	0.1383	0.1394	0.1343	0.1378
Hexanal	0.1367	0.1416	0.1422	0.1366	0.1413
Nonanal	0.1403	0.1324	0.1334	0.1304	0.1320
Octanal	0.1385	0.1353	0.1363	0.1321	0.1348
Pentanal	0.1384	0.1449	0.1462	0.1409	0.1451
Acetone	0.1606	0.1490	0.1486	0.1555	0.1493
Benzophenone	0.1916	N/A	N/A	N/A	N/A
Cyclohexanone	0.1386	0.1381	0.1474	0.1424	0.1435
Ethylisopropyl ketone	0.1419	0.1342	0.1412	0.1373	0.1351
3-Heptanone	0.1360	0.1353	0.1412	0.1349	0.1348
2-Heptanone	0.1375	0.1368	0.1377	0.1349	0.1364
2-Hexanone	0.1392	0.1398	0.1408	0.1379	0.1396
3-Hexanone	0.1482	0.1377	0.1447	0.1379	0.1375
Methylethyl ketone	0.1451	0.1458	0.1469	0.1475	0.1465
Methylisobutyl ketone	0.1440	0.1366	0.1373	0.1373	0.1375
Butyl acetate	0.1381	0.1317	0.1321	0.1296	0.1308
Ethyl acetate	0.1439	0.1334	0.1342	0.1351	0.1335
Ethyl benzoate	0.1443	0.1276	0.1266	0.1270	0.1260
Ethyl butyrate	0.1362	0.1315	0.1518	0.1296	0.1308
Ethyl formate	0.1604	0.1359	0.1392	0.1439	0.1365
Ethyl propionate	0.1388	0.1328	0.1587	0.1320	0.1325
Methyl acetate	0.1534	0.1323	0.1330	0.1394	0.1325
Methyl acrylate	0.1563	0.1322	0.1332	0.1353	0.1330
Methyl benzoate	0.1536	0.1304	0.1292	0.1289	0.1286
Propyl acetate	0.1409	0.1329	0.1336	0.1320	0.1325
Diethanol amine	0.2089	0.1638	N/A	N/A	0.1655
Diethyl amine	0.1341	0.1403	0.1456	0.1458	0.1400
Di-isopropyl amine	0.1132	0.1282	0.1268	0.1359	0.1289
Dipropyl amine	0.1288	0.1387	0.1405	0.1372	0.1369
Ethyl amine	0.1861	0.1617	0.1598	0.1744	0.1602
Ethylenediamine	0.2322	0.1712	0.1744	0.1745	0.1719
Diethyl amine	0.1341	0.1403	0.1456	0.1458	0.1400
Isopropyl amine	0.1381	0.1437	0.1436	0.1605	0.1437
Methyl amine	0.2049	0.1635	N/A	0.1974	0.1520
Propyl amine	0.1723	0.1539	0.1559	0.1610	0.1564
Acetamide	0.2627	N/A	N/A	0.1704	N/A
Benzamide	0.2097	N/A	N/A	N/A	N/A
Formamide	0.3530	0.1816	N/A	0.1847	0.1823

Table C.7 Continued.

N-Methyl acetamide	0.1670	0.1498	N/A	0.1547	0.1593
N,N-Dimethyl formamide	0.1840	0.1461	N/A	0.1415	0.1477
Acrylic acid	0.1576	N/A	0.1674	0.1652	N/A
Benzoic acid	0.1698	N/A	N/A	N/A	N/A
Acetic acid	0.1609	N/A	0.1749	0.1753	N/A
Butyric acid	0.1466	N/A	0.1578	0.1568	N/A
Decanoic acid	0.1464	N/A	0.1307	N/A	N/A
2-Ethyl butanoic acid	0.1458	0.1453	0.1452	0.1447	0.1448
2-Ethyl hexanoic acid	0.1432	0.1373	0.1374	N/A	0.1375
Formic acid	0.2698	0.1905	N/A	0.1933	0.1925
Heptanoic acid	0.1424	N/A	0.1421	N/A	N/A
Isobutyric acid	0.1405	0.1558	0.1548	0.1560	0.1552
dichlorodiethylsilane	0.1359	NA	NA	NA	0.1132
dimethyldichlorosilane	0.1317	NA	NA	NA	0.1123
dimethyldimethoxysilane	0.1133	NA	NA	NA	0.1167
ethyltrichlorosilane	0.1312	NA	NA	NA	0.1091
hexamethyldisiloxane	0.1288	NA	NA	NA	0.1113
methyl trichlorosilane	0.1443	NA	NA	NA	0.1089
methyl vinyl dichlorosilane	0.1000	NA	NA	NA	0.1135
trimethoxysilane	0.1419	NA	NA	NA	0.1164
vinyltrichlorosilane	0.1315	NA	NA	NA	0.1093
octamethyltrisiloxane	0.1303	NA	NA	NA	0.1069
benzotrifluoride	0.1065	0.1096	0.1135	0.1109	0.1115
fluorobenzene	0.1261	0.1289	0.1280	0.1311	0.1293
hexafluorobenzene	0.0883	0.0930	0.0949	0.1017	0.0927
perfluoromethylcyclopentane	0.0590	NA	0.0727	0.0699	NA
perfluoro-n-heptane	0.0597	0.0687	0.0681	0.0630	0.0692
perfluoro-n-hexane	0.0623	0.0685	0.0679	0.0628	0.0685
perfluoro-n-nonane	0.0575	0.0678	0.0673	0.0636	0.0697
perfluoro-n-octane	0.0609	0.0684	0.0678	0.0633	0.0695
perfluoro-n-pentane	0.0605	0.0672	0.0668	0.0628	0.0671

Table C.8. Liquid specific heat at 298 K.

Compound	C_p - Lit. (J mol^{-1} K^{-1})	C_p - Pred. (J mol^{-1} K^{-1})
		JR
Nonane	284.09	286.32
Undecane	345.80	347.13
Butane	140.45	142.33
Tetradecane	438.30	439.47
Tridecane	407.98	408.69
Chloroethane	106.30	106.21
Chloroform	113.65	113.29
1-Chloropropane	131.75	133.46
Decane	314.99	316.58
Nonadecane	587.86	592.91
Acetylene	118.97	84.41
1-Butene	128.26	129.60
cis-2-Butene	127.40	124.53
trans-2-Butene	127.86	124.53
1-Decene	299.74	303.12
Ethylene	187.01	84.32
1-Heptene	211.76	213.83
1-Hexene	182.94	185.08
Methyl acetylene	106.46	96.35
Propylene	108.55	103.17
1-Butyne	137.54	122.49
1-Decyne	306.35	294.58
1-Heptyne	217.77	205.88
3-Hexyne	167.25	169.62
1-Hexyne	190.15	177.39
2-Hexyne	170.60	169.62
3-Methyl-1-butyne	162.15	146.36
1-Nonyne	276.57	264.54
1-Octyne	245.32	234.95
2-Pentyne	142.18	141.48
Benzyl alcohol	216.94	237.28
1-Butanol	177.77	208.02
2-Butanol	196.52	203.75
1-Decanol	370.71	400.37
Ethanol	112.28	146.74

Table C.8 Continued.

1-Heptanol	278.83	303.39
2-Heptanol	279.46	298.79
1-Hexanol	242.02	271.27
2-Hexanol	257.43	266.75
Methanol	81.14	117.09
Anisole	199.75	182.24
Benzyl ethyl ether	230.54	243.15
Dibutyl ether	278.03	281.67
Diethyl ether	175.58	164.48
Diphenyl ether	267.57	268.14
Ethylhexyl ether	282.59	281.67
Ethylisopropyl ether	193.31	189.42
Ethylpropyl ether	197.20	192.91
Tetrahydrofuran	123.94	127.80
Methylbutyl ether	192.77	334.69
Benzene	136.46	126.39
Propylbenzene	214.20	216.91
p-Dichlorobenzene	169.34	174.36
Biphenyl	249.70	238.94
m-Xylene	182.62	188.96
Butylbenzene	243.06	247.43
Chlorobenzene	150.11	149.68
Cumene	209.18	212.80
m-Dichlorobenzene	170.68	174.36
Ethylbenzene	183.16	186.87
Cyclobutane	109.57	109.04
Cyclohexane	154.79	149.77
Cyclohexene	148.36	141.97
Cyclopentane	127.18	129.17
Cyclopentene	122.67	121.38
Cyclopropane	89.29	89.60
Ethylcyclohexane	211.53	206.98
Ethylcyclopentane	186.06	185.63
Propenylcyclohexene	218.56	214.25
1,1-Dimethylcyclohexane	209.18	199.90
Propionaldehyde	133.79	133.84
Acetaldehyde	112.61	105.81
Butyraldehyde	163.65	162.60
Decanal	325.28	345.98

Table C.8 Continued.

Formaldehyde	70.33	96.98
Heptanal	248.81	252.42
Hexanal	215.90	221.96
Nonanal	295.14	314.51
Octanal	268.81	283.29
Pentanal	188.87	192.00
Acetone	126.28	127.20
Benzophenone	291.57	N/A
Cyclohexanone	185.19	170.32
Ethylisopropyl ketone	209.77	211.25
3-Heptanone	245.70	245.58
2-Heptanone	242.10	245.58
2-Hexanone	213.14	215.19
3-Hexanone	216.59	215.19
Methylethyl ketone	158.63	155.93
Methylisobutyl ketone	213.82	211.25
Butyl acetate	226.44	233.57
Ethyl acetate	170.76	174.03
Ethyl benzoate	234.94	257.41
Ethyl butyrate	226.97	233.57
Ethyl formate	146.63	157.80
Ethyl propionate	195.56	203.53
Methyl acetate	141.99	145.13
Methyl acrylate	161.74	160.85
Methyl benzoate	209.00	225.91
Propyl acetate	197.86	203.53
Diethanol amine	269.43	N/A
Diethyl amine	173.80	175.64
Di-isopropyl amine	226.29	227.17
Dipropyl amine	216.67	234.96
Ethyl amine	133.32	125.04
Ethylenediamine	172.58	170.86
Diethyl amine	173.80	175.64
Isopropyl amine	163.79	150.09
Methyl amine	103.68	97.08
Propyl amine	162.77	153.72
Acetamide	140.65	142.55
Benzamide	239.12	N/A
Formamide	108.28	119.77

Table C.8 Continued.

N-Methyl acetamide	135.13	164.28
N,N-Dimethyl formamide	150.41	157.69
Acrylic acid	144.70	161.94
Benzoic acid	187.36	N/A
Acetic acid	123.83	144.75
Butyric acid	177.70	207.01
Decanoic acid	350.20	N/A
2-Ethyl butanoic acid	236.06	267.38
2-Ethyl hexanoic acid	295.52	N/A
Formic acid	99.38	146.23
Heptanoic acid	266.15	N/A
Isobutyric acid	181.65	202.42
Chloroethane	106.30	106.21
Chloroform	113.65	113.29
1-Chloropropane	131.75	133.46
p-Dichlorobenzene	169.34	174.36
m-Dichlorobenzene	170.68	174.36
dichlorodiethylsilane	215.53	NA
dimethyldichlorosilane	168.00	NA
dimethyldimethoxysilane	218.16	NA
ethyltrichlorosilane	172.04	NA
hexamethyldisiloxane	311.26	NA
methyl trichlorosilane	163.11	NA
methyl vinyl dichlorosilane	173.17	NA
trimethoxysilane	204.95	NA
vinyltrichlorosilane	174.78	NA
octamethyltrisiloxane	355.61	NA
benzotrifluoride	188.75	189.64
fluorobenzene	147.21	142.67
hexafluorobenzene	221.35	226.11
perfluoromethylcyclopentane	211.97	278.57
perfluoro-n-heptane	417.41	377.14
perfluoro-n-hexane	380.54	332.16
perfluoro-n-nonane	500.35	466.58
perfluoro-n-octane	454.58	422.05
perfluoro-n-pentane	347.70	287.47

APPENDIX D

DATA USED FOR DEVELOPMENT OF GC METHODS FOR ORGANOSILICON COMPOUNDS

Table D.1. Melting point data for organosilicon compounds.

Compounds	T_m - Lit. (K)	T_m - Pred. (K)	Absolute deviation (%)
dichlorodiethylsilane	174.10	173.28	0.47
dimethyldichlorosilane	197.05	161.36	18.11
dimethyldimethoxysilane	193.00	223.42	15.76
ethyltrichlorosilane	167.50	168.06	0.33
hexamethyldisiloxane	204.93	177.11	13.58
methyl trichlorosilane	195.35	155.69	20.30
methyl vinyl dichlorosilane	178.15	183.23	2.85
trimethoxysilane	159.60	240.87	50.92
vinyltrichlorosilane	178.35	178.35	0.00
octamethyltrisiloxane	187.15	181.97	2.77
[3-(mercapto)propyl]triethoxysilane	210.00	305.49	45.47
(3-methylacryloxypropyl)trichlorosilane	220.00	258.60	17.55
3-(triethoxysilyl)propionitrile	204.55	322.58	57.70
3-(trimethoxysilyl)-1-propanethiol	200.00	246.44	23.22
γ-aminopropyltriethoxysilane	140.00	322.57	130.41
bis[3-(trimethoxysilyl)propyl]disulfide	250.00	367.22	46.89
bis[3-(triethoxysilyl)propyl]disulfide	270.00	381.49	41.29
decamethylcyclopentasiloxane	235.15	235.79	0.27
decamethyltetrasiloxane	205.15	186.67	9.01
dimethylchlorosilane	162.15	162.12	0.02
diphenyldichlorosilane	251.15	317.77	26.52
dodecamethylcyclohexasiloxane	270.15	262.67	2.77
dodecamethylpentasiloxane	192.00	191.23	0.40
eicosamethylnonasiloxane	202.15	208.17	2.98
hexacosamethyldodecasiloxane	206.00	219.71	6.65
hexadecamethylcyclooctasiloxane	304.70	305.09	0.13
hexadecamethylheptasiloxane	195.15	199.94	2.46
methyl dichlorosilane	182.55	156.48	14.28
methyl silicate	273.85	261.43	4.53

Table D.1 Continued.

octadecamethyloctasiloxane	210.15	204.11	2.87
octamethylcyclotetrasiloxane	290.80	202.89	30.23
phenylmethyldichlorosilane	229.65	259.40	12.95
phenyltrichlorosilane	233.20	256.51	9.99
tetrachlorosilane	204.30	149.79	26.68
tetradecamethylhexasiloxane	214.15	195.65	8.64
tetraethoxysilane	190.97	280.59	46.93
tetraethyl silane	190.65	212.25	11.33
tetramethylsilane	174.07	172.09	1.14
trichlorosilane	144.95	150.61	3.91
trimethyl silanol	282.65	246.07	12.94
trimethylchlorosilane	215.45	166.82	22.57
tris(2-methoxyethoxy)vinylsilane	143.15	325.15	127.14
vinyltrimethoxysilane	176.15	256.56	45.65

Table D.2. Normal boiling point data for organosilicon compounds.

Compounds	T_b - Lit. (K)	T_b - Pred. (K)	Absolute deviation (%)
dichlorodiethylsilane	403.15	361.00	10.46
dimethyldichlorosilane	343.55	327.17	4.77
dimethyldimethoxysilane	354.55	387.11	9.18
ethyltrichlorosilane	371.05	371.67	0.17
hexamethyldisiloxane	373.67	370.49	0.85
methyl trichlorosilane	339.55	339.55	0.00
methyl vinyl dichlorosilane	366.95	360.84	1.67
trimethoxysilane	357.50	412.36	15.35
vinyltrichlorosilane	363.85	371.52	2.11
octamethyltrisiloxane	425.70	423.87	0.43
[3-(mercapto)propyl]triethoxysilane	498.80	546.20	9.50
(3-methylacryloxypropyl)trichlorosilane	523.80	520.60	0.61
3-(triethoxysilyl)propionitrile	512.06	544.28	6.29
3-(trimethoxysilyl)-1-propanethiol	487.15	452.18	7.18
γ-aminopropyltriethoxysilane	493.05	538.44	9.21
bis[3-(trimethoxysilyl)propyl]disulfide	599.50	663.25	10.63
bis[3-(triethoxysilyl)propyl]disulfide	731.40	689.78	5.69
decamethylcyclopentasiloxane	484.10	482.84	0.26
decamethyltetrasiloxane	467.50	466.89	0.13
dimethylchlorosilane	308.65	300.81	2.54
diphenyldichlorosilane	577.25	565.43	2.05
dodecamethylcyclohexasiloxane	518.15	523.41	1.02
dodecamethylpentasiloxane	503.10	502.93	0.03
eicosamethylnonasiloxane	609.50	607.24	0.37
hexacosamethyldodecasiloxane	654.00	662.29	1.27
hexadecamethylcyclooctasiloxane	576.50	587.43	1.90
hexadecamethylheptasiloxane	559.94	561.14	0.21
methyl dichlorosilane	314.70	314.70	0.00
methyl silicate	393.27	449.49	14.30
octadecamethyloctasiloxane	583.60	585.38	0.31
octamethylcyclotetrasiloxane	448.15	433.18	3.34
phenylmethyldichlorosilane	477.35	476.77	0.12
phenyltrichlorosilane	474.95	483.18	1.73
tetrachlorosilane	330.00	351.28	6.45
tetradecamethylhexasiloxane	532.90	533.93	0.19
tetraethoxysilane	440.90	493.85	12.01

Table D.2 Continued.

tetraethyl silane	426.56	423.58	0.70
tetramethylsilane	299.80	300.12	0.11
trichlorosilane	305.00	327.77	7.47
trimethyl silanol	372.15	382.19	2.70
trimethylchlorosilane	330.75	314.06	5.05
tris(2-methoxyethoxy)vinylsilane	550.25	578.86	5.20
vinyltrimethoxysilane	397.40	443.18	11.52

Table D.3. Critical temperature data for organosilicon compounds.

Compounds	T_c - Lit. (K)	T_c - Pred. (K)	Absolute deviation (%)
dichlorodiethylsilane	595.75	535.20	10.16
dimethyldichlorosilane	520.35	502.55	3.42
dimethyldimethoxysilane	524.00	555.14	5.94
ethyltrichlorosilane	559.95	547.80	2.17
hexamethyldisiloxane	518.70	518.70	0.00
methyl trichlorosilane	517.00	517.00	0.00
methyl vinyl dichlorosilane	544.10	538.52	1.03
trimethoxysilane	525.00	574.75	9.48
vinyltrichlorosilane	543.15	550.94	1.43
octamethyltrisiloxane	564.40	558.49	1.05
[3-(mercapto)propyl]triethoxysilane	647.50	730.64	12.84
(3-methylacryloxypropyl)trichlorosilane	708.10	701.27	0.96
3-(triethoxysilyl)propionitrile	672.10	734.62	9.30
3-(trimethoxysilyl)-1-propanethiol	657.60	645.40	1.85
γ-aminopropyltriethoxysilane	634.60	734.97	15.82
bis[3-(trimethoxysilyl)propyl]disulfide	736.20	854.41	16.06
bis[3-(triethoxysilyl)propyl]disulfide	900.30	878.40	2.43
decamethylcyclopentasiloxane	619.15	619.15	0.00
decamethyltetrasiloxane	599.40	592.43	1.16
dimethylchlorosilane	472.00	466.17	1.23
diphenyldichlorosilane	814.00	784.09	3.67
dodecamethylcyclohexasiloxane	645.80	661.31	2.40
dodecamethylpentasiloxane	628.40	622.02	1.02
eicosamethylnonasiloxane	703.50	712.74	1.31
hexacosamethyldodecasiloxane	735.00	763.11	3.83
hexadecamethylcyclooctasiloxane	689.20	727.83	5.61
hexadecamethylheptasiloxane	671.80	671.80	0.00
methyl dichlorosilane	483.00	483.00	0.00
methyl silicate	562.80	616.90	9.61
octadecamethyloctasiloxane	688.90	693.18	0.62
octamethylcyclotetrasiloxane	586.50	567.55	3.23
phenylmethyldichlorosilane	689.00	683.76	0.76
phenyltrichlorosilane	688.00	690.47	0.36
tetrachlorosilane	507.00	530.60	4.66
tetradecamethylhexasiloxane	653.20	648.25	0.76
tetraethoxysilane	592.20	659.73	11.40

Table D.3 Continued.

tetraethyl silane	606.00	592.84	2.17
tetramethylsilane	450.40	470.61	4.49
trichlorosilane	479.00	498.69	4.11
trimethyl silanol	526.50	557.03	5.80
trimethylchlorosilane	497.75	487.13	2.13
tris(2-methoxyethoxy)vinylsilane	723.90	748.56	3.41
vinyltrimethoxysilane	553.70	613.51	10.80

Table D.4. Critical pressure data for organosilicon compounds.

Compounds	P_c - Lit. (bar)	P_c - Pred. (K)	Absolute deviation (%)
dichlorodiethylsilane	30.60	30.02	1.89
dimethyldichlorosilane	34.90	33.56	3.83
dimethyldimethoxysilane	26.60	29.32	10.22
ethyltrichlorosilane	33.30	31.72	4.76
hexamethyldisiloxane	19.14	17.09	10.73
methyl trichlorosilane	35.30	35.65	1.00
methyl vinyl dichlorosilane	29.40	31.61	7.51
trimethoxysilane	28.90	33.05	14.35
vinyltrichlorosilane	30.60	33.48	9.40
octamethyltrisiloxane	14.40	12.35	14.20
[3-(mercapto)propyl]triethoxysilane	18.63	18.41	1.20
(3-methylacryloxypropyl)trichlorosilane	21.13	20.91	1.03
3-(triethoxysilyl)propionitrile	17.61	19.82	12.54
3-(trimethoxysilyl)-1-propanethiol	23.33	24.91	6.78
γ-aminopropyltriethoxysilane	19.11	18.94	0.90
bis[3-(trimethoxysilyl)propyl]disulfide	13.09	13.90	6.18
bis[3-(triethoxysilyl)propyl]disulfide	10.22	10.83	5.94
decamethylcyclopentasiloxane	11.60	11.29	2.70
decamethyltetrasiloxane	12.27	10.11	17.60
dimethylchlorosilane	36.20	36.51	0.86
diphenyldichlorosilane	23.30	23.30	0.00
dodecamethylcyclohexasiloxane	9.61	9.99	4.00
dodecamethylpentasiloxane	9.45	8.87	6.11
eicosamethylnonasiloxane	5.41	7.04	30.23
hexacosamethyldodecasiloxane	4.22	6.61	56.83
hexadecamethylcyclooctasiloxane	6.91	8.51	23.12
hexadecamethylheptasiloxane	6.77	7.63	12.63
methyl dichlorosilane	39.50	38.95	1.38
methyl silicate	28.73	28.67	0.21
octadecamethyloctasiloxane	6.24	7.28	16.74
octamethylcyclotetrasiloxane	13.32	13.32	0.00
phenylmethyldichlorosilane	28.70	27.54	4.03
phenyltrichlorosilane	29.60	28.98	2.10
tetrachlorosilane	35.90	37.99	5.82
tetradecamethylhexasiloxane	8.04	8.12	0.97
tetraethoxysilane	20.45	19.12	6.50

Table D.4 Continued.

tetraethyl silane	24.00	20.98	12.60
tetramethylsilane	28.14	29.99	6.59
trichlorosilane	41.70	41.70	0.00
trimethyl silanol	38.09	36.83	3.31
trimethylchlorosilane	32.00	31.69	0.98
tris(2-methoxyethoxy)vinylsilane	17.79	16.38	7.92
vinyltrimethoxysilane	26.85	27.49	2.40

Table D.5. Critical volume data for organosilicon compounds.

Compounds	V_c - Lit. (cc mol^{-1})	V_c - Pred. (cc mol^{-1})	Absolute deviation (%)
dichlorodiethylsilane	455.63	405.77	10.94
dimethyldichlorosilane	358.00	349.49	2.38
dimethyldimethoxysilane	441.00	409.19	7.21
ethyltrichlorosilane	414.00	395.78	4.40
hexamethyldisiloxane	601.00	648.31	7.87
methyl trichlorosilane	340.00	339.50	0.15
methyl vinyl dichlorosilane	409.00	392.57	4.02
trimethoxysilane	408.00	368.55	9.67
vinyltrichlorosilane	408.00	382.58	6.23
octamethyltrisiloxane	868.00	927.12	6.81
[3-(mercapto)propyl]triethoxysilane	736.00	741.47	0.74
(3-methylacryloxypropyl)trichlorosilane	664.00	676.35	1.86
3-(triethoxysilyl)propionitrile	743.00	730.70	1.66
3-(trimethoxysilyl)-1-propanethiol	578.00	519.38	10.14
γ-aminopropyltriethoxysilane	799.00	753.41	5.71
bis[3-(trimethoxysilyl)propyl]disulfide	1110.00	1151.76	3.76
bis[3-(triethoxysilyl)propyl]disulfide	1500.00	1476.84	1.54
decamethylcyclopentasiloxane	1216.00	1216.03	0.00
decamethyltetrasiloxane	1157.00	1205.93	4.23
dimethylchlorosilane	299.00	299.00	0.00
diphenyldichlorosilane	674.00	721.47	7.04
dodecamethylcyclohexasiloxane	1610.00	1457.64	9.46
dodecamethylpentasiloxane	1509.00	1484.75	1.61
eicosamethylnonasiloxane	2600.00	2600.00	0.00
hexacosamethyldodecasiloxane	3390.00	3436.44	1.37
hexadecamethylcyclooctasiloxane	2260.00	1940.88	14.12
hexadecamethylheptasiloxane	2133.00	2042.37	4.25
methyl dichlorosilane	289.00	289.00	0.00
methyl silicate	445.00	448.89	0.87
octadecamethyloctasiloxane	2466.00	2321.19	5.87
octamethylcyclotetrasiloxane	970.00	974.41	0.45
phenylmethyldichlorosilane	508.00	535.48	5.41
phenyltrichlorosilane	499.00	525.49	5.31
tetrachlorosilane	326.00	329.50	1.07
tetradecamethylhexasiloxane	1808.00	1763.56	2.46
tetraethoxysilane	645.00	665.61	3.20

Table D.5 Continued.

tetraethyl silane	587.00	594.61	1.30
tetramethylsilane	357.00	369.49	3.50
trichlorosilane	268.00	279.00	4.10
trimethyl silanol	326.00	331.75	1.76
trimethylchlorosilane	366.00	359.49	1.78
tris(2-methoxyethoxy)vinylsilane	870.00	863.05	0.80
vinyltrimethoxysilane	439.00	472.12	7.55

Table D.6. Data for acentric factor of organosilicon compounds.

Compounds	ω - Lit.	ω - Pred.	Absolute deviation (%)
dichlorodiethylsilane	0.3189	0.2908	8.81
dimethyldichlorosilane	0.2675	0.2479	7.33
dimethyldimethoxysilane	0.2629	0.3823	45.40
ethyltrichlorosilane	0.2691	0.2917	8.37
hexamethyldisiloxane	0.4152	0.3553	14.41
methyl trichlorosilane	0.2634	0.2487	5.59
methyl vinyl dichlorosilane	0.2928	0.2807	4.14
trimethoxysilane	0.3224	0.4036	25.20
vinyltrichlorosilane	0.2815	0.2815	0.01
octamethyltrisiloxane	0.5328	0.4654	12.65
[3-(mercapto)propyl]triethoxysilane	0.8370	0.6361	24.00
(3-methylacryloxypropyl)trichlorosilane	0.6267	0.6239	0.45
3-(triethoxysilyl)propionitrile	0.7179	0.6361	11.39
3-(trimethoxysilyl)-1-propanethiol	0.6472	0.2456	62.06
γ-aminopropyltriethoxysilane	0.8895	0.8605	3.26
bis[3-(trimethoxysilyl)propyl]disulfide	1.1551	1.1551	0.00
bis[3-(triethoxysilyl)propyl]disulfide	0.8888	1.4569	63.92
decamethylcyclopentasiloxane	0.6658	0.6164	7.42
decamethyltetrasiloxane	0.6726	0.5744	14.60
dimethylchlorosilane	0.2526	0.2015	20.22
diphenyldichlorosilane	0.4283	0.6109	42.64
dodecamethylcyclohexasiloxane	0.7462	0.7462	0.00
dodecamethylpentasiloxane	0.7257	0.6813	6.12
eicosamethylnonasiloxane	1.0916	1.0818	0.90
hexacosamethyldodecasiloxane	1.2990	1.3536	4.20
hexadecamethylcyclooctasiloxane	0.8829	0.9933	12.51
hexadecamethylheptasiloxane	0.8871	0.8872	0.01
methyl dichlorosilane	0.2758	0.2023	26.64
methyl silicate	0.4442	0.5190	16.84
octadecamethyloctasiloxane	0.9839	0.9859	0.21
octamethylcyclotetrasiloxane	0.5890	0.4832	17.97
phenylmethyldichlorosilane	0.4022	0.4299	6.88
phenyltrichlorosilane	0.3956	0.4307	8.87
tetrachlorosilane	0.2318	0.2495	7.64
tetradecamethylhexasiloxane	0.7850	0.7857	0.08
tetraethoxysilane	0.6325	0.7623	20.52

Table D.6 Continued.

tetraethyl silane	0.4002	0.4200	4.94
tetramethylsilane	0.2240	0.2462	9.93
trichlorosilane	0.2031	0.2031	0.00
trimethyl silanol	0.6341	0.6085	4.04
trimethylchlorosilane	0.2701	0.2470	8.54
tris(2-methoxyethoxy)vinylsilane	0.7150	0.9803	37.10
vinyltrimethoxysilane	0.5514	0.4841	12.19

Table D.7. Surface tension data at 298 K for organosilicon compounds.

Compounds	σ - Lit. (dynes cm^{-1})	σ - Pred. (dynes cm^{-1})	Absolute deviation (%)
dichlorodiethylsilane	13.63	18.75	37.49
dimethyldichlorosilane	19.62	18.12	7.61
dimethyldimethoxysilane	21.81	19.84	9.05
ethyltrichlorosilane	22.96	19.64	14.47
hexamethyldisiloxane	15.40	16.66	8.22
methyl trichlorosilane	19.54	19.02	2.69
methyl vinyl dichlorosilane	20.94	19.86	5.16
trimethoxysilane	20.02	19.96	0.28
vinyltrichlorosilane	22.88	20.75	9.32
octamethyltrisiloxane	16.66	16.99	1.96
[3-(mercapto)propyl]triethoxysilane	32.13	32.23	0.32
(3-methylacryloxypropyl)trichlorosilane	34.66	36.88	6.41
3-(triethoxysilyl)propionitrile	32.44	37.32	15.06
3-(trimethoxysilyl)-1-propanethiol	41.45	25.06	39.55
γ-aminopropyltriethoxysilane	36.76	33.12	9.89
bis[3-(trimethoxysilyl)propyl]disulfide	40.90	23.71	42.03
bis[3-(triethoxysilyl)propyl]disulfide	34.40	27.58	19.84
decamethylcyclopentasiloxane	18.41	19.09	3.66
decamethyltetrasiloxane	17.31	17.31	0.00
dimethylchlorosilane	13.62	15.61	14.64
diphenyldichlorosilane	37.82	60.12	58.96
dodecamethylcyclohexasiloxane	19.00	19.00	0.00
dodecamethylpentasiloxane	17.77	17.64	0.74
eicosamethylnonasiloxane	19.16	18.94	1.16
hexacosamethyldodecasiloxane	19.21	19.91	3.68
hexadecamethylcyclooctasiloxane	19.43	18.83	3.07
hexadecamethylheptasiloxane	18.50	18.29	1.14
methyl dichlorosilane	18.03	16.50	8.44
methyl silicate	58.31	23.33	59.98
octadecamethyloctasiloxane	18.61	18.61	0.00
octamethylcyclotetrasiloxane	18.20	19.17	5.34
phenylmethyldichlorosilane	31.73	39.12	23.31
phenyltrichlorosilane	30.67	40.01	30.45
tetrachlorosilane	18.80	19.91	5.89
tetradecamethylhexasiloxane	18.31	17.96	1.87

Table D.7 Continued.

tetraethoxysilane	21.28	25.91	21.75
tetraethyl silane	22.51	18.83	16.35
tetramethylsilane	12.28	16.34	33.11
trichlorosilane	17.40	17.40	0.00
trimethyl silanol	18.58	24.33	30.93
trimethylchlorosilane	17.25	17.23	0.12
tris(2-methoxyethoxy)vinylsilane	35.65	32.36	9.23
vinyltrimethoxysilane	25.31	23.32	7.89

Table D.8. Enthalpy of vaporization data at 298 K for organosilicon compounds.

Compounds	H_{vap} - Lit. (kJ mol^{-1})	H_{vap} -Pred. (kJ mol^{-1})	Absolute deviation (%)
dichlorodiethylsilane	43.47	33.43	23.08
dimethyldichlorosilane	32.11	28.52	11.16
dimethyldimethoxysilane	34.68	35.65	2.80
ethyltrichlorosilane	36.55	35.44	3.04
hexamethyldisiloxane	36.29	33.55	7.56
methyl trichlorosilane	29.85	30.53	2.26
methyl vinyl dichlorosilane	35.24	32.34	8.23
trimethoxysilane	35.61	39.92	12.11
vinyltrichlorosilane	34.21	34.34	0.38
octamethyltrisiloxane	46.59	42.58	8.61
[3-(mercapto)propyl]triethoxysilane	65.38	80.93	23.77
(3-methylacryloxypropyl)trichlorosilane	70.75	70.05	0.98
3-(triethoxysilyl)propionitrile	68.38	80.75	18.09
3-(trimethoxysilyl)-1-propanethiol	46.05	50.94	10.61
γ-aminopropyltriethoxysilane	55.66	79.54	42.91
bis[3-(trimethoxysilyl)propyl]disulfide	101.66	123.29	21.28
bis[3-(triethoxysilyl)propyl]disulfide	103.20	149.88	45.23
decamethylcyclopentasiloxane	59.01	56.12	4.90
decamethyltetrasiloxane	54.62	51.61	5.51
dimethylchlorosilane	25.23	25.22	0.04
diphenyldichlorosilane	81.14	72.29	10.91
dodecamethylcyclohexasiloxane	64.99	64.99	0.00
dodecamethylpentasiloxane	61.92	60.65	2.06
eicosamethylnonasiloxane	92.85	96.77	4.22
hexacosamethyldodecasiloxane	123.87	123.87	0.00
hexadecamethylcyclooctasiloxane	79.68	82.75	3.85
hexadecamethylheptasiloxane	78.52	78.71	0.25
methyl dichlorosilane	27.23	27.23	0.00
methyl silicate	49.92	46.78	6.28
octadecamethyloctasiloxane	83.76	87.74	4.76
octamethylcyclotetrasiloxane	54.94	47.24	14.01
phenylmethyldichlorosilane	53.93	50.41	6.53
phenyltrichlorosilane	52.41	52.41	0.00
tetrachlorosilane	29.69	32.53	9.56
tetradecamethylhexasiloxane	71.41	69.68	2.42
tetraethoxysilane	53.59	64.51	20.37

Table D.8 Continued.

tetraethyl silane	44.48	44.16	0.73
tetramethylsilane	24.37	24.52	0.60
trichlorosilane	26.83	29.23	8.93
trimethyl silanol	50.92	48.51	4.73
trimethylchlorosilane	29.83	26.52	11.08
tris(2-methoxyethoxy)vinylsilane	74.60	89.75	20.31
vinyltrimethoxysilane	43.44	45.03	3.66

Table D.9. Liquid viscosity data at 298 K for organosilicon compounds.

Compounds	η - Lit. (cP)	η - Lit. (cP)	Absolute deviation (%)
dichlorodiethylsilane	0.6359	0.6317	0.67
dimethyldichlorosilane	0.4616	0.4192	9.20
dimethyldimethoxysilane	0.3588	0.4524	26.08
ethyltrichlorosilane	0.4361	0.6786	55.62
hexamethyldisiloxane	0.4816	0.7298	51.52
methyl trichlorosilane	0.4673	0.4661	0.25
methyl vinyl dichlorosilane	0.4928	0.4500	8.69
trimethoxysilane	0.3752	0.4242	13.08
vinyltrichlorosilane	0.4969	0.4969	0.01
octamethyltrisiloxane	0.8291	1.1343	36.81
[3-(mercapto)propyl]triethoxysilane	1.5897	1.6926	6.47
(3-methylacryloxypropyl)trichlorosilane	2.4610	2.2815	7.29
3-(triethoxysilyl)propionitrile	1.5784	1.5784	0.00
3-(trimethoxysilyl)-1-propanethiol	2.1167	1.6670	21.25
γ-aminopropyltriethoxysilane	1.4738	2.0939	42.07
bis[3-(trimethoxysilyl)propyl]disulfide	17.0551	5.6602	66.81
bis[3-(triethoxysilyl)propyl]disulfide	2.6004	5.3301	104.98
decamethylcyclopentasiloxane	3.8006	3.8005	0.00
decamethyltetrasiloxane	1.2988	1.5387	18.48
dimethylchlorosilane	0.2806	0.2806	0.00
diphenyldichlorosilane	2.0205	1.3936	31.03
dodecamethylcyclohexasiloxane	6.7989	4.5607	32.92
dodecamethylpentasiloxane	1.8417	1.9432	5.51
eicosamethylnonasiloxane	4.2527	3.5612	16.26
hexacosamethyldodecasiloxane	6.4005	4.7746	25.40
hexadecamethylcyclooctasiloxane	14.2053	6.0809	57.19
hexadecamethylheptasiloxane	2.9502	2.7522	6.71
methyl dichlorosilane	0.3302	0.3275	0.81
methyl silicate	0.6008	0.5794	3.55
octadecamethyloctasiloxane	3.5188	3.1567	10.29
octamethylcyclotetrasiloxane	2.1978	3.0404	38.34
phenylmethyldichlorosilane	1.4939	0.9064	39.33
phenyltrichlorosilane	1.3553	0.9533	29.66
tetrachlorosilane	0.4539	0.5130	13.01
tetradecamethylhexasiloxane	2.3478	2.3477	0.00
tetraethoxysilane	0.6678	0.3594	46.18

Table D.9 Continued.

tetraethyl silane	0.6065	1.1753	93.79
tetramethylsilane	0.8720	0.3253	62.69
trichlorosilane	0.3266	0.3744	14.65
trimethyl silanol	4.7182	2.6588	43.65
trimethylchlorosilane	0.3722	0.3722	0.00
tris(2-methoxyethoxy)vinylsilane	2.4493	1.2098	50.61
vinyltrimethoxysilane	0.5467	0.5467	0.00

Table D.10. Specific heat data at 298 K for organosilicon compounds.

Compounds	C_p - Lit. (J mol^{-1} K^{-1})	C_p - Pred. (J mol-1 K^{-1})	Absolute deviation (%)
dichlorodiethylsilane	215.53	182.96	15.11
dimethyldichlorosilane	168.02	153.57	8.60
dimethyldimethoxysilane	218.16	217.97	0.09
ethyltrichlorosilane	172.04	178.84	3.95
hexamethyldisiloxane	311.26	259.51	16.62
methyl trichlorosilane	163.12	149.45	8.38
methyl vinyl dichlorosilane	173.17	176.95	2.18
trimethoxysilane	204.95	237.30	15.78
vinyltrichlorosilane	174.78	172.84	1.11
octamethyltrisiloxane	355.61	357.22	0.45
[3-(mercapto)propyl]triethoxysilane	342.71	432.99	26.34
(3-methylacryloxypropyl)trichlorosilane	312.35	349.34	11.84
3-(triethoxysilyl)propionitrile	356.03	385.32	8.23
3-(trimethoxysilyl)-1-propanethiol	232.06	254.67	9.74
γ-aminopropyltriethoxysilane	459.76	451.99	1.69
bis[3-(trimethoxysilyl)propyl]disulfide	539.41	645.55	19.68
bis[3-(triethoxysilyl)propyl]disulfide	617.66	833.67	34.97
decamethylcyclopentasiloxane	599.72	591.96	1.29
decamethyltetrasiloxane	513.62	454.93	11.43
dimethylchlorosilane	158.40	148.92	5.98
diphenyldichlorosilane	325.13	320.97	1.28
dodecamethylcyclohexasiloxane	705.70	706.94	0.18
dodecamethylpentasiloxane	624.29	552.63	11.48
eicosamethylnonasiloxane	889.07	943.47	6.12
hexacosamethyldodecasiloxane	1207.21	1236.59	2.43
hexadecamethylcyclooctasiloxane	862.23	936.90	8.66
hexadecamethylheptasiloxane	820.26	748.05	8.80
methyl dichlorosilane	150.10	144.80	3.53
methyl silicate	240.51	274.14	13.98
octadecamethyloctasiloxane	845.20	845.76	0.07
octamethylcyclotetrasiloxane	507.55	476.98	6.02
phenylmethyldichlorosilane	253.82	237.27	6.52
phenyltrichlorosilane	218.29	233.15	6.81
tetrachlorosilane	145.33	145.33	0.00
tetradecamethylhexasiloxane	747.11	650.34	12.95
tetraethoxysilane	364.18	399.56	9.71

Table D.10 Continued.

tetraethyl silane	295.10	279.39	5.32
tetramethylsilane	191.90	161.80	15.68
trichlorosilane	132.16	140.68	6.45
trimethyl silanol	240.74	169.65	29.53
trimethylchlorosilane	180.44	157.68	12.61
tris(2-methoxyethoxy)vinylsilane	403.32	535.95	32.89
vinyltrimethoxysilane	254.40	269.45	5.92

APPENDIX E

DATA USED FOR DEVELOPMENT OF GC METHOD FOR RADIATIVE FORCING

Table E.1. Data used for development of group contribution method for radiative forcing.

Compounds	RF - Lit. ($W\ m^{-2}$)	RF - Pred. ($W\ m^{-2}$)	Absolute deviation (%)
CH_3OCH_2F	0.154	0.135	12.329
CH_3OCHF_2	0.210	0.246	16.986
CF_3OCH_3	0.243	0.298	22.653
CHF_2OCHF_2	0.484	0.418	13.603
CF_3OCHF_2	0.470	0.471	0.114
$CH_3OCH_2CF_3$	0.240	0.216	9.846
$CF_3OCH_2CH_3$	0.259	0.298	15.076
$CH_3OCF_2CHF_2$	0.345	0.329	4.640
$CHF_2OCH_2CF_3$	0.389	0.389	0.036
$CH_3OCF_2CF_3$	0.448	0.354	20.950
$CHF_2OCF_2CHF_2$	0.554	0.501	9.480
$CHF_2OCF_2CH_2F$	0.455	0.418	8.121
$CHF_2OCHFCF_3$	0.529	0.476	10.074
$CF_3OCHFCHF_2$	0.479	0.503	4.997
$CF_3OCF_2CF_2H$	0.568	0.554	2.490
$CF_3OCH_2CHF_2$	0.366	0.416	13.684
$CF_3OCH_2CF_3$	0.439	0.441	0.509
$CF_3OCHFCF_3$	0.528	0.528	0.016
$CH_3OCH_2CF_2CF_3$	0.320	0.300	6.346
$CH_3OCH_2CF_2CHF_2$	0.221	0.275	24.227
$CHF_2OCH_2CF_2CHF_2$	0.447	0.447	0.007
$CH_3OCF_2CF_2CHF_2$	0.401	0.412	2.821
$CH_3OCF_2CF_2CF_3$	0.434	0.437	0.798
$CHF_2OCF_2CHFCF_3$	0.633	0.586	7.385
$CF_3OCH_2CF_2CF_3$	0.525	0.525	0.085
$CF_3OCF_2CHFCF_3$	0.641	0.639	0.370
$CHF_2OCH_2CF_2CF_3$	0.479	0.472	1.424

Table E.1 Continued.

$CH_3OCH(CF_3)_2$	0.36	0.360	0.123
$CH_3OCF(CF_3)_2$	0.439	0.458	4.318
$CH_2FOCH(CF_3)_2$	0.424	0.421	0.616
CF3OCH(CF3)2	0.563	0.584	3.805
$CH_3CH_2OCF_2CF_2H$	0.37	0.329	11.083
$CH_3CH_2OCF_2CF_3$	0.488	0.354	27.430
$CF_3CH_2OCH_2CF_3$	0.398	0.360	9.659
$CHF_2CF_2OCH_2CF_3$	0.516	0.472	8.492
$CF_3CH_2OCF_2CF_3$	0.531	0.497	6.341
$CH_3OCF_2CF_2CF_2CF_3$	0.552	0.521	5.655
$CHF_2OCH_2CF_2CHFCF_3$	0.486	0.532	9.425
$CH_3OCF_2CH(CF_3)_2$	0.489	0.497	1.704
$CHF_2CF_2OCH_2CF_2CHF_2$	0.529	0.530	0.255
CHF2CF2OCH2CF2CF3	0.582	0.556	4.553
$CH_3CH_2OCF_2CHFCF_3$	0.431	0.414	3.999
$CF_3CH_2OCF_2CHFCF_3$	0.593	0.557	6.079
$CF_3CHFOCF_2CF_2CF_3$	0.636	0.668	4.953
$CF_3CHFCF_2OCH_2CF_2CHF_2$	0.621	0.615	0.946
$CF_3CHFCF_2OCH_2CF_2CF_3$	0.67	0.640	4.437
$CH_3OCH_2CF_2CF_2CF_2CHF_2$	0.406	0.441	8.666
CCl_3F	0.28	0.185	34.051
CCl_2F_2	0.34	0.141	58.580
$CClF_3$	0.26	0.172	33.868
CCl_2FCClF_2	0.319	0.268	15.994
$CClF_2CClF_2$	0.31	0.224	27.694
$CClF_2CF_3$	0.227	0.255	12.451
$CHClF_2$	0.223	0.147	34.174
$CHCl_2CF_3$	0.199	0.201	0.852
$CHClFCF_3$	0.223	0.232	3.841
CH_3CCl_2F	0.155	0.156	0.583
CH_3CClF_2	0.194	0.112	42.230
$CF_3CF_2CHCl_2$	0.268	0.284	5.976
CF_2ClCF_2CHFCl	0.284	0.284	0.080
CHF_3	0.268	0.256	4.298
CH_2F_2	0.173	0.173	0.029
CHF_2CF_3	0.271	0.261	3.607
CHF_2CHF_2	0.195	0.236	21.064
CH_2FCF_3	0.217	0.178	18.067
CHF_2CH_2F	0.135	0.153	13.069

Table E.1 Continued.

CH_3CF_3	0.171	0.143	16.264
CH_3CHF_2	0.127	0.118	7.057
CH_3CH_2F	0.036	0.035	3.874
CF_3CHFCF_3	0.346	0.346	0.000
$CF_3CH_2CF_3$	0.274	0.286	4.517
$CHF_2CH_2CF_3$	0.284	0.261	8.019
CH_3CC1_3	0.079	0.086	9.191
HFE7200	0.3	0.521	73.595
HFE7100	0.31	0.521	67.995

APPENDIX F

OCTANOL-WATER PARTITIONING COEFFICIENT AND WATER SOLUBILITY

Octanol-water partitioning coefficient (*k*-O/W) and water solubility (*x*-H_2O) were estimated using KOWWIN v1.68 and WSKOW v1.42 packages available with the software EPI Suite, EPI 4.10 from US EPA.

Table F.1. Octanol-water partitioning coefficient and water solubility of heat transfer fluids.

Name	Formula	log(*k*-O/W)	*x*-H_2O (mg L^{-1})
(E)-1,1,1-trifluoro-3-methylpent-2-ene	$C_6H_9F_3$	3.545	80.05
(E)-5,5,5-trifluoro-4,4-dimethylpent-2-ene	$C_7H_{11}F_3$	3.869	36.87
(E)-6,6,6-trifluorohex-2-ene	$C_6H_9F_3$	3.489	89.40
(E)-prop-1-en-1-ylcyclobutane	C_7H_{12}	3.378	45.39
1,1,1,4,4,4-hexafluoro-2,2-dimethylbutane	$C_6H_8F_6$	4.008	3.21
1,1,1,4,4,4-hexafluoro-2-methylbutane	$C_5H_6F_6$	3.555	9.18
1,1,1,5,5,5-hexafluoro-3-methylpentane	$C_6H_8F_6$	4.046	2.98
1,1,1,5,5,5-hexafluoropentane	$C_5H_6F_6$	3.628	7.94
1,1,1,5,5-pentafluorohexane	$C_6H_9F_5$	4.179	2.81
1,1,1-trifluoro-2,2-dimethylpentane	$C_7H_{13}F_3$	4.084	4.29
1,1,1-trifluoro-2,3,3-trimethylbutane	$C_7H1_3F_3$	4.010	4.95
1,1,1-trifluoro-2,3-dimethylpentane	$C_7H_{13}F3$	4.048	4.60
1,1,1-trifluoro-3-(2,2,2-trifluoroethoxy)propane	$C_5H_6F_6O$	2.372	432.00
1,1,1-trifluoro-3-methoxybutane	$C_5H_9F_3O$	1.883	2025.00
1,1,1-trifluoro-3-methoxypropane	$C_4H_7F_3O$	1.465	5248.00
1,1,1-trifluoro-3-methyl-2-(trifluoromethyl)butane	C6H8F6	3.972	3.44
1,1,1-trifluoro-3-methylpentane	$C_6H_{11}F_3$	3.630	12.03
1,1,1-trifluorobutan-2-one	$C_4H_5F_3O$	0.672	25410.00
1,1,1-trifluorohexane	$C_6H_{11}F_3$	3.704	10.41

Table F.1 Continued.

1,1,2,2-tetramethyl-3-(trifluoromethyl)cyclopropane	$C_8H_{13}F_3$	4.278	2.58
1,1,2-trimethyl-2-(trifluoromethyl)cyclopropane	$C_7H_{11}F_3$	3.860	6.79
1-fluoro-1-methyl-3-methylenecyclobutane	C_6H_9F	2.925	371.20
1-methoxybutane	$C_5H_{12}O$	1.540	4807.00
2,2-difluoro-3-methyl-3-(trifluoromethyl)pentane	$C_7H_{11}F_5$	4.559	1.14
2,2-difluoro-4-methyl-3-(trifluoromethyl)pentane	$C_7H_{11}F5$	4.523	1.22
2-(2,2-difluoropropoxy)-1,1,1-trifluoropropane	$C_6H_9F_5O$	2.849	177.10
3,3-difluoroheptane	$C_7H_{14}F_2$	4.254	3.66
3-ethoxy-1,1,1-trifluoropropane	$C_5H_9F_3O$	1.956	1752.00
3-methyl-3-(trifluoromethyl)pent-1-ene	$C_7H_{11}F_3$	3.947	31.59
4,4,4-trifluoro-2,3,3-trimethylbut-1-ene	$C_7H_{11}F_3$	4.004	28.29
4,4,4-trifluorobutan-2-one	$C_4H_5F_3O$	0.672	25410.00
4-methyl-3-(trifluoromethyl)pent-1-ene	$C_7H_{11}F_3$	3.911	33.90
5,5,5-trifluoro-2-methylpent-1-ene	$C_6H_9F_3$	3.624	68.58
6,6,6-trifluorohex-1-ene	$C_6H_9F_3$	3.567	76.60
methyl 3,3,3-trifluoropropanoate	$C_4H_5F_3O_2$	1.280	6625.00
1,1,1-trifluoro-2-(2,2,2-trifluoroethoxy)ethane	$C_4H_4F_6O$	1.881	1333.00
1-ethoxybutane	$C_6H_{14}O$	2.031	2128.00
Methanol	CH_4O	-0.632	1000000.00
Dimethoxydimethylsilane	$C_4H_{12}O_2Si$	0.585	31710.00
ethyldimethylsilane	$C_4H_{12}Si$	2.662	669.30
HFE7000	$C_4H_3F_7O$	2.668	230.30
HFE7200	$C_6H_5F_9O$	3.828	10.62
PF5060	C_6F_{14}	4.610	0.15

APPENDIX G

COSMO-RS

Conductor-like screening model for realistic solvation (COSMO-RS) was developed by Klamt [1] and combines quantum chemical calculations with statistical thermodynamics for prediction of thermodynamic properties of fluids and fluid mixtures. The method is implemented in the software COSMOTherm available from COSMOlogic GmbH & Co. KG, Leverkusen, Germany. In the present work, COSMO-RS was used for the prediction of vapor-liquid equilibria of HFE 7200 + methanol mixture. The basic idea behind COSMO-RS is the dielectric continuum solvation approximation of Born [2] which treats a solvent as a continuous medium of finite dielectric constant.

The first step in COSMO-RS is to calculate the charge distribution of the solute molecule using density functional theory. The solute is then introduced in the solvent by constructing a cavity (~ 20 % larger than solute's van der Waals radius) in the solvent. In COSMO-RS, a scaled conductor approximation is used instead of the exact dielectric boundary condition as it considerably simplifies the mathematics of dielectric continuum solvation models, with very small loss of accuracy. Therefore, the solvent is first treated as a perfect conductor and the polarization charge density on the cavity surface caused by the solute is calculated. The charge density (σ) for a solvent with finite dielectric constant (ε) is then calculated using the scaled-conductor approximation as follows:

$$\sigma = \frac{\varepsilon - 1}{\varepsilon + 0.5}\sigma^{*} \qquad \text{(G.1)}$$

where σ^* is the charge density calculated by treating the solvent as a perfect conductor. The interaction energy between the solvent and solute molecule are then calculated. All relevant intermolecular interactions such as van der Waals, electrostatic, and hydrogen bonding are taken into account.

Thermodynamic properties are calculated using statistical thermodynamics by factoring the partition function into three contributions, $Z = Z^0 Z^C Z^R$. The first factor, Z^0, is the ideal entropic contribution arising from permutations of identical particles. The second factor (Z^C), called the combinatorial factor, is due to steric interactions taking into account all size and shape effects of the molecules. The third factor (Z^R), called the residual factor arises from all non-steric interactions between the molecules. The residual contribution is computed by considering pair-wise interactions of surface segments with the assumption that all surface segments are distinguishable. To calculate the residual part, the 3D information on polarization charge densities (σ) on the molecular surface is converted to a histogram $p(\sigma)$ which indicates the surface available in the polarization interval $\sigma \pm d\sigma/2$. Such a histogram is called the sigma profile, and the profile of water is shown in Figure G.1 with its sigma surface as inset. Once the partition function is known, all relevant solution thermodynamic properties can be calculated.

In COSMO-RS, quantum chemical calculations are usually performed using density functional theory with Becke-Perdew (BP) functional TZVP basis set [3]. In addition, COSMO-RS uses 8 adjustable parameters (and 1 additional parameter for each element). Solvent-water partition, vapor pressure, activity coefficient in aqueous infinite dilution of 800 small molecules built of elements H, C, N, O, F, Cl, Br, I and S were used

for its parameterization. The parameterizations were evaluated on a validation test set of 2000 data points, consisting of temperature dependent activity coefficients, Henry law constants, and vapor pressures for various solutes in different solvents. Chemical potential differences were reproduced with a RMS accuracy of ~0.35 kcal mol^{-1}. [3]

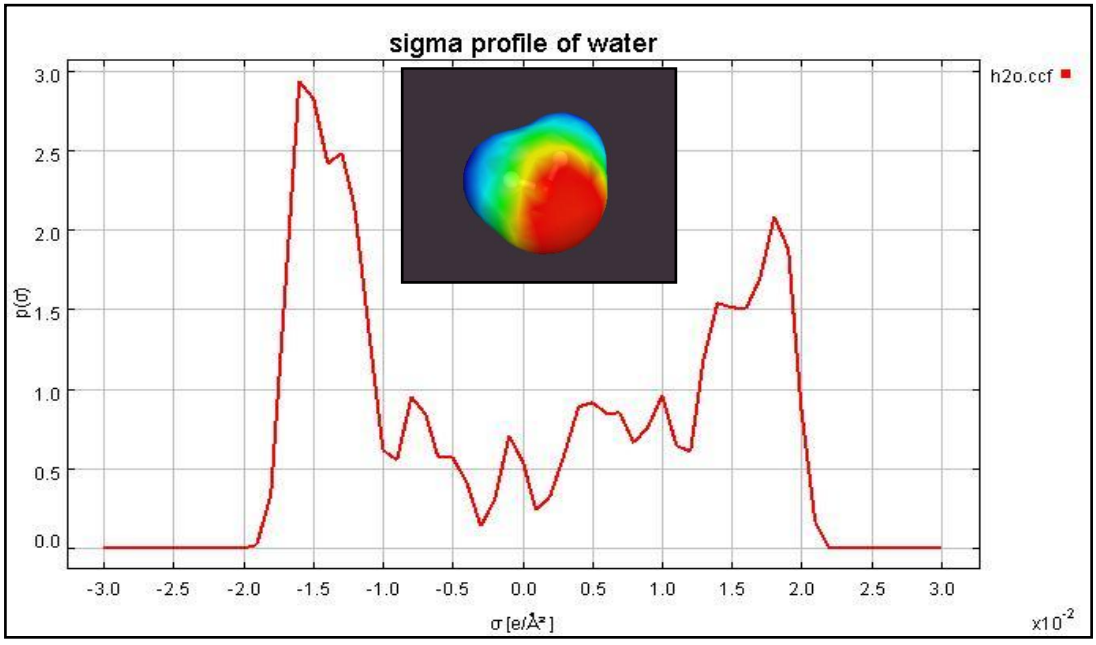

Figure G.1. Sigma profile of water calculated at BP/TZVP level of theory.

The COSMOTherm software allows for estimation of liquid viscosity using a QSPR method. The COSMO-QSPR method for liquid viscosity is given as:

$$\ln(\eta) = C_{area}A + C_{M2}M^2 + C_{N,ring}N^{ring} + C_{TS}TS + C_0 \qquad \text{(G.2)}$$

The descriptors for the liquid viscosity are the compounds surface area (A) as read from its COSMO-file, the second σ-moment (M^2) of the compound, the number of ring atoms in the compound (N^{ring}), and the pure compound entropy (S) times temperature (T). The

COSMO-QSPR method for liquid viscosity was also evaluated in this work and compared with GC methods described in Chapter 2.

The quantitative structure property relationship (QSPR) method described above was evaluated with particular emphasis on fluorinated and organosilicon compounds. The numbers of compounds used in evaluation of COSMO method are listed in Table G.1. The other organics include 2-3 compounds from all other classes of compounds (except F and Si) used in evaluation of GC method. Figure G.2 compares AADs of COSMO method with those of MG method.

Table G.1. Number of compounds used for the evaluation of COSMO-QSPR method.

	COSMO-QSPR	MG
F	12	12
Si	9	NA
Other organics	28	28
Total	49	49

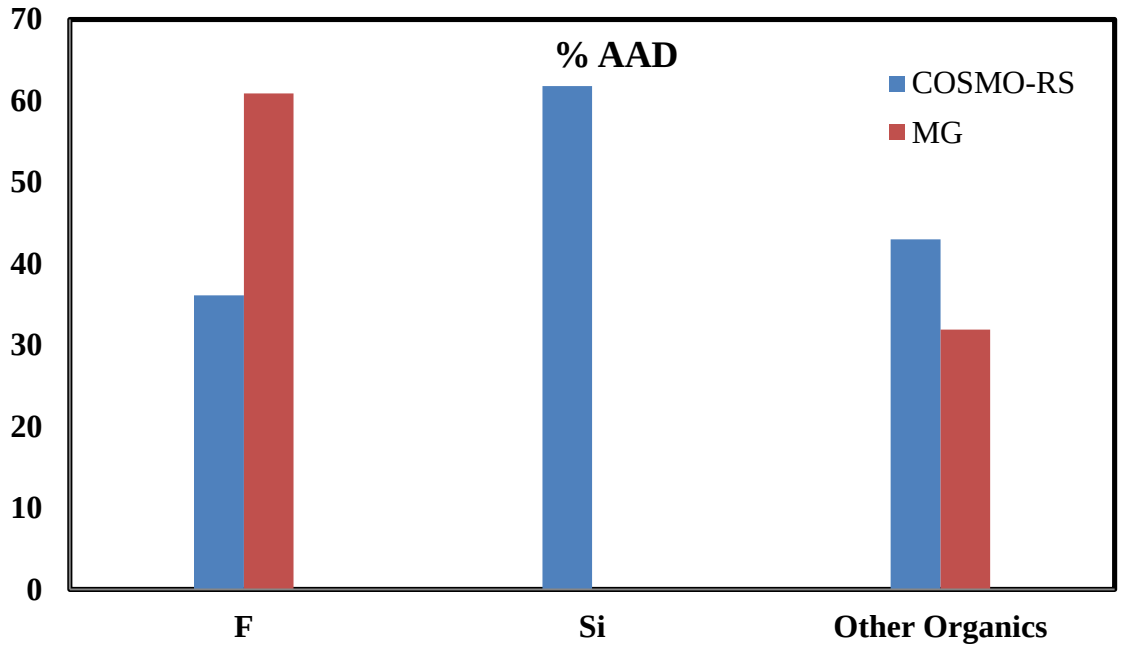

Figure G.2. Comparison of COSMO-QSPR with the MG method for the prediction of liquid viscosity at 298 K.

It can be observed that while COSMO-QSPR method has relatively lower error for fluorinated compounds, its overall AAD is higher than GC methods.

G.1 References

1. Klamt, A., *COSMO-RS From quantum chemistry to fluid phase thermodynamics and drug design*, 2005. Amsterdam, The Netherlands: Elsevier.

2. Born, M., *Volumes and Hydration Warmth of Ions*, Zeitschrift fur Physik, 1920, **1**: p. 45-46

3. COSMO-RS theory and background available from COSMOlogic, http://www.cosmologic.de/index.php?cosId=4201&crId=4